The novel role of Syndecan 3 in bone metabolism

Thesis submitted in accordance with the requirements of the University of Liverpool for the degree of Doctor in Philosophy

By

Francesca Manuela Johnson de Sousa Brito

September 2019

Abstract

Syndecan-3 (Sdc3), a transmembrane heparan sulphate proteoglycan receptor, is highly expressed in periosteal osteoblasts during skeletal development, but its role in the adult skeleton is unknown. Sdc3 knock-out (Sdc3 KO) mice have normal musculature and are resistant to diet-induced obesity. Here I analysed the role of Sdc3 in bone metabolism using a Sdc3 KO mouse.

At 3 months there was a decrease in bone volume in Sdc3 KO tibias, compared to WT mice. Cortical analysis of tibias of Sdc3 KO mice showed decreased cortical thickness, overall bone perimeter and bone strength, as compared to male WT mice. When analysing trabecular and cortical bone of femurs, similar results were also observed. At 6-months differences between Sdc3 KO mice were maintained. Furthermore, the 5th lumbar vertebrae (L5) also showed decreased bone volume at 3 months of age in Sdc3 KO mice compared to WT mice.

Interestingly, Sdc3 appears to have a differential effect on pre and postnatal bone development as Sdc3 KO P2 pups have significantly increased tibial length and bone volume as compared to WT pups.

Dynamic bone histomorphometric analysis at 3 months of age revealed significant reduction in bone formation of Sdc3 KO mice when compared to WT mice. Similar results were observed at 6 months of age in Sdc3 KO mice compared to WT. Histomorphometric quantification of osteoclasts in Sdc3 KO mice at 3 months of age revealed a significant reduction in osteoclast numbers, when compared to male 3-month-old WT mice. This difference was maintained at 6 months of age. Bone marrow adiposity was also quantified at 3 and 6 months of age and revealed a 60-fold increase and 2-fold increase in bone marrow adipocytes in 3-month-old and 6-month-old Sdc3 KO mice, respectively, vs WT mice of the same age.

Assessment of anabolic response of bone to mechanical loading using dynamic histomorphometry revealed that Sdc3 KO mice have a blunted response to mechanical loading when compared to WT mice.

In vitro studies mirrored the *in vivo* findings, revealing that there was an approximately 50% decrease in Sdc3KO osteoclast number compared to WT, although interestingly, Sdc3 KO osteoclasts had increased resorptive activity *in vitro* when compared to WT. Gene expression studies revealed a decrease in *Tnfrsf11a* (encoding RANK) and in *Fzd7* in M-CSF-dependent Sdc3 KO macrophages versus WT.

In vitro studies on osteoblasts revealed a reduction in mineralisation in Sdc3 KO osteoblast cultures generated from bone chips, bone marrow stromal cells (BMSCs) and from calvaria together with the observation of the presence of fat cells in these cultures, in contrast to WT. Osteoblast differentiation markers: *Alpl, Runx2* and *Bglap* showed a significant decrease in Sdc3 KO by qPCR. Interestingly *Lgr4* expression was also significantly decreased in Sdc3 KO cultures suggesting inhibition of Wnt signalling. Protein studies showed decreased non-phosphorylated β-catenin after Wnt3a stimulation in Sdc3 KO cultures suggesting that the canonical Wnt signalling pathway may be impaired in the absence of Sdc3.

These results indicate that the low bone volume phenotype in Sdc3 KO mice is due to reduced bone formation, likely due to impaired differentiation and/or function of osteoblasts. Increased osteoclast activity, despite decreased osteoclastogenesis, may be contributing to the phenotype. The underlying mechanism may involve disruption of the Wnt signalling pathway. These data provide first evidence of the novel role of Sdc3 in regulating bone metabolism in adult mice.

List of presentations

Oral Communications

Brito F, Pisconti A, Prior A, Charlesworth G, Bou-Gharios G, van 't Hof RJ, Daroszewska A. Novel role of Syndecan-3 (Sdc3) in maintaining bone mass. European Calcified Tissue Society (ECTS) Annual Conference, 2018, Valencia, Spain. **Oral presentation** and **poster**

Brito F, Pisconti A, Prior A, Charlesworth G, Bou-Gharios G, van 't Hof RJ, Daroszewska A. Novel role of Syndecan-3 in maintaining bone mass. IACD Musculoskeletal Biology Science day 2017. **Oral presentation**

Poster communications

Butcher A, **Brito F,** Charlesworth G, Prior A, Bou-Gharios G, Pisconti A, van 't Hof RJ, Daroszewska A. Novel role of Syndecan 3 in regulating osteoblastogenesis through the Wnt signalling pathway. ECTS Annual Conference, 2019, Budapest, Hungary. **Poster presentation**

Butcher A, **Brito F,** Bou-Gharios G, Pisconti A, Daroszewska A, van 't Hof RJ. Syndecan 3 deletion leads to premature bone ageing. ECTS Annual Conference, 2018, Valencia, Spain. **Oral presentation** and **poster**

Liew J., **Brito F**, Charlesworth G, van 't Hof RJ, Daroszewska A. Age-related increased osteoclastogenesis is due to increased phosphorylation of p38 and enhanced expression of V-ATPase. ECTS Annual Conference, 2018, Valencia, Spain. **Poster presentation**

Brito F, Pisconti A, Prior A, Charlesworth G, Bou-Gharios G, van 't Hof RJ, Daroszewska A. Role of Syndecan-3 (Sdc3) in maintaining bone mass. ECTS Annual Conference, 2017, Salzburg, Austria. **Poster presentation**

Brito F, Pisconti A, Prior A, Charlesworth G, Bou-Gharios G, van 't Hof RJ, Daroszewska A. Syndecan-3 is important for maintaining bone mass. IACD Musculoskeletal Biology Science day, 2016. **Poster presentation**

Brito F, Pisconti A, Prior A, Charlesworth G, Bou-Gharios G, van 't Hof RJ, Daroszewska A. Syndecan-3 is important for maintaining bone mass. Bone Research Society (BRS) Annual Meeting, 2016, Liverpool. **Poster presentation**

Brito F, Bou-Gharios G, van 't Hof RJ, Daroszewska A. Understanding the mechanisms underlying bone cell ageing. IACD Musculoskeletal Biology Science day 2015. **Poster presentation**

You can't and you won't.
I can, I will, I have.

Acknowledgments

It would be fair to say that this PhD has been quite a journey. There have been many highs and many lows, but this has been a truly life-changing experience. I could not have done it without the support and guidance I have received from some amazing people.

First and foremost, I would like to thank the Institute of Ageing and Chronic Disease for funding my PhD.

To my primary supervisor, Dr. Anna Daroszewska, thank you for the opportunity to pursue this PhD. For the support, guidance and encouragement throughout these 4 years, especially through my thesis writing. It has been a great honour to be your PhD student and I hope I have done you proud. You pushed me hard to be the best I can be. Thank you.

To Professor Rob van' t Hof, I am thankful for his contagious enthusiasm for science, for all he has taught me and for allowing me to grow as a scientist. He has been a great mentor to me.

I would also like to thank my third supervisor, Professor George Bou-Gharios. His challenging questions made me work even harder to prove I was indeed deserving of this position. I hope I have proven him worthy of it.

To Dr. Dada Pisconti, thank you for asking us to investigate the Sdc3 KO mouse in the first place. I have thoroughly enjoyed working on this project and will be sad when I finally move on to something new.

To the amazing lab group I have worked with these last 4 years, I am immensely grateful. Gemma, Mandie and Cath have been essential throughout my lab work years, always lending a helping hand, a hug or even a slice of cake. Jacqueline, my conference buddy, thank you for all her support and encouragement, and the biggest of smiles. To our most recent lab member, Andy, thank you for all your help in those final months in lab, your great sense of humour and the funniest nights out. To Mikele, I couldn't have asked for a better partner to start and end this adventure with. He is an amazing scientist but most importantly a great friend and my family away from home. He provided me with a home when I didn't have one, endless hugs, a shoulder to cry on and many fun late nights/ early mornings climbing lamp posts or lions, destroying our livers, but it was all worth it.

I would like to give a special thank you to Dr. James Henstock. He managed to drag my confidence back up again when it was at its lowest and help me both professionally and financially through some of my hardest months. To Dr. Aphodite Vasilaki, thank you for all the support during the most emotionally challenging aspects of my PhD. She has been a safe haven to go to when I was most down, offering endless support and hugs. She has provided an excellent example of a successful and extremely smart woman in science. To Prof. Jim Gallagher, thank you for being my advisor, offering great discussions and for lending me your reflected light microscope for my osteoclast work. And I can't go without thanking Dr. Sarah Taylor for all the demonstrating jobs which were an immense financial help and a great confidence booster. I must also thank Dr Blandine Poulet for teaching me how to perform mechanical loading and for then letting me use it for my loading experiments.

I have met some amazing people through this journey which I can call friends. I'm thankful for Jess and Rhiannon, my write-up room buddies, who have made those

long days so much easier and enjoyable. I can't wait to celebrate the end of this journey with you! Brendan and Eddie, my desk neighbours, we've spent such fun times together and I will never forget you.

Ifi the small tornado with the biggest heart, thank you for your friendship. Steph, what a roller-coaster. Our adventures and journey to the end of crazy! We survived my friend. Adam, how can I ever thank someone, who didn't know me that well but put a roof over my head, I thank you from the bottom of my heart. I've had an amazing time sharing a home with you, Euan and Jude, discovering the gift of cleaning I have and that I cook a lot of pasta. But you can never do too much of those, can you?

To Euan, my knight in shining armour that saved me from so many things, including myself. He is the kindest most loving person I have ever been so lucky to meet. I never expected to meet someone that would change my life so much, for the better, and all because you made fun of Portugal and the music I like. Your never-ending love, support, encouragement and especially patience, I am so very grateful.

To my friends outside of my PhD, Ana Xavier, Soledad and Ana Luisa who have always been a text or a phone call away, I thank you.

I would like to make a special acknowledgment to Andrew, who sadly passed away at the start of my PhD. I could never have imagined how much of an impact you were going to have on my years in Liverpool. I am so thankful to have had you in my life. During one of the most tragic and heart-breaking moments in our lives, you brought me closer to two very important people in my life and for that I will always be grateful. Alan and Robina, thank you so much for all the love and support you have given me throughout my PhD. I am grateful for all the weekends I have spent in your lovely home, making my time away from home so much more bearable. I hope that as much as you have helped me, I have also been able to help you.

To my Titi, thank you for always checking up on me during these four years, for the warmest and most loving hugs you gave me whenever I went home and for always supporting me no matter what. It breaks my heart that I didn't get the chance to tell you I finally finished but I know you were there in that room with me.

And finally, but certainly not the least, I would like to thank my parents and my sister. My parents have provided both my sister and I unconditional love and support throughout our lives, always receiving us, together with Max, with the warmest of welcomes and the biggest hugs. I thank my sister for all her advice and support, always trying to be the big sister even though she is the baby of the family. Our family have been through some tough times recently, but we have come out stronger than ever. As much as I hope I have made you proud, I want you to know how proud I am of how amazingly strong you have all been in these past few years, especially recently. To my parents, you have supported me throughout all my pursuits, providing both Jessica and I with a loving home and always encouraging me to go further. Thank you for believing in me when I didn't, for loving me unconditionally and for allowing me to pursue all my dreams. You are the most important people in my world and to you I dedicate this thesis.

List of Figures

List of Tables

Abbreviations

ADIPOQ	adiponectin
AKP	alkaline phosphatase
AKT	protein kinase B
ALP	alkaline phosphatase
ANK	ankylosis gene
AP-1	activator protein-1
ATF4	activating transcription factor 4
AXIN2	axis inhibition protein 2
AWERB	Animal welfare and Ethical Review Body
BCA	bicinchoninic acid
Bcl-2	B-cell leukemia/lymphoma2
BFR/BS	bone formation rate per bone surface
BGLAP	osteocalcin
BGP	β-Glycerophosphate
BMC	Bone mineral content
BMD	bone mineral density
BMP	Bone morphogenic protein
BMSC	bone marrow mesenchymal stem cell(s)
BRU	bone remodeling unit
BS	bone surface
BV	bone volume
BV/TV	bone volume per tissue volume
CAII	carbonic anhydrase II
Calv	calvaria
CBF1	c promoter-binding factor 1
cDNA	complementary deoxyribonucleic
c-Fms	colony-stimulating factor-1 receptor
CKI	casein kinase I
CNS	central nervous system
Col1a1	type 1 collagen

Cort.Th	cortical thickness
CS	chondroitin sulphate
Csf-1	colony stimulating factor 1
CT	computerised tomography
CTNNB1	β-catenin
CTSK	cathepsinK
DAP	DNAX-activation protein
DC-STAMP	dendrocyte expressed seven transmembrane protein
Dhh	desert hedgehog
DKK1	dickkopf
DMEM	Dulbecco's Modified Eagle's medium
DS	dermatan sulphate
Dsh	dishevelled
DXA	dual-energy x-ray absorptiometry
ECM	extracellular matrix
ENPP1	ectonucleotide pyrophosphatase/phosphodiesterase 1
E.Pm	endosteal perimeter
ERK	extracellular signal regulated kinase
EtOH	ethanol
ETS	E26 transformation-specific
F	female
FcRϒ	Fc receptor common ϒ subunit
FCS	foetal calf serum
FGF	fibroblast growth factor
FGFR	fibroblast growth factor receptor
Fmax	maximum force
FRAX	fracture risk assessment tool
Fzd	frizzled
g	gram
GAG	glycosaminoglycans
Grb2	growth factor receptor bound protein 2

GSK-3β	glycogen synthase 3 β
h	hour(s)
Hes	hairy enhancer of split
Hh	hedgehog
HB-GAM	heparin-binding growth-associated molecule
HMBS	hydroxymethylbilane synthase
HMG	high mobility group
HS	heparan sulphate
HSC	haematopoietic stromal cells
HSPG	heparan sulphate proteoglycan
IBMX	3-Isobutyl-1-methylxanthine
Ihh	indian hedgehog
IKK	NF- κB kinase
IP	intra-peritoneal
ITAM	Immunoreceptor tyrosine-based activation motif
JNK	c-Jun N-terminal kinase
KO	knockout
KS	keratan sulphate
L5	lumbar vertebrae 5
Lag-1	longevity assurance gene-1
Lef	lymphoid-enhancing factor
LRG4	leucine-rich repeat-containing G-protein coupled receptor 4
LRG6	leucine-rich repeat-containing G-protein coupled receptor 6
LRP5	low density lipoprotein receptor-related protein 5
LRP6	low density lipoprotein receptor-related protein 6
M	male
MAPK	Mitogen-activated protein kinase
MAR	mineral apposition rate
M-CSF	macrophage colony stimulating factor
MEA	2-methoxyethyl acetate
mg	milligram

ml	milliliter
MGP	Matrix gla-protein
min	minutes(s)
MITF	Microphthalmia transcription factor
ml	milliliter
mM	millimole
MMA	methyl methacrylate
MMI	mean polar moment of inertia
mMolar	millimolar
MMP	matrix metalloproteases
MO	macrophage
mRNA	messenger ribonucleic acid
MS/BS	mineralising surface per bone surface
MSC	mesenchymal stromal cell
N	newtons
NEMO	NF- κB essencial modulator
NFATc1	nuclear factor of activated T cells 1
NF-kB	nuclear factor-kappa B
ng	nanogram
NICD	Notch intracellular domain
nMoles	nanomoles
N.Oc.	number of osteoclasts
N.Oc/BS	number of osteoclasts per bone surface
N.Oc/BV	number of osteoclasts per bone volume
N.Oc/TV	number of osteoclasts per tissue volume
Ob	osteoblast
Oc	osteoclast
Oc./BS	osteoclasts per bone surface
OC-STAMP	osteoclast stimulatory transmembrane protein
ON	osteonectin
OPG	osteoprotegerin

OSCAR	osteoclast-associated receptor
PBS	phosphate buffered saline
PCR	polymerase chain reaction
PI-3K	phosphatidylinositol-3 kinase
PKCα	protein kinase Cα
PLCϒ	phospholipase C ϒ
POc	pre-osteoclast
POSTN	periostin
PPARϒ	peroxisome proliferator-activated receptors ϒ
PPi	inorganic pyrophosphatase
P.Pm	periosteal perimeter
PS1	presenilin 1
PS2	presenilin 2
PTH	parathyroid hormone
qPCR	quantitative polymerase chain reaction
RANK	receptor activator for NF-kB
RANKL	receptor activator for NF-kB ligand
ResSurf/Oc	resorption surface per osteoclast
RGD	Arg-Gly-Asp
RIPA	radio-immunoprecipitation assay
RNA	ribonucleic acid
ROI	region of interest
R-SMAD	Receptor regulated SMAD
RSPO	R-spondin
RT	reverse transcriptase
RT-qPCR	reverse transcription quantitative polymerase chain reaction
Runx2	Runt-related transcription factor 2
SARA	SMAD anchor for receptor activation
SD	standard deviation
Sdc1	syndecan 1
Sdc2	syndecan 2

Sdc3	syndecan 3
Sdc3 KO	Sdc3 knock-out
Sdc4	syndecan 4
SDS	sodium dodecyl sulphate
Shh	sonic hedgehog
SLRP	small leucine-rich proteoglycan
SMAD	mothers against decapentaplegic homolog
SMI	structure model index
SOST	sclerostin
Su(H)	suppressor of hairless
TAB	TAK-1-binding protein
TACE	tumour necrosis factor-α-converting enzyme
TAK	TGF-β-activated kinase
Tb.N	trabecular number
Tb.Pf	trabecular pattern factor
Tb.Sp	trabecular separation
TBS-T	Tris Buffer Saline and Tween
Tb.Th	trabecular thickness
Tcf	T-cell factor
TFE3	transcription factor binding to IGHM enhancer 3
TGF-β	transformation growth factor-beta
TNAP	tissue-nonspecific alkaline phosphatase
TNFR	tumour necrosis factor receptor
TNFRSF11A	tumour necrosis factor receptor superfamily member 11A (RANK)
TNFSF11	tumour necrosis factor ligand superfamily member 11 (RANKL
TRAcP	tartrate-resistant acid phosphatase
TRAF	TNFR-associated cytoplasmic factor
TV	tissue volume
VDBP	vitamin-D-binding protein
Wif1	Wnt inhibitory factor 1
Wnt	wingless signaling

WNT3A	wingless family member 3A
WT	wild type
αMEM	α-Modified Eagle's Medium
µCT	MicroCT
µg	microgram
µl	microliter
µm	micrometer
%	percent

Table of Contents

1 Introduction

1.1 Bone: Function, structure and matrix

The skeletal system is composed mainly of cartilage and over 200 bones, which are mesoderm-derived tissues[1]. Bone, a specialised connective tissue, is a dynamic tissue able to adapt to mechanical stimuli and is constantly regenerated throughout life due to bone turnover[2–4]. It has several functions, such as protecting the internal organs and structures, aiding in mobility by providing levers for the muscles, housing bone marrow, and therefore playing a role in haematopoiesis, actively participating in mineral homeostasis, and serves as the biggest reservoir of minerals, including calcium and phosphate, and also contains growth factors and cytokines[5].

There are two types of bone structure in long bones, cortical (compact) bone, which is the outer casing of bones, and cancellous (trabecular, spongy) bone, which is located internally to cortical bone at the epiphysis and metaphysis of long bones and the interior of vertebrae[2]. In cortical bone, as can be seen in **Figure 1.1**, densely packed fibrils form concentric lamellae which form cortical osteons, and between the lamellae are lacunae where osteocytes are entrapped[5–8]. The cortical osteons are known as Haversian systems which surround the Haversian canal where we can find small blood vessels and nerves[5]. These blood vessels can interconnect forming Volkmann's canals. Cortical bone has an outer and an inner surface, the periosteal and the endosteal surfaces, respectively[5]. The compact arrangement of cortical bone allows it to have mechanical and protective functions[6].

Trabecular bone, which is the metabolically active component of the bone, is made up of plates and rods which are connected between each other giving it a spongy/honeycomb appearance which helps provide structural support[9]. In between the trabecular bone we can find bone marrow and blood vessels. Although trabecular bone is not compact like cortical bone, and therefore has reduced strength, it has a higher surface area which allows it to be in close contact with bone marrow, vessels and compact bone facilitating its role in haematopoiesis[2,10].

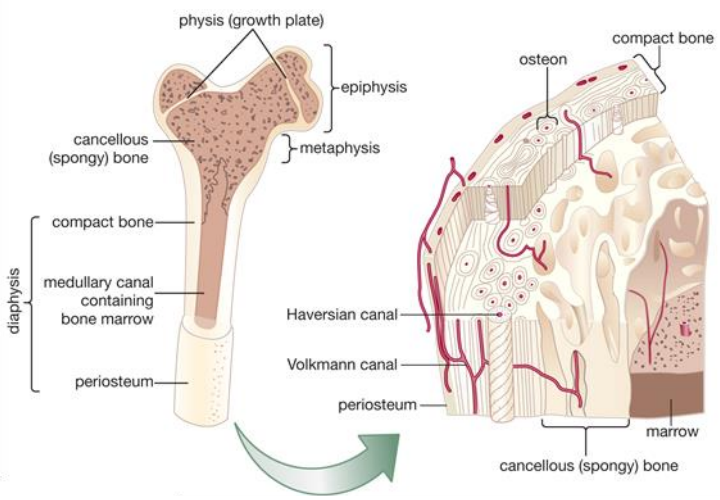

Figure 1.1: Representation of the internal structure of a human femur together with a close up of the interior of cortical and trabecular bone. The cylindrical bone shaft, called the diaphysis, which expands near the end to form the metaphysis where trabecular bone can be found. At the end of the bone is the epiphysis. The outer layer of the cortical bone is the periosteum. The Haversian system, also known as osteon, has a central canal called Haversian canal surrounded by concentric layers of matrix called lamellae which are the building blocks of the Haversian system[9].
(https://www.britannica.com/science/cancellous-bone/media/1/92222/66017)

Bone is a composite tissue made up of an organic matrix and an inorganic matrix, which allows the skeleton to be both rigid and strong but also maintain some form of elasticity[3]. The organic matrix of bone contains predominantly type I collagen, osteocalcin, osteonectin, osteopontin, fibronectin, bone morphogenic proteins (BMPs), cytokines and growth factors[11], all aiding in cell differentiation and bone growth and differentiation.

Collagen in bone, and other tissues, is arranged in fibrils which group together to form collagen fibres[10,12], as can be seen in **Figure 1.2**. This is what gives bone its flexibility and provides the tensile and compressive strength of bone. Collagen Type I is the most abundant type of collagen in bone and is the major protein in bone[12]. The remaining non-collagenous components, such as proteoglycans, which will be described in greater detail later on in this chapter in section 1.7, and glycosylated proteins, may only make up to 10% of the organic matrix but have important functions during mineralisation, osteoblast function and bone remodelling[10,13]. The inorganic matrix is made up of mineral crystals of calcium and phosphate in the form

of hydroxyapatite, $Ca_{10}(PO_4)_6(OH)_2$, which are associated with collagen fibril surfaces and allow bone its stiffness[14–16].

Bone is also composed of four different cell types, osteoclasts, osteoblasts, osteocytes and bone lining cells.

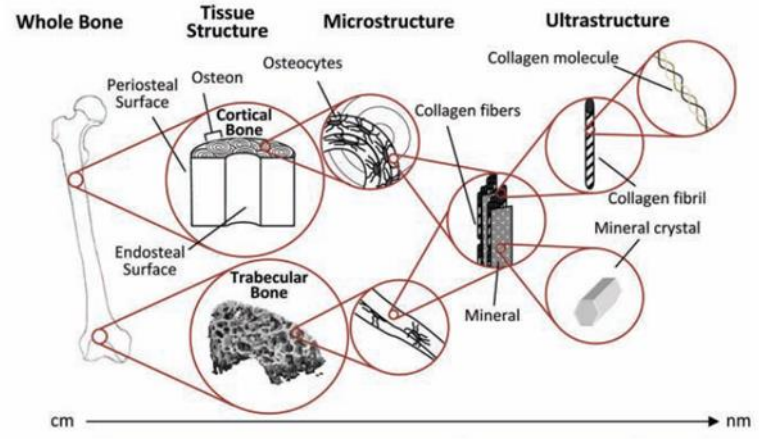

Figure 1.2: Hierarchical structural levels of bone. Cortical bone, which is the compact bone, surrounds the bone marrow and is made up of organised cortical osteons (also called Haversian systems) where osteocytes can be found. Trabecular bone is less organised and made up of connected plates and rods and is mostly found in the metaphysis and epiphysis of long bones and in the interior of vertebrae. Both types of bone contain both collagen fibres and mineral[14].

1.2 Bone cells

Bone cells are derived from haematopoietic stromal cells (HSCs) and from mesenchymal stromal cells (MSCs). HSCs give rise to the bone resorbing cells known as osteoclasts and MSCs give rise to the cells involved in bone formation and mineralisation, osteoblasts and osteocytes[17].

1.2.1 Osteoclasts

Osteoclasts are multinucleated cells, derived from HSCs and formed by fusion of mononuclear progenitors of the monocyte/macrophage lineage[18]. Osteoclasts are present in all mineralised tissue, having the capacity to resorb the mineralised tissue, and also cartilage and teeth[19], playing a central role in bone remodelling.

There are two cytokines essential and sufficient to promote osteoclastogenesis, macrophage-colony stimulating factor (M-CSF; also known as CSF-1)[18], and receptor activator of nuclear factor-κB ligand (RANKL)[20], as can be seen in **Figure 1.3**. M-CSF stimulates proliferation and survival of osteoclast precursors[21], motility and cytoplasmic spreading of mature osteoclasts[22], and induces expression of receptor activator of nuclear factor-κB (RANK)[23].

Another factor which plays a role in regulation of osteoclastogenesis is osteoprotegerin (OPG)[24]. It is now known that OPG, which acts as a decoy receptor for RANKL, is able to bind to RANK blocking RANKL's capacity to bind RANK[20], and it is the balance between OPG and RANKL that regulates osteoclastogenesis and therefore bone resorption[25].

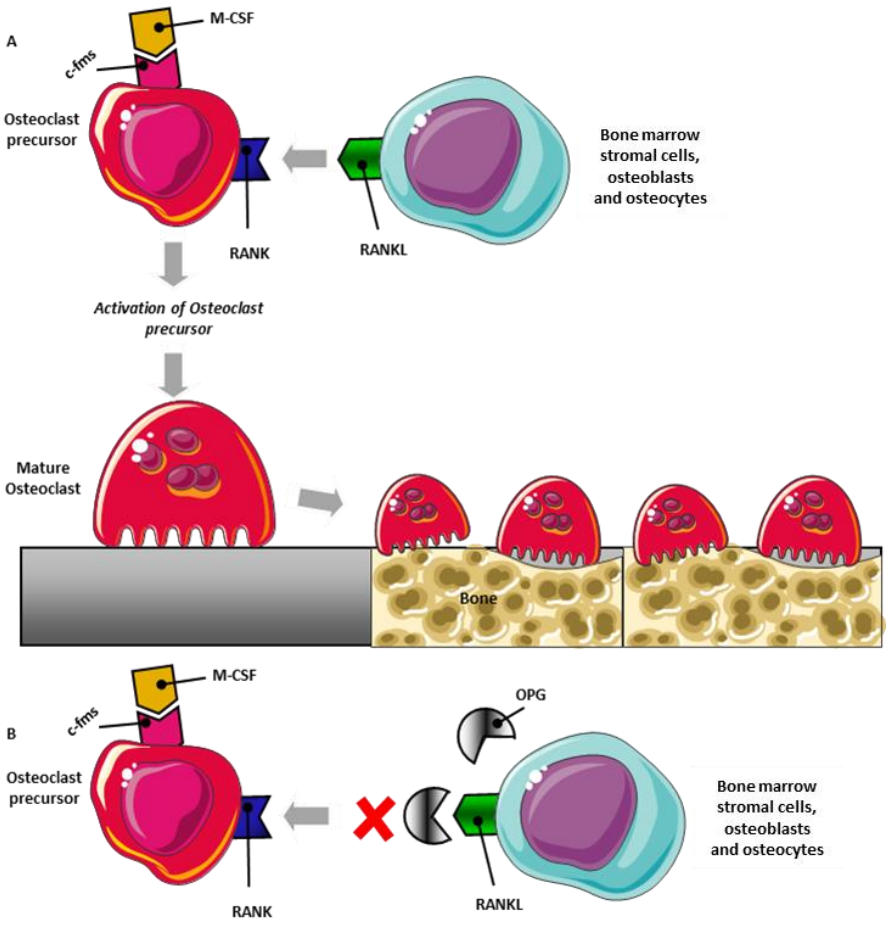

Figure 1.3: Mechanisms involved in osteoclastogenesis. (A) BMSCs, osteoblasts and osteocytes express M-CSF and RANKL. When M-CSF interacts with c-fms and RANKL interacts with its receptor RANK, this activates the osteoclast precursor promoting cell fusion in order to form a mature osteoclast which is then capable of resorbing bone. **(B)** OPG interacts with RANKL and inhibits osteoclastogenesis.

When M-CSF binds to its receptor c-Fms, this results in the recruitment of adaptor molecule c-Src[22] which in turn stimulates phosphatidylinositol-3 kinase (PI-3K) activity[26], stimulating protein kinase B (AKT) pathway activation, which stimulates cell survival[27]. On the other hand, c-Fms can interact with growth factor receptor bound protein 2 (Grb2) which mediates the activation of extracellular signal-regulated kinases (ERK)[28]. The activation of the ERK pathway leads to phosphorylation of microphthalmia transcription factor (MITF) and a partner protein, transcription factor binding to IGHM enhancer 3 (TFE3), resulting in activation of transcription factors therefore stimulation of osteoclast development and function[29] (**Figure 1.4**). M-CSF is also able to stimulate the expression of RANK in precursor cells, which allows the cells to respond to RANKL[23].

PU.1, a transcription factor part of the E26 transformation-specific (ETS) family which is only present in hematopoietic cells[30], is essential for macrophage and osteoclast development as mice lacking PU.1 have osteoclast-deficient osteopetrosis due to an arrest in macrophage and osteoclast development[31]. This transcription factor has therefore been shown to be important at an earlier stage during osteoclastogenesis.

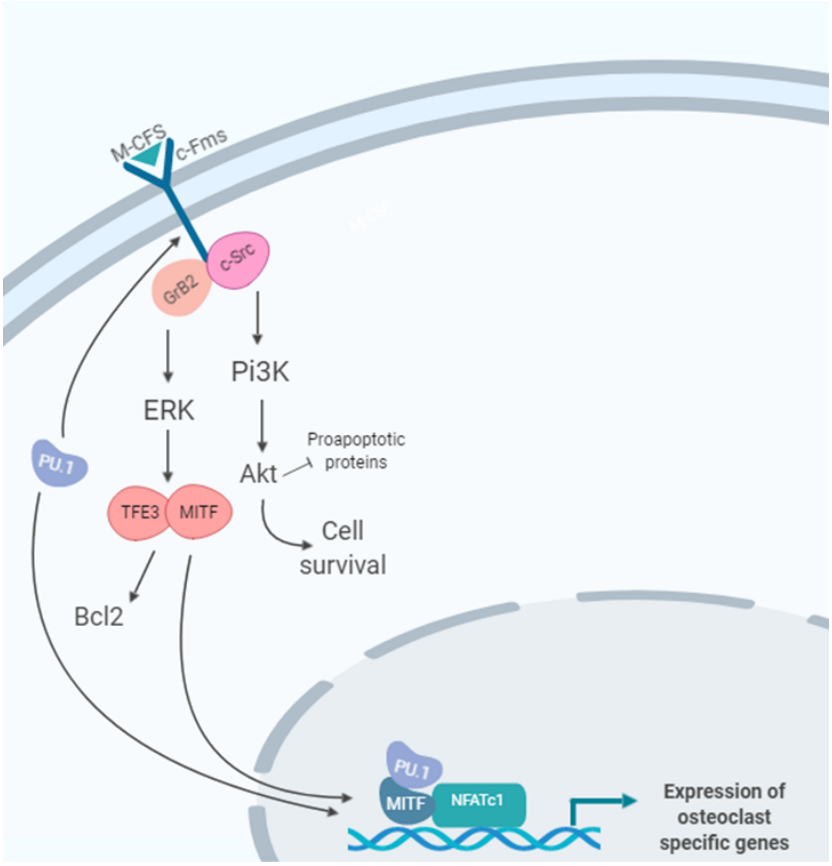

Figure: 1.4: M-CSF/C-FMS signalling pathway in. M-CSF induced activation of c-fms, whose expression is regulated by PU.1, results in the proliferation and survival of osteoclast precursor cells through activation of the ERK and Pi3K pathways. (Created with BioRender.com)

When RANKL binds to RANK it activates at least five different signalling cascades that regulate osteoclast differentiation, maturation and activation. These are inhibitor of NF-κB kinase (IKK), c-Jun N-terminal kinase (JNK), p38, extracellular signal-regulated kinase (ERK) and Src pathways[32] (**Figure 1.5**). An initial step upstream of these pathways is the binding of TNFR-associated cytoplasmic factors (TRAFs) to the cytoplasmic domain of RANK[33,34]. TRAF2[35], TRAF5[36] and TRAF6[37,38] are the three TRAFs that have been shown to bind to RANK after its activation but binding of TRAF6 to RANK has been shown to be essential for osteoclastogenesis as its deletion leads to osteopetrosis due to lack of osteoclast activity[38,39]. Recruitment of TRAF6 to RANK results in the formation of the signalling complex which contains transforming growth factor beta (TGF-β)-activated kinase (TAK)1 and TAK-1-binding protein (TAB)2 which activates all three mitogen-activated protein kinase (MAPK) pathways[40], ERK, by

activation of MEK1/2[41], JNK, by activation of MKK7[42], and p38, by activation of MKK3/8[43,44]. These induce activation of their downstream activator protein-1 (AP-1), through the induction of its critical component c-Fos, and MITF. After TRAF6 recruitment, there is also the activation of the NF-κB pathway by activation of inhibitory complex formed of κB protein kinases (IKK) -α, -β and -ϒ, known as NF-κB essential modulator (NEMO) which induces phosphorylation and degradation of IκB-α and the release of p65/p50 heterodimers, which translocate into the nucleous[45]. This then induces the expression of transcription factors c-Fos and nuclear factor of activated T-cells, cytoplasmic 1 (NFATc1), necessary for osteoclast differentiation[45]. Initial activation of NFATc1 via TRAF6 binding to RANK is not enough to fully activate it[46].

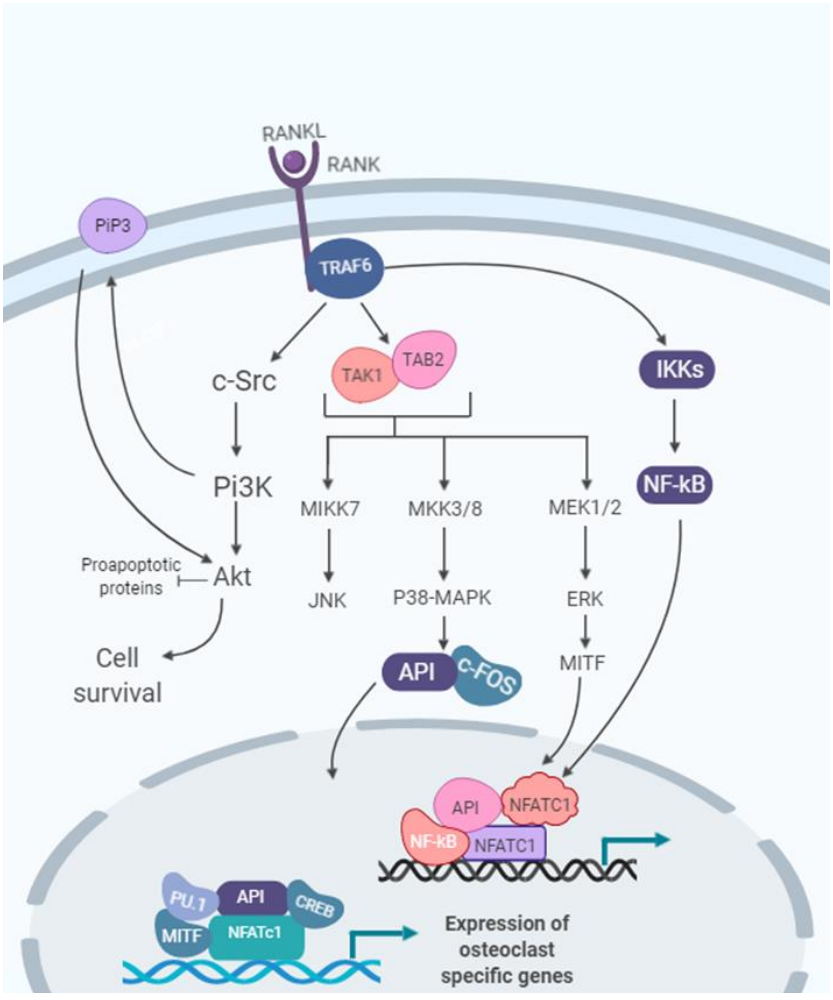

Figure 1.5: RANK/RANKL signalling in osteoclasts. Binding of RANKL to its receptor RANK recruits TRAF6. This in turn activates downstream pathways MAPK, JNK, ERK, Pi3K and NF-κB through IKKs, promoting differentiation of osteoclast precursors to osteoclasts. (Created with BioRender.com)

In order to fully stimulate NFATc1 the calcineurin pathway needs to be activated[46,47] (**Figure 1.6).** Firstly, the binding of RANKL to RANK phosphorylates Fc receptor common ϒ subunit (FcRϒ) and DNAX-activating protein (DAP)12 molecules[48]. These associate with triggering receptor expressed in myeloid cells-2 (TREM2) and osteoclast-associated receptor (OSCAR)[49]. FcRϒ harbours the immunoreceptor tyrosine-based activation motif (ITAM)[49]. Phosphorylation of ITAM activates phospholipase C ϒ (PLCϒ)[50] and Ca^{2+} signalling, in a Syk-dependent manner[51] crucial for total activation of NFATc1[49]. Activated PLCϒ activates calcium signalling and the CaMK/CREB pathway[52]. Activation of calcium signalling also activates calmodulin-dependent phosphatase calcineurin[53]. Calcineurin then dephosphorylates serine residues in NFATc1 which allows for its nucleus translocation and activation[54]. This then allows NFATc1 to bind to its own promoter which results in the autoamplification of NFATC1 expression[46]. On the other hand, the CREB pathway and its subsequent translocation in to the nucleus induces c-Fos which is required for NFATc1 expression[52].

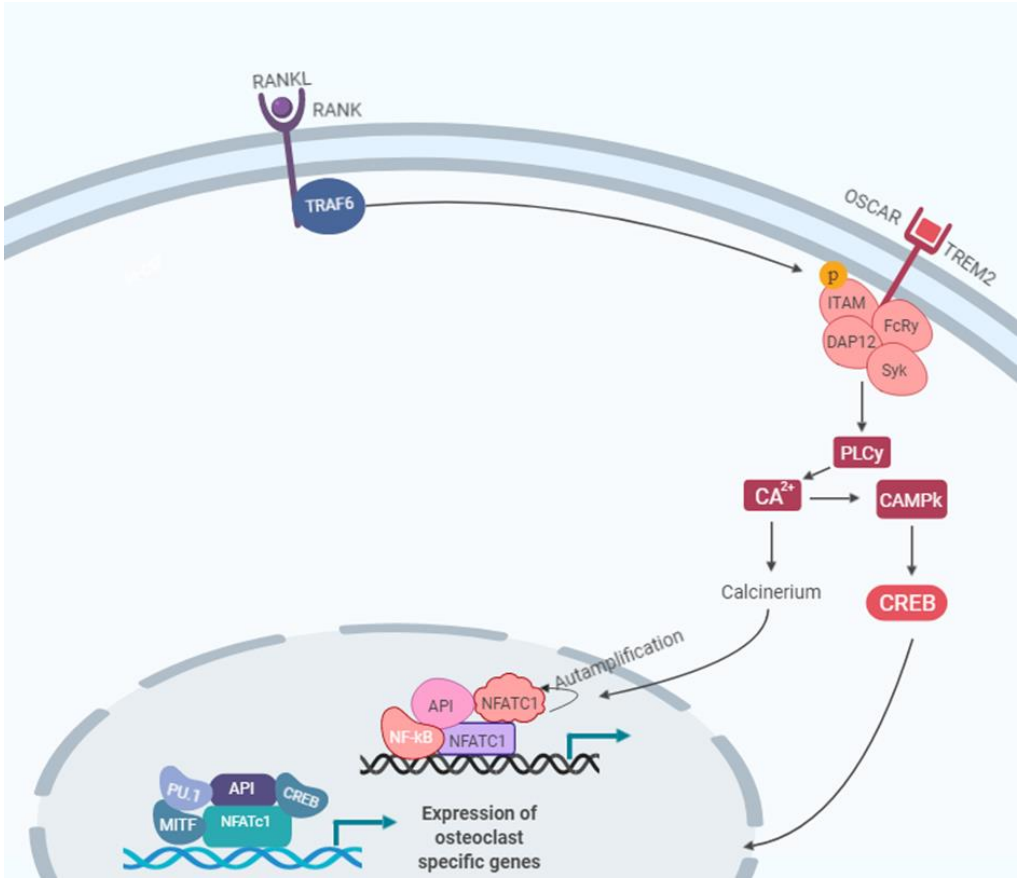

Figure 1.6: Co-stimulatory calcium signalling in osteoclasts. In addition to RANKL signalling, the calcium pathway also plays a costimulatory role in osteoclastogenesis providing robust NFATc1 activation. (Created with BioRender.com)

RANKL also activates the PI3K/AKT pathway through binding of TRAF6 to RANK coupled with activation of c-SRC[55]. C-SRC activation leads to activation of PI3K, which generates phosphatidylinositol-(3,4,5)-phosphate (PIP3) at the cell membrane which then recruits Akt[56]. Activation of Akt is important for cell survival and osteoclast differentiation due to inactivation of proapoptotic proteins[55].

It is the interaction between these different pathways that then allows for the expression of osteoclast-specific genes (**Figure 1.7**).

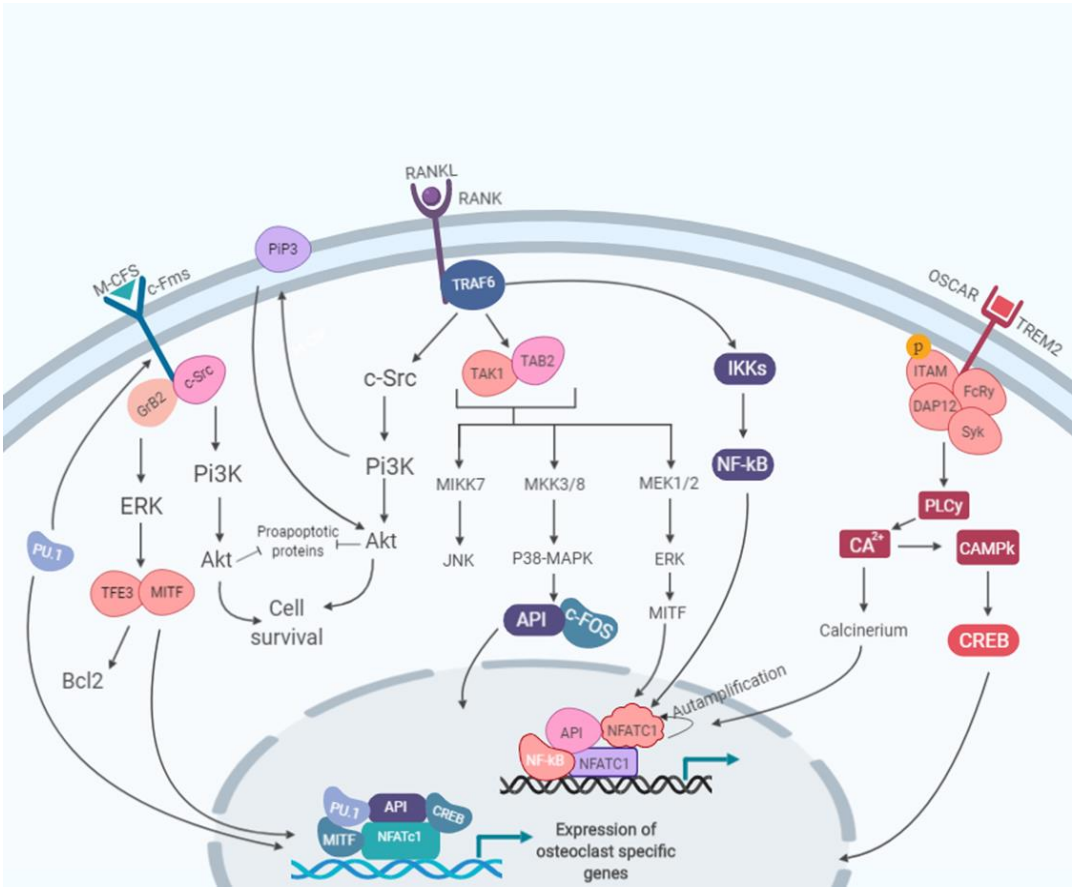

Figure 1.7: Signalling pathways involved in osteoclast differentiation. M-CSF and RANKL are the main two cytokines essential for osteoclastogenesis. Binding of M-CSF to its receptor c-FMS induces the activation of ERK and Akt pathways which are important for cell proliferation and survival of osteoclast precursor cells. Binding of RANKL to RANK recruits TRAF6 which in turn activates the Akt, JNK, MAPK and ERK pathway and also NF-κB promoting osteoclast differentiation. Costimulatory calcium signalling increases NFATc1 induction. (Created with BioRender.com)

Bone resorption requires multiple steps in which mature osteoclasts need to adhere to the bone and only then can they degrade the organic and inorganic phases of bone[57]. The initial step required for osteoclast resorptive capacity is osteoclast polarization. This requires αvβ3 integrin, which is the most important integrin for bone resorption as mice lacking β3 are osteosclerotic due to dysfunctional osteoclasts[58]. Integrins are heterodimeric membrane receptors that mediate the interactions between the cell-cell, cell-extracellular matrix and can mediate osteoclastic bone recognition[59,60]. This integrin is able to recognize the amino acid motif Arg- Gly- Asp (RGD), present in bone-residing proteins, including fibronectin,

vitronectin, osteopontin and bone sialoprotein[61,62]. In osteoclasts, these integrins cluster at adhesive sites called podosomes[63]. Podosomes enable osteoclasts to spread and attach to the bone substrate, creating a sealing zone and inducing osteoclast polarization[61,64]. Osteoclasts resorb bone by secreting proteases, mainly cathepsin K and hydrochloric acid that dissolve the matrix and release the mineral into the extracellular space under the ruffled border, the resorption lacuna, also known as the Howship's lacuna[65,66]. The sealing zone is made of podosomes rich in filamentous actin (F-actin) that form a ring adjacent to the ruffled border[67,68]. The ruffled border is a resorbing organelle formed by fusion of intracellular acidic vesicles facing the resorption lacuna[67,69]. The low pH in the resorption lacuna is generated via an active secretion of protons, initiated by the activity of carbonic anhydrase II (CAII) and followed by the action of vacuolar H^+-adenosine triphosphate (H^+-ATPase) pump, both at the ruffled border membrane and in intracellular vacuoles[69–72]. An energy dependent chloride/bicarbonate (Cl^-/HCO_3^-) exchange on the cell surface is responsible for maintaining intra-osteoclastic pH[73]. Electroneutrality is maintained by a high number of ruffled membrane Cl^- channels, which allows a flow of chloride anions into the resorptive lacuna, an action parallel to the H^+-ATPase[74]. This coupled action determines and limits secretion of HCl into the resorptive microenvironment[74]. This acidification leads to solubilization of the mineral phase of bone, therefore exposing the organic phase. The products of this degradation are endocytosed by the osteoclast and transported to and released at the cells antiresorptive surface to the extracellular matrix[75,76].

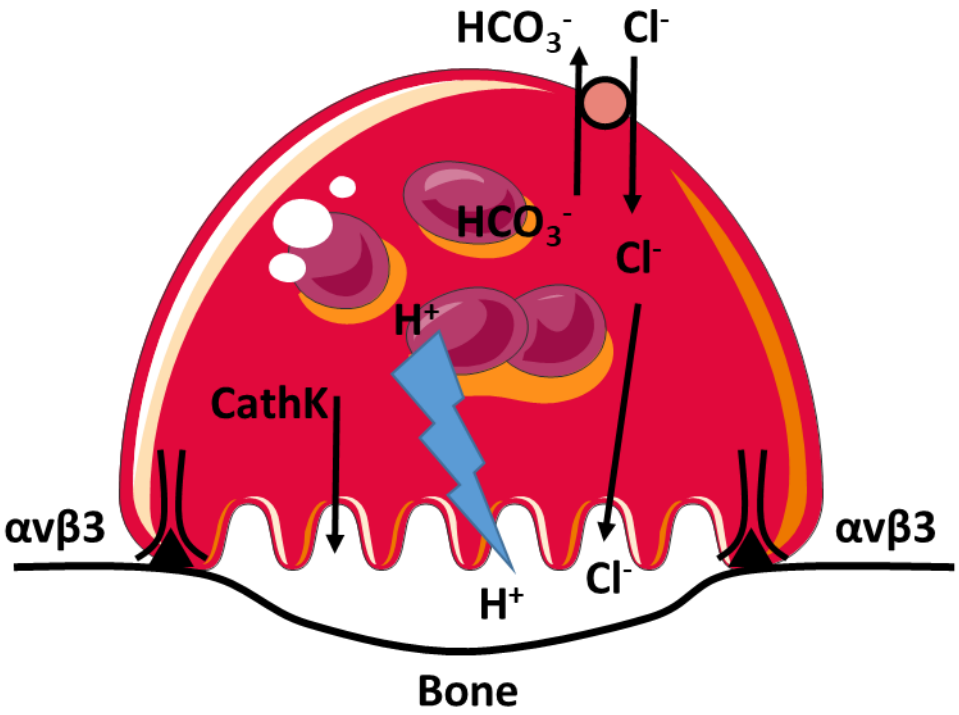

Figure 1.8: Mechanism of osteoclastic bone resorption. Osteoclasts adhere to the bone surface through integrin αvβ3 which creates a sealing zone made up of podosomes rich in F-actin forming an actin ring. Hydrochloric acid and acidic protease cathepsin K are secreted into the resorption lacunae. The acid is generated via a combined action of a vacuolar H^+-ATPase pump, coupled with a chloride channel and a chloride-bicarbonate exchanger situated on the cells non-resorptive surface. The acidic environment in the resorption lacunae leads to solubilization of the mineral phase of the bone, exposing the organic phase which is degraded by cathepsin K.

1.2.2 Osteoblasts

Osteoblasts, the bone-forming cells, are derived from mesenchymal stromal cells, a non-hematopoietic pluripotent stromal cell that also gives rise to a variety of other skeletal component cells, including chondrocytes, adipocytes, myoblasts, tendon cells and fibroblasts[77,78]. Unlike osteoclasts, osteoblasts are mononucleated cells. The primary function of osteoblasts is to form bone by the synthesis and secretion of bone extracellular matrix (ECM) proteins able to induce mineralisation of this ECM[79]. Integrins regulate osteoblast adhesion enabling them to form a monolayer which is linked by cadherins[80,81]. Upon activation, osteoblast secrete matrix which includes collagen type I, and noncollagenous proteins such as osteopontin, osteonectin, bone sialoprotein, matrix gla-protein (MGP) and

osteocalcin[82,83]. Ectoproteins are also important for bone formation. These include ectonucleotide pyrophosphatase/Phosphodiesterase 1 (ENPP1) which hydrolyses ATP generating inorganic pyrophosphate (PP_i), an inhibitor of hydroxyapatite formation[84]. Another important ectoprotein is tissue-nonspecific alkaline phosphatase (TNAP), which has a crucial role in mineralisation of the extracellular matrix[85–89] as it hydrolyses PP_i generating phosphate for the formation of hydroxyapatite[90]. Progressive ankylosis gene (ANK), also an ectoprotein, exports pyrophosphate generated intracellularly to the extracellular domain[91].

Osteoblast commitment, differentiation and function all depends on a number of signalling pathways, which include TGF-β/bone morphogenic protein (BMP) signalling, wingless-type MMTV integration site (Wnt) signalling, Hedgehogs (Hh), Notch and fibroblast growth factors (FGFs)[78].

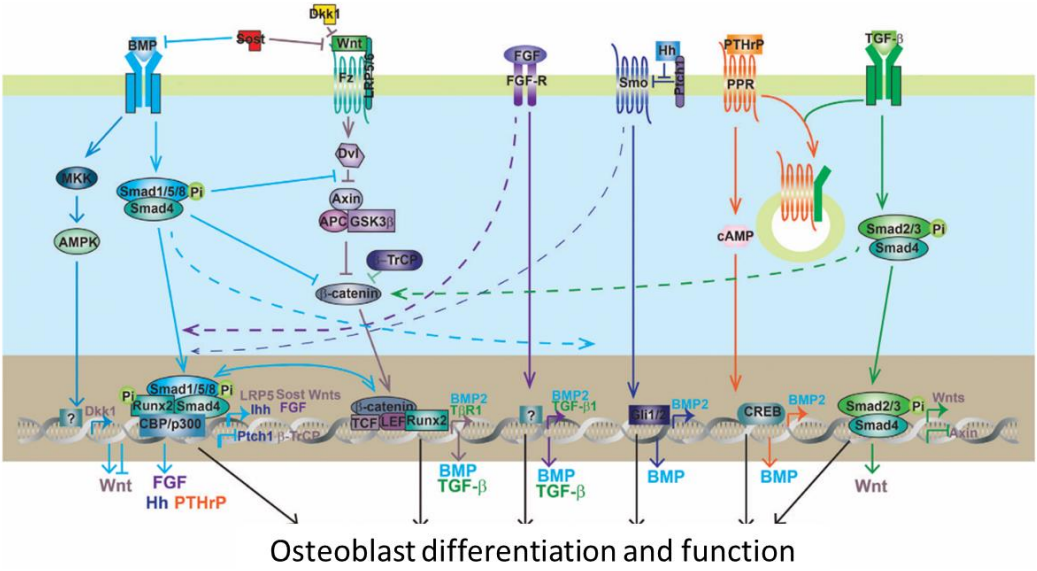

Figure 1.9: Different signalling pathways regulating osteoblast differentiation. Osteoblast differentiation is regulated by various developmental signals and a series of signalling pathways, including BMP, Wnt, FGF, Hh, PThrP and TGF-β pathways.[92]

BMP signalling

At an initial stage in osteoblast differentiation, BMP2 or BMP4, members of the TGFβ family originally discovered as inducers of ectopic bone[93,94], bind to their type I and type II BMP receptor on the MSC surface resulting in the recruitment and phosphorylation of small mother against decapentaplegic (SMAD) proteins SMAD1, SMAD5 or SMAD8[95]. SMADS are cytoplasmic signal transducers from the membrane to the nucleous[95]. These then form a complex with SMAD4 which translocates into the nucleus regulating gene expression by activating Runt-related transcription factor 2 (Runx2)[96]. Runx2 has been shown to be a master transcription factor essential in osteoblastogenesis as Runx2-deficient mice die shortly after birth due to complete lack of osteoblasts and bone[97].

Runx2 positively regulates the expression of osteoblast marker genes collagen type 1 (*Col1a1*), alkaline phosphatase (*ALP*), osteopontin (*OPN*), osteonectin (*ON*) and osteocalcin (*OC*)[98–100], and can also regulate the expression of zinc-finger-containing transcription factor Osterix[101]. Osterix forms a complex with NFAT2 that binds to DNA and controls the transcription of target genes OC, OPN, ON and Col1a1[100]. Although Runx2 is a major transcription factor regulating osteoblast commitment and differentiation, it has been shown that at a later stage Runx2 negatively controls osteoblast differentiation as 3-week-old mice overexpressing Runx2 have osteopenia as a result of reduced number of mature osteoblasts[102].

BMP-2 is also able to stimulate the expression of a number of nuclear transcription factors such as homeobox-containing transcription factors Distal-less homeobox 5 (Dlx5)[103] and glioma-associated oncogene family zing finger 2 (Gli2)[104], which can either stimulate Runx2 expression, or act as co-activators of Runx2.

TGF-β signalling

Similar to BMP signalling, TGF-β, whose members of its pathway also include BMPs, first binds to receptor type II and then is recognized by receptor type I forming a complex in which receptor type II phosphorylates receptor type I allowing signal transduction[105]. After phosphorylation, receptor regulated SMADs (R-SMADS) bind to receptor type I promoted by an adaptor protein, SMAD anchor for receptor activation (SARA)[106]. The interaction of SARA with receptor type I recruits SMAD2[107–109] and

SMAD3[110,111] to the activated receptor complex. This in turn leads to phosphorylation of SMAD2 and SMAD3 and association of Co-SMAD SMAD4[111–114]. Thereafter, the SMAD complex translocates into the nucleus where they form a complex with FAST-1 which in turn activates transcription of target genes[115].

Both BMP and TGF-β signal through SMAD4, which has been shown to be important for positive regulation of osteoblast formation and function, and skeletal development[92]. Studies on mutations in SMAD4 have demonstrated its importance during embryonic development[116], bone homeostasis[117] and growth plate formation and organization[118]. In humans, inactivating mutations in SMAD4 causes a disease called Myhre syndrome characterized by short stature and facial dysmorphism[119,120].

Wnt signalling

The Wnt signalling pathway is also important during osteoblast differentiation[121]. It can be divided into three categories: the Wnt/β-catenin pathway, which is also known as the canonical Wnt pathway[122], the noncanonical Wnt/planar cell polarity[123] and the Wnt/calcium pathway[124]. In humans there are 19 Wnt proteins, while in mice there are 18[125]. Wnt proteins have been classified into canonical (Wnt1, Wnt2, Wnt2b/13, Wnt3, Wnt3a, Wnt8a/d, Wnt8b, Wnta10a, Wnta10b, Wnt9a/14, Wnt9b/15 and Wnt16) and non-canonical (Wnt4, Wnt5a, Wnt5b, Wnt6, Wnt7a, Wnt7b, Wnt11 and Wnt16)[126]. From the 19 Wnt proteins,Wnt1, Wnt3a, Wnt4, Wnt5a, Wnt7b, Wnt10b and Wnt16 are expressed in osteoblasts and play a role in bone[127].

Canonical signalling is initiated by binding of Wnt ligands to a dual receptor complex comprised of a transmembrane G-protein coupled receptors of the frizzled (Fzd) family, of which there are a total of ten, and a co-receptor of the LRP family, LRP5 or LRP6[128]. In addition to the usual Wnt ligands, mammals also express endogenous enhancers with the most known being the R-spondins (RSPO) ligand family[129]. These are a group of four secreted proteins that can bind to Fzd receptors together with an lipoprotein receptor-related protein (LRP) co-receptor, possibly LRP6[129,130], but more recently it was proven that they function as ligands of LGR4 (also known as Grp48), LGR5 and LGR6 which in turn potentiates Wnt/β-catenin signalling[131]. The binding of Wnt to the Fzd receptor results in the phosphorylation of

the LRP co-receptors which in turn leads to the recruitment of Axin and the tumour repressor protein APC through the interaction with dishevelled (DVL)[132], forming a complex that also includes glycogen synthase 3 β (GSK-3β)[133], casein kinase I (CKI)[134,135] and FRAT1, which all together form a complex[136,137] (**Figure 1.10**). This complex prevents phosphorylation of β-catenin and subsequent proteosomal degradation resulting in the stabilization of β-catenin[136,138]. This in turn leads to accumulation of β-catenin in the cytoplasm which then translocates into the nucleus where it associates with the lymphoid-enhancing factor/T-cell factor (Lef/Tcf) family of high mobility group (HMG)-type transcription factor and displace Groucho[139], stimulating the expression of target genes *Lef1*, *Tcf7*, *Nkd2* and *Axin2*[138,140–143], and also *Runx2* during osteogenesis[144] and *OPG* in mature osteoblasts[145]. In the absence of Wnt β-catenin is phosphorylated in the Axin complex by CKI and then by GSK-3β which in turn targets it for ubiquitin-mediated degradation[132,135,146–149].

LGRs function as agonists of the Wnt pathway. *Lgr5* knockout mice have been shown to have total neonatal lethality due to ankyloglossia and gastrointestinal distension, but showed no skeletal defects[150]. On the other hand, LGR4 has been shown to play a major role in bone formation and remodelling, and osteoblast maturation and mineralisation as studies of mice lacking *Lgr4* have delayed embryonic bone formation and decreased differentiation and function of osteoblasts, and also decreased postnatal bone formation and bone volume[151]. This was due to a downregulation of activating transcription factor 4 (ATF4) and its downstream targets, osteocalcin, bone sialoprotein and collagen[151]. It has also been shown that ATF4 can directly interact with Runx2[152], which is essential for osteoblast differentiation, demonstrating how the different pathways interact with each other. Wnt signalling is not just modulated by these agonists but also by extracellular antagonists which include secreted frizzled-related proteins (Sfrps) and Wnt inhibitory factor 1 (Wif1), which act as decoy receptors and directly sequester Wnt ligands inhibiting both canonical and non-canonical signalling[153,154]. Sclerostin[155,156] and Dickkopf (DKK1)[157,158] function by binding to LRP5/6 and Kremen 1/2 allowing specific inhibition of canonical Wnt signalling[154].

The canonical Wnt pathway has been shown to be important in bone homeostasis and osteoblast formation due to studies of patients with mutations in

proteins, which are part of this pathway, that cause diseases with either high bone mass (sclerosteosis[159] and Van Buchem disease[160,161]) and low bone mass (osteoporosis pseudoglioma syndrome[162]). Van Buchem disease is associated with the deletion of an enhancer regions downstream in the Wnt/β-catenin signalling which causes reduced expression of the Wnt antagonist sclerostin (SOST)[160,161].

Similar to van Buchem disease, sclerosteosis is a rare autosomal recessive disease in which the *SOST* gene is also affected but in this case it is due to loss-of-function mutations which cause skeletal malformations in the hand, thickened and sclerotic bones due to unrestricted bone growth and therefore increased bone mass[159,163]. Osteoporosis pseudoglioma syndrome is associated with a loss of function mutation in the low-density LRP5 which causes severe reduction in trabecular bone which leads to multiple fractures and bone deformities[162].

Due to the number of human diseases associated with mutations in this pathway and the variety of mutations, there is huge interest in the canonical Wnt pathway as its study could further the understanding of the mechanisms involved in bone homeostasis and be used to develop new therapeutic approaches to treat disease characterised by low bone mass such as osteoporosis. Indeed some advances have already been made, including the anabolic agent, romosozumab, an anti-sclerostin antibody that inhibits sclerostin, stimulating modelling-based bone formation[164]. And while it is a promising form of treatment, there are some limitations to the drug such as the inconvenient treatment administration, although not as inconvenient as teriparatide which is administered sub-cutaneous daily. However, romosozumad also has side-effects, such as increased cardio-vascular disease risk[164], highlighting the need for alternative anabolic agents for treatment of osteoporosis.

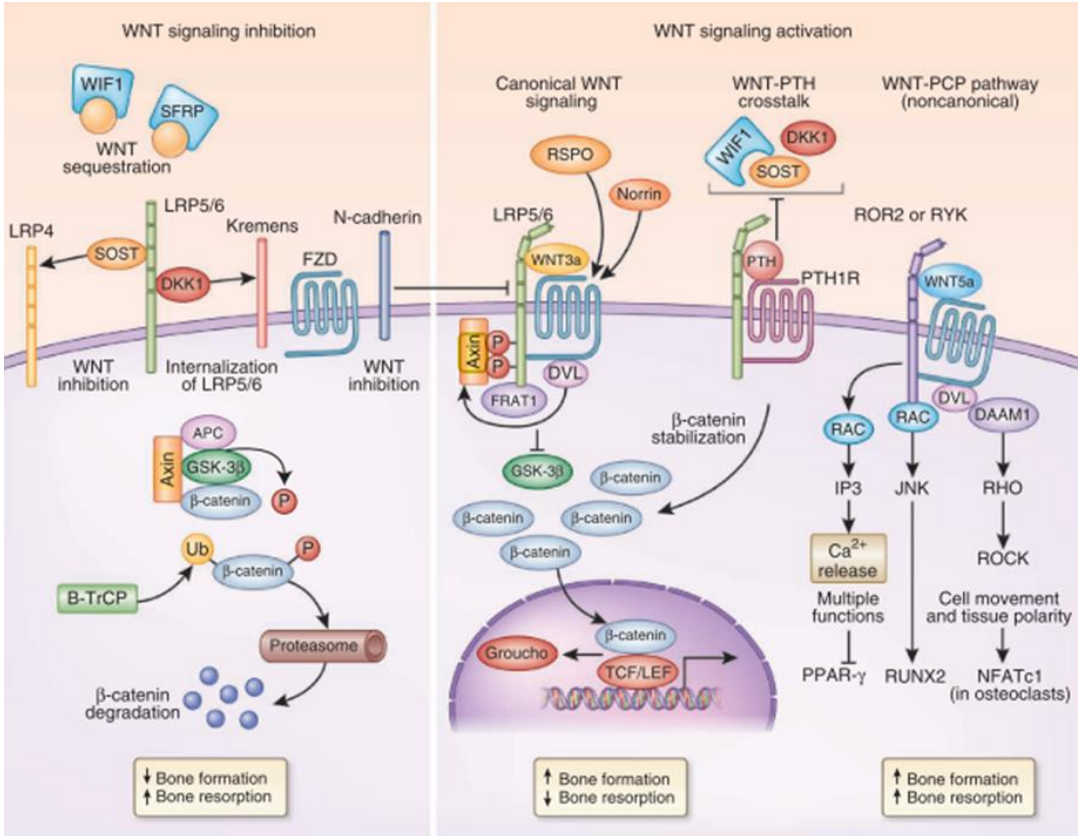

Figure 1.10: Wnt signalling pathway in osteoblastogenesis. In the absence of Wnt ligands, β-catenin is phosphorylated and degraded. In the presence of Wnt ligands, these bind to a complex formed by Frizzled (FZD) and co-receptors LRP5/6. Axin then binds to this complex, which together with dishevelled (DVL) inhibits β-catenin phosphorylation. B-catenin can then accumulate in the cytoplasm, translocating into the nucleus where it associates with TCF/LEF transcription factors, which displaces Groucho, controlling target gene transcription (Adapted from Baron & Kneissel, 2013[137]).

Hedgehog Signalling

The Hedgehog (Hh) signalling pathway plays a critical role in bone development and homeostasis. The segment polarity gene *Hedgehog* was originally discovered in *Drosophila*[165]. The Hh signalling pathway regulates the transcription of many target genes[166]. In mammals there are three different *Hedgehog* genes, *Indian hedgehog* (*Ihh*), *Sonic hedgehog* (*Shh*) and *Desert hedgehog* (*Dhh*),which are found in different tissues and have different functions[166]. Ihh was found to be crucial for osteoblast development and differentiation and skeletal morphogenesis, since Ihh

null mice completely lack osteoblasts in endochondral bones, in part due to failure to express *Runx2*[167,168].

Notch signalling

Notch signalling is also important in osteoblastogenesis. The Notch receptor family comprises a group of type I transmembrane proteins that control cellular fate decisions during development[169,170]. Notch is a single pass transmembrane receptor that is activated by direct contact with the membrane-bound ligands Delta 1-4 and Serrate/Jagged 1 and 2 which leads to the cleavage of the Notch extracellular domain near the transmembrane region and release of the Notch intracellular domain (NICD)[170–172]. Cleavage of the NICD is mediated by the γ-secretase complex which contains either presenilin 1 (PS1) or 2 (PS2) as the catalytic subunit[173]. As a result of this cleavage, NICD translocates into the nucleus where it interacts and forms a complex with members of the CSL (CBF1/Su(H)/Lag-1) family of transcription factors, c promoter-binding factor 1 (CBF1), suppressor of hairless [Su(H)] and longevity assurance gene-1 (Lag-1)[169,170]. This interaction converts the CSL receptors from transcriptional repressors to activators[169]. Activation of Notch induces gene expression of Hairy Enhancer of Split (*Hes*) 1 or 5[174,175], and HES-related repressor protein 1-3[176]. In osteoblasts, the expression of *Hey1*, a Notch target gene, was shown to interact with Runx2 inhibiting its transcriptional activity which in turn inhibited the differentiation of MSCs in to osteoblasts[172,177].

In muscle satellite cells, Notch has been shown to cooperate with syndecan 3[178], a transmembrane proteoglycan which will be explained later in this chapter. Sdc3 and Notch reside in a complex where Sdc3 can facilitate Notch processing by ADAM17/ tumour necrosis factor-α-converting enzyme (TACE) and NICD generation[178].

FGF signalling

Fibroblast growth factors (FGF) are a family of polypeptides, comprising of 22 members, that control proliferation and differentiation of various cells types[179,180] and are also known regulators of bone formation and development[181,182]. In osteoblasts, FGFs, which include FGF2 and FGF23, interact with their FGF receptors

(FGFRs) inducing receptor dimerization and autophosphorylation, and downstream kinase cascades[180,183,184]. The interaction between FGF2/23 and its receptor requires the intervention of heparin sulphate proteoglycans (HSPGs) that bind both the ligand and the receptor stabilizing them[185,186]. In osteoblasts, FGF2 activates various pathways which include MAP kinases, ERKs, p38 MAP kinase and PKC[187–189]. FGF2 signalling through ERK stimulates AP1 expression and can also mediate phosphorylation and transcriptional activity of Cbfa1/Runx2[188,190,191]. This also involves activation of the PKC pathway, affecting osteocalcin gene expression, therefore demonstrating the importance of FGF signalling in the control of osteoblast differentiation[188,190,191]. P38 MAP kinase was also shown to be involved in increased IL6 synthesis which is induced by FGF in osteoblasts[192].

Osteoblasts are also regulators of bone resorption by secreting M-CSF and RANKL, which are essential in osteoclastogenesis[19]. Osteoblasts are also able to secrete OPG, a decoy receptor for RANKL, a key extracellular regulator of osteoclast development[20].

After osteoblasts have fulfilled their main function of forming bone, they either undergo programmed cell death (apoptosis)[193], become flattened cells on the bone surface called bone lining cells[17], or become entrapped within lacunae of mineralised matrix as osteocytes[194].

1.2.3 Osteocytes

Osteocytes are the most abundant cells of mature mammalian bones, comprising 95% of all bone cells in and adult skeleton[195]. Once osteoblasts are embedded into the bone matrix, they cease their activity becoming osteocytes. Osteocytes are small dendritic-like cells with numerous long and thin processes which connect with each other and with cells on the bone surface[7]. The osteocyte resides within a lacuna and their processes are contained within canals called canaliculi, and this system, the lacunocanalicular system, acts as a channel for metabolic exchange[196,197]. The interconnected network formed by osteocytes allows them to sense and respond to local and systemic stimuli to regulate bone remodelling[198]. It is thought that osteocytes regulate bone remodelling by regulating both osteoclasts

and osteoblasts via the release of soluble mediators. A major way in which osteocytes regulate osteoclast activity is through osteocyte death which occurs at microdamaged bone sites, and targets the osteocytes for removal by osteoclasts[199]. Studies by Nakashima *et al*. and Xiong *et al*. showed that osteocytes are the main source of RANKL, the major osteoclast differentiation factor, which shows their importance in osteoclastogenesis[200,201]. But both groups provided evidence that osteocytes play a role in regulating the effects of mechanical loading on bone remodelling[200,201]. By deleting RANKL specifically in osteocytes, the mice developed a severe osteopetrotic phenotype, and by unloading the mice Xiong *et al*. reported that there was an increase in RANKL produced by osteocytes during tail suspension[201].

The Wnt pathway plays a major role during osteoblastogenesis. There are two antagonists of this pathway produced by osteocytes, Sclerostin and DKK1, able to regulate bone remodelling by inhibiting bone formation[202,203]. A study by Robling *et al*.[204] showed that mechanical loading decreased the expression of sclerostin and DKK-1 in osteocytes. The decrease in the production of these Wnt pathway antagonists by osteocytes resulted in upregulation of β-catenin signalling in osteoblasts accompanied by an increase in bone formation. On the other hand, unloading resulted in increased expression of sclerostin and DKK-1 and reduction in bone formation.

1.3 Bone development

Skeletogenesis is a key event during embryonic development. It starts once multipotent mesenchymal cells arise from the ectoderm and mesoderm. These layers give rise to multiple early derivatives, including ectoderm-derived neural tube, mesoderm-derived notochord, paraxial mesoderm and lateral plate mesoderm which in turn give rise to the skeleton and other organs[205]. The neural crest cells from the dorsal margins of the closing neural tube migrate into the anterior part of the skull, where they give rise to many of the skeletal and connective tissue components of the head, while prechordal mesodermal cells produce cartilage and bones in the posterior part of the skull[205]. The Paraxial mesoderm gives rise to somites which form

the axial skeleton, whereas lateral plate mesodermal cells form the appendicular skeleton[205,206]. Once cells migrate to specific sites of the future bones in the body, and commit to a skeletal fate they start to produce a matrix rich in components which are tightly controlled in a spatial and temporal manner[205,207]. These mesenchymal cells gather, forming high density cell condensations that outline the shape and size of future bones, with a high up-regulation in versican, tenascin, syndecan 3, N-CAM and N-cadherin[208]. Within these condensations, the transformation of the mesenchymal cells leads to two major modes of bone formation, or osteogenesis: endochondral bone formation and intramembranous bone formation.

1.3.1 Endochondral bone formation

The process by which a cartilage intermediate is formed and replaced by bone is called endochondral ossification (**Figure 1.11**). Endochondral ossification is responsible for the development of the appendicular skeleton, facial bones, vertebrae and the medial clavicles[209]. In foetal development, the process of endochondral ossification begins with the formation of mesenchymal condensations of osteochondroprogenitors[208,210]. The cells in the condensations can differentiate into chondrocytes which secrete a matrix rich in type II collagen and the proteoglycan aggrecan, and have a genetic program driven by SOX9[211]. The primordial cartilage continues growing and elongating through recruitment of more mesenchymal progenitors and proliferation of chondrocytes which mature, exit the cell cycle, downregulate type II collagen expression and undergo hypertrophy, forming an avascular cartilaginous template surrounded by the perichondrium[210]. These mature hypertrophic chondrocytes secrete a unique extracellular matrix, different from that of proliferating chondrocytes, composed of collagen X[212]. At the same time, hypertrophic chondrocytes attract blood vessels through the secretion of angiogenic factors, and direct adjacent perichondral cells to differentiate into osteoblasts which secrete bone matrix, forming a bone collar surrounding the hypertrophic chondrocytes[1,210]. The invasion of blood vessels allows for the influx of osteoblast precursors, osteo(chondro)clasts and hematopoietic cells[209]. The osteoblasts that invade the cartilage lay down bone matrix upon the cartilaginous mould to form trabecular bone while the osteo(chondro)clasts degrade the extracellular

cartilaginous matrix through secretion of matrix metalloproteases (MMPs), such as MMP9[213]. These events result in the formation of the primary ossification centres that propagate towards the distal ends of the budding bone[214]. Through continuous proliferation of chondrocytes, the mould enlarges further and secondary ossification centres are formed together with a change of chondrocyte shape and size forming columns of stacked cells in a specific orientation which direct the lengthening of the bone[211,215]. This developmental structure is called the growth plate and is found in both ends (e.g. long bones) of the bone called epiphyses[1,209,210]. Postnatally, this growth plate continues to be responsible for linear bone growth until skeletal maturity is reached in which the growth plate disappears (e.g. in humans during adolescence)[210]. In smaller mammals such as mice or rats the growth plate does not disappear with ageing but longitudinal growth ceases[216].

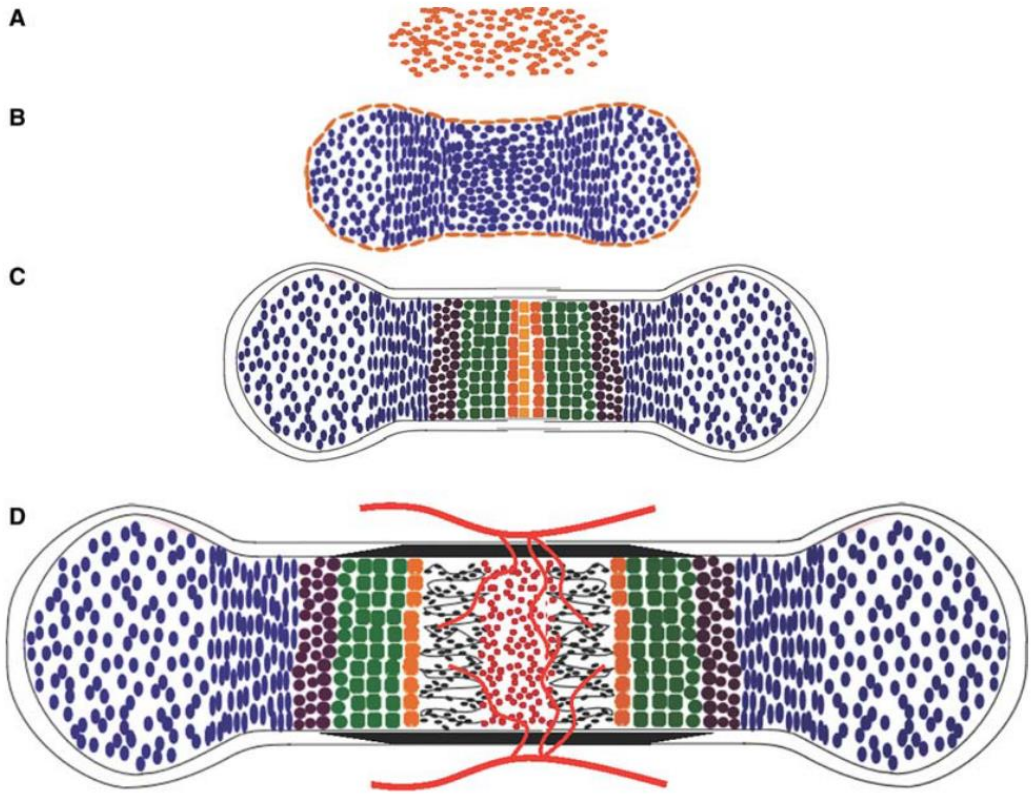

Figure 1.11: Endochondral ossification. Mesenchymal cells agglomerate together forming condensations (**A**). These cells then differentiate into chondrocytes (blue) which are surrounded by the perichondrium (orange) (**B**). Chondrocytes then continue to proliferate and undergo maturation, becoming prehypertrophic chondrocytes (brown) to then hypertrophic chondrocytes (green) and later terminal hypertrophic chondrocytes (orange) forming a template of the future bone at which point they may undergo apoptosis (yellow) (**C**). These hypertrophic chondrocytes attract blood vessels (red lines) through the secretion of angiogenic growth factors, which in turn attracts osteoblasts which secrete bone matrix (black), forming the bone collar (black) which surrounds the hypertrophic chondrocytes (**D**). (Adapted from Long & Ornitz, 2013)[211]

The growth plate is characterized by four populations of cells organized into morphologically different zones: the resting cell zone, composed of round chondrocytes, the proliferation zone, composed of proliferating chondrocytes organized into longitudinal columns, the maturation or prehypertrophic zone, comprises maturing chondrocytes which express *Ihh* (encoding the paracrine factor Indian hedgehog) and *Col10a1* (encoding collagen X), and the hypertrophic zone, which is formed by enlarged chondrocytes in which the extracellular matrix becomes calcified before the cells are eventually invaded by blood vessels[210] (**Figure 1.12**).

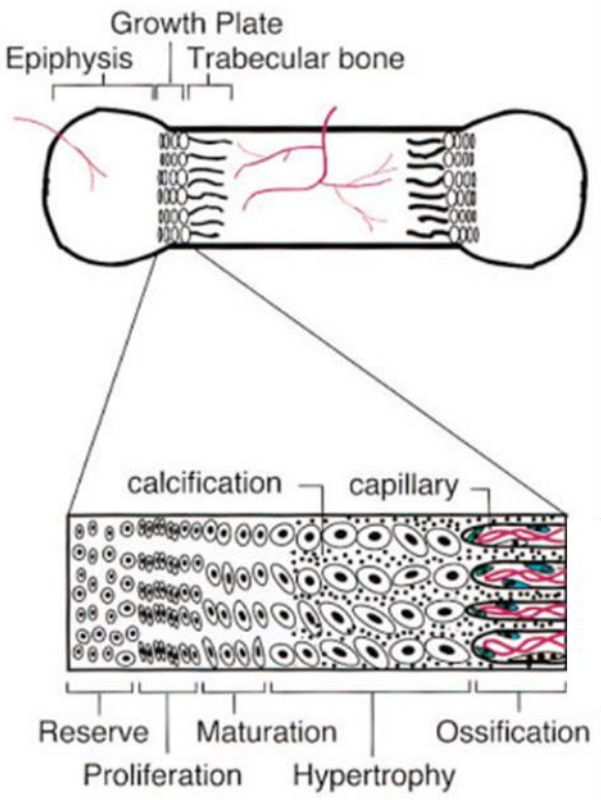

Figure 1.12. Diagram of a growth plate showing the different cartilage zones. (Adpated from Vu *et al*.[213])

1.3.2 Intramembranous bone formation

Compared to endochondral bone formation, intramembranous bone formation is the least understood. It is the process by which many of the flat bones, such as craniofacial bones and the clavicle, are formed[217]. In intramembranous ossification, which occurs during embryonic development, multipotent mesenchymal cells in condensations differentiate directly into osteoblasts, due to an upregulation of Wnt/β-catenin signalling[218]. These cells are then able to produce a collagenous matrix rich in collagen type I, osteopontin and osteocalcin, and can synthesize bone matrix resulting in the formation of the flat bones[210].

1.4 Bone modelling

During development and growth, bones continuously increase in mass and length, achieving their final mass and shape by a process called bone modelling[219]. During bone modelling, bone is removed from one site and deposited at a different one, a process that depends on genetic, dietary, hormonal and physical factors[17,219]. During bone modelling, bone formation and bone resorption are not coupled biologically[220], for example, with ageing there may be widening of the bones due to endosteal resorption of old bone and periosteal apposition of new bone[5].

According to Wolff's law, bone adapts and changes in response to the stresses it is placed under[221]. Bone modelling primarily occurs during growth and is less frequent in adults, however, modelling may be increased in the adult skeleton such as during increases in mechanical loading. Examples of this are the arm used for serving in tennis players which has increased bone mass compared to the other arm[222] or after daily administration of teriparatide via sub-cutaneous injection[223,224].

1.5 Bone remodelling

Bone has the capacity of growth but also the capacity of regeneration and remodelling throughout life. Bone undergoes a continual adaptation during vertebrate life to attain and preserve skeletal size, shape and structural integrity, and its overall homeostasis[225]. This is due to bone remodelling, which is the process responsible for the removal and repair of damaged bone to maintain the integrity of the adult skeleton and mineral homeostasis until death[225]. In contrast to bone modelling in which there is either bone formation or resorption occurring in one area, remodelling involves the coordinated actions of osteoclasts, osteoblasts and osteocytes. Together, these cells are called a bone remodelling unit (BRU).

There are four distinct and sequential phases of bone remodelling: quiescence, resorption, reversal and formation, illustrated schematically in **Figure 1.13**. Bone remodelling starts and ends at the quiescent phase.

Quiescence

During the quiescent phase there is no bone resorption or formation until the next remodelling cycle begins. At this stage bone contains osteocytes embedded within its matrix and bone lining cells covering the bone surface[226].

Resorption

A remodelling signal, which may be in the form of a mechanical strain on the bone or a hormonal signal (e.g. by the parathyroid hormone (PTH)), which is detected by osteocytes initiates the remodelling cycle[227]. It has been suggested that osteocytes are able to sense mechanical stress which in turn leads to the recruitment of osteoclast progenitors and osteoblasts[228]. After bone lining cells retract, these produce collagenase and, together with matrix metalloproteinases (MMPs) released by osteoblasts, digest the unmineralised matrix[229,230]. The recruited osteoclast precursors differentiate into multinucleated osteoclasts which in turn degrade the mineralised matrix[225], through a process described in detail in section 1.2.1. Briefly, mature osteoclasts bind to the bone becoming polarised and forming a sealed compartment in which the pH reduces to 4.5 through the action of proton pumps and Cl- channels[72,231]. Cathepsin K then degrades the exposed organic matrix which is then endocytosed and transported to the basolateral surface and released into the extracellular matrix[75,76]. This results in the formation of the "Howship's lacunae" where osteoclasts remain resorbing bone for up to 12 days[17].

Reversal

Once the resorption phase is complete, reversal phase is initiated with osteoclasts undergoing apoptosis and being removed by phagocytosis, leaving the Howship's lacuna free of osteoclasts[3]. It is also at this stage that osteoblasts are recruited to initiate the bone formation phase. The mechanisms by which osteoblasts are recruited are still not fully understood but it is thought that during resorption, factors such as TGF-β and insulin-like growth factors I and II (IGF1/2), which were embedded within the bone matrix are released[232] or that osteoclasts are in fact the ones that produce these factors which recruit osteoblasts[233]. Interestingly, a recent study by Ikebuchi *et al*. reported that RANK produced by maturing osteoclasts, binds

osteoblastic RANKL triggering RANKL reverse signalling, which in turn activates Runx2 therefore promoting bone formation[234]. This is an indication that the processes of bone resorption and bone formation are coupled.

Formation

This phase may take up to 6 months to complete as opposed to the resorption phase that takes just up to 12 days[235]. Osteoblasts can synthesize collagenous organic matrix and are able to form new bone through a process explained in detail in section 1.2.2. Briefly, osteoblasts secrete collagen type I and other non-collagenous proteins in order to form an organic nonmineralised matrix which later is mineralised with the help of ALP[82,83].

Once formation is complete, osteoblasts either undergo apoptosis, become embedded within the matrix becoming osteocytes or differentiate into bone lining cells which cover the bone surface[17,193,194]. This new environment is maintained in a quiescent phase until the next remodelling cycle is activated.

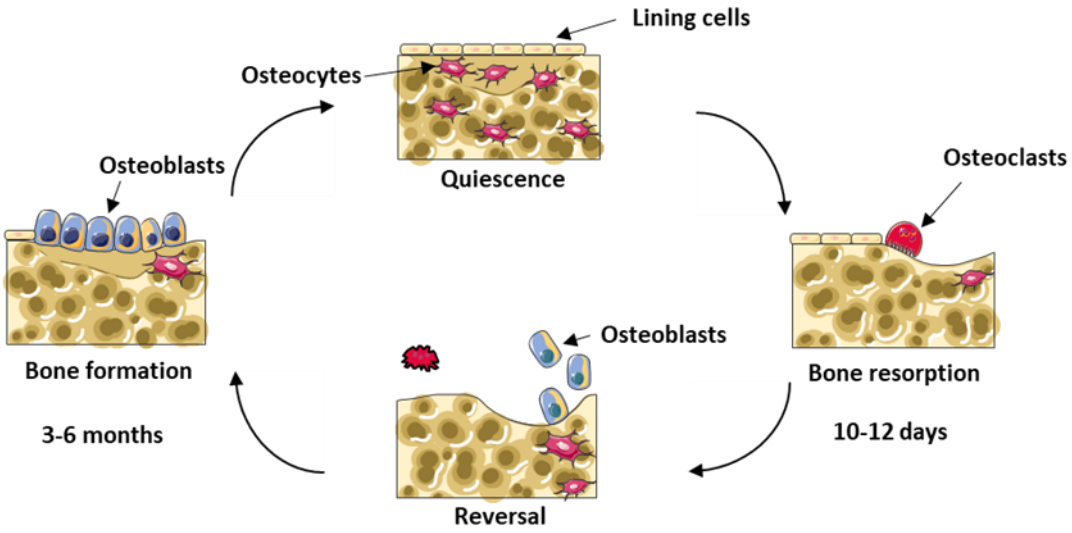

Figure 1.13: Bone remodelling cycle. The remodelling cycle is composed of a quiescent phase, a resorption phase in which osteoclasts resorb bone, a reversal phase in which osteoclasts undergo apoptosis and osteoblasts are recruited to begin the formation phase, forming new bone and finally returning to the quiescent phase until a new remodelling signal leads to activation of another remodelling cycle.

1.6 Systemic regulation of bone remodelling

Bone undergoes continuous remodelling cycles carried out by bone resorbing osteoclasts and bone forming osteoblasts while also under the control of mechanosensing osteocytes in order to maintain a healthy skeleton. The balance between these processes controls bone homeostasis, and all the cells interact with each other through the duration of the cycle. Apart from cellular factors, hormonal factors such as vitamin D_3, PTH, calcitonin, and oestrogen, also play a major role in the maintenance of skeletal integrity throughout ageing (**Figure 1.14**).

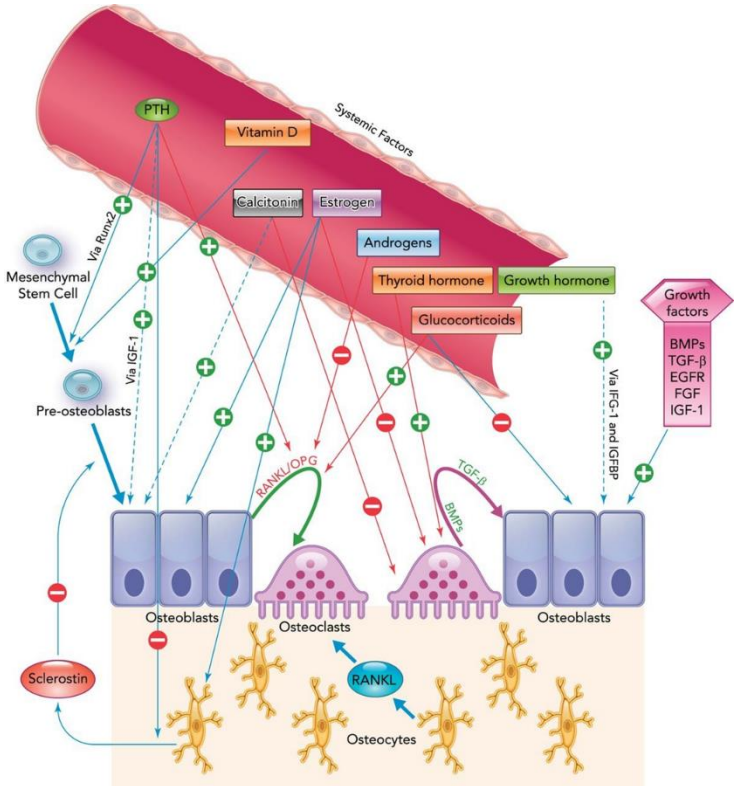

Figure 1.14: Systemic regulation of bone remodelling. The bone remodelling process is controlled by bone cells, which include osteoclasts, osteoblasts, osteocytes and bone lining cells which are controlled by various systemic factors, such as vitamin D, oestrogen, PTH, calcitonin and other hormones all of which positively or negatively regulate bone remodelling. Image adapted from Siddiqui *et al.*[236].

Vitamin D

Vitamin D is a secosteroidal prohormone whose role is to regulate metabolism of calcium and phosphate by promoting their absorption from the gut and decrease PTH concentrations, essential for bone remodelling[237,238]. Vitamin D has two major

isoforms: Vitamin D_2 (ergocalciferol) which is synthesized from ergosterol by ultraviolet (UV) B radiation in plants, fungi and yeast; and Vitamin D_3 (cholecalciferol), which is synthesized by 7-dehydrocholesterol on the skin surface[238].Both vitamins D_2 and D_3 can be obtained in small quantities through diet but only D_3 is obtained through exposure to UVB light. Vitamin D needs both 25- and 1α-hydroxylation to become the active hormone 1,25-dihydroxyvitamin D (1,25- $(OH)_2D$)[239].

Vitamin D (both vitamin D2 and D3) binds to vitamin D-binding protein (VDBP) in circulation and is first delivered to the liver. In the liver, vitamin D is metabolized by vitamin D 25-hydroxylases (including mitochondrial P450 enzymes CYP2R1 and CYP27A1) to 25-hydroxyvitamin D (25(OH)D, also known as calcitriol), which is the major circulating form of vitamin D in serum[238,240].

The second important site where 25(OH)D is further metabolized is the kidney, where it is converted into the hormonally active 1,25$(OH)_2D$, by the enzyme 25(OH)D 1α-hydroxylase (CYP27B1) in the proximal tubule[238,240]. 1α,25$(OH)_2D$ is the active form of vitamin D and when entering the blood, is delivered to different targets such as the intestine, bone and kidneys where it is known to regulate calcium and phosphate metabolism[240]. 1,25$(OH)_2D$ can then open up the calcium channels in the intestine which in turn stimulates the formation of calcium binding protein in the intestinal cells stimulating the absorption of calcium and phosphate from the intestine[240]. This in turn facilitates mineralisation of bone.

A stimulator of renal synthesis of 1α,25$(OH)_2D$ is PTH, which if increased stimulates the production of 1α,25$(OH)_2D$[241,242]. But due to a feedback loop, elevated serum levels of active vitamin D lead to a decrease in the release of PTH[240].

The kidney also produces the inactivating enzyme 25(OH)D 24-hydroxylase (24,25$(OH)_2D$, also known as CYP24), which catabolizes both 25(OH)D and 1,25$(OH)_2D$ into biologically inactive calcitroic acid[239].

Vitamin D deficiency can lead to decreased calcium in circulation, called hypocalcemia, which leads to the increase of PTH levels, known as secondary hyperparathyroidism, in order to stimulate hydroxylation of 25(OH)D in the kidney to its active form 1α,25$(OH)_2D$. In turn, increased levels of PTH leads to increased bone turnover, which leads to bone loss[243].

Parathyroid Hormone

The parathyroid hormone (PTH) is secreted by the parathyroid glands in response to reduced levels of serum calcium, therefore maintaining calcium homeostasis[244]. It acts peripherally on the kidneys and on bone and indirectly on the intestine to maintain serum calcium homesotasis[225,245]. In bone, PTH binds to a seven-transmembrane G-protein-linked receptor, the PTH receptor, on the surface of osteoblasts and stromal cells[242,245]. This in turn, activates protein kinase A, protein kinase C, and calcium intracellular signalling pathways in these cells and induces transcriptional responses that lead to the expression of M-CSF and RANKL, therefore inducing osteoclast differentiation and activation, which later leads to bone resorption[245].

Oestrogen

Oestrogen, the main female sex hormone, is one of the major inhibitors of osteoclastogenesis. In osteoclasts, oestrogen suppresses RANKL and M-CSF-induced activator protein-1-dependent transcription through a reduction of c-Jun activity, thus directly suppressing RANKL-induced osteoclast differentiation[246]. Moreover, oestrogen can stimulate the expression of OPG, the RANKL antagonist, in osteoblasts therefore inhibiting osteoclastogenesis[247]. During oestrogen deficiency, osteoclast differentiation and activity is increased due to a higher expression of RANKL[248,249], but also an increase in production of M-CSF by bone marrow cells[250]. In osteoblasts and osteocytes, oestrogen has an antiapoptotic effect due to the activation of Src/Shc/ERK signalling pathway[251] and the downregulation of JNK[252], therefore enhancing osteogenic differentiation and activity. Oestrogen has the ability to modulate bone cell activity therefore playing an essential role in maintaining bone homeostasis.

Calcitonin

Calcitonin is one of the hormones which play a role in bone remodelling. It binds exclusively to osteoclasts through calcitonin receptors and causes a rapid decrease in resorptive activity[253]. Calcitonin is secreted mainly by thyroid C cells in response to elevated serum calcium levels[254]. The main functions of calcitonin in calcium homeostasis are to inhibit bone resorption, decrease calcium reabsorption

in the kidney, thus increasing urinary calcium excretion, and to regulate 1α,25$(OH)_2D_3$ production in the kidney[254]. There is, however, no evidence for an important physiologic effect of calcitonin in adults, as thyroidectomy, which leads to calcitonin deficiency, does not lead to osteoporosis as would be expected[255].

FGF23

FGF23 is a hormone produced by osteocytes whose main function is to regulate phosphate homeostasis and vitamin D metabolism (**Figure 1.15**)[256]. Unlike other FGFs, FGF23 has a low affinity to heparin sulphate, and can therefore easily enter circulation and act as an endocrine hormone[256].

In the kidney, together with its co-receptor Klotho, FGF23 decreases the threshold for renal tubular reabsorption of phosphate by decreasing the abundance of phosphate transporters[256]. Therefore, when FGF23 is increased, serum phosphate levels are maintained at significantly lower levels than normal[257]. In addition, FGF23 regulates vitamin D by increasing the expression of 24-hydroxylase and inhibiting the expression of 1α-hydroxylase, thus reducing the concentration of active 1,25$(OH)_2D$, a critical regulator of calcium homeostasis[256,257]. Abnormally increased levels of FGF23 result in lower circulating levels of 1,25$(OH)_2D$ which may contribute to the low concentration of serum phosphate, as intestinal phosphate absorption is regulated by 1,25$(OH)_2D$[257].

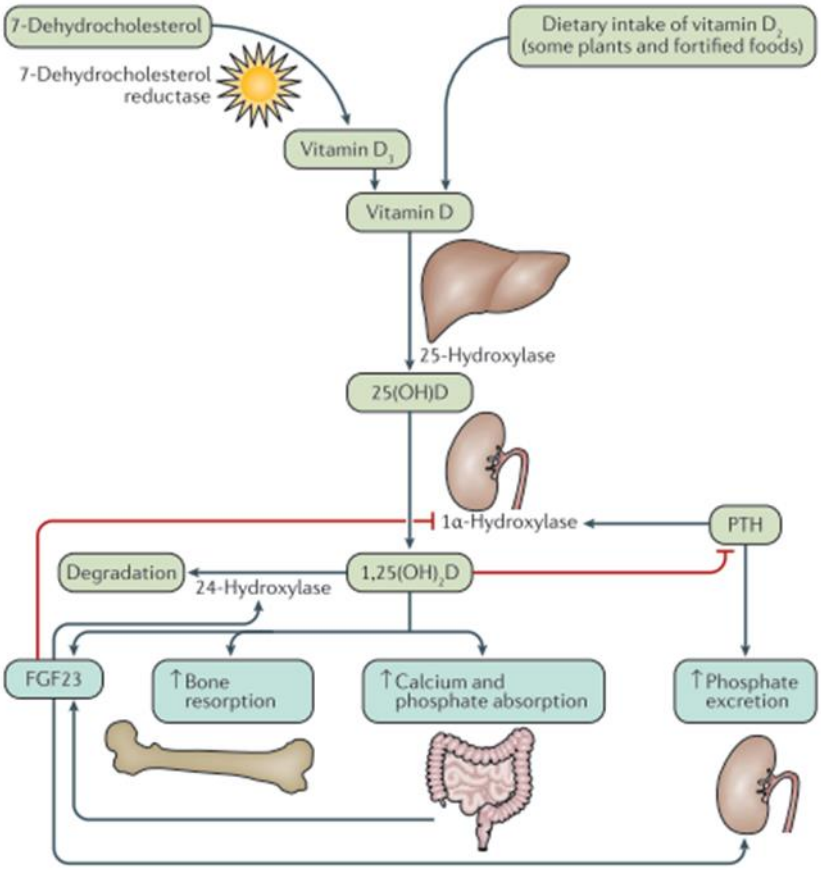

Figure 1.15: Regulation of calcium and phosphate homeostasis. Serum calcium and phosphate levels are regulated by the action of $1,25(OH)_2D$, FGF23 and PTH on the intestine, bone and kidney. (Adapted from Carpenter *et al*.)[257]

Central Nervous System

Increased body weight has been shown to have a strong correlation with bone mass, and obesity has been considered a protective factor against osteoporosis especially in postmenopausal women[258]. It has been demonstrated previously that signalling between the brain and bone tissue is fundamental in mediating bone metabolism and energy regulation[259]. This idea that the brain and bone are connected was initially a product of the discovery of Leptin in 1994[260].

Leptin is a small polypeptide hormone secreted primarily by adipocytes and is involved in the regulation of food intake and energy expenditure[258]. Obese people have increased circulating levels of leptin, however interestingly, Ducy *et al*. first reported that leptin-deficient mice (*Ob/Ob*) and leptin receptor deficient mice (*db/db*) had increased bone mass phenotype due to increased bone formation which

suggest leptin is an inhibitor of bone formation[261]. Intracerebroventricular infusion of leptin were also performed on these mice which corrected the increased bone phenotype which suggested that the effects of leptin are controlled by the central nervous system (CNS)[261]. It was thought that if leptin is an inhibitor of bone formation and obese individuals have increased levels of this hormone that they have decreased bone mass and not increased bone mass, but it was later shown that most obese individuals lack sensitivity to leptin[262].

This strengthens the idea of crosstalk not just between the CNS and bone but also between adipocytes and bone.

1.7 Proteoglycans

Proteoglycans are glycoproteins composed of a specific core protein substituted with one or more glycosaminoglycan (GAG) polysaccharide chains covalently linked, with the exception of hyaluronan which lacks a protein core[263,264]. Proteoglycans are part of ECM, but also present in every tissue compartment, on the cell surface, intracellularly in granules and in the nucleus[264]. They can be divided into small leucine-rich proteoglycans (SLRPs), modular proteoglycans and cell-surface proteoglycans, which some SLRPs can also be part of (**Figure 1.16**)[265,266]. Functions depend on their location, but they are known to stabilize ligand-receptor interactions or cell-cell interactions, regulate cell proliferation, migration and sensitivity to growth factors, and activate signalling pathways, all through their GAG chains[267].

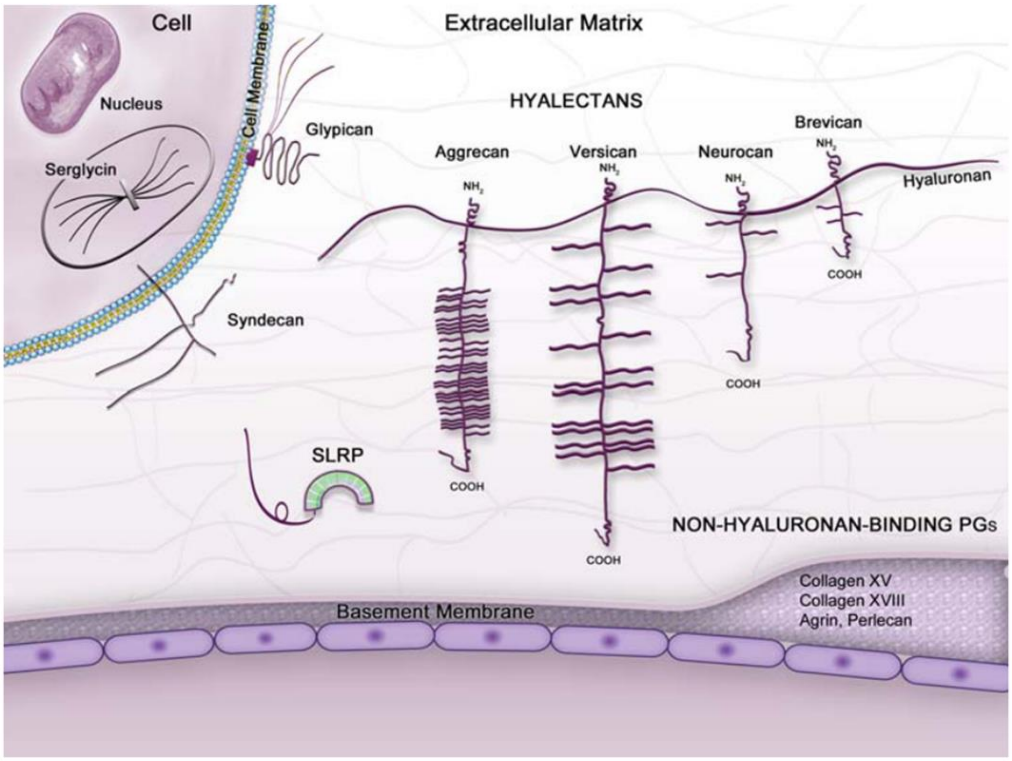

Figure 1.16: Proteoglycan classification. Based on location and binding, proteoglycans can be divided into small leucine-rich proteoglycans (SLRPs), modular proteoglycans, which include hyalectans and non-hyaluronan-binding proteoglycans, and cell-surface proteoglycans, which include syndecans and glypicans[265,266]. (Adapted from Schaefer and Schaefer, 2010)

GAGs consist of repeating disaccharide structures which contain galactose and hexosamine[267]. They can be divided into sulphated and non-sulphated GAGs[268]. In the sulphated GAGs there are keratan sulphates (KS), chondroitin sulphates (CS), dermatan sulphates (DS) and heparan sulphates (HS), with only hyaluronan being part of the non-sulphated GAGs[266,268]. GAGs are a key component of bone matrix and cell surface helping modulate the activity of growth factors important for bone cell formation and activity and increase bone toughness[269,270]. However, ageing results in a reduction of GAGs in bone matrix and therefore a decrease in toughness of bone possibly contributing to the decline of bone quality[271]. Research has shown that GAGs, including sulphated hyaluronan and CS, can inhibit sclerostin, a known Wnt pathway inhibitor, therefore enhancing bone regeneration[272]. It has also been shown that HS GAGs improve osteogenesis by modulating Wnt signalling[273].

1.7.1 Heparan Sulphate proteoglycans

Heparan sulphate proteoglycans (HSPGs) are the most ubiquitous cell surface and ECM glycoproteins, with the common characteristic of containing one or more HS chains[274–276]. HSPGs can be divided into different groups based on the structure of their core protein, those being glypicans, syndecans and perlecans. Glypicans and perlecans bear only HS GAG chains, while syndecans have both HS and, in some cases, CS chains[277]. Perlecans are secreted and mainly distributed in the ECM, whereas glypicans and syndecans are cell surface HSPGs linked to the cell membrane via glycosylphosphatidylinositol linkage or through a transmembrane domains, respectively[278,279].

1.7.1.1 Syndecans

Syndecans are a family of four (in mammals) type I transmembrane glycoproteins that have HS chains attached to their extracellular domains and in the cases of syndecan1 and 3, CS chains too[274] (**Figure 1.17**). As only syndecans 1 and 3 contain HS and CS chains and syndecans 2 and 4 contain only HS chains, they can be divided into two subfamilies[280,281]. Syndecans contain three distinct domains in their core protein, N-terminal polypeptide domains, an ectodomain where GAGs are attached to specific serine residues, a single hydrophobic transmembrane domain and a short C-terminal cytoplasmic domain, composed of a variable (V) region flanked by two conserved C1 and C2 regions[274,282]

Syndecans can bind a variety of extracellular ligands increasing their concentration at the cell surface and mediate several cell-cell and cell-matrix interactions via their covalently attached HS chains[280]. By associating with the cytoskeleton, syndecans aid in cell adhesion by stabilizing the cytoskeleton and in turn increasing adhesion strength[280]. Additionally, syndecans have the ability to shed their extracellular domain by proteolytic cleavage which may reflect their distinct functions between the different members of the syndecan family, although this is still unclear[283].

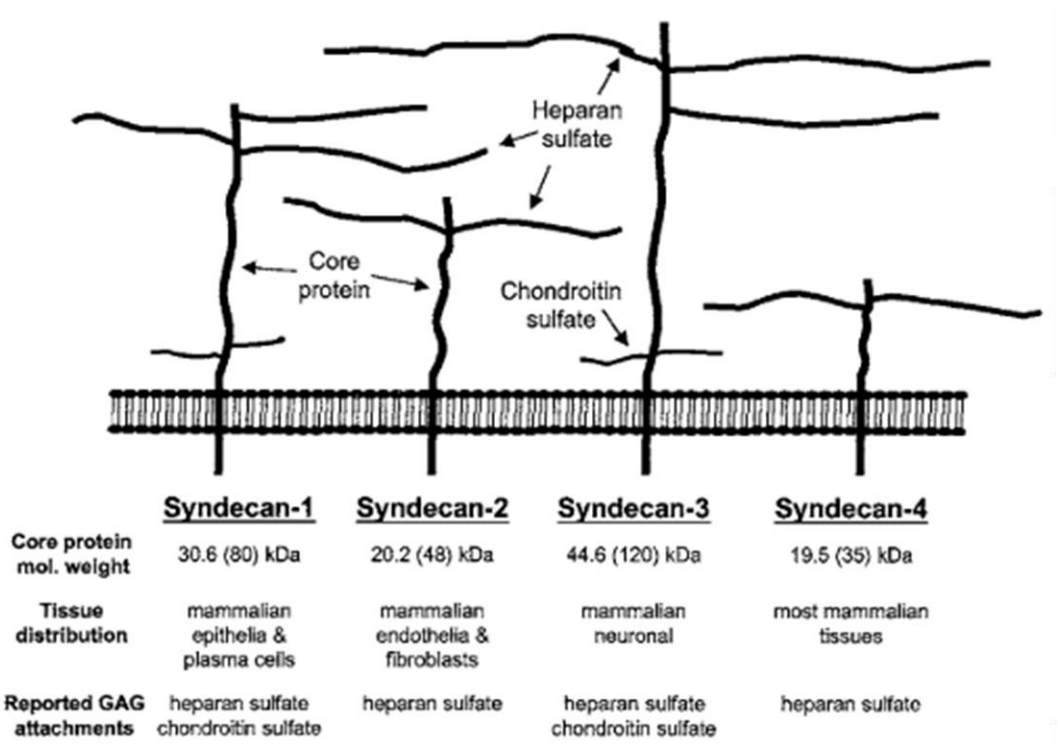

	Syndecan-1	Syndecan-2	Syndecan-3	Syndecan-4
Core protein mol. weight	30.6 (80) kDa	20.2 (48) kDa	44.6 (120) kDa	19.5 (35) kDa
Tissue distribution	mammalian epithelia & plasma cells	mammalian endothelia & fibroblasts	mammalian neuronal	most mammalian tissues
Reported GAG attachments	heparan sulfate chondroitin sulfate	heparan sulfate	heparan sulfate chondroitin sulfate	heparan sulfate

Figure 1.17: The Syndecan family. Syndecans are a family of four transmembrane proteoglycans. All four have heparan sulphate GAG attachments with the exception of Syndecan 1 and 3 which also have chondroitin sulphate attachments. In parenthesis is their molecular weight based on SDS-PAGE migration of the core protein without GAG chains[284]. (Adapted from Bellin *et al*., 2003)

Syndecans are named based on the order they were discovered and the tissue from which they were originally cloned. Syndecan 1, the first syndecan to be cloned, is found in epithelial and plasma cells[285], whereas Syndecan 2, also known as fibroglycan, is mainly expressed in mesenchymal cells[286,287], such as fibroblasts and smooth muscle. Syndecan 3, first described as N-syndecan, the least studied of the syndecans, was first discovered in the rat brain and can also be found in developing musculoskeletal tissues[288,289]. On the other hand, syndecan 4, also known as ryudocan and amphiglycan, is ubiquitously expressed[279,290].

1.7.1.1.1 Syndecan 1

Syndecan 1 was the first mammalian syndecan to be cloned[285], but its existence was known before this. Studies identified an HSPG intercalated in the plasma membrane of mouse mammary gland epithelial cells and rat

hepatocytes[278,291]. It was found to be predominantly expressed on the basolateral surface of epithelial cells where it associates with the actin cytoskeleton[292]. The major function of syndecan 1 appears to be to negatively regulate the adhesion and migration of leucocytes[293,294].

However, syndecan 1 appears to play a role in endothelial mechanosensing and regulation of endothelial phenotype[295]. Voyvodic *et al*. investigated the role of syndecan 1 in controlling the shear stress-induced signalling and flow-mediated phenotypic modulation in endothelial cells[295]. By performing studies on mice lacking syndecan 1 it was reported that these mice have a pro-inflammatory phenotype in endothelial cells with an altered response to atheroprotective flow[295]. However, Sdc1 KO mice have increased inflammation due to increased ICAM-1 and leukocyte recruitment, highlighting the role of Sdc1 in immune responses[296].

On the other hand, a study by Ren *et al*. demonstrated that syndecan 1 plays an important role in multiple myeloma mediating increased Wnt/β-catenin signalling and cell growth[297]. They also demonstrated that Wnts bind to HS side chains of Sdc1 which in turn activates the Wnt pathway through Wnt receptor Frizzled[297]. This study also demonstrated that Sdc1 binds osteoblast-produced R-spondin through its HS chains which in turn activates LGR4 therefore repressing Fzd degradation, all of which is essential for optimal stimulation of Wnt signalling in multiple myeloma[297].

Although Sdc1 plays a major role in cell adhesion and motility, it has not yet been shown to play a role in the skeleton.

1.7.1.1.2 Syndecan 2

Syndecan 2 was originally known as fibroglycan, but later Bernfield *et al*. changed its nomenclature to what it is currently known as[274]. It is mainly produced by mesenchymal cells, which explains where its original name of fibroglycan originated from, but unlike Sdc1, it was not found to be expressed by epithelial cell lines[286,298]. Sdc2 is also expressed in the adult brain, heart, kidney, liver, spleen and cultured hepatocytes, fibroblasts and neurectodermal cells[287,298]. During development, syndecan 2 is expressed at sites of cell-cell and cell-matrix interactions especially in mesenchymal condensations, and continues to be expressed in the

perichondrium, periosteum, and connective tissue cells[299]. David *et al*. found Sdc2 was highly expressed in the periosteum during early osteogenesis and its expression increased during osteoblast differentiation, therefore being linked to osteoblast differentiation both during development and adulthood[299].

Studies by Mansouri *et al*., found overexpression of Sdc2 lead to the enrichment on the bone surface with HS resulting in increased bone mass due to bone resorption inhibition[273]. However, this overexpression also lead to decreased osteoblasts, possibly due to decreased Runx2 expression, and osteoclasts together with RANKL levels[273]. Syndecan 2 overexpression was also associated with bone marrow cell apoptosis, although osteoblast survival and activity was not altered, which was suggested to be due to the downregulatory effect it had on Wnt/β-catenin signalling in particular through deregulation of the GSK3 pathway[273]. This study therefore highlighted the effect syndecans have on the Wnt pathway, essential for osteogenesis and bone development but also the importance of HS GAGs in osteoblast differentiation and activity.

1.7.1.1.3 Syndecan 3

Syndecan 3 is the least studied of the syndecans. It was first described by Carey *et al*. in neonatal rat Schwann cells and was therefore given the name of N-syndecan[288]. It was thought to provide cell surface binding sites for extracellular proteins, such as ECM adhesion proteins, growth factors and cell-cell adhesion molecules[288]. Syndecan 3 was later found to be highly expressed in the embryonic chicken limb bud by Gould *et al.* and was given the name by which it is currently recognised, Syndecan 3[289]. It was also shown to be highly expressed in mesenchymal condensations during chondrogenesis and therefore thought to mediate the adhesive cell-matrix interactions and cytoskeleton reorganization involved in the process of condensation[289]. Further studies were performed in order to understand the role syndecan 3 played in limb development and it was later reported that it is expressed in the progress zone beneath the apical ectodermal ridge and precartilage condensations in the developing limb bud[300]. It was suggested that syndecan 3 may be involved in the maturation of chondrocytes during endochondral ossification by playing a role in the regulation of the proliferative phase of the process[300,301].

Syndecan 3 was also shown to be highly expressed in the peripheral layers of the periosteum around the diaphysis where osteoblasts are differentiating and depositing the intramembranous bone collar[300,302]. This indicates that syndecan 3 may play a role in regulating osteoblast differentiation and osteogenesis. On the other hand, syndecan 3 was found to be highly expressed in the calvaria, which is formed through intramembranous ossification, differently from long bone development, highlighting its role in osteoblast differentiation[300]. Therefore, it was suggested that syndecan 3 may be important during early development of the skeleton especially during condensations, essential for the formation of the skeleton[300].

Interestingly, a study by Koyama *et al*., reported that syndecan 3 was involved in skeletal development due to the increased expression of syndecan 3 in the epiphysis and the perichondrium which surrounds the mesenchymal condensations of long bones[303].

Syndecan 3 has since been shown to be a cell surface receptor for heparin binding growth-associated molecule (HB-GAM)[304], which, similar to syndecan 3, is highly expressed by differentiating osteoblasts during the formation of the periosteal bone collar[305].

Sdc3 KO mice were shown to exhibit muscular dystrophy with extensive fatty infiltrations in the muscles, reduced locomotion, hyperplasia of myonuclei and satellite cells, and an increase of centrally nucleated myofibers in uninjured muscles[306]. It was later reported that Sdc3 KO satellite cells proliferate at a slower rate and have increased apoptosis due to an impairment of the Notch signalling pathway by reduced Notch target gene induction and impaired NICD accumulation[178]. More recently it was reported that Sdc3 deletion leads to improved muscle regeneration after repeated acute muscle injuries, rescued muscle histopathology and function in dystrophic muscle tissue and improves muscle ageing reducing fat infiltration in the muscle[307].

The co-expression of syndecan 3 and HB-GAM in differentiating osteoblasts during bone formation and the role syndecan 3 plays in regulating chondrocyte proliferation in developing limbs suggests Sdc3 is involved in skeletogenesis[308], however the exact role of Sdc3 in bone homeostasis is still not fully understood.

1.7.1.1.4 Syndecan 4

Syndecan 4, the last member of the syndecan family to be identified, can promote intracellular adhesion, similarly to syndecan 1[309]. It was also found to be expressed during wound healing after incisional wounding of the skin[310]. Woods and Couchman found syndecan 4 to be associated with focal adhesion that contain vinculin and either integrin β1 or β3[311]. Syndecan 4 also has the ability to bind fibronectin through its GAG chains, activate protein kinase Cα (PKCα) and the small GTPase RhoA[311]. These together with the integrins stabilize focal adhesion sites[311].

Interestingly, a study on Xenopus by Muñoz *et al*., found that syndecan 4 regulates non-canonical Wnt signalling by forming a complex with Frizzled 7 and interacts with Dishevelled (Dsh), activating its translocation to the plasma membrane which leads to activation of the non-canonical Wnt pathway[312]. It was also shown that syndecan 4 is essential for convergent and extension movements in *Xenopus* embryos[312].

Syndecan 4 not only plays a role in wound healing, it also appears to support fracture repair as its loss leads to impaired fracture healing and proinflammatory signals in adults[313]. Bertrand *et al.* reported that Sdc4 deletion was associated with inhibition of chondrocyte proliferation and reduced aggrecanase activity in uncalcified cartilage of the epiphysis although this did not lead to a growth phenotype at birth[313]. However, Sdc4 did not play any major role during endochondral bone development as no prominent differences were observed in early development between Sdc4 KO and WT mouse embryos[313]. These findings highlighted Sdc4 redundancy during skeletal development[313]. This was associated with a compensatory up-regulation of syndecan 2 in developing cartilage in the Sdc4 KO mice[313].

1.8 Osteoporosis

Our bones constantly undergo changes throughout our lives. Humans reach peak bone mass in their late 20s by which point they start to slowly loose bone, although during the menopause women suffer rapid bone loss. This is due to an imbalance between bone formation and bone resorption during remodelling, where,

in ageing, bone formation is unable to keep up with the increase in bone resorption therefore there is a decrease in bone accrual. This may lead to osteoporosis.

Osteoporosis, which literally means “porous bone”, has been defined as an age-related metabolic bone disorder, characterised by low bone mass and microarchitectural deterioration of bone tissue, which consequently leads to enhanced bone fragility and therefore increased susceptibility to fracture[314]. It is a huge and increasing public health problem as it affects millions of people worldwide, predominantly postmenopausal women. Osteoporosis is considered a silent disease as it may be symptomless in the absence of fractures, however fractures are a complication of this process which may lead to increased pain, disability and even death. The most common osteoporotic fractures are vertebral compression fractures, fractures of the hip, proximal humerus and forearm[315], but when bone density is reduced the fracture risk in other bones is also increased[316]. Another consequence of age-related bone loss is the increase in bone marrow adiposity which also contributes to increased fragility[317]. Despite the progress made over the years in prevention and treatment options there are still many challenges to overcome in these areas.

1.8.1 Epidemiology

Incidence and prevalence

Osteoporosis is an age-related disease which affects millions of people world-wide making it a serious public health burden. According to the International Osteoporosis Foundation, 1 in 3 women and 1 in 5 men aged fifty and over are at risk of an osteoporotic fracture[318]. The prevalence of osteoporosis increases with age and is twice as high in women than in men of the same ages, and adults with prior fractures are 50-100% more likely to sustain another fracture in a different bone[315,319]. The reason for women being at higher risk is due to their peak bone mass being lower than men’s and the rapid bone loss observed after the menopause. It is also known that women live longer than men which also increases their risk of osteoporotic fracture[315]. With the exception of lung cancer, osteoporotic fractures account for more combined deaths than any cancer[320].

Osteoporosis causes over 8.9 million fractures annually worldwide, which accounts for approximately 1000 fractures per hour[321]. Western countries have a higher incidence of fractures than other regions in the worlds. In Europe, the prevalence of osteoporosis was estimated at 27.6 million people in 2010, of which 22 million were women[322]. In the year 2000 there were an estimated 9 million osteoporotic fractures, 1.6 million of those were of the hip, 1.7 million were of the forearm and 1.4 million were of the spine[321]. In 2010, the economic cost of these fractures was 37 billion euros in Europe and up to 20 billion dollars in the United States of America[322,323].

Globally, major osteoporotic fracture frequency varies greatly being highest in Europe and lowest in Africa (**Table 1.1**)[321]. Interestingly, within Europe, Eastern Mediterranean has the lowest values while Scandinavia has the highest[321]. The geographical variation between fracture incidence is most marked for hip fractures with Europe showing higher values of incidence and Western Pacific and Americas not being too far off[321]. Reports have shown that hip fracture rates in northern Europe and North America have started to decline among both men and women which has been associated with an increase in BMD in the elderly, thought to be due to an increase in obesity[324]. Developing countries such as in Africa have a lower incidence partly due to the lower risk but also because of lower life expectancy[325]. In Asian countries such as China, osteoporotic hip fractures, have increased dramatically between 1990 and 1992 and 2002 and 2006, and this is thought to be due to westernization of the population[326]. Due to urbanization, walking, which protects against hip fractures, has reduced due to an increase reliance on cars and buses. Squatting, which strengthens the spine, has also become uncommon due to the use of chairs and western-style toilets. A decrease in sun exposure, which leads to vitamin D deficiency, due to people moving into multi-storey buildings with no outdoor space[326]. It is still unclear why there are such differences in prevalence of fractures in different regions worldwide but this can be partly explained by the heritability of skeletal size which is greater in those of African heritage and lowest in those of Caucasian heritage[327]. Diet and exercise is also related to differences in bone mass worldwide as climate may be too[327].

Osteoporotic fractures lead to a great degree of disability, which in some cases can even cause death, and have huge medical costs worldwide. As longevity of the population is increasing, the frequency of osteoporotic fractures is predicted to rise, although this increase in fracture rates may also be due to the increase in sedentarism.

Table 1.1: Estimated number of osteoporotic fractures in men and women aged 50 or over in 2000 by WHO region ([a] includes Australia, China, Japan, New Zealand and the Republic of Korea)[321].

	Expected number of fractures by site (thousands)				**All osteoporotic fractures**	
WHO region	Hip	Spine	Proximal Humerus	Forearm	No.	%
Africa	8	12	6	16	75	0.8
Americas	311	214	111	248	1406	15.7
South-East Asia	221	253	121	306	1562	17.4
Europe	620	490	250	574	3119	34.8
Eastern Mediterranean	35	43	21	52	261	2.9
Western Pacific	432	405	197	464	2535	28.6
Total	1672	1416	706	1660	8959	100

Genetic Factors

Genetic risk factors play a major role in the development of osteoporosis. Studies with twins have demonstrated that over 50% of the variance in bone mass is genetically determined[328]. Although it was determined that there is a stronger genetic component to the determination of bone mass in the spine but not as much in the proximal femur and forearm, suggesting that environmental factors may play a more important role in determining bone mass variation in these last sites as opposed to what is observed in the spine[328]. Another twin study also found that the

age in which women start the menopause is genetically determined[329], providing evidence that, at least in women, genetic factors play an important role in determining bone loss[330]. Makovey *et al*., also performed a large twin study investigating the genetic effects on bone loss and found that at least 40% of the variance in bone loss for the spine, forearm, and whole body in peri- and postmenopausal women is genetically determined, although this excluded the femoral neck as there was no significant difference[331]. Similar studies were performed with male twins, which in contrast to studies with female twins, during a 16 year period, no genetic effects on bone loss in the radial bone were found[332]. Indeed, it was suggested that environmental factors were the major cause in the variation observed in bone mass and density loss with ageing[332].

Genome-wide linkage studies which included over 200 thousand individuals have revealed 56 loci related to BMD variation which clustered within the RANK-RANKL-OPG, MSC differentiation, endochondral ossification and Wnt-signalling pathways[333]. Fourteen of those loci were also associated with fracture risk including *LRP5* and *DKK1*[333]. In addition to these genes, *WNT3a* was also shown to be strongly associated with deceased hip BMD, *LRP4* was associated with decreased BMD in the lumbar spine and *DKK2* was shown to be associated with decreased BMD in the femoral neck, but these last 2 genes showed lower significance[334]. There have been many other genes identified which are associated with osteoporosis, but these require further studies as there are many other factors that can regulate gene expression including epigenetic and environmental factors. Therefore, before the identified variants can be used in the risk assessment, they would require further *in vivo* and *in vitro* studies.

1.8.2 Pathophysiology

As mentioned earlier, peak bone mass is reached in the second decade of human life. However, the skeleton constantly undergoes a process called bone remodelling. The process of remodelling requires the activity of bone resorbing osteoclasts, which remove mature and damaged bone, and bone forming osteoblasts, which replace this with new bone. This process allows the skeleton to maintain its structural integrity and is controlled by mechanical and endocrine

stimuli. Osteocytes first sense mechanical strain which leads to the activation of bone remodelling where, in normal physiological conditions, osteoclasts resorb a specific amount of bone and then through the action of osteoblasts, new bone matrix is deposited. The process of mineralisation is controlled by the endocrine system which includes the actions of PTH, oestrogens and vitamin D.

Bone remodelling in osteoporosis

Osteoclast-mediated bone resorption is a fast process as osteoclasts typically undergo apoptosis within approximately 12 days. In contrast, bone formation can take up to 6 months which means that if there is an increase in osteoclast function and an inadequate response in bone formation this can result in loss of bone mass and microarchitectural deterioration of the skeleton[315]. This is what happens in the ageing skeleton, in which there is a negative imbalance in the remodelling cycle. It was originally thought that osteoporosis was only due to oestrogen deficiency[335], but subsequently it was proposed that there were two forms of osteoporosis, either related to oestrogen deficiency due to the menopause or due to calcium deficiency and ageing of the skeleton[336]. Although it is known that oestrogen plays a major role in the differentiation and activation of bone cells, it is now known that that there are multiple factors controlling bone remodelling and can cause bone mass loss and deterioration of the skeleton leading to osteoporosis.

In age related osteoporosis, which affects both sexes later in life, osteoblasts are less capable of refilling the resorption pits which leads to decreased trabecular and cortical thickness[337]. In contrast, postmenopausal osteoporosis is characterised by a marked decrease in oestrogen levels which leads to an increase in osteoclastogenesis and subsequently osteoclast activity, but also to an increase in the activation frequency of BRUs and bone marrow adipocyte number and size[249,338,339]. This increased osteoclast activity in postmenopausal osteoporosis not only leads to rapid trabecular and cortical thinning but also leads to an increase in perforated trabecular plates which can lead to crush fractures, for example of the vertebrae[338]. Postmenopausal women will therefore suffer from both postmenopausal bone loss and age related bone loss which can therefore explain why women are more prone to developing osteoporotic fractures than men[338] (**Figure 1.18**).

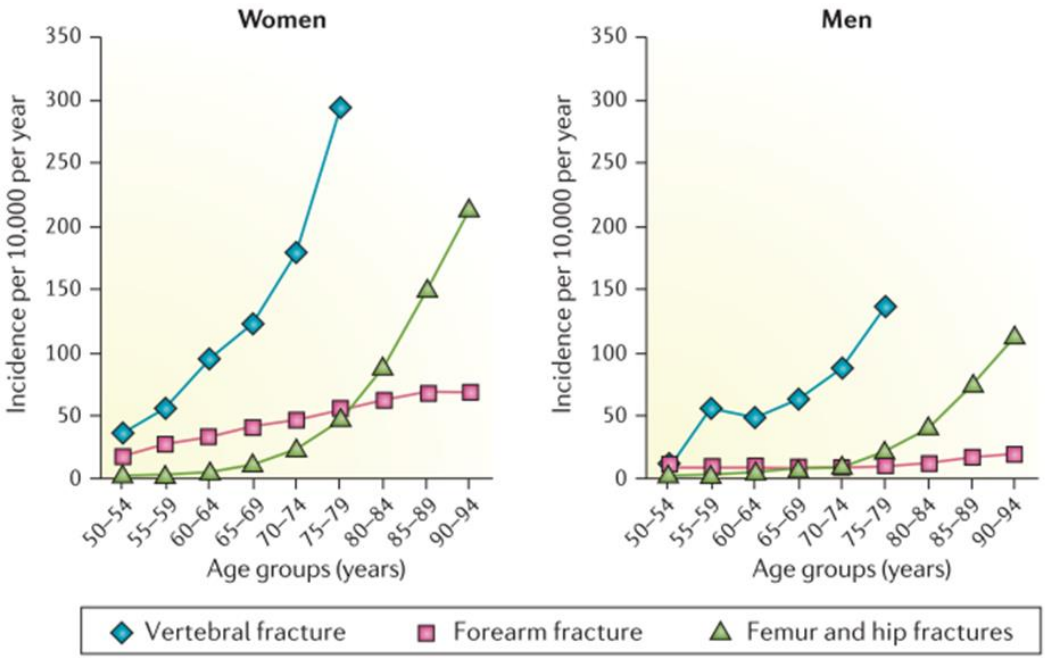

Figure 1.18: Fracture incidence with increasing age in women and men. Data shown is incidence of vertebral, forearm, and femur and hip fractures in women and men, also demonstrating the difference in fracture incidence observed between women and men. Adapted from Eastell *et al.*[315].

Oestrogens and osteoporosis

Oestrogen deficiency is critical to the pathogenesis of osteoporosis and although it was originally thought that age-related bone loss was caused by an increase in bone resorption it is now known that impaired bone formation also contributes to this process. Ivey and Baylink[340] found that bone formation was unable to adequately compensate to the increase in bone resorption caused by oestrogen deficiency. It has been shown that the reduced bone formation during oestrogen deficiency is due to a lack of response to mechanical loading, which is required for the activation of bone remodelling[341]. Osteocytes are the major producers of sclerostin, a Wnt signalling antagonist, which is inhibited during mechanical loading therefore enhancing Wnt signalling and consequently osteoblastogenesis and later bone formation[202]. However, during oestrogen deficiency sclerostin synthesis is enhanced due to lack of response of osteocytes to mechanical loading therefore inhibiting bone formation[342,343].

Although men do not have the equivalent of the menopause and testosterone is the main male sex steroid, it has been found that oestrogen deficiency is closely related to decreased distal forearm BMD in older men[344].

Fat mass also has an effect on BMD as it has been shown that increased body weight is associated with increased BMD[345]. But interestingly, the enzyme aromatase, which is found in gonadal tissue and highly expressed in white adipose tissue, can convert adrenal androgens such as androstenedione, or testosterone to oestrogen, protecting the skeleton against osteoporosis[346]. On the other hand, oestrogen downregulates adipogenic differentiation and maturation but during oestrogen deficiency, especially after the menopause, adipocyte infiltration precedes osteoblastogenesis which is accompanied by a decline in bone mass[347].

Calcium, vitamin D and parathyroid hormone in osteoporosis

Parathyroid hormone and 1,25-dihydroxyvitamin D are important in the pathogenesis of osteoporosis. With age, there is a decrease in calcium intake and sometimes vitamin D deficiency, due to diet, immobilization or being housebound due to other pathologies and side-effects from the medication, and therefore reduced sunlight exposure. Intestinal absorption of calcium and renal function also decreases in ageing. There is a decrease in the capacity kidneys have to hydroxylate 25-hydroxyvitamin D into its active form[348]. The active form of vitamin D, 1,25 (OH_2) D^3, is both necessary for intestinal absorption of calcium and phosphorus and can also inhibit PTH synthesis[348]. The reduced calcium supply leads to secondary hyperparathyroidism where the parathyroid glands increases PTH secretion which will in turn stimulate bone resorption to release calcium and later the hydroxylation of vitamin D in the kidney to the active form[243]. The raised serum PTH stimulates bone remodelling units which consequently leads to bone loss[243]. Vitamin D deficiency and hyperparathyroidism can also contribute to neuromuscular impairment which increases the risk of falls and consequently the risk of fractures[349,350].

RANK/RANKL/OPG pathway in osteoporosis

RANKL is required for osteoclastogenesis. RANKL, produced by osteoblasts and osteocytes, is a ligand for the receptor activator of NF-κB (RANK) found on

osteoclast progenitors and is capable of activating osteoclast differentiation and function[19]. On the other hand, OPG, a decoy receptor for RANKL, is also produced by osteoblasts and osteocytes and acts by blocking RANKL/RANK interactions therefore inhibiting osteoclastogenesis[20]. *In vitro* studies with bone marrow cells from untreated postmenopausal women have found that there is increased surface expression of RANKL on these cells, compared with bone marrow cells obtained from oestrogen replete women, thus contributing to increased bone resorption during postmenopausal oestrogen deficiency[249]. Interestingly, it has also been shown that oestrogen enhances osteoblastic OPG secretion therefore playing a major role in downregulating bone resorption[351]. During oestrogen deficiency, OPG levels decrease, while RANKL expression is increased leading to increased osteoclast differentiation and activity therefore contributing to the development of osteoporosis[248,249]. It has since been shown that oestrogen replacement can partially reverse these effects by decreasing surface expression of RANKL on bone marrow cells, and oestrogen replacement improves BMD in postmenopausal osteoporosis[249].

1.8.3 Clinical aspects

1.8.3.1 Clinical features

As uncomplicated osteoporosis is an asymptomatic disease it only becomes apparent when a patient suffers a fragility fracture due to minimal trauma. The most common osteoporotic fractures are of the hip, wrist and vertebrae, although later in life fractures of the femur become more common[352]. In patients with osteoporosis and in older people, fractures are often the result of a fall or due to a minimal trauma[338,353]. Vertebral collapse without symptoms is also a very common clinical feature, although some patients may present with acute onset of sharp pain over the involved region or discomfort[352]. This may later lead to loss of height and dorsal kyphosis, which is also known as dowager's hump[352].

1.8.3.2 Diagnosis

The World Health Organization defines osteoporosis by BMD, measured by dual-energy x-ray absorptiometry (DXA) at the lumbar spine, total hip or femoral neck

of 2.5 standard deviations (SD) or more bellow the population mean for young healthy adults[327] (**Table 1.2**). DXA is an X-ray-based technique that quantifies bone mineral content (BMC) by using X-ray sources of different energies allowing subtraction of the attenuation of radiation by soft tissues from the total attenuation to determine the attenuation caused by bone mineral[315].

Women and men over the age of 50, and especially postmenopausal women should be assessed for osteoporosis. This risk is evaluated in the individual based on the presence of clinical risk factors, which include previous fragility fractures, genetic predisposition, smoking, alcohol consumption, early-onset menopause, decreased BMI and other factors involved in secondary osteoporosis such as anorexia nervosa, type 1 and type 2 diabetes, certain drugs and gastrointestinal diseases, among others[315]. There are also conditions related to increased risk of falling that lead to greater risk of hip fractures which include Parkinson's disease, dementia, vertigo, vision impairment and alcoholism[316,354].

Table 1.2: World Health Organisation Diagnostic Criteria for Osteoporosis[327].

Group	Diagnostic criteria
Normal BMD	BMD within 1 SD of the mean of a young adult reference population
Osteopenia	BMD between 1.0 and 2.5 SD below the mean of a young adult reference population
Osteoporosis	BMD 2.5 or more SD below the mean of a young adult reference population
Severe Osteoporosis	Osteoporosis with one or more fragility fractures

Other than DXA, considered the gold standard for diagnosis[327], quantitative computed tomography can also be used to diagnose osteoporosis and is proven most useful in assessing cancellous bone density rather than cortical bone. Although one of the main advantages is that it provides a measure of true volumetric density rather than an area adjusted result as is the case of DXA, it also has disadvantages which include a high exposure to radiation[354]. Simple radiographs can also be used to diagnose in the presence of fractures such as subclinical vertebral fractures, which is a strong risk factor for subsequent fractures[354].

A prerequisite for the definition of primary osteoporosis is that diseases and drugs that cause secondary osteoporosis are excluded[327]. Low bone density can be secondary to hyperthyroidism, primary hyperparathyroidism, hypercortisolism, myeloma, or osteomalacia (**Table 1.3**)[354].

Table 1.3: List of drugs and disease that are associated with increased fracture risk (adapted from Eastell *et al*.[315]).

Drugs and diseases associated with secondary osteoporosis	
Drugs	**Rheumatological diseases**
- Glucocorticoids	- Rheumatoid arthritis
- Aromatase inhibitors	- Ankylosing spondylitis
- Proton pump inhibitors	**Haematological diseases**
- Glitazones	- Multiple myeloma
- Anti-epileptics	- Systemic mastocytosis
- Loop-acting diuretics	- Leukaemia
- Heparin and warfarin	**Neurological diseases**
- Antidepressants	- Stroke
Endocrine diseases	- Immobilization
- Anorexia nervosa	- Parkinson disease
- Hypogonadism	**Other diseases**
- Cushing syndrome	- Congestive cardiac failure
- Vitamin D deficiency	- Chronic obstruction lung disease
- Hyperparathyroidism	- Chronic renal insufficiency
- Hyperthyroidism	- Osteogenesis imperfecta
- Diabetes mellitus	- Marfan syndrome
Gastrointestinal disease	- Ehlers-Danlos syndrome
- Malabsorption	- Human immunodeficiency virus infection (and its treatment)
- Inflammatory bowel diseases	

Apart from the above-mentioned diagnostic tools, risk assessment tools have also been developed such as the Fracture Risk Assessment Tool (FRAX). FRAX is an algorithm which was developed in 2008 to evaluate fracture risk of patients based on individual patient models that integrate the risks associated with clinical risk factors with or without BMD and is now incorporated into clinical practice guidelines[355]. It estimates the 10 year probability of major osteoporotic fractures and a 10 year probability of hip fracture alone[356]. But like many algorithms FRAX has its limitations such as only taking into account an average dose or exposure[322].

1.8.4 Management

In the management of osteoporosis, the aims of intervention are to prevent bone loss in individuals at risk of osteoporosis or in patients with osteoporosis and reduce the incidence of osteoporotic fractures[325].

The choice of intervention and the cost-effectiveness of any management strategy is determined by absolute fracture risk, therefore younger people at a lower risk will receive lifestyle recommendations whereas older people at a higher risk will receive pharmacological interventions[325]. When considering pharmaceutical intervention, general preventive measures should be implemented for at risk patients and these include avoidance of modifiable risk factors such as smoking and excessive alcohol consumption. Patients should start vitamin D and calcium supplementation, increase protein intake, and weight-bearing[322]. These general measures can slow down bone loss but do not restore BMD and cannot be used as a form of therapy for patients at high risk of fracture[356].

Medications used in the treatment of osteoporosis are divided in to two categories: antiresorptive therapy, such as bisphosphonates, oestrogens, calcitonin and denosumab (monoclonal antibody to RANKL); and bone forming treatments, such as teriparatide and most recently, Romosozumab[325].

1.8.4.1 Antiresorptive agents

Antiresorptive agents target the formation, function and survival of osteoclasts therefore reducing bone resorption rates but this is followed by a decrease in osteoblast activity[357].

Bisphosphonates include alendronate, risedronate, ibandronate and zoledronic acid, and are the most commonly used agents for managing osteoporosis. They are synthetic analogues of the naturally occurring compound pyrophosphate and act by binding to calcium phosphate mineral component of bone. Osteoclasts can then resorb the calcium phosphate with the bound bisphosphonate which subsequently suppresses osteoclast activity[358]. They have been shown to reduce hip fracture risk by up to 50%[359] and vertebral fracture by 40 to 70%[360].

Bisphosphonates can be administered orally, however ibandronate and zoledronate can be given intravenously. The choice between the different treatments depends on side-effects, compliance, cost and convenience. Due to the fact that they are poorly absorbed by the intestine, oral bisphosphonates should be administered in the morning on an empty stomach with water, 30 to 60 minutes prior to a meal and patients should remain upright for at least 30 minutes post administration[361]. The reason being is that oral bisphosphonates can cause gastrointestinal disturbances such as in cases of gastro-oesophageal reflux. On the other hand, intravenous bisphosphonates can cause flu-like symptoms and in addition patients with severe pre-existing kidney disease may suffer acute renal failure and all bisphosphonates are contraindicated in severe kidney impairment[315]. Furthermore, there are potential concerns with long-term suppression of bone turnover associated with prolonged treatment with bisphosphonates as there are reports of this leading to atypical femoral fractures[362]. A rare side-effect associated with high dose intravenous bisphosphonate therapy is osteonecrosis of the jaw which is defined as the presence of exposed and necrotic bone in the maxillofacial region[363]. The occurrence of such side-effects and the administration methods may account for poor treatment compliance.

Another type of antiresorptive treatment is denosumab, a monoclonal antibody directed against RANKL which is administered every 6 months for 36 months via subcutaneous injections[315]. It acts by binding to RANKL and preventing the

interaction of RANKL with its receptor RANK which results in rapid and profound inhibition of bone resorption[364]. Denosumab reduces the risk of vertebral and non-vertebral fractures, and hip fractures in women with osteoporosis[364]. As denosumab is administered every 6 months as a subcutaneous injections it encourages greater adherence to treatment than that observed during bisphosphonate treatment, although denosumab is also associated with atypical femoral fractures and osteonecrosis of the jaw[364].

1.8.4.2 Anabolic agents

Teriparatide, which is a recombinant human parathyroid hormone peptide, and PTH, a recombinant human PTH, are anabolic treatments that increase bone formation and lead to large increases in BMD in the spine[320]. They are both administered daily by subcutaneous injection for a limited time of 18-24 months due to the increased risk of bone tumours observed in rodents when treated with high doses of teriparatide[356,365]. For this reason, patients that have had previous radiation therapy to the skeleton or skeletal malignancies should not receive this type of treatment.

Romosozumab, a more recent therapy, is a humanized monoclonal antibody that inhibits sclerostin which is applied subcutaneously once a month[164]. Phase III FRAME trials in female patients suffering from postmenopausal osteoporosis showed increases in BMD of 13% and 17% at the lumbar spine and hip, respectively, and reduced risk of vertebral and clinical fractures upon transitioning to denosumab[366]. However, treatment with romosozumab lead to serious adverse effects such as cardiovascular events compared with alendronate but not a placebo, therefore further studies are being performed[367].

1.8.4.3 Hormone replacement therapy

Oestrogen replacement therapy, with or without progestin administration, has been shown to prevent bone loss and to reduce fracture risk of the spine and hip in postmenopausal women[368]. However, oestrogen treatment can lead to increased cardiovascular events, stroke and breast cancer risk, therefore it is only used short-term[369], and should not be administered to women with thrombophlebitis or

thromboembolic disorders, or with breast or uterine cancers[325]. Although this treatment has a lower cost than other anti-osteoporosis treatments the risk outweigh the benefits and therefore there is a lot of uncertainty about prescribing this form of therapy[369].

Due to the ageing population and the increase in osteoporosis among the population, and despite the increasing number of effective drugs to treat osteoporosis there is still a need to develop new therapies that have less side-effects and simpler treatment protocols which in turn will lead to a higher treatment compliance.

1.9 Aims

Studies have shown that there are a number of genetic risk factors that can play a major role in bone loss and osteoporosis, but research is still required to identify genes that regulate bone mass and other markers of osteoporotic phenotypes[370–372]. Osteoporosis is considered polygenic and although there are various studies identifying genes that impact bone mass it is still unclear how these genes interact with each other and how this affects bone development and maintenance[371,372]. Varanasi *et al.* identified the proteoglycan syndecan-mediated signalling pathway as being one of the top three site-specific pathways preferentially induced in the spine, which bears mechanical stress, versus the iliac crest, which bears less mechanical stress, in humans[371]. As previously mentioned, syndecans are a family of four of transmembrane haparan sulphate proteoglycans[274,276], of which Syndecan 3 is the least studied of all syndecans. Syndecans 1, 2 and 3 have been shown to be important during bone development due to their expression levels in endochondral and periosteal bone and syndecan 4 is expressed in chondrocytes and osteoblasts and has been shown to have an important role in osteoarthritis[299,373]. As with other members of the syndecan family, syndecan 3 functions as an extracellular matrix receptor and as co-receptor for growth factors [308]. It plays a central part in condensations, a crucial phase of skeletogenesis, such as precartilage condensations, by setting boundaries which limits the condensation size[208,300] and has a role during

limb development by regulating chondrocyte proliferation[301,374,375]. Syndecan 3 has also been demonstrated to be involved in the development and differentiation of the central nervous system, lens, sclerotomes and feather buds[300]. It is highly expressed in differentiating periosteal osteoblasts and calvaria, suggesting it may be involved in regulating chondrogenesis and osteogenesis[289,300,308]. Interestingly, Sdc3 knock-out (Sdc3 KO) mice have improved regeneration in repeatedly injured muscle and muscle ageing [178] and are resistant to diet-induced obesity[376]. So far, its role in the adult skeleton and age-related bone loss is unknown, but it was observed by our collaborator, Dr. Addolorata Pisconti, that while handling the Sdc3 KO mice for experimental purposes, their bones would often break easily. Therefore, the overall aim of this project was to investigate the role of syndecan 3 in bone metabolism. The specific aims were as followed:

1. Determine the effect Sdc3 deletion on bone volume and architecture in a Sdc3 KO transgenic mouse.
2. Determine the effect of Sdc3 deletion on bone turnover using dynamic bone histomorphometry.
3. Determine the effect of Sdc3 deletion on bone response to mechanical loading in the Sdc3 KO mouse.
4. Determine the role of Sdc3 deletion on osteoclast and osteoblast differentiation and activity *in vitro*.

2 Materials and methods

2.1 Reagents

Table 2.1: List of reagents.

Reagent	Catalogue number	Company
4-nitrophenol solution	N7660	Sigma Aldrich, UK
αMEM	32571	Life Technologies, USA
Accutase	A1110501	Fisher Scientific, USA
Acetic acid	305238	Scientific Laboratory Supplies, UK
Acid Fuchsin	F8129	Sigma Aldrich, UK
Alexa Fluor 488		Life technologies, USA
Alexa Fluor 800		Life technologies, USA
Alizarin Red S	A5533	Sigma Aldrich, UK
Alamar Blue	DAL1025	Fisher Scientific, USA
Analine Blue	415049	Sigma Aldrich, UK
Anti-Ki67 rabbit antibody	Ab15580	Abcam, UK
B-glycerol phosphate	G9422	Sigma Aldrich, UK
Blocking buffer	(TBS)927-50010	LICOR, UK
Calcein Blue	M1255	Sigma Aldrich, UK
Calcein Green	C0875	Sigma Aldrich, UK
Cetylpyridinium Chloride	C0732	Sigma
Chloroform	C2432	Sigma Aldrich, UK
Collagenase, type 1a	C9891	Sigma Aldrich, UK
Dexamethasome	D4902	Sigma Aldrich, UK
Di-butyl phthalate	524980	Sigma Aldrich, UK
Diethanolamine	D8885	Sigma Aldrich, UK
Dimethylformamide	D4551	Sigma Aldrich, UK
DMEM	D5671	Sigma Aldrich, UK
DMSO	0231	VWR, USA
EDTA	E6758	Sigma
Ethanol Absolute	E7023	Honeywell, USA
Ethanol (histology)		Fisher scientific
EvoScript Universal cDNA Master	07912455001	Roche, Switzerland
Ferric acid	F7134	Sigma Aldrich, UK
Formical 2000	DCF20GAL	American Master Tech, USA
Glacial acetic acid	305238	Scientific Laboratory Supplies, UK
Harris Hematoxylin	3801560BBE	Leica, UK
HBSS	14025	Life Technologies, USA
HEPES	H3874	Sigma Aldrich, UK
Hydrochloric acid	320331	Honeywell,USA
IBMX	15879	Scientific Laboratory Supplies, UK

Insulin	15500	Scientific Laboratory Supplies, UK
Isopropanol	278475	Sigma Aldrich, UK
L-Ascorbic acid	49752	Sigma Aldrich, UK
Lightcycler 480 probes master	04887301001	Roche, Switzerland
Light green	214566	Sigma Aldrich, UK
M-CSF	Cyt-439	Prospec
Methoxyethyl acetate	109886	Honeywell, USA
Methyl methacrylate	1955909	Sigma Aldrich, UK
MgCl2	M2670	Sigma Aldrich, UK
NaCl	S7653	Sigma Aldrich, UK
Naphtol AS BI phosphate	N2125	Sigma Aldrich, UK
Naphtol AS TR phosphate	N6125	Sigma Aldrich, UK
Neutral buffered formalin		Leica, UK
Non-immune goat serum		Vector, USA
Non-phosphorilated β-catenin rabbitantibody	Ab32572	Abcam, UK
Orange G	03756	Sigma Aldrich, UK
Paraformaldehyde		Sigma Aldrich, UK
Pararosanaline	MKBP3538V	Sigma Aldrich, UK
PBS	D8537	Sigma Aldrich, UK
Phosphotungstic acid	P4006	Sigma Aldrich, UK
B-actin mouse antibody	Ab8226	Abcam, UK
Perilipin rabbit antibody	Ab61682	Abcam, UK
Qiazol		Qiagen, Germany
Recombinant Wnt3a antibody	Ab219412	Abcam, UK
RNeasy Micro kit		Qiagen, Germany
SDS	L4509	Sigma Aldrich, UK
Sodium acetate anhydrous	S2889	Sigma Aldrich, UK
Sodium hydroxude	655104	Sigma Aldrich, UK
Sodium phosphate	342483	Sigma Aldrich, UK
Surgipath Paraplast formula R		Leica, UK
Tris HCl	T3253	Sigma Aldrich, UK
Triton X-10	T6878	Rohn & Haas Company, Germany
Trizol		Qiagen, Germany
Tween 20	P7949	Sigma Aldrich, UK
Uni-Trieve	NB325	Innovex biosciences, USA
Urea	U6504	Sigma Aldrich, UK

Vectashield mounting medium with DAPI	H1200	Vector, USA
Xylene	X0250	Fisher scientific, USA

2.2 General

2.2.1 Animals

Sdc3 KO mice on a C57Bl6 background[377] were obtained from the laboratory of Dr. Addolorata Pisconti, University of Liverpool, United Kingdom. Animals were housed in a pathogen-free facility, at the University of Liverpool. All procedures were in accordance with the Animals (Scientific Procedures) Act 1986 and the EU Directive 2010/63/EU and after the local ethical review and approval by Liverpool University's Animal Welfare and Ethical Review Body (AWERB). Sdc3 KO were generated from heterozygote breeding. Control mice were littermates and age- and sex-matched on the C57Bl6 background.

2.2.2 Mechanical testing by three-point bend test

To determine bone stiffness and breaking strength three-point bending tests were performed with a material testing machine (Zwick/ Roell Z0.5, Switzerland) fitted with a 50 N load cell. Femurs were mounted on two supports 8mm apart with the anterior part facing upwards (**Figure 2.1**). All femurs were mounted in the same way to reduce variability between specimens.

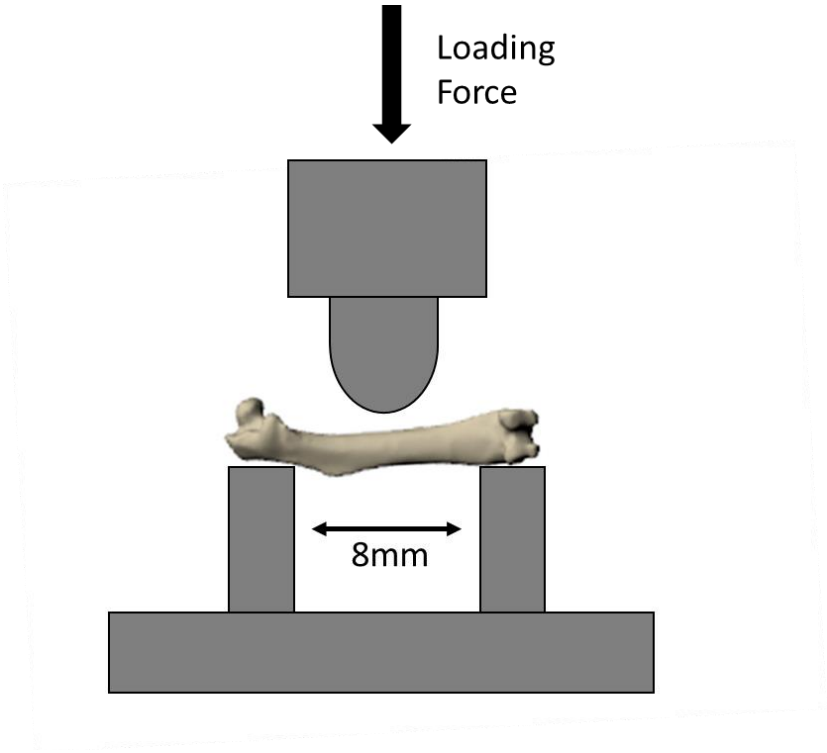

Figure 2.1: Diagram of a three-point bending test.

Axial bending load was applied to the femurs of 3-month-old wild-type (WT) and Sdc3 KO male mice and tested until failure, at which point the bones fracture. The cross-head was lowered at 1mm/min and force was recorded after every 0.7 µm change in deflection. Failure and fractured points were identified from the load-extension curve as the point of maximum load and where the load rapidly decreased to zero, respectively. The stiffness was defined as the slope of the linear portion of this curve.

2.2.3 Bone imaging by microCT

Left legs, right legs and spines of WT and Sdc3 KO mice at 3 and 6-months-old were harvested and fixed overnight in Neutral buffered formalin and stored in 70% ethanol. Bones were then scanned by µCT using a Skyscan 1272 system (SKYSCAN, Belgium) with a rotation step size of 0.3° over 180°, an isotropic resolution set at 4.5µm, X-ray source at 50 kV and 200 µA, 0.5 mm aluminium filter, no camera binning and no averaging. Images were reconstructed using Skyscan "NRecon" software (SKYSCAN, Belgium) which provides images of the analysed bones slice-by-slice. The reconstructed set of slices were then viewed in Skyscan's "-Data-Viewer-" software

(SKYSCAN, Belgium) to allow reorientation of the scans and select a defined volume of interest for analysis (**Figure 2.2**). Using Skyscan "CT-Analyser" (SKYSCAN, Belgium) or "CTAN" software (SKYSCAN, Belgium) the data set was then analysed for morphometry using a macro (details in appendix) with a fixed threshold to differentiate mineralised bone from soft tissue. For trabecular analysis measurements were taken from 200 slices immediately distal to the growth plate of tibias and immediately proximal to the growth plate of femurs. For cortical analysis 100 slices immediately distal the end of the trochanter of the femur and proximal to the tibio-fibular junction of the tibia (**Figure 2.2**). Trabecular bone was separated from cortical bone using a CTAN macro (details in Appendix), and the same macro then performed measurements of the cortical and trabecular parameters according to ASBMR guidelines[378]. Spines were also scanned with the same parameters as described above and analysed with the volume of interest being between the growth plates of the lumbar vertebrae 5 (L5) (**Figure 2.3**). With CTAN, a circle of approximately 0.9mm was used to delineate the area of interest of the vertebrae, encompassing as much trabecular bone as possible excluding cortical bone and then analysed with a macro (details in Appendix) to measure trabecular bone only. For the 2-day-old pups, whole skeletons were scanned at a resolution of 9 µm and reconstructed as detailed above. The data set was analysed with Skyscan CTAN with a macro (details in Appendix) which allowed to differentiate soft tissue from bone using a fixed threshold and tibial bone volume measured between the proximal and distal growth plates.

For tibial length measurements of 3-month-old mice, the distance between proximal and distal growth plates was measured on the µCT scans described above using Data Viewer. For the tibial length measurements of the pups, the full length of mineralised tibial diaphysis at P2 was measured on µCT longitudinal scans of 9µm scans using Data Viewer.

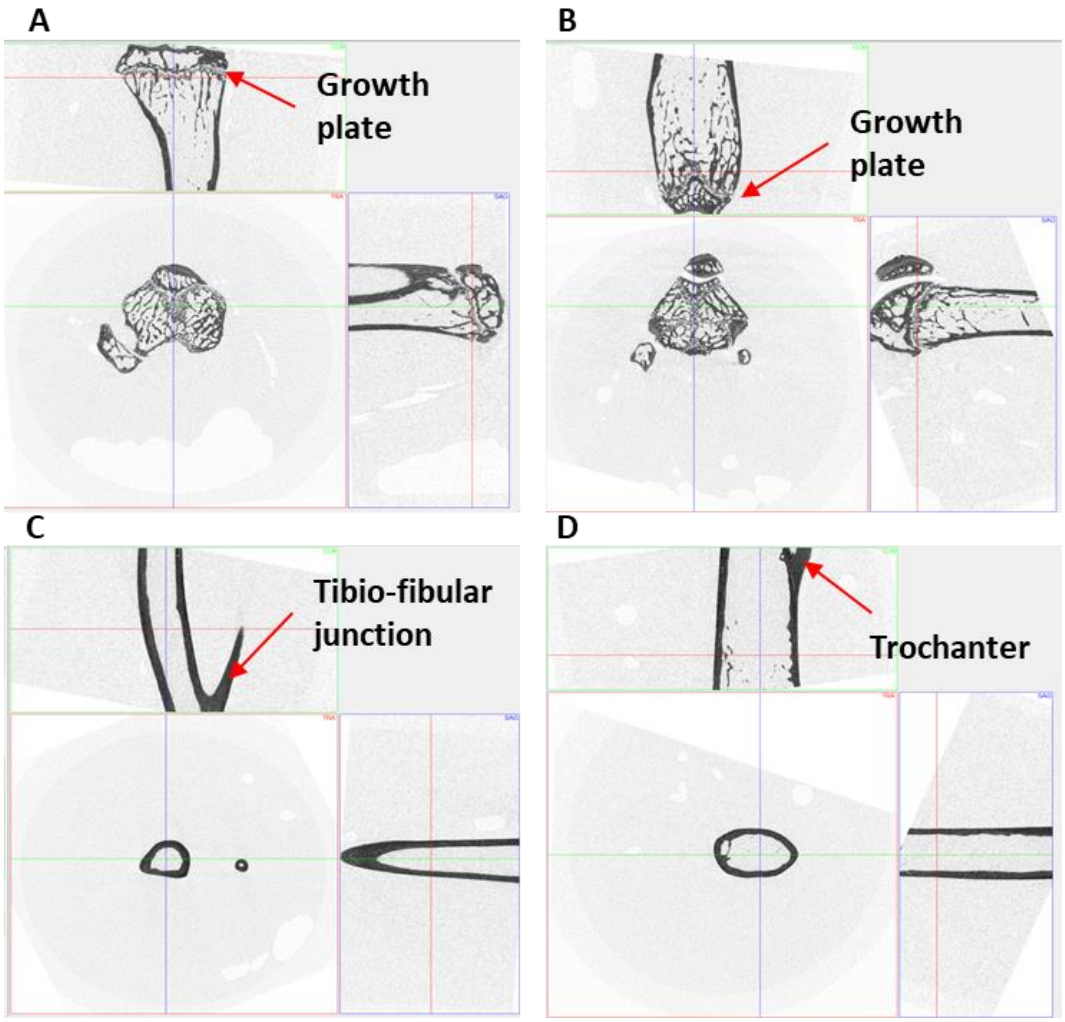

Figure 2.2: Screenshots from Skyscan "Data-Viewer" – software. Images illustrate the selected regions for trabecular analysis of tibias (**A**) and femurs (**B**) and for cortical analysis of tibias (**C**) and femurs (**D**)

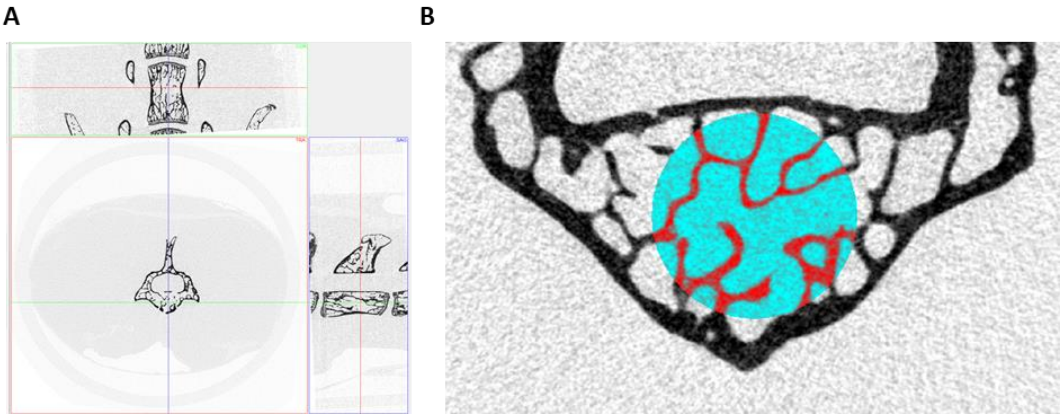

Figure 2.3: Screenshots taken from Skyscan "Data-viewer"- software (A) and CT-AN – software (B). Images show selected regions for trabecular analysis of the L5 **(A)** and the region of interest **(B).**

2.3 Histology

2.3.1 Bone histomorphometry

Mice received two intra-peritoneal (IP) injections of calcein (200µl IP injection of 2mg/ml) 5 days and 2 days before culling. Legs were then fixed in neutral buffered formalin for 24 hours and then stored in 70% ethanol. After µCt analysis, tibia samples were processed with a Leica ASP300 tissue processor (Leica Microsystems, UK) and dehydrated through a series of alcohol washes and cleared in xylene (**Table 2.1**). Samples were then infiltrated at 4°C under vacuum with a mixture of 88.99% methyl methacrylate (MMA), 10% di-butyl phthalate, 1% Perkadox 16 and 0.01% Tinogard for 7 days. Next, Teflon embedding blocks were filled with methyl methacrylate and bones were placed in the sample wells. The wells were sealed with air-tight lids and the blocks were left to polymerise in a water bath at 30°C at least overnight until polymerisation was complete. Then, lids were removed and embedding rings were attached by adding a mixture of two parts yellow cold curing resin powder with one-part Technovit mounting media. Blocks were left to harden for at least 2 days before sectioning at 5µm with a Leica RM2265 motorised microtome (Leica Microsystems, UK) fitted with a tungsten steel D-profile knife. Sections were mounted on to Leica X-tra slides, covered with kissol film and placed under pressure with a slide-press in a dry incubator at 37°C for 48 hours. This protocol is based on a protocol described by van 't Hof *et al.*[379].

Table 2.2: Dehydration steps.

Steps	Solution in basket	Processing Time
1	70% EtOH	30min
2	80% EtOH	2h
3	96% EtOH	2h
4	100% EtOH	3h
5	100% EtOH	3h
6	Xylene	1h
7	Xylene	12h

2.3.1.1 Calcein staining

For analysis of bone formation, sections were stained, without being deplasticised, for 3 minutes in 0.1% Calcein Blue, pH8. The sections were washed 3 times in water, dehydrated though a decreasing alcohol series, cleared in xylene and

coverslipped using the automatic coverslipper of a Leica auto stainer. The sections were then visualised using the Zeiss Axio Scan.Z1 slide scanner (Carl Zeiss LTd., UK) with a monochrome camera and a 20x lens resulting in a pixel size of 0.227 µm. Bone histomorphometric analysis of bone formation parameters was performed using a custom in-house developed image analysis program based on ImageJ, available at https://www.liverpool.ac.uk/ageing-and-chronic-disease/bone-hist/ (developed by Prof. Rob van 't Hof[379]).

2.3.1.2 Tartrate-resistant acid phosphatase (TRAcP) staining

For analysis of bone resorption parameters, sections were stained for tartrate-resistant acid phosphatase (TRAcP), to identify osteoclasts, and Aniline Blue, to identify bone. This staining method was based on the method described by Chappard *et al.* [380] and Van 't Hof *et al.* [379]. Sections were deplasticised in 3 changes of 2-methoxyethyl acetate (MEA), cleared in two changes of Xylene and taken through a decreasing alcohol series to water **(Table 2.3)**. The sections were incubated at 37°C for up to 2 hours in a staining solution of naphtol ASBI-phosphate (1.4mg/ml) and fast red (1.4 mg/ml) in a 0.2 M acetate buffer (pH 5.2) containing 50 mM sodium tartrate. After the TRAcP stain the sections were washed in two changes of distilled water and counterstained for 15 min using 0.33 g/l Aniline Blue and 6g/l phosphotungstic acid in water, and briefly washed in three changes of water. The sections were then coverslipped using Apathy's serum. For the imaging of the TRAcP stained sections, a Zeiss Axio Scan.Z1 slide scanner (Carl Zeiss Ltd., UK) in brightfield mode was used with a 10× lens together with a colour camera resulting in a pixel size of 0.442 µm. Analysis was performed using a custom in-house developed analysis program based on ImageJ, available at https://www.liverpool.ac.uk/ageing-and-chronic-disease/bone-hist/ (developed by Prof. Rob van 't Hof[379]).

Table 2.3: Deplasticizing steps. Steps performed to remove the resin from the sections to allow stains to penetrate the tissue.

Steps	Solution in basket	Processing time
1	MEA	20min
2	MEA	20min
3	MEA	20min
4	Xylene	10min
5	Xylene	10min
6	100% EtOH	2min
7	100% EtOH	2min
8	80% EtOH	1min
9	70% EtOH	1min
10	50% EtOH	1min
11	Distilled water	1min

2.3.1.3 Goldner's Trichrome staining

For bone marrow fat analysis, sections were deplasticized, following the parameters described in Table 2.3, and placed in freshly made Weigert's Solution[381], which is made up of equal parts of Weigert's Iron Haematoxylin solution A and Weigert's Iron Haematoxylin solution B, for 30 minutes. Next, sections were washed in running tap water for 10 minutes, rinsed with distilled water then stained in Ponceau Acid Fuchsin for 30 minutes. Next, sections were rinsed in 1% Acetic acid, placed in Phosphomolybdic Acid-Orange G solution for 5 minutes, rinsed in 1% acetic acid for 30 seconds, stained in Light Green stock solution for 10-15 minutes and rinsed again in 1% acetic acid for 5 minutes. Sections were then blotted dry, dehydrated in 3 baths of 2-propanol and 2 baths of 70% EtOH and finally slides were coverslipped using the Leica CV5030 automated coverslipper (Leica Microsystems, UK). For imaging of Goldner's Trichrome stained sections, a Zeiss LSM800 confocal microscope (Carl Zeiss Ltd., UK) on brightfield mode using a 10x lens and quantified using and in-house developed program (FatHisto) based on ImageJ developed by Prof. Rob van' t Hof. For details on solutions please see Appendix 1.

2.3.2 Immunohistochemistry

For immunohistochemistry analysis, tibias were dissected and cleared of soft tissue, placed in neutral buffered formalin for 24 hours and then stored in 70% ethanol. After µCT analysis, samples were decalcified in Formical 2000 decalcification solution overnight on a rocking platform at room temperature. Samples were then processed using a Leica ASP300 tissue processor (Leica Microsystems, UK) as described in **table 2.4**.

Table 2.4: Wax processing steps.

Solution	Duration	Temperature
70% EtOH	15min	Room temperature
90% EtOH	60min	Room temperature
100% EtOH	20min	Room temperature
100% EtOH	40min	Room temperature
100% EtOH	60min	Room temperature
100% EtOH	120min	Room temperature
Xylene	20min	Room temperature
Xylene	40min	Room temperature
Xylene	60min	40°C
Wax	30min	62°C
Wax	60min	62°C
Wax	150min	62°C

After processing, samples were embedded within Surgipath Paraplast into embedding cassettes with the aid of the Leica EG1150 H embedding station. Next, tissue was sectioned using a Thermo-Fisher HM 355S Automatic microtome fitted with a Cool-cut Section Transfer System (Thermo-Fisher, USA).

2.3.2.1 Perilipin immunostaining

Sections were dewaxed (**Table 2.5**), incubated in Unitrieve solution for 30 minutes in an oven at 50°C. The Unitreve solution was then removed and the sections blocked in non-immune goat serum for 30 minutes. Next, sections were incubated in

primary rabbit perilipin antibody at 1:500 dilution in blocking buffer overnight at 4°C. After primary antibody incubation, samples were washed 3 times in PBS, incubated for an hour in a 1:200 dilution of secondary goat anti rabbit Alexa Fluor 594 (Invitrogen), washed again 3 times in PBS and coversliped with Vectorshield containing DAPI and sealed with nail varnish. Controls exposed to no primary antibody were also performed to confirm specificity of staining. The sections were then visualised using the Zeiss Axio Scan.Z1 slide scanner (Carl Zeiss Ltd., UK) with a monochrome camera and a 20x lens resulting in a pixel size of 0.227 µm.

Table 2.5: Dewax steps. Steps performed to remove the wax from the sections to allow stains to penetrate the tissue.

Steps	Solution in basket	Processing time
1	Xylene	2min
2	Xylene	2min
3	100% EtOH	1min
4	90% EtOH	1min
5	70% EtOH	1min
6	Distilled water	1min

2.3.3 *In vivo* loading

The right tibia of 10-week old WT (N=6) and Sdc3 KO (N=8) male mice were loaded in accordance to the model described by De Souza *et al.* for investigating tibial cancellous and cortical bone response to loading[382]. Mice were kept under isoflurane anaesthetic throughout the procedure in order to keep tibias positioned correctly. Tibias were held between padded cups vertically, as shown in **Figure 2.4**, with both knee and ankle in deep flexion. Dynamix axial loads were applied with a mechanical test instrument (ElectroForce 3100, TA instruments, USA) through the knee joint via the upper loading cup, attached to the actuator, for 40 cycles at 11N and a frequency of 0.1 Hz, with 10 second rest between cycles, three times a week over 2 weeks[382]. The lower cup was linked to the load cell allowing the applied load to be monitored. The left tibia was used as a contra-lateral control. To assess bone formation, each

mouse received IP injections of calcein (200µl IP injection at 2mg/ml) 5 days and 2 days before culling. Histomorphometry analysis was performed as described above.

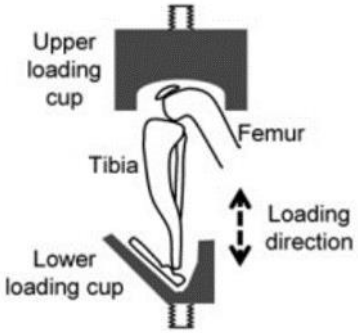

Figure 2.4: Diagrammatic representation of the loading model. Estimated position of the flexed mouse hind limb when placed in the loading apparatus, showing approximate position of the bones relative to the upper and lower loading cups and the loading direction[383].

2.4 Tissue culture

2.4.1 Isolation and culture of bone marrow macrophages and osteoclasts

Bone marrow was obtained from 8-week-old WT and Sdc3 KO female mice. First, after culling, animals were skinned and hind limbs were removed. All soft tissue was removed from bones by scraping the bones thoroughly with the aid of a scalpel. Tibias and femurs were separated, and the epiphyses were cut off. The diaphysis were opened using a 27 gauge hypodermic needle. Bones of each limb were then put in to a 500µl Eppendorf containing a hole in the bottom of the tube. This small Eppendorf was contained in a 1.5ml Eppendorf with 125µl of complete αMEM (supplemented with 10% FCS and 1% P/S). The Eppendorfs were centrifuged in a 1-14 Microfuge (Sigma, UK) at 800x*g* for 3 minutes at room temperature. This resulted in the bone marrow being flushed out of the bones and collected in the larger Eppendorf. The pellets of each Eppendorf were resuspended, collected and transferred to a petri dish containing 10ml of standard αMEM supplemented with M-CSF at 100 ng/ml. Cells were incubated for 3 days at 37°C in a humidified 5% CO_2 atmosphere to allow the attachment of the cells. After 3 days medium was removed, cells were washed in PBS to remove all non-adherent cells and fresh media supplemented with M-CSF at 100ng/ml. Cells were left to grow until confluent with medium changes performed every 3 days.

For osteoclast generation, confluent macrophages were lifted by removing medium, washing in PBS and adding 2.5ml of Accutase. Cells were then incubated for 3 minutes at 37°C in a humidified 5% CO_2 atmosphere to allow cells to detach. When detached, 5.5 ml of medium was added to the tissue culture dish and the resulting cell suspension transferred to a 15ml tube making sure most of the cells were transferred. The cell suspension was then centrifuged at 300x*g* for 3 minutes. Supernatant was discarded and pellet resuspended in 5 ml of medium. Cells were then counted with the aid of a TC20 automated cell counter (Bio-Rad, USA).

For RANKL dose response assays cells were plated ($15x10^4$ cells/ml) in a 96-well plate in a total volume of 150µl, 5 wells for each RANKL concentration (0, 10, 25, 50 and 100ng/ml). Cells were incubated at 37°C in a humidified 5% CO_2 atmosphere in standard αMEM supplemented with 25ng/ml of M-CSF and the appropriate concentration of RANKL (kindly donated by Dr Jim Dunford, University of Oxford, Oxford, UK) for up to 7 days with medium changes every other day.

For resorption assays, prior to seeding, dentin slices were sterilised and placed in the well of a 96-well plate. Next, cells were added ($15x10^4$ cells/well) to the dentin slice in a drop of 25µl, incubated for 1 hour for cells to attach to the dentin slice and the remaining 125µl of medium added containing M-CSF at 1:4000 dilution and 100ng/ml of RANKL. Cells were incubated at 37°C in a humidified 5% CO_2 atmosphere with half the medium exchanges performed every 2-3 days.

To obtain RNA, macrophages were plated on 6-well plates ($6x10^5$ cells/well) and cultured in complete αMEM. For generation of macrophages, the culture media was supplemented with M-CSF (100ng/ml) while to generate pre-osteoclasts and osteoclasts media was supplemented with M-CSF (25ng/ml) and RANKL (100ng/ml). Macrophages were cultured until confluent, pre-osteoclasts were cultured for approximately 2 days and osteoclasts were cultured for 5 to 6 days.

2.4.1.1.1 Tartrate resistance acid phosphatase (TRAcP) staining

After end of the culture period, cells were fixed in 4% PFA for 10 minutes and washed twice in PBS. For TRAP staining solution I mixed solution 1 and 2 together (**details of solutions can be found in appendix 1**), filtered the solution mix and added 50µl of the mix to each well. The plate was incubated for at least 30 minutes at 37°C.

Before removing the stain, plates were checked under the microscope for red osteoclasts. After confirming osteoclasts were stained, staining solution was removed, cells were washed in distilled water and stored in 70% ethanol at 4°C until osteoclast counts were performed. For the osteoclast counts, TRAP positive cells with more than 3 nuclei were counted with the aid of a microscope. Osteoclast nuclei counts were taken from wells stimulated with 100ng/ml of RANKL, also of TRAP-positive cells containing more than 3 nuclei.

2.4.1.1.2 Resorption assay

After 14 days of culture (as detailed in section 2.3.1), medium was removed, cells were washed in PBS and fixed in 4% PFA for 10 minutes at room temperature. Cells were then stained for TRAP and TRAP positive cells were counted using a microscope. Next, dentin slices were cleaned and imaged using an Olympus reflected light microscope fitted with a 5x lens and a Zeiss camera. Pits are visible as dark areas on a light grey background using this technique (see figure 5.3 in chapter 5). Resorption was measured using custom software based on ImageJ developed by Prof van 't Hof.

2.4.1.1.3 RNA extraction of osteoclasts and macrophages

Extraction of RNA was performed using the RNeasy Micro kit (Qiagen, Germany) according to the manufacturer's instructions as follows: Medium was removed from wells and cells were washed gently once in PBS. To the washed cells, 700µl of Qiazol was added to each well to lyse the cells. The cell lysates were collected through thorough scraping. This was transferred into separate microcentrifuge tubes.

The lysates were vortexed for 1 minute in order to homogenize the samples. The lysates were incubated at room temperature for 5 minutes. To each sample, 140µl of chloroform was added and then shaken vigorously. The samples were incubated at room temperature for 2-3 minutes and then centrifuged in a 5415 R centrifuge (Eppendorf, Germany) at 12,000g for 15 minutes at 4°C. The upper aqueous phase (~350µl) was transferred to a new microcentrifuge tube and 1.5 times the volume in the tube (~525µl) of 100% ethanol was added and mixed by pipetting up and down.

To the spin columns provided by the kit, 700µl of the sample was added and these were centrifuged at 8,000g for 15 seconds at room temperature. Flow-through was discarded and procedure was repeated if needed. To each sample, 500µl of RPE buffer was added and the tubes were centrifuged at 8,000g for 15 seconds at room temperature. Flow-through was discarded and 500µl of RPE was added again and tubes centrifuged at 8,000g for 2 minutes at room temperature.

To elute the RNA from the spin columns, they were transferred to a new Eppendorf and 30µl of RNase-free water was added. Tubes were centrifuged at 8,000g for 1 minute, at room temperature. A further 30µl of RNase-free water was added and tubes were centrifuged at 8,000g for 1 minute. Finally, RNA quantities and purities were assessed using the NanoDrop 2000^{TM} spectrophotometer (Thermo Fisher, USA). RNA samples were stored at -80°C until used.

2.4.2 Osteoblast culture

2.4.2.1 Osteoblasts isolation

Bone chips

To isolate osteoblasts from bone chips, after obtaining bone marrow from femurs and tibias as described above, the clean bones were cut into small fragments using a scalpel. The fragments were then transferred to a T25 flask containing 5ml of 1mg/ml collagenase. Flasks were then incubated in a shaking water bath at 37°C for 1 hour. Next, the supernatant was discarded and bone chips were washed vigorously in HBS at least 3 times until fragments were separated from each other. When fragments were no longer clumping together, HBS was removed and 5ml of complete αMEM added. Flasks were incubated for 5 days in a humidified incubator at 37°C with 5% CO_2. After 5 days, medium was removed, bone chips were washed in PBS and fresh medium was added. Flasks were maintained for up to 1 month, with half medium changes performed twice a week, until confluency was reached at which point cells were trypsinized, bone chips removed and cells transferred to a T75 flask and cultured until confluent. When confluency was reached, the cells were plated in 6 well plates ($6x10^5$ cells/well) for RNA/DNA/Protein studies and grown in complete αMEM until confluent, in 12 well plates (100 000cells/well) for mineralisation assays by growing cells in complete DMEM (supplemented with 10% FCS and 1% P/S)

containing 2mM of BGP and 50µg/ml of L-Ascorbic Acid for 21 days with half medium changes performed every other day, in 96-well plates (15 000 cells/well) for alkaline phosphatase assays and on coverslips in 12-well plates (100 000 cells/well) for cell proliferation assays.

Calvaria

For isolation of osteoblasts from calvaria, WT and Sdc3 KO 2-day old pups were sacrificed, sprayed with 70% ethanol and the scalp was delicately removed. Then, coronal and lambdoid sutures were identified and cuts were performed around them with the aid of scissors. The calvarial bones were removed and transferred to a petri dish containing 10 ml of PBS. After all calvaria were dissected from an individual litter, these were transferred to a T25 flask and washed twice in HBS. After washes, HBS was removed, 5ml of 1mg/ml collagenase was added and flasks were incubated in a shaking water bath at 37°C for 10 minutes. Then, supernatant was discarded and a second collagenase digestion was performed for 30 minutes. Next, supernatant was kept in a 15 ml falcon tube which was then centrifuged at 300g for 3 minutes, supernatant discarded, the pellet was resuspended in 1 ml of complete αMEM and the tube was set to one side. The flask containing the calvaria was washed twice in PBS and 5ml of 4mM EDTA was added. Flasks were incubated in a shaking water bath at 37°C for another 10 minutes. Next, the supernatant was kept as described before and flask containing calvaria was washed twice in HBS and a final collagenase digest was performed for 30 minutes. After, supernatant was kept as described before and all 3 fractions were combined and transferred to a T75 flask and medium was added to make up 15 ml. to the flask containing the calvaria, fresh medium was added. Both flasks were incubated in a humidified incubator at 37°C with 5% CO_2 until cells reached confluence. When confluence was reached, cells were plated in 12-well plates (100 000cells/well) and after reaching confluence were grown in osteogenic medium made up of complete DMEM containing 2mM of BGP and 50µg/ml of L-Ascorbic Acid for 21 days with half medium changes performed every other day.

Bone marrow stromal cells

For isolation of MSCs, bone marrow was extracted as described previously **(2.4.1**), transferred to a 15ml falcon tube and resuspended in 12ml of complete αMEM. Next, the cells were plated directly in to 12-well plates, 1 ml per well, and grown until confluent. When confluence was reached cells were grown in either osteogenic conditions, made up of complete DMEM containing 2mM of BGP and 50µg/ml of L-Ascorbic acid or adipogenic conditions, made up of 1µM of Dexamethasome, 0.5mM of IBMX and 10µg/ml of insulin in complete αMEM.

2.4.2.2 Mineralisation assay

For mineralisation assays, cells grown in 12-well plates in osteogenic medium were fixed, after 21 days, in ice cold 70% ethanol, washed with water and stained with 40mM Alizarin Red S for 20 minutes on a rocker. Next, plates were washed overnight in water and air dried. To destain and quantify the mineralised nodules, experimental wells were incubated in a destaining solution made of 10% (w/v) cetylpyridinium chloride in 10mM sodium phosphate (pH 7) for 30 minutes on a rocker at room temperature. The de-staining solution was then harvested from the wells and added to a 96-well plate together with standards made up of the destaining solution. Plates were read on a SPECTROstar nano plate reader (BMG LABTECH, Germany) measuring absorbance at 562nm analysed with the plate reader software MARS (BMG LABTECH, Germany).

2.4.2.3 Alkaline phosphatase assay

For the ALP assay, osteoblasts from bone chips were plated at $15x10^3$ cells/well in a 96-well plate and cultured in 150µl complete αMEM with 10% FCS for 24 hours (or to confluency). Cell viability was determined by, performing an Alamar blue assay. Alamar Blue (100µl/well) was added to the osteoblast cultures containing fresh DMEM, and the plates were incubated in the dark for 2 hours at 37°C. Alamar blue signal was quantified by fluorescence using a FLUOstar Optima plate reader (BMG LABTECH, Germany) with plate reader software (BMG LabTech, Germany), set to excitation 560nm and emission 590nm. Next, the medium with Alamar blue was removed, cells were washed and fixed in 4% PFA and stored in the freezer until the

ALP assay was performed. To perform the ALP assay, plates were defrosted overnight at 4°C, 100µl of substrate solution (20mM paranitrophenyl phosphate (PNPP) in 1M Diethanolamine and 1mM MgCl2, pH 9.8) was added to experimental wells and standards, a serial dilution of paranitrophenyl which is the reaction product, were added to blank wells. This assay involved a colour change from colourless to yellow relative to enzyme activity. Alkaline phosphatase enzyme activity was measured using the conversion of PNPP by measuring absorption at 405 nm on a SPECTROstar nano plate reader (BMG LABTECH, Germany) at 1 min intervals for 30 minutes. The slope of the resulting curve was calculated using Excel. Alkaline phosphatase measurements were corrected for cell number by dividing by the Alamar Blue signal.

2.4.2.4 Cell proliferation assay

For proliferation assays, cells plated on to coversilps and cultured until semi confluent were fixed in methanol, permeabilized with 0.1% Triton X-10 and blocked in 10% FCS in PBS. Coverslips containing cells were then incubated in a 1:250 dilution of Anti-Ki67 rabbit primary antibody, washed in PBS, incubated in a secondary goat-anti-rabbit Alexa Fluor 488 antibody at 2µg/ml, and washed again in PBS. Immunostained coverslips were finally mounted on a slide with Vectashield mounting medium containing DAPI. Imaging was performed using a Zeiss Axio Scan.Z1 slide scanner (Carl Zeiss Ltd., UK) in fluorescence mode for DAPI and AF488 using a 10x lens, and Ki-67 positive (green and blue) and negative (blue) nuclei quantified using a macro on ImageJ.

2.4.3 Adipocytes

For adipocyte generation, MSCs were obtained as mentioned above, grown to confluence and then stimulated for up to 17 days with adipogenic medium by adding 1µM of Dexamethasome, 0.5mM of IBMX and 10µg/ml of insulin to complete αMEM. At the end of the culture period, RNA was extracted by the triple extraction method described below.

2.5 Molecular analysis

2.5.1 RNA, DNA and Protein extraction

Cells were lysed with Trizol and triple extraction was performed as previously described[384]. Briefly, each well was washed in PBS and 700µl of Trizol was added to each well. Then, cell lysates were collected with the aid of a cell scraper and pipetted into a microcentrifuge tube. Tubes were vortexed for approximately 1 minute to homogenize cells. Tubes were incubated at room temperature for 5 minutes. Then, 140µl of chloroform was added to each tube and then shaken vigorously. Tubes were incubated at room temperature for 2-3 minutes and then centrifuged at 12,000g for 15 minutes at 4°C. The upper aqueous phase (350µl) was transferred to a new microcentrifuge tube. The remaining phases were kept on ice to later extract DNA and protein.

For RNA:

To the tube containing the aqueous phase, 350µl of isopropanol was added, tubes were shaken vigorously and incubated at room temperature for 10 minutes. Next, the tubes were centrifuged at 12,000g for 15 minutes at 4°C. Supernatant was discarded and the pellets were washed in 525µl of 100% ethanol and 21µl of 3M sodium acetate. The tubes were centrifuged at 7500g for 5 minutes at 4°C. Supernatant was discarded, and the pellets washed again in 700µl of 100% ethanol and centrifuged at 7500g for 5 minutes at 4°C. The supernatant was discarded, and the pellets were left to airdry for 5-10 minutes. 40µl of RNase free water was added to tubes which were then incubated at room temperature for 1 minute. Finally, tubes were incubated at 55.5°C for 10-15 minutes and stored at -80°C until used.

For DNA:

The remaining aqueous phase overlying the interphase was removed carefully and 300µl of 100% ethanol was added to each tube. Tubes were mixed vigorously without vortex and incubated for 2-3 minutes at room temperature. Tubes were then centrifuged at 2000g for 5 minutes at 4°C to pellet the DNA. The phenol-ethanol supernatant was transferred to a new tube and kept on ice until protein isolation was performed. To the tube containing the pellet of DNA, 700µl of 0.1M sodium citrate in 10% ethanol, pH 8.5, was added to resuspend the pellet. Tubes were centrifuged at 2000g for 5 minutes at 4°C and supernatant was discarded. The resuspension step

was repeated, the supernatant discarded and pellet was resuspended in 1.05ml of 75% ethanol. Tubes were incubated for 10-20 minutes with occasional mixing by gentle inversion. After incubation, tubes were centrifuged at 2000g for 5 minutes at 4°C and supernatant was discarded. DNA pellet was airdried for 5-10 minutes and then resuspended in 300µl of 8mM NaOH. Tubes were centrifuged at 12,000g for 10 minutes at 4°C to remove insoluble materials and supernatant was transferred to a new Eppendorf and pH was adjusted with 1M HEPES buffer to pH 7-8 and 1mM EDTA was added. DNA was stored at -20°C for future work.

For protein:

The phenol-ethanol supernatants were loaded into dialysis membranes which were then transferred into a large beaker containing 0.1% SDS solution. Membranes were left to dialyse for 16 hours at 4°C. After 16 hours, the SDS solution was refreshed and membranes were incubated for a further 4 hours at 4°C. After 4 hours, the solution was refreshed again, and membranes were incubated for 2 hours at 4°C. During dialysis, the samples partitioned in to three phases: a colourless supernatant, a globular mass and a colourless, viscous liquid. After 2 hours, the globular mass was removed from the membrane and resuspended in 200µl total solvent in 8M urea in Tris-HCl, pH 8 and 1% SDS in molecular-grade water with a 1:1 ratio of the Tris-HCl and the SDC. Protein samples were stored at -20°C until further use.

2.5.2 cDNA synthesis

cDNA was synthesized using the EvoScript Universal cDNA Master (Roche, Switzerland) according to the manufacturer's instructions. Briefly, before setting up reactions all reagents were vortexed and centrifuged briefly. To a new Eppendorf, 1µg of RNA sample was added, 4µl of 5x concentrated reaction buffer and PCR grade water to a final volume of 18µl. Tubes were mixed well, centrifuged briefly and incubated for 5 minutes at room temperature. After incubation, 2µl of 10x concentrated enzyme mix was added and mixed well. Tubes were then placed in a SimpliAmp Thermal Cycler (Thermo Fisher, USA) and the following protocol was followed:

Table 2.6: Reverse transcription protocol performed on a thermal cycler.

Step	Temperature	Duration
1	42°C	15min
2	85°C	5min
3	65°C	15min
4	4°C	∞

2.5.3 Quantitative PCR

For gene expression studies, the LightCycler 480 probes master (Roche, Switzerland) was used. Firstly, a master mix was prepared as follows:

Table 2.7: RT-qPCR master mix ingredient list. A different master mix was made up for each gene of interest.

Reagent	Volume for 1 sample
Probes Master (2x)	5µl
Primer forward	0.4µl
Primer reverse	0.4µl
Probe	0.2µl
Water	3µl

Table 2.8: RT-qPCR master mix ingredient list for primer/probe assays. A different master mix was made up for each gene of interest.

Reagent	Volume for 1 sample
Probes Master (2x)	5µl
Primer/Probe assay	0.5µl
Water	3.5µl

After master mix was prepared, for each sample 9µl of master mix and 1µl of cDNA was added to a well in a 96-well PCR plate making up a total reaction volume of 10µl. For all RT-qPCR, the Mono Color Hydrolysis Probe/UPL protocol was followed using the following settings:

Table 2.9: RT-qPCR run program.

Step	Cycle(s)	Temperature	Time
Pre-incubation	1	95°C	10min
Amplification	45	95°C	10sec
		60°C	30s
		72°C	1s
Cooling	1	40°C	30s

All RT-qPCR was performed using the Lightcycler 480 (Roche, Switzerland) and every sample was analysed in triplicate. CT values were obtained and expression relative to HMBS (housekeeping gene) was calculated. The housekeeping gene (HMBS) was chosen based on a study by Stephens *et al.*[385]. All primer/probe sets (**Table 2.10**) used had either been pre-validated by the lab group or validated Roche or Taqman RealTime ready single assays (**Table 2.11**).

Table 2.10: Primer/ probe sets.

Gene name	Forward (5'-3')	Reverse (5'-3')	Probe
Hmbs	TCCCTGAAGGATGTGCCTAC	AAGGGTTTTCCCGTTTGC	79
TnfrsfF11a	GTGCTGCTCGTTCCACTG	AGATGCTCATAATGCCTCTCCT	25
Dcstamp	ACAAACAGTTCCAAAGCTTGC	GACTCCTTGGGTTCCTTGCT	11
Nfatc1	TCCAAAGTCATTTTCGTGGA	TTTGCTTCCATCTCCCAGAC	50
Ctsk	CGAAAAGAGCCTAGCGAACA	TGGGTAGCAGCAGAAACTTG	18
Sdc3	CAGCTCCCTCAGAAGAGCATA	CAGGAAGGCAGCGAAGAG	12
Runx2	CCACAAGGACAGAGTCAGATTACA	TGGCTCAGATAGGAGGGGTA	60
Alpl	AAGGCTTCTTCTTGCTGGTG	GCCTTACCCTCATGATGTCC	16
Bglap	AGACTCCGGCGCTACCTT	CTCGTCACAAGCAGGGTTAAG	32
Tnfrsf11	TGAAGACACACTACCTGACTCCTG	CCACAATGTGTTGCAGTTCC	88
Opg	ATGAACAAGTGGCTGTGCTG	CAGTTTCTGGGTCATAATGCAA	69
Col1a1	CTCCTGGCAAGAATGGAGAT	AATCCACGAGCACCCTGA	79
Fgf2	TATGGATCTCCACGGCAAC	GTCCACTGGCGGAACTTG	26

Table 2.11: RealTime ready single assays.

GENE	Assay ID	Company
***Pparg* (BC006779)**	313623	Roche
Adipoq	310252	Roche
Axin2	315714	Roche
Wnt10b	310539	Roche
Ctnnb1	300053	Roche
Lgr4	318678	Roche
Atf4	318371	Roche
Lgr5	310756	Roche
Lgr6	318676	Roche
Lrp5	310507	Roche
Lrp6	310543	Roche
Wnt3a	301106	Roche
Smad6	300938	Roche
Postn	316725	Roche
On	313324	Roche
Sdc1	Mm00448918_m1	Taqman
Sdc2	Mm04207492_m1	Taqman
Sdc4	Mm00488527_m1	Taqman
Fzd1	317881	Roche
Fzd7	310548	Roche

2.5.4 Western blotting

Osteoblasts (6x10^5 cells/well) were cultured in 6 well plates, serum starved overnight and stimulated with Wnt3a at 50ng/ml. After stimulation, the cells were lysed with Trizol as described above (**2.4.1**) and the protein concentration was determined by BCA protein assay. Twenty to 30 µg of protein were separated by denaturing 10% polyacrylamide gel (BioRad, UK) electrophoresis and transferred to a nitrocellulose membrane with a semi-dry Trans-Blot Turbo Transfer System (BioRad, UK) for 7 minutes at 25 volts and 2.4 amps. Membranes were blocked in LICOR blocking buffer for 1 hour at room temperature and incubated in non-phosphorylated (active) β-catenin rabbit primary antibody at 1:1000 dilution in LICOR blocking buffer overnight at 4°C. Following 3x 15-minute washes in TBS-T, membranes were incubated for 1 hour in secondary goat-anti-rabbit Alexa Fluor 800 antibody at 1:10000 dilution. Following further washes in TBS-T membranes were reprobed with primary β-actin mouse antibody at 1:5000 dilution for 1 hour at room temperature, washed in TBS-T and incubated in secondary rabbit-anti-mouse Alexa Fluor 680

antibody at 1:10000 dilution for one hour at room temperature. After 3 final washes in TBS-T, membranes were visualised using the Odyssey CLx imaging system and analysed using Image Studio lite.

3. Syndecan-3 deletion induces a low bone volume phenotype in adult mice

3.1 Introduction

The skeleton plays an important role in providing support, protection of vital organs, aiding movement, providing an environment for bone marrow, thus playing a role in haematopoiesis, storage of minerals such as calcium and phosphorus and a reservoir of growth factors and cytokines, having also an important endocrine function [386–388]. Bone is a metabolically active dynamic tissue that undergoes continuous changes with development and ageing [14,225,389]. The two processes which are involved in the development and maintenance of bone are remodelling and modelling[225]. Bone remodelling begins during foetal development and continues throughout adult life, during which there is a coordinated turnover of bone by bone resorbing osteoclasts and bone forming osteoblasts, both of which work at the same bone remodelling unit (BRU)[315,337,390]. In ageing and especially in post-menopausal women there is an imbalance during bone turnover at each BRU which can lead to bone loss and a variety of metabolic disorders of the skeleton, such as osteoporosis[337,390–393]. In contrast to remodelling, bone modelling is a process in which bone is first formed and undergoes shaping or reshaping [337,387,390]. Unlike what happens in bone remodelling, where osteoclast and osteoblast function is coupled, in modelling these cells work independently from one another [337,387]. The process of modelling happens in response to mechanical loading and physiologic influences which allow the skeleton to adapt to the prevailing loads[4,5,337,390].

Osteoporosis is a skeletal disease characterized by low bone mass and microarchitectural deterioration of bone tissue with a consequent increase in bone fragility and susceptibility to fracture [316]. This disease causes more than 8.9 million fractures annually worldwide, with one in three postmenopausal woman and one in five men being affected by it worldwide [320,394,395]. Over the years several drugs have been developed that can prevent fractures due to osteoporosis. In the past two decades, bisphosphonates have been used as primary treatment for osteoporosis due to their low cost and efficacy[315]. They have a high affinity to bone and when taken

up by osteoclasts they are able to inhibit bone-resorbing activity[315,360]. Unfortunately, there is poor patient compliance and persistence to the treatment due to side-effects, strict dosing requirements and because osteoporosis is a silent disease patients cannot detect improvement in symptoms and fail to appreciate the benefits of the treatment[396,397]. As such, it is important to continue to do research into possible new therapeutic approaches, especially anabolic, which have the capacity to stimulate bone formation[398,399], that are more effective, less disruptive to the daily routine of the patient and perhaps with fewer side-effects. As I have outlined in detail in the Introduction in Chapter 1, current anabolic treatments available for patients with severe osteoporosis include Teriparatide (recombinant parathyroid hormone) and Romosozumab (anti-sclerostin antibody) but these also have limitations such as cost, subcutaneous administration and side-effects, hence the importance of research into other forms of anabolic teatment[391].

The understanding of which pathways and what factors may be controlling the process of bone ageing is still incomplete, oversimplified and one of the most difficult challenges in the field of osteoporosis [390,400,401]. Identification of the mechanisms of action involved in osteoporosis could lead to exciting new approaches to diagnosis and treatment and also improved use of existing treatments for diseases such as osteoporosis [337,390].

To ascertain the role of Sdc3 in the maintenance of prenatal and postnatal bone morphology I used microCT to analyse bones of Sdc3 KO and WT mice.

3.2 Methods

To assess the effect of knocking out Sdc3 on bone morphometry, left hind legs and spines of WT and Sdc3 KO mice aged 3 and 6-months and whole skeletons of 2-day old pups were harvested and fixed overnight in paraformaldehyde (4%) and stored in 70% ethanol. Bones were then scanned by µCT using a Skyscan 1272 (Bruker, Belgium) and trabecular and cortical morphometry was analysed and leg lengths were measured (for details please see Chapter 2). Measurements of Sdc3 KO were normalised to those of the WT.

In addition, flexural strength of femurs from 3-month-old mice was evaluated by dynamic three-point bending test on unfixed femurs of WT and Sdc3 KO mice using the ZWICK-mechanical testing machine (ZWICK, Switzerland).

The weights of female and male WT and Sdc3 KO mice were recorded from week 1 after birth until 24 weeks of age.

Statistical analysis of the data was performed by an unpaired Student's *t* test.

3.3 Results

3.3.1 Mouse weights

Body weights of WT and Sdc3 KO mice were taken weekly, from week 1 after birth to 24 weeks of age (N number can be found in Table 3.1). Although there was variation at different weeks of age, there were no significant differences noted between WT and Sdc3 KO males (**Figure 3.1**) or females (**Figure 3.2**).

Figure 3.1: Weight of male WT and Sdc3 KO mice. No significant differences were seen during the 24 weeks of weighing. Values shown are means ± SD. N number can be found in table 3.1.

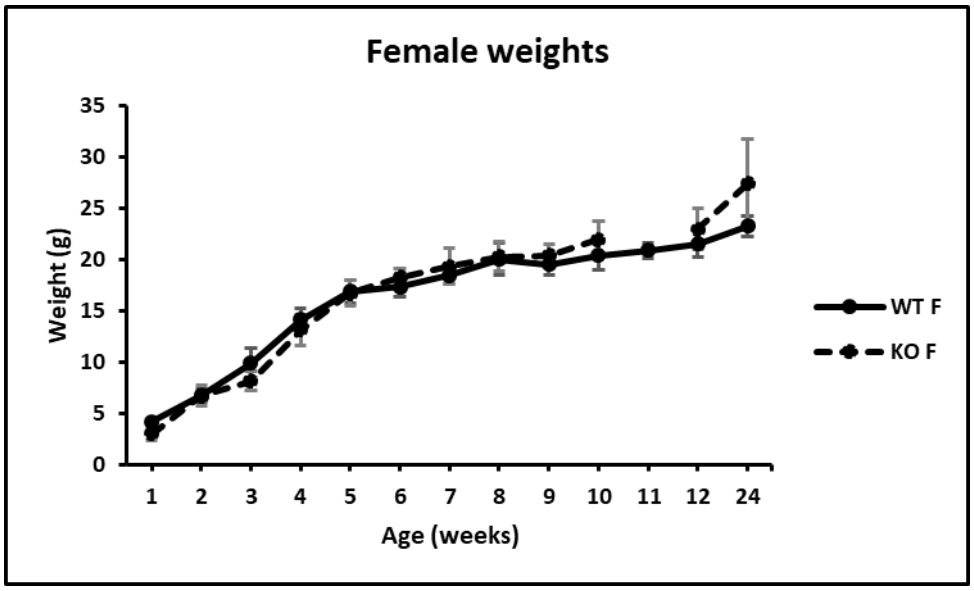

Figure 3.2: Weight of female WT and Sdc3 KO mice. No significant changes seen between WT and Sdc3 KO weights during the 24 weeks. Values shown are means ± SD. N numbers can be found in table 3.1.

Table 3.1: Number of mice (N) by age, gender and genotype. There is a higher variability in N number in the Sdc3 KO due to the collaborative nature of this work.

Week	WT		Sdc3 KO	
	Female	Male	Female	Male
1	10	12	9	11
2	10	13	26	26
3	10	13	14	14
4	10	13	33	39
5	10	13	30	32
6	10	13	30	30
7	10	13	21	21
8	10	13	38	34
9	10	13	14	30
10	10	13	27	43
11	10	13	-	-
12	10	13	27	12
24	5	4	37	9

3.3.2 Morphometry of tibias and femurs of 3-month-old mice

Trabecular analysis

Trabecular analysis of tibias (**Figure 3.3 A; Table 3.2**) and femurs (**Figure 3.3 B; Table 3.2**) of male Sdc3 KO mice showed a significant reduction in bone volume, when compared to male WT control mice. There was a 34% ($p<0.001$), 13% ($p<0.001$) and 24% ($p<0.001$) decrease in bone volume per tissue volume (BV/TV), trabecular thickness (Tb.Th) and trabecular number (Tb.N), respectively, of Sdc3 KO tibias. On the other hand, there was an increase of 10% ($p<0.01$), 50% ($p<0.001$) and 20% ($p<0.001$) in trabecular separation (Tb.Sp), trabecular pattern factor (Tb.Pf) and structure model index (SMI), respectively, in Sdc3 KO tibias, as shown in Figure 3.3 A. As Tb.Pf and SMI are increased in Sdc3 KO this suggests trabeculae are less connected and are more 'rod-like' than 'plate-like'. The morphometric analysis of the trabecular bone of femurs showed very similar values to those found in the analysis of the tibias. Sdc3 KO mice showed a 30.5% ($p<0.001$), 12.5% ($p<0.001$) and a 21% ($p<0.01$) decrease in BV/TV, Tb.Th and Tb.N, respectively. There was an increase of 9% ($p<0.05$), 50% ($p<0.001$) and 18% ($p<0.01$) in Tb.Sp, Tb.Pf and SMI, respectively, in Sdc3 KO compared to WT mice, as shown in Figure 3.3B. These results demonstrate that Sdc3 KO mice have a low bone volume phenotype, which is illustrated in Figures 3.3 C-F. Crossectional images of 3D µCT reconstructions show a decrease in trabecular bone of Sdc3 KO tibias (**Figure 3.3 D**) and femurs (**Figure 3.3 F**), showing the rod-like appearance of the Sdc3 KO trabeculae in comparison to the plate-like trabeculae of WT mice.

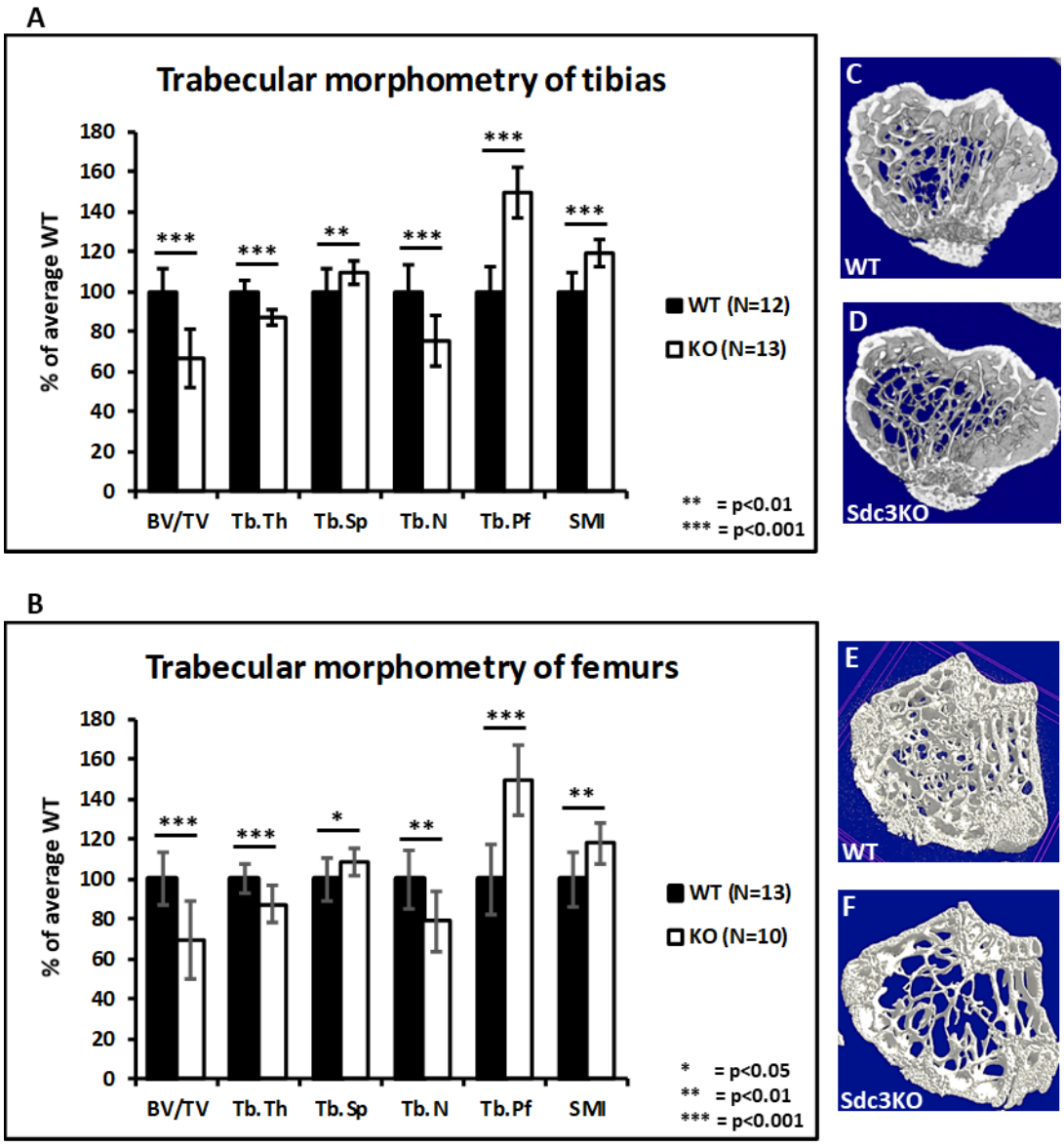

Figure 3.3: Trabecular morphometry of tibias and femurs of 3-month-old WT and Sdc3 KO mice. Morphometry analysis of trabecular bone from the tibias (**A**) and femurs (**B**) of 3-month old male Sdc3 KO (N=13 and N=10, respectively) shows a decrease in bone volume per tissue volume (BV/TV), trabecular thickness (Tb.Th), and trabecular number (Tb.N), and an increase in trabecular separation (Tb.Sp), trabecular pattern factor (Tb.Pf) and structure model index (SMI) as compared to WT (N=12 and N=13, respectively). Crossectional images of 3D µCT reconstructions of whole bone from tibias (**C** and **D**) and Femurs (**E** and **F**) show altered trabecular bone architecture and low bone volume in Sdc3 KO (**D** and **F**) as compared to WT (**C** and **E**). Images of a stack of 200 slices were taken from 20 slices away from the growth plates. Note the decrease in trabecular bone volume and connectivity, and the rod-like appearance in Sdc3 KO, as opposed to WT. Measurements shown in **A** and **B** relating to Sdc3 KO are shown as percentage of average WT. Data are shown as means ±SD. Significance is denoted by *p<0.05, **p<0.01, ***p<0.001.

Table 3.2: MicroCT analysis of trabecular bone in tibias and femurs of WT and Sdc3 KO male mice at 3-months of age. Tibias and femurs of WT mice have significantly higher bone volume per tissue volume (BV/TV), trabecular thickness (Tb.Th), and trabecular number (Tb.N) and significantly lower trabecular separation (Tb.Sp), trabecular pattern factor (Tb.Pf) and structure model index (SMI), than Sdc3 KO mice. Values shown are means ± SD. Significance (Sdc3 KO vs WT mice) denoted by *p<0.05, **p<0.01, ***p<0.001.

	Tibias		**Femurs**	
	WT (N=12)	**Sdc3 KO (N=13)**	**WT (N=13)**	**Sdc3 KO (N=6)**
BV/TV (%)	20 ± 2	**13 ± 2*****	20 ± 3	**14 ± 3*****
Tb.Th (µm)	56 ± 3	**49 ± 2*****	57 ± 4	**50 ± 5*****
Tb.Sp (µm)	170 ± 20	**187 ± 11****	181 ± 19	**197 ± 14***
Tb.N (mm)	4 ± 1	**3 ± 0.3*****	4 ± 0.5	**3 ± 0.4****
Tb.Pf (1/mm)	18 ± 4	**25 ± 3*****	15 ± 3	**22 ± 4*****
SMI	2 ± 0.17	**2 ± 0.14*****	2 ± 0.2	**2 ± 0.2****

Cortical analysis

Cortical analysis of tibias of male Sdc3 KO mice showed a decrease of 4% (p<0.01), 8% (p<0.001), 9% (p<0.05) and 28% (p<0.05) in BV/TV, cortical thickness (Cort.Th), periosteal perimeter (P.Pm) and mean polar moment of inertia (MMI; predictor of bone strength), respectively, as compared to male WT mice (**Figure 3.4 A; Table 3.3**). Endosteal perimeter (E.Pm) was decreased by 5% in Sdc3 KO tibias but did not reach significance (p=0.06). When analysing femurs, there was a significant decrease of 5% (p<0.05) and 9% (p<0.01) in P.Pm and E.Pm, respectively (**Figure 3.4 B; Table 3.3**). BV/TV, Cort.Th and MMI of femurs showed no significant differences between genotypes. Together with the overall decrease in trabecular bone volume, these data suggest that Sdc3 KO mice may have weaker bones than WT mice.

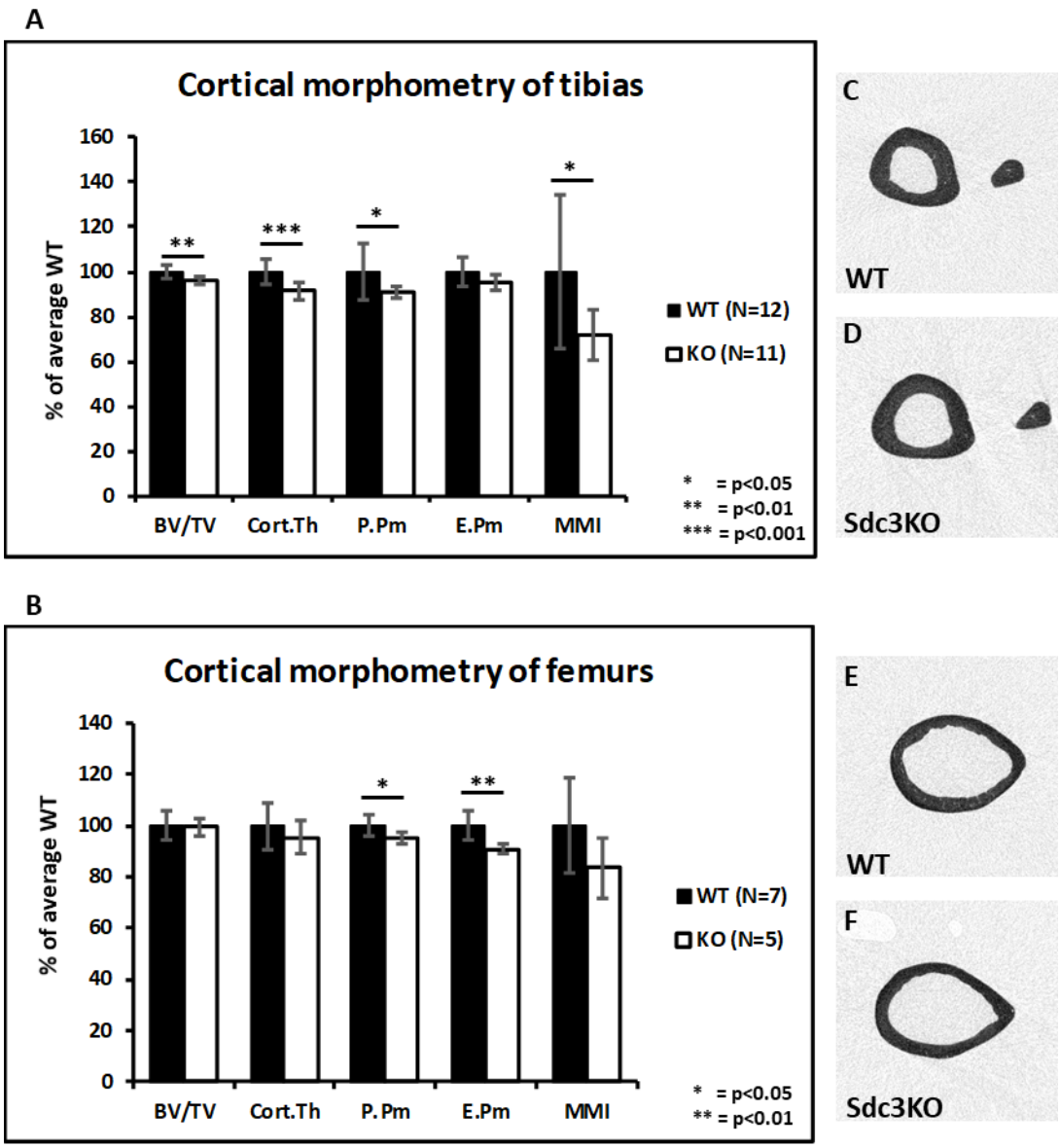

Figure 3.4: Cortical morphometry of tibias and femurs of 3-month-old WT and Sdc3 KO mice. Cortical analysis of tibias (**A**) showed a significant decrease in bone volume per tissue volume (BV/TV), cortical thickness (Cort.Th), periosteal perimeter (P.Pm) and mean polar moment of inertia (MMI) in Sdc3 KO male mice (N=11) as compared to WT male mice (N=12). Analysis of the femurs (**B**) showed that overall P.Pm and endosteal perimeter (E.Pm) were decreased in Sdc3 KO male mice (N=5) as compared to WT male mice (N=7). Measurements shown in **A** and **B** relating to Sdc3 KO are shown as percentage of average WT. Data are shown as means ±SD. Significance is denoted by *p<0.05, **p<0.01, ***p<0.001.

Table 3.3: MicroCT analysis of cortical bone in tibias and femurs of male WT and Sdc3 KO mice at 3-months of age. Cortical analysis of tibiae shows a decrease in cortical thickness (Cort.Th), periosteal perimeter (P.Pm) and mean polar moment of inertia (MMI) in Sdc3 KO mice when compared to WT mice. Cortical analysis of femurs shows a significant decrease in P.Pm and endosteal perimeter (E.Pm) of Sdc3 KO when compared to WT mice. Values shown are means ± SD. Significance (Sdc3 KO vs WT mice) denoted by *p<0.05, **p<0.01, ***p<0.001.

	Tibias		**Femurs**	
	WT (N=12)	**Sdc3 KO (N=11)**	**WT (N=7)**	**Sdc3 KO (N=5)**
Cort.Th (µm)	260 ± 16	**238 ± 10*****	217 ± 20	207 ± 14
P.Pm (mm)	4 ± 0.5	**4 ± 0.1***	6 ± 0.23	**6 ± 0.1***
E.Pm (mm)	2 ± 0.2	2 ± 0.1	5 ± 0.3	**4 ± 0.1****
MMI (mm^4)	0.2 ± 0.1	**0.1 ± 0.02***	0.6 ± 0.1	0.5 ± 0.1

3.3.3 Morphometry of tibias and femurs of 6-month-old mice

Trabecular analysis

Trabecular analysis of tibias (**Figure 3.5 A; Table 3.4**) and femurs (**Figure 3.5 B; Table 3.4**) of male Sdc3 KO mice continued to show a significant reduction in bone volume at 6-months of age, when compared to male WT control mice of the same age. There was a 31% (p<0.001), 13% (p<0.001) and 21% (p<0.01) decrease in bone volume per tissue volume (BV/TV), trabecular thickness (Tb.Th) and trabecular number (Tb.N), respectively, of Sdc3 KO tibias. On the other hand, there was an increase of 55% (p<0.01) and 17% (p<0.001) in, trabecular pattern factor (Tb.Pf) and structure model index (SMI), respectively, in Sdc3 KO tibias, as shown in Figure 3.5 A. As Tb.Pf and SMI continue to be increased in Sdc3 KO at 6-months of age, it suggests trabeculae remain less connected and are more 'rod-like' than 'plate-like'. The morphometric analysis of the trabecular bone of femurs showed very similar values to those found in the analysis of the tibias. Sdc3 KO mice showed a 36% (p<0.001), 17% (p<0.001) and a 23% (p<0.01) decrease in BV/TV, Tb.Th and Tb.N, respectively. There was an increase of 64% (p<0.001) and 17% (p<0.001) in Tb.Pf and SMI, respectively, in Sdc3 KO compared to WT mice, as shown in Figure 3.5 B. Both tibias and femurs showed no significant difference in trabecular separation (Tb.Sp) between Sdc3 KO and WT mice.

A

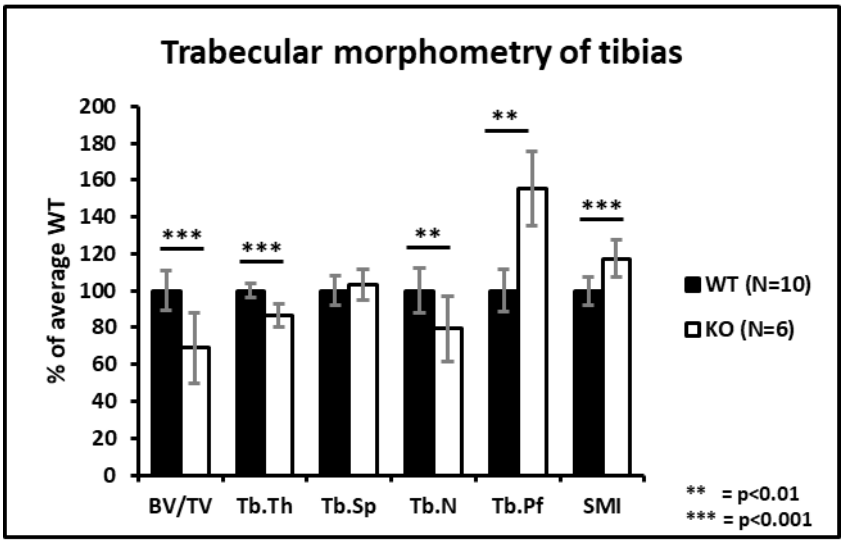

B

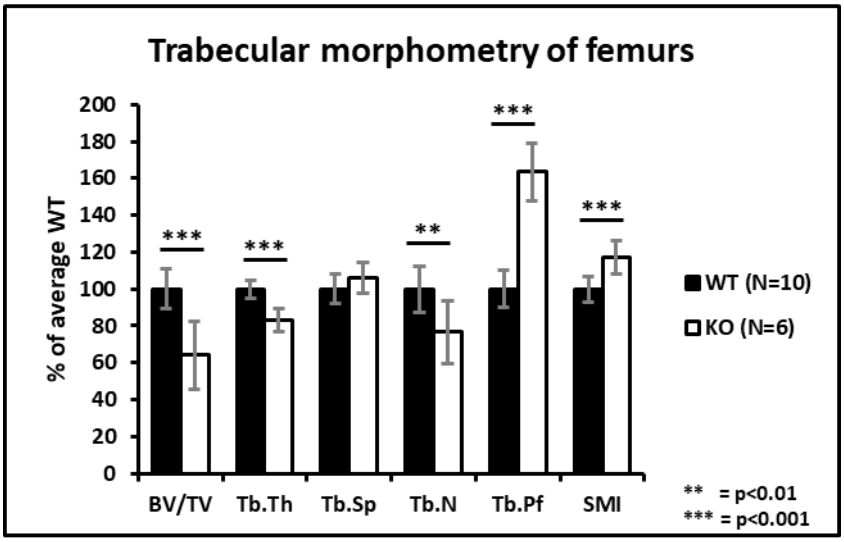

Figure 3.5: Trabecular morphometry of tibias and femurs of 6-month-old WT and Sdc3 KO mice. Trabecular analysis of tibias (**A**) and femurs (**B**) showed a significant decrease in bone volume per tissue volume (BV/TV), trabecular thickness (Tb.Th) and trabecular number (Tb.N), and an increase in trabecular pattern factor (Tb.Pf) and structure model index (SMI) in 6-month-old Sdc3 KO male mice (N=6 for both tibias and femurs) as compared to WT male mice (N=10 for both tibias and femurs). Measurements shown in **A** and **B** relating to Sdc3 KO are shown as a percentage of average WT. Data are shown as means ±SD. Significance is denoted by **p<0.01, ***p<0.001.

Table 3.4: MicroCT analysis of trabecular bone in tibias and femurs of male WT and Sdc3 KO mice at 6-months of age. Tibias and femurs of WT mice have significantly higher bone volume per tissue volume (BV/TV), trabecular thickness (Tb.Th), and trabecular number (Tb.N) and significantly lower trabecular separation (Tb.Sp), trabecular pattern factor (Tb.Pf) and structure model index (SMI), than Sdc3 KO mice. Values shown are means ± SD. Significance (Sdc3 KO vs WT mice) denoted by **p<0.01, ***p<0.001.

	Tibias		**Femurs**	
	WT (N=10)	**Sdc3 KO (N=6)**	**WT (N=10)**	**Sdc3 KO (N=6)**
BV/TV (%)	18 ± 2	**13 ± 2*****	19 ± 2	**12 ± 2*****
Tb.Th (µm)	62 ± 2	**54 ± 3*****	64 ± 3	**53 ± 3*****
Tb.Sp (µm)	204 ± 16	211 ± 18	212 ± 17	225 ± 19
Tb.N (mm)	3 ± 0.4	**2 ± 0.4****	3 ± 0.4	**2 ± 0.4*****
Tb.Pf (1/mm)	15 ± 2	**24 ± 5*****	14 ± 2	**23 ± 4*****
SMI	2 ± 0.1	**2 ± 0.2*****	2 ± 0.1	**2 ± 0.2*****

Cortical analysis

Cortical analysis of tibias of male 6-month-old Sdc3 KO mice showed a decrease of 13% (p<0.001), 21% (p<0.01), 12% (p<0.001) and 53% (p<0.015) in cortical thickness (Cort.Th), periosteal perimeter (P.Pm), endosteal perimeter (E.Pm) and mean polar moment of inertia (MMI; predictor of bone strength), respectively, as compared to male WT mice (**Figure 3.6 A; Table 3.5**). BV/TV showed no significant change between Sdc3 KO and WT tibias at 6 months of age. When analysing femurs, there was a significant decrease of 5% (p<0.01), 11% (p<0.001), 15% (p<0.001) and 35% (p<0.001) in Cort.Th, P.Pm, E.Pm and MMI, respectively (**Figure 3.6 B; Table 3.5**). BV/TV of femurs showed a significant increase of 5% (p<0.01) in Sdc3 KO compared to WT mice. Together with the overall decrease in trabecular bone volume, these data continue to suggest that Sdc3 KO mice may have weaker bones than WT mice.

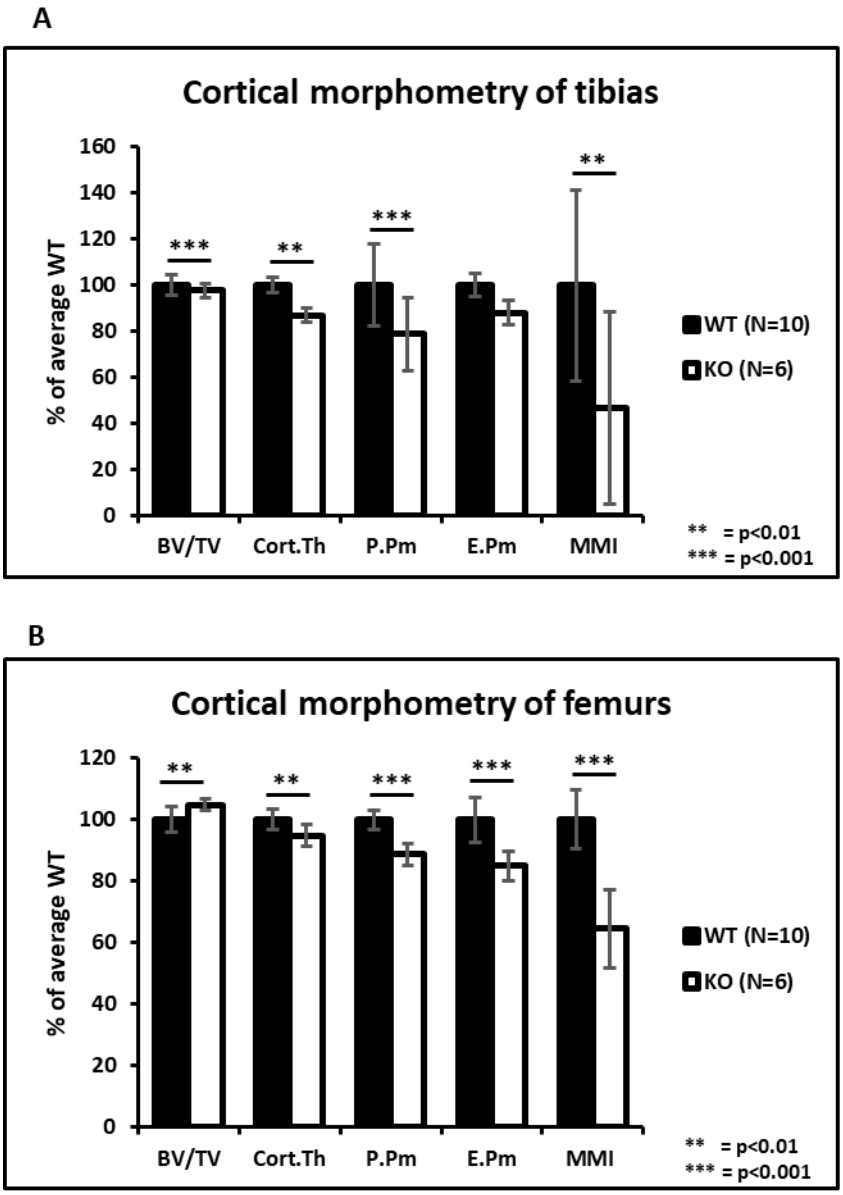

Figure 3.6: Cortical morphometry of tibias and femurs of 6-month-old WT and Sdc3 KO mice. Cortical analysis of tibias (**A**) showed a significant decrease in bone volume per tissue volume (BV/TV), cortical thickness (Cort.Th), periosteal perimeter (P.Pm) and mean polar moment of inertia (MMI) in Sdc3 KO male mice (N=6) as compared to WT male mice (N=10). Analysis of the femurs (**B**) showed a significant decrease in BV/TV, Cort.Th, P.Pm, endosteal perimeter (E.Pm) and MMI in Sdc3 KO male mice (N=6) as compared to WT male mice (N=10). Measurements shown in **A** and **B** relating to Sdc3 KO are shown as percentage of average WT. Data are shown as means ±SD. Significance is denoted by **p<0.01, ***p<0.001.

Table 3.5: MicroCT analysis of cortical bone in tibias and femurs of male 6-month old WT and Sdc3 KO mice. Although cortical thickness (Cort.Th) and endosteal perimeter (E.Pm) increase in Sdc3 KO as they age, these values are still reduced in comparison with WT mice. Periosteal perimeter (P.Pm) and mean polar moment of inertia (MMI) are all significantly reduced in SDC3 KO when compared to WT. Values shown are means ± SD. Significance (Sdc3 KO vs age-matched WT mice) denoted by *p<0.05, **p<0.01, ***p<0.001.

	Tibias		**Femurs**	
	WT (N=10)	**Sdc3 KO (N=6)**	**WT (N=10)**	**Sdc3 KO (N=6)**
Cort.Th (µm)	272 ± 9	**236 ± 7*****	227 ± 7	**215 ± 8****
P.Pm (mm)	6 ± 1	**4 ± 1***	6 ± 0.2	**6 ± 0.2*****
E.Pm (mm)	3 ± 0.1	**2 ± 0.1*****	5 ± 0.4	**4 ± 0.2*****
MMI (mm^4)	0.4 ± 0.2	**0.2 ± 0.1****	1 ± 0.1	**1 ± 0.1*****

3.3.4 Analysis of WT and Sdc3 KO 2-day-old pups

I have shown in the previous section that Sdc3 deletion induces a low bone volume phenotype in adult mice. However, it has previously been shown that Sdc3 is involved in skeletal development[300,302]. Therefore, to understand whether the adult low bone volume mouse phenotype could be due to impaired skeletal development I analysed the skeletons of 2-day old pups.

Analysis of whole skeletons

To understand the possible effects of knocking out Sdc3 on skeletal development, whole skeletons of 2-day-old WT and Sdc3 KO mice were anatomically examined. This showed no obvious defects in the anatomy of Sdc3 KO pups when compared to WT pups (**Figure 3.7 A** and **B**). Both WT and Sdc3 KO pups seem to have developed at the same rate.

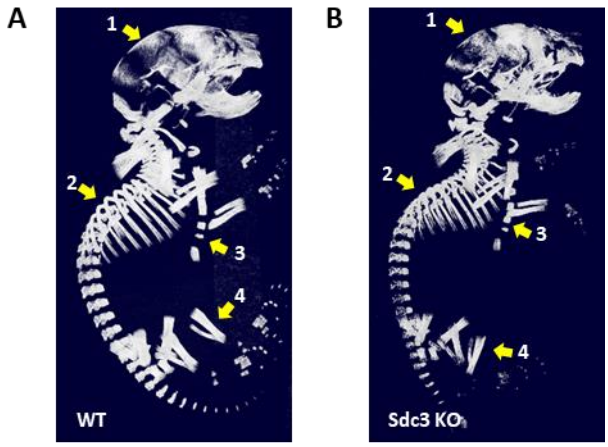

Figure 3.7: Whole skeleton of P2 mice. Analysis of the whole skeletons of P2 pups shows no major anatomical differences in the skull (**1**), spine (**2**), sternum (**3**) and tibias (**4**), between WT (**A; N=15**) and Sdc3 KO (**B; N=17**) mice.

Bone volume analysis of tibias

The right whole tibias of 2-day-old WT and Sdc3 KO mice were analysed by µCT. There was an increase of 0.33 mm^3 in tibia bone volume in the Sdc3 KO pups when compared to the WT pups ($p<0.001$; **Figure 3.8**).

A

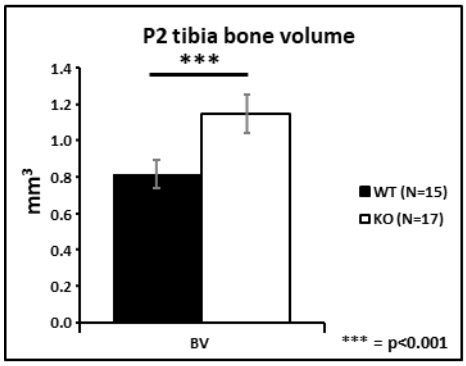

B

	WT (N=15)	Sdc3KO (N=17)
BV (mm^3)	0.82±0.08	1.15±0.11

Figure 3.8: Bone volume analysis of tibias of 2-day-old pups. (A) Analysis of tibias shows a 0.33 mm^3 increase in bone volume (BV) in Sdc3 KO mice, significantly different from WT mice ($p<0.001$). **(B)** Sdc3 KO average bone volume was 1.15 mm^3 ±SD, which is higher than WT control mice whose average bone volume was 0.82mm^3 ±SD.

Tibia length assessment

Next, I measured the full length of the mineralised diaphysis of the tibias of 2-day-old WT and Sdc3 KO pups with the aid of Data Viewer (Bruker, Belgium). Sdc3 KO

pups have longer tibias than WT with these measuring 3.17 mm on average and Sdc3 KO measuring 3.40 mm ($p<0.05$; **Figure 3.9**).

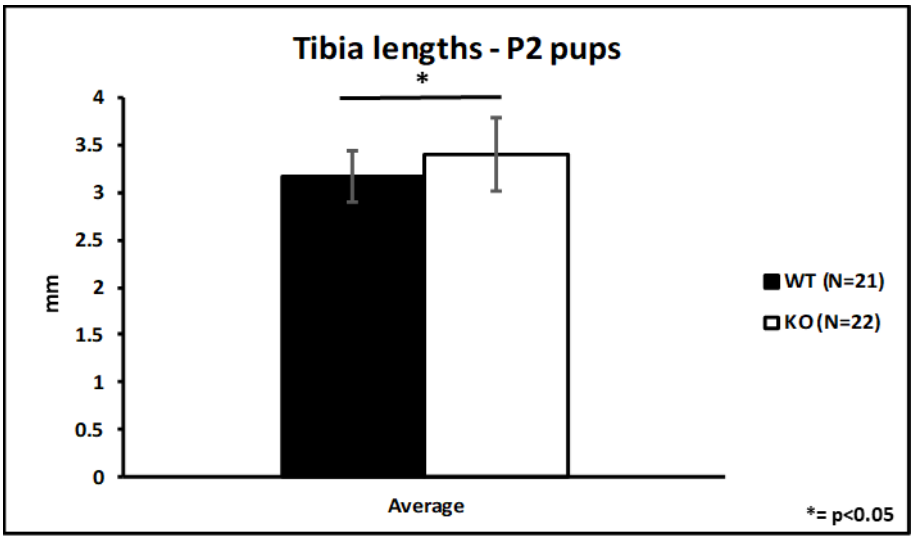

Figure 3.9: Tibia lengths of 2-day old WT and Sdc3 KO pups. P2 Sdc3KO mice have significantly longer tibias than WT mice. Error bars show SD, significance is denoted by *$p<0.05$.

3.3.5 Tibial length in adult mice

In order to assess whether the difference in long bone length is maintained in adulthood, the length of the tibiae of 3- and 6-month-old male WT and Sdc3 KO mice were measured and compared. With the aid of Data Viewer (Bruker, Belgium), measurements were taken from the middle of the condyles to the point of the distal tibiofibular junction.

In contrast to what was seen in the 2-day-old pups, Sdc3 KO mouse tibias were shorter than those of WT mice at 3 months of age (**Figure 3.10**). Although the difference may seem very small with WT tibias measuring 10.57 mm and Sdc3 KO tibias measuring 10.33 mm, this difference was highly significant ($p<0.001$).

At 6 months of age, tibial length of WT and Sdc3 KO mice was measured using the exact same method as used for the 3-month-old mice. Analysis of the tibia lengths showed a difference of 0.4mm with WT measuring 10.9 mm and KO measuring 10.5 mm (**Figure 3.10**). As with the 3-month old mice, Sdc3 KO tibiae were significantly shorter than tibias of WT mice at 6 months of age ($p<0.01$).

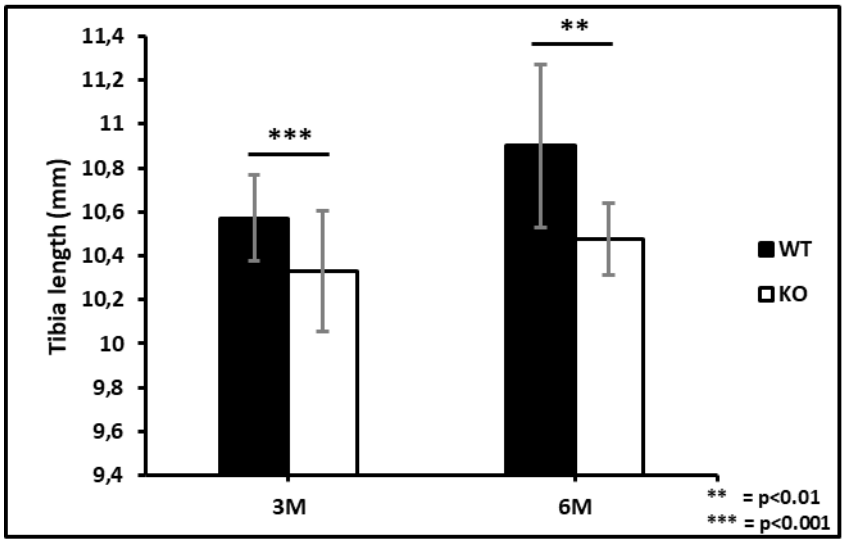

Figure 3.10: Length of tibiae at 3 and 6 months of age of WT and Sdc3 KO mice. Sdc3 KO mouse (N=7) tibiae lengths are significantly shorter than tibias of WT mice (N=6) at 3 months of age. Sdc3 KO mice are still significantly different than WT mice at 6 months of age with WT mice (N=14) increasing their tibiae lengths by 0.33 mm and Sdc3 KO mice (N=10) only increasing by 0.17 mm as they mature. Error bars show SD, significance is denoted by **p<0.01 and ***p<0.001.

3.3.6 Three-point bending test of femurs of 3-month-old WT and Sdc3 KO mice

The biomechanical properties of the long bones of Sdc3 KO mice were likely to be altered due to the changes in bone morphometry. Sdc3 KO mice show differences in both trabecular and cortical parameters, in which MMI suggests they are weaker than WT mice, so indeed to investigate the strength of the femurs of 3-month-old male WT and Sdc3 KO mice, 3-point bending was carried out (**Figure 3.11**). Bone strength was significantly lower in Sdc3 KO vs WT mice, as evidenced by the 27% ($p<0.001$), 41% ($p<0.001$) and 18% ($p<0.05$) reduction of the maximum force required to break, work to break and stiffness, respectively, of Sdc3 KO mice femurs in comparison to WT mouse femurs. This reduction in Sdc3 KO bone strength is expected and reflects the lower periosteal and endosteal perimeter, cortical thickness and MMI of Sdc3 KO mice revealed by the µCT analysis.

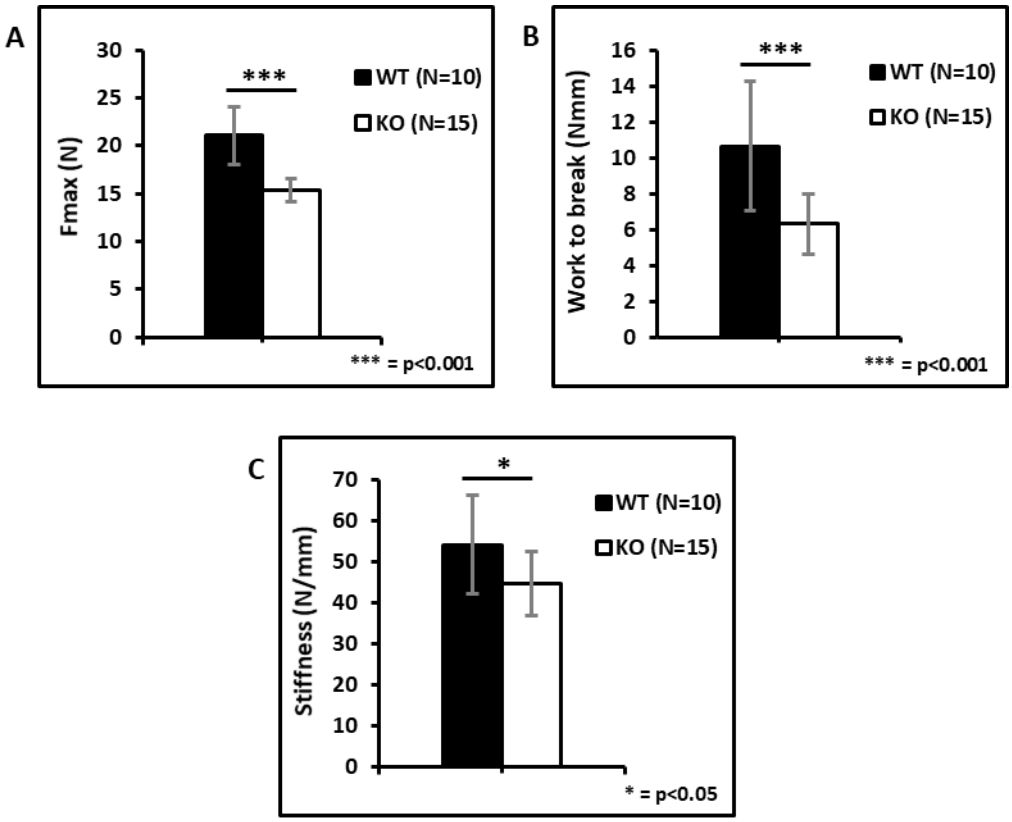

Figure 3.11: Three-point bend test at 3 months of age. Three-point bend test shows a reduction in the mechanical strength, work to break and stiffness of Sdc3 KO femurs (N=15) when compared to WT mouse femurs (N=10). Graphs show Sdc3 KO femurs require less work to fracture which indicates they are weaker than WT mouse femurs. Maximum load was defined as the highest point on the Load-extension curve. Work to break was defined as the total area under the Load-extension curve. Stiffness was defined as the slope of the linear region of the Load-extension curve. Error bars show SD, significance is denoted by *p<0.05 and ***p<0.001.

3.3.7 Morphometry of WT and Sdc3 KO mouse spines

Trabecular analysis of 3-month-old mouse spines

Micro-Ct analysis of the 5th lumbar vertebrae (L5) of 3-month-old male WT (N=11) and Sdc3 KO (N=11) mice showed a decrease, in Sdc3 KO as compared to WT mice, of 18% in BV/TV (p<0.001) mostly due to a 17% decrease in trabecular thickness (p<0.001) as trabecular number was not affected (**Figure 3.12**).

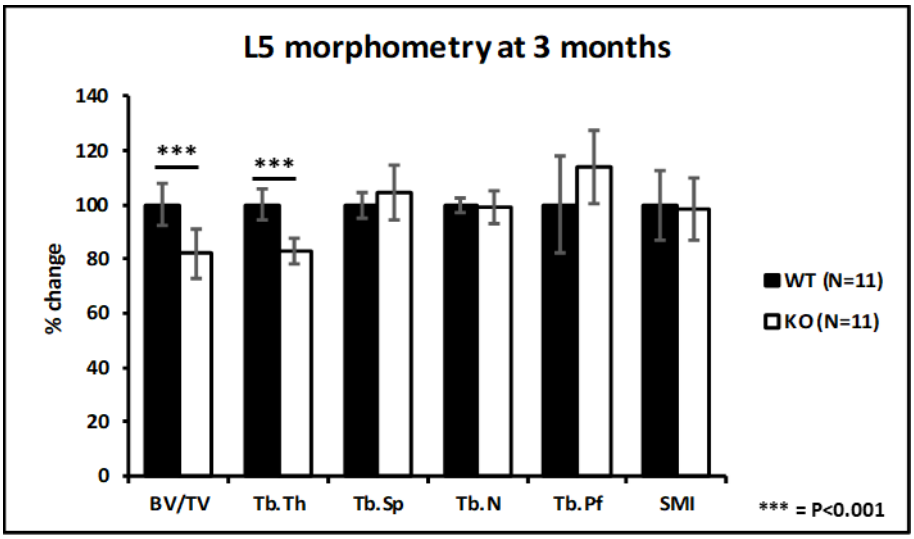

Figure 3.12: Analysis of L5 morphometry at 3 months of age. µCT analysis shows a decrease in overall bone volume/tissue volume (BV/TV) and a reduction in trabecular thickness (Tb.Th) in Sdc3 KO mice when compared to WT mice. Measurements were normalised to 100% for the WT. Error bars show SD, significance is denoted by ***p<0.001.

Trabecular analysis of 6-month-old mouse spines

Micro-CT analysis of the L5 of 6-month-old male WT (N=6) and Sdc3 KO (N=7) mice showed no significant difference was reached possibly due to low N number (**Figure 3.13**).

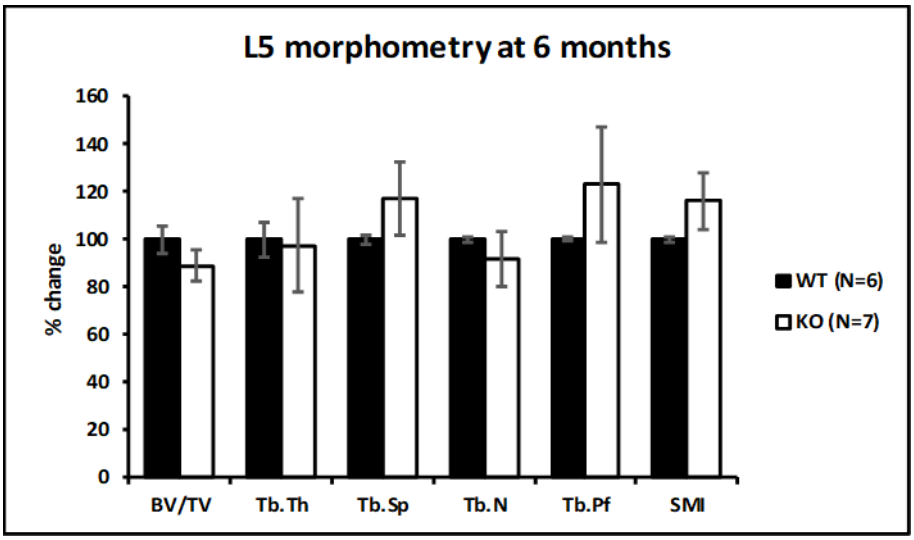

Figure 3.13: Analysis of L5 shows no significant changes at 6 months of age. Bone volume/Tissue volume (BV/TV), trabecular thickness (Tb.Th), trabecular separation (Tb.Sp), trabecular number (Tb.N), trabecular pattern factor (Tb. Pf) and structure model index (SMI) showed no significant difference between Sdc3 KO and WT mice. Measurements were normalised to 100% for the WT. Error bars show SD.

3.4 Discussion

Syndecans, a family of transmembrane proteoglycans, are known to function as membrane receptors to a wide variety of ligands and participate in cellular interactions [280,402]. Syndecans appear to play a role during bone development by regulating chondrocyte proliferation, regulating skeletogenic condensations and chondrogenesis and osteogenesis[208,301,306,313,374,375]. Syndecan 3 is the least studied of all four syndecans and it is still unknown whether syndecan 3 may be involved in maintenance of the adult skeleton. In this chapter, the results have provided evidence that deletion of *Sdc3* leads to a decrease in overall bone volume and an increase in bone fragility in adult mice.

In this chapter I have shown that male Sdc3 KO mice have decreased trabecular bone volume by at least 30% in tibias and femurs at 3 months of age (**Figure 3.3**). They have a decrease in trabecular number, poor connectivity and trabeculae are more "rod like" than "plate like", which can lead to an increase in bone fragility. Furthermore, these mice show cortical thinning and a decrease in overall bone perimeter (**Figure 3.4**). These architectural changes lead to a low MMI, a geometric predictor of whole bone strength meaning that these bones could be prone to fragility fractures. The low MMI correlated with the decrease in maximum force required to break, work to break and stiffness in Sdc3 KO mouse femurs (**Figure 3.11**). At 6-months of age similar values were observed between Sdc3 KO and WT tibias and femurs as those seen at 3 months of age. These findings suggest these mice suffer with early onset osteoporosis. They may also suggest that Sdc3 may be important for up regulation of bone formation and adult bone mass maintenance. However, it is unclear whether the low bone volume phenotype of Sdc3 KO mice is due to a decrease in bone formation or increase in bone resorption or both.

A study by Strader and colleagues has shown that Sdc3 KO mice are resistant to diet-induced obesity and are leaner than WT mice when given a high fat diet [376]. They studied the effects of a high-fat and low-fat diets on Sdc3 KO mice and their wild-type controls. Interestingly, they demonstrated that when given a high-fat diet, Sdc3 KO mice were partially resistant to obesity due to a reduction in food intake by male mice and an increase in energy expenditure in females, relative to that of WT

controls[376]. It has been shown that there is a link between appetite, energy metabolism and bone remodelling which may indicate that the underlying mechanisms involved in this link may also play a role in development of the Sdc3 KO phenotype[403]. Given the importance of the effect of weight on bone mass, the weights of my Sdc3 KO and WT control mice were taken from 1 to 24 weeks of age with ad libitum access to a chow diet. No significant differences were seen in both male and female Sdc3 KO and WT mice therefore the change in bone volume cannot be explained by a change in weight (**Figure 3.1 and 3.2**).

Findings by Koyama *et al.*[302] suggested that syndecan 3 may play a role during early development by demonstrating that during the development of chick limbs the mesenchymal condensations are surrounded by a thick layer of connective tissue, the perichondrium, that is rich in syndecan 3. It was later shown that syndecan 3 is important during the condensation phase in development as it is able to set boundaries and limit condensation size[208]. It has also been shown that syndecan 3 is highly expressed in the periosteum of developing long bones of chicks and in association with the differentiating osteoblasts of the periosteum[300]. This suggests syndecan 3 may be important during skeletogenesis and in regulating the onset of bone differentiation possibly due to a role in cell-cell interactions, which are crucial during development, and interactions between cells and the extracellular matrix. Although syndecan 3 is found in early development its exact role is still unclear. Although I have found that Sdc3 KO mice have low bone volume in adulthood, it is still unknown whether this could be early onset osteoporosis or a change during early development. In order to further understand this, the whole skeletons and tibias of 2-day-old pups were analysed (**Figure 3.7, 3.8 and 3.9**). Remarkably, the opposite of what is seen in the adult Sdc3 KO mice was observed in the 2-day-old pups, with the phenotype being reversed. At first, when observing the whole skeletons there are no major anatomical differences between Sdc3 KO and WT pups but upon closer investigation, Sdc3 KO tibias were longer and had increased overall bone volume when compared to WT. As Sdc3 is known to play a role in restricting condensation size in early skeletal development, knocking Sdc3 out may cause the difference in tibiae length as this inhibition or restriction may be released, thus explaining the longer bones seen in of Sdc3KO P2 pups[264,274,280,404–407]. The data found in these

papers highlights the importance of Sdc3 during early development possibly by having a role in regulating cell proliferation and interactions.

Measurements of tibia lengths were also taken at 3 and 6 months of age. Although at 2 days old Sdc3 KO pups had longer tibias than those of WT pups, at 3 months of age they become shorter compared to WT mice and remain shorter than controls as they mature (**Figure 3.9 and 3.10**). Although the difference in leg lengths at 3 and 6 months was significant this was only a 2% and a 4% change from WT, respectively. This absolute difference in tibial length was so small that there was no need to change the height, during microCT analysis, of the stack of slices as this would only equate to approximately 2 slices which is within the margin of error of the ROI.

The spines of 3 and 6-month old mice were also analysed showing only a significant decrease in BV/TV in 3-month-old Sdc3 KO mice which reflects a highly significant decrease in trabecular thickness, when compared to age matched WT mice (**Figure 3.12**). At 6 months of age no significant changes were observed between Sdc3 KO and WT mice (**Figure 3.13**). This may be due to the fact that long bones loose bone volume at a faster rate than vertebral bones, but most likely due to the low number of replicates used in this analysis[408,409].

Given the global burden of osteoporosis it would be of interest to understand whether Syndecan 3 could be used as a therapeutic approach, possibly by overexpressing it in certain cells. Interestingly, a recent paper by Mansouri *et al*.[410] investigated the function of endogenous cellular GAGs during bone remodelling by using a transgenic mouse model overexpressing Sdc2 in osteoblasts. This led to an increase in bone volume in mice due to an enrichment in heparan sulphate on the bone surface. They saw a significant increase in trabecular bone volume and number in both young and mature mice and a decrease in trabecular separation in mature mice, but no changes in cortical bone. In contrast, overexpression of Sdc2 also inhibited resorption by inhibiting osteoclastogenesis and therefore decreasing bone remodelling, modulated bone formation by increasing osteoblast activity in younger mice but reduced osteoblast number in older mice which led to a decrease in bone formation rate in the older mice. It also appeared to have different impacts on angiogenesis depending on the age of the mice, by increasing pro-osteogenic endothelium in young mice, which also supports osteogenesis, but strongly

decreasing these types of vessels in the mature mice overexpressing Sdc2. This proteoglycan overexpression also inhibited the Wnt- β-catenin pathway and increased apoptosis in mesenchymal precursors in bone marrow. They concluded that GAGs could have an important role during osteogenesis but may also interfere with the crosstalk between the bone surface and marrow cells, altering osteoblast function[273]. These findings highlight how these proteoglycans have different effects at different ages and in different cells which is also comparable to the syndecan 3 knockout in which I see an increase in bone volume in early developmental stages but then see a decrease in bone volume in young adulthood when comparing to WT mice of the same ages. And although Sdc3 and Sdc2 are structurally different and have different expression patterns this study by Mansouri *et al*.[410] highlights the importance of investigating the different effects Sdc3 may have on different bone cells and how these cells could affect each other.

In another study Bertrand *et al*.[313], analysed the functional role of Sdc4 during normal bone development and during bone fracture repair by using Sdc4 KO mice generated via a lacZ-knockin strategy. As with Sdc3 KO mice, the Sdc4 KO pups showed no obvious postnatal abnormalities, although no measurements of long bones were taken, when compared to their WT littermates. In this study they showed that the deletion of Sdc4 was associated with only minor changes in bone development, with Sdc4 KO mice having no major anatomical differences in the skeleton, no major differences in size and morphometric analysis of calcified tissue showed no significant differences when compared to WT littermates. They also found that the loss of Sdc4 is compensated for by a marked up-regulation of Sdc2 during bone development, but there is a lack of this compensation in adult bones during fracture repair. This could be due to age or the activity of cytokines involved in inflammation[313]. Taking this into account it is important to understand whether the remaining syndecans have any compensatory effect in the absence of Sdc3, which seems unlikely during adulthood when considering the significant low bone volume seen in the adult Sdc3 KO mice. But, on the other hand, this could possibly explain why during early development Sdc3 KO pups have increased bone volume when compared to WT pups, although the effect of other syndecans on early skeletogenesis is unknown. Interestingly, a recent paper by Kehoe *et al.*[411] that aimed to examine

the role of Sdc3 in joint inflammation, showed that Sdc3 also has a role during stress conditions such as arthritis, having both pro- and anti-inflammatory properties depending on the tissue and the nature of the inflammatory insult. They showed that in the joint Sdc3 is pro-inflammatory due to the fact its deletion reduces leukocyte recruitment and the clinical manifestation of arthritis. Though it seems that in the skin and in the cremaster muscle Sdc3 is anti-inflammatory due to an enhanced leukocyte interaction with the endothelium and recruitment after deletion of the proteoglycan[411]. These studies demonstrate how different syndecans have very distinct functions which could be due to diverse extracellular domain sequences, respective GAG chain structures and specific GAG binding sites, and glycosylation variation of the extracellular domain, with the cytoplasmic domain having the most conserved areas but still some variation among the family of four[313,407,412,413]. These structural features allow syndecans to interact with different types of ligands, such as growth factors, cytokines, extracellular matrix proteins and glycoproteins, and other proteins which could promote different responses in the cell which may also be dependent on different syndecans[406,407].

Studies, such as that done by Shimazu *et al*.[301], have shown the importance of Sdc3 in chondrogenesis and regulation of chondrocyte proliferation, but none have yet shown the importance of syndecans in bone homeostasis[289,301,308]. Therefore, considering that this model has shown that by knocking Sdc3 out, mice have a low bone volume phenotype it is important to investigate osteoblast and osteoclast function *in vivo* and *in vitro* as it is possible that this phenotype is due to decreased bone formation, or increased bone resorption, or possibly a combination of both. In the next chapters I will be looking into this on a cellular level.

4 Low bone volume phenotype in Sdc3 KO mice is associated with reduced bone remodelling

4.1 Introduction

In the previous chapter I have described µCT morphometric analysis of long bones and spine of Sdc3 KO mice. Adult Sdc3 KO mice have decreased trabecular and cortical bone volume. By performing 3-point bend tests on the mouse femurs, it was shown that there is less force required to break Sdc3 KO bones versus WT bones, which indicates that the bones of Sdc3 KO mice are more fragile than bones of the WT. Interestingly Sdc3 KO pups were shown to have longer tibias with increased bone volume when compared to WT pups. This suggests syndecan 3 to be important for normal bone maintenance in adulthood but also *in utero* given the difference in phenotype in early development when compared to adult and mature mice.

It is known that syndecan 3 plays an important role in the condensation phase, critical during skeletogenesis, and is a regulator of chondrocyte proliferation[208,300,375,414]. It has increased expression during limb development, where it is found in the perichondrium and periosteum, and in the developing calvaria, but its exact role is still unknown[300,302]. Sdc3 also plays an important role in growth plate proliferation and maturation of chondrocytes[301]. However, the role and mechanisms in which Sdc3 is involved and its specific function in the maintenance of adult bone homeostasis is unclear. Apart from syndecan 3, so far only syndecan 2 has been shown to have a role in bone. Sdc2, which also has a role during condensation of prechondrogenic core and the perichondrium, was found to be highly expressed during osteoblast differentiation[410]. Therefore, Mansouri *et al*. created a mouse model with syndecan 2 overexpression in osteoblasts to further understand its role in osteogenesis[273]. They found that Sdc2 overexpression in osteoblasts lead to increased bone formation but also found that Sdc2 can support osteoclastogenesis, osteogenesis and other mesenchymal precursor populations[273]. Taking this study into account it may be of interest to investigate osteoblast function and bone formation in the Sdc3 KO as a reduction in osteoblastogenesis may be a reason for the low bone mass phenotype. But it is also important to investigate osteoclast function as Sdc3

KO may possibly have increased osteoclastogenesis or overactive osteoclasts. In order to fully understand the mechanisms underlying the low bone volume phenotype of Sdc3 KO mice, dynamic bone histomorphometry of Sdc3 KO and WT adult mice was performed.

Mechanical loading is an important factor for the maintenance of bone mass[415]. Studies have shown that increased mechanical loading results in an increase in bone mass while in contrast, lack of mechanical loading leads to a rapid bone loss[415]. Therefore, the effect of mechanical loading on Sdc3 KO and WT mice was also investigated. As human osteoporosis is associated with increased bone marrow adiposity[416–419] and whilst preforming histology, voids in the bone marrow of Sdc3 KO mice were observed suggestive of the presence of an increased number of adipocytes, quantification of the bone marrow adipose tissue was also performed in Sdc3 KO versus WT mice.

4.2 Methods

Male Sdc3 KO and WT mice (3 and 6 months old) received two injections of calcein (200µl IP injection of 2mg/ml) 5 days and 2 days before euthanizing. Mouse skins were removed and the hind limbs were fixed overnight in 4% PFA. Tibias were then dissected and fixed in neutral buffered formalin for 24 hours and stored in 70% ethanol at room temperature. After µCT analysis, the left tibia was processed for MMA embedding and the right tibia for paraffin embedding.

For analysis of bone formation, MMA embedded sections of the left tibia taken from 3-month-old WT (N=12) and Sdc3 KO mice (N=11) and from 6-month-old WT (N=8) and Sdc3 KO mice (N=7) were stained, without being deplasticised, with Calcein Blue (Sigma). The sections were dehydrated through an alcohol series, cleared in xylene and coverslipped using the automatic coverslipper in the Leica auto stainer. These were then visualised using the Zeiss Axio Scan.Z1 slide scanner with a monochrome camera and a 20x lens resulting in a pixel size of 0.227 µm.

For analysis of bone resorption parameters, MMA embedded sections of the left tibia taken from 3-month-old WT (N=13) and Sdc3 KO mice (N=13) and from 6-month-old WT (N=10) and Sdc3 KO mice (N=7) were deplasticised in monoethanolamine (MEA) and stained for tartrate resistant acid phosphatase

(TRAcP) activity to visualise osteoclasts and counterstained using Aniline Blue to visualise bone, as described by Van ´t Hof *et al.*[379] and adapted from Chappard *et al.*[380] (for details please see Chapter 2). For the imaging of the TRAcP stained sections, a Zeiss Axio Scan.Z1 slide scanner was used with a 10× lens together with a colour camera resulting in a pixel size of 0.442 µm.

For quantification of bone marrow adiposity, MMA embedded sections of left tibias of 3-month-old WT (N=6) and Sdc3 KO mice (N=4) and 6-month-old WT (N=6) and Sdc3 KO mice (N=6) were deplasticised in MEA and stained with Goldners Trichrome method. To confirm the presence of fat cells in the marrow space, a Perilipin (Abcam) immunostain was performed on dewaxed paraffin embedded sections of 3-month-old WT (N=3) and Sdc3 KO mice (N=3). Sections were incubated in Unitreve solution, blocked with goat serum and incubated in a 1:500 dilution of perilipin rabbit primary antibody, washed in PBS, incubated in 1:200 dilution of the secondary goat anti rabbit Alexa fluor 594 (Invitrogen). Imaging was performed using the Zeiss LSM800 confocal microscope with a colour camera and a 10x lens, resulting in a pixel size of 0.908 µm.

To assess for anabolic response to mechanical loading, the right tibias of 3-month-old male Sdc3 KO (N=11) and WT (N=8) mice where held in the loading cups and dynamic axial loads where applied through the knee joint three times a week (Mondays, Wednesdays and Fridays) for 2 consecutive weeks (for details please refer to Chapter 2). During the final week of loading mice received two injections of calcein (200µl IP injection of 2mg/ml) 7 days and 3 days before euthanizing. After euthanizing, mouse skins were removed and hind limbs dissected and placed in 4% PFA to fix overnight. The left (not loaded) and right (loaded) mouse tibias were then dissected and fixed in neutral buffered formalin for 24 hours and stored in 70% ethanol at room temperature until analysed by µCT. After µCT analysis, histomorphometric analysis of bone formation was performed as described above.

All bone histomorphometric analysis of measurements of the region of interest, which included proximal tibial metaphysis and excluded primary spongiosa, was performed using a custom in-house developed image analysis program based on ImageJ, available at https://www.liverpool.ac.uk/ageing-and-chronic-disease/bone-hist/ (developed by Prof. Rob van 't Hof[379]). For bone marrow adiposity

quantification, the same program was used but set to quantify the circular voids within the bone marrow.

Statistical analysis was performed using a paired two-tailed Student's *t* test for mechanical loading, and otherwise an unpaired two-tailed Student's *t* test.

For details on the methods used in this chapter please see **Chapter 2.**

4.3 Results

4.3.1 Dynamic bone histomorphometry analysis

3-month-old mice

Dynamic histomorphometric analysis of bone formation in male 3-month-old Sdc3 KO mice (N=11) showed a significant reduction in BV/TV of 35% ($p<0.01$), mineralising apposition rate (MAR) of 21% ($p<0.01$), mineralising surface per bone surface (MS/BS) of 38% ($p<0.01$) and in bone formation rate per bone surface (BFR/BS) of 51% ($p<0.001$), when compared to male 3-month-old WT mice (N=12) (**Figure 4.1, A; Table 4.1**). Calcein double labelling showed a striking decrease of double label surface in Sdc3 KO compared to WT mice (**Figure 4.1, B and C**). These results support the µCT data from the previous chapter, suggesting that lack of Sdc3 significantly reduces bone formation in long bones.

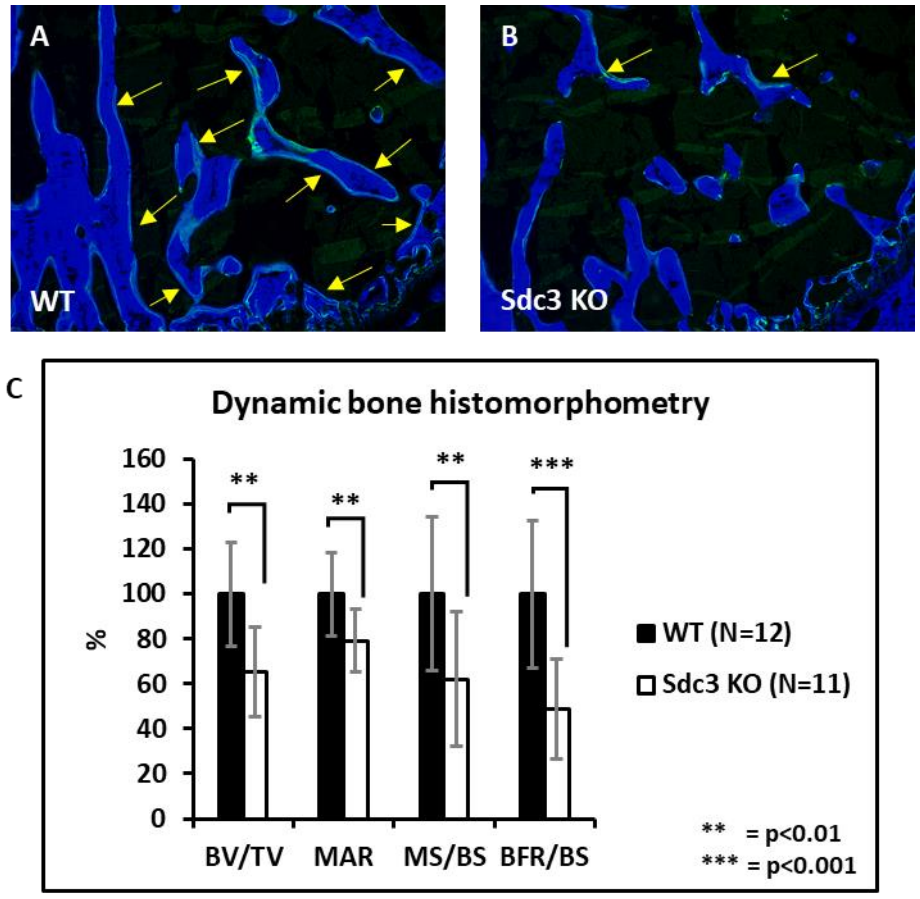

Figure 4.1: Dynamic bone histomorphometry analysis at 3 months of age. Analysis of bone formation parameters (**A**) in tibias from 3-month-old male Sdc3 KO (N=11) shows a significant decrease in bone volume per tissue volume (BV/TV), mineral apposition rate (MAR), mineralising surface per bone surface (MS/BS) and bone formation rate per bone surface (BFR/BS) as compared to WT (N=12). Fluorescent microscopy of tibias from WT and Sdc3 KO mice with calcein double-labelling and Calcein Blue counterstain show many areas with double label (indicated by yellow arrows) in the WT mice (**B**), compared with significantly less double label surface in Sdc3 KO (**C**). Note that the Sdc3 KO mouse appears to have more single labels. Measurements were normalised to 100% for the WT in **A**. Data in A are means ± SD. Significance is denoted by **p<0.01 and ***p<0.001.

6-month-old mice

Analysis of bone formation (**Figure 4.2, A; Table 4.1**) from male 6-month-old Sdc3 KO mice (N=7) showed a significant reduction in MS/BS of 30% ($p<0.05$) and in BFR/BS of 43% ($p<0.05$), when compared to male 6-month-old WT mice (N=8). BV/TV and MAR showed no significant difference between Sdc3 KO and WT mice. Although the difference in bone formation parameters - MAR, MS/BS and BFR/BS - is more significant at 3 months of age the data analysed at 6 months of age still shows an impairment in bone formation, suggesting impaired osteoblast function.

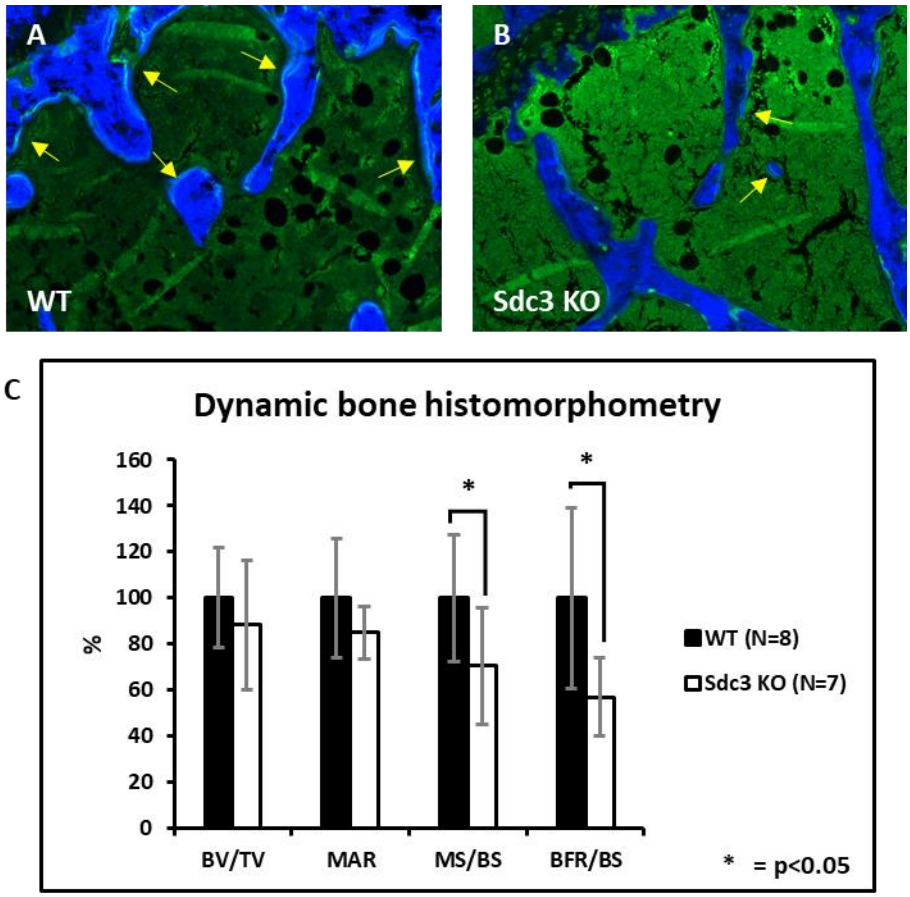

Figure 4.2: Dynamic bone histomorphometry analysis at 6 months of age. Analysis of bone formation parameters (**A**) in tibias of 6-month-old male Sdc3 KO (N=7) shows a significant decrease in mineralising surface per bone surface (MS/BS) and bone formation rate per bone surface (BFR/BS) as compared to WT (N=8). Bone volume per tissue volume (BV/TV) and mineral apposition rate (MAR) showed no significant difference between Sdc3 KO and WT mice. Fluorescent microscopy of tibias from WT and Sdc3 KO mice with calcein double-labelling and Calcein Blue counterstain shows a higher amount of calcein double label in in the WT mice (**B**) compared to very little double label in Sdc3 KO (**C**), with calcein double labels (in green) indicated by yellow arrows. Measurements were normalised to 100% for the WT in **A**. Data in **A** are means ± SD. Significance is denoted by *p<0.05.

Table 4.1: Dynamic histomorphometry analysis of bone formation parameters in WT and Sdc3 KO male mice at 3 and 6 months of age. Significant differences can be observed between Sdc3 KO and WT mice at both 3 and 6 months of age. Values shown are means ± SD. Significance (Sdc3 KO vs age-matched WT mice) denoted by *p<0.05, **p<0.01, ***p<0.001.

	3-month-old		6-month-old	
	WT (N=12)	**Sdc3 KO (N=11)**	**WT (N=8)**	**Sdc3 KO (N=7)**
BV/TV (%)	17 ± 4	**11 ± 3*****	13 ± 3	12 ± 4
MAR (µm/day)	2 ± 0.4	**2 ± 0.3****	1 ± 0.3	1 ± 0.1
MS/BS (%)	32 ± 11	**20 ± 10****	20 ± 6	**14 ± 5***
BFR/BS ($\mu m^3/\mu m^2$/day)	0.6 ± 0.2	**0.3 ± 0.1*****	0.2 ± 0.1	**0.1 ± 0.04***

4.3.2 Histomorphometric quantification of osteoclasts

3-month-old mice

Surprisingly, histomorphometric analysis of tibias (**Figure 4.3, A; Table 4.2**) from male 3-month-old Sdc3 KO mice (N=13) showed a significant reduction in osteoclast surface per bone surface (Oc.S/BS) of 44% ($p<0.05$), number of osteoclasts per bone surface (N.Oc/BS) of 44% ($p<0.01$) and number of osteoclasts per tissue volume (N.Oc/TV) of 57% ($p<0.01$), when compared to male 3-month-old WT mice (N=13). Number of osteoclasts per bone volume (N.Oc/BV) showed no significant difference between Sdc3 KO mice and WT mice. These data suggest that the reduced bone volume phenotype of Sdc3 KO, analysed by µCT is not due to an increase in osteoclast numbers but due to impaired osteoblast function in the Sdc3 KO mice. These data suggest that Sdc3 KO mice have reduced osteoclastogenesis.

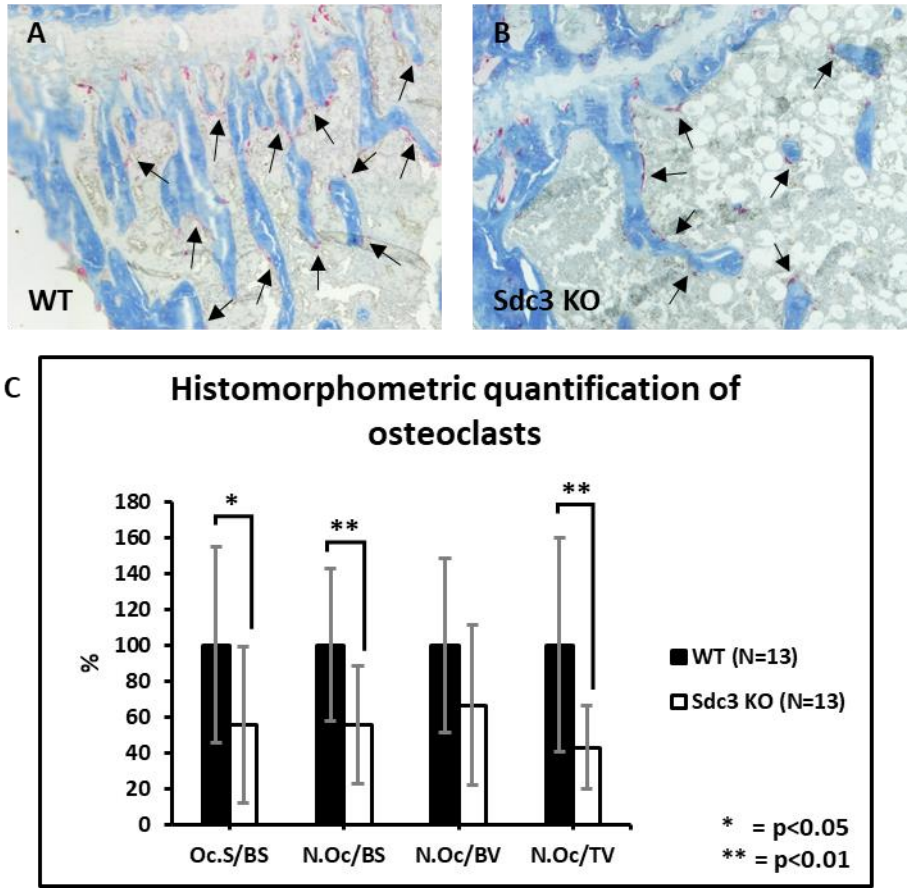

Figure 4.3: Histomorphometric quantification of osteoclasts in 3-month-old mice. Analysis of histomorphometric parameters (**A**) of tibias of 3-month-old male Sdc3 KO (N=13) shows a significant decrease in osteoclast surface per bone surface (Oc.S/BS), number of osteoclasts per bone surface (N.Oc/BS) and number of osteoclasts per tissue volume (N.Oc/TV) as compared to WT (N=13). Aniline Blue and TRAcP stain of a tibia from WT and Sdc3 KO mice show higher number of osteoclasts in the WT (**B**) compared to a reduced number of osteoclasts in Sdc3 KO mice (**C**), with osteoclasts (stained red) indicated by arrows. Measurements were normalised to 100% for the WT in **A**. Data in **A** are means ± SD. Significance is denoted by *p<0.05 and **p<0.01.

6-month-old mice

Histomorphometric quantification of osteoclasts in tibias (**Figure 4.4, A; Table 4.2**) from male 6-month-old Sdc3 KO mice (N=7) showed a significant reduction in Oc.S/BS of 53% ($p<0.01$), N.Oc/BS of 61% ($p<0.01$), N.Oc/BV of 62% ($p<0.01$) and N.Oc/TV of 70% ($p<0.001$) when compared to male 6-month-old WT mice (N=10).

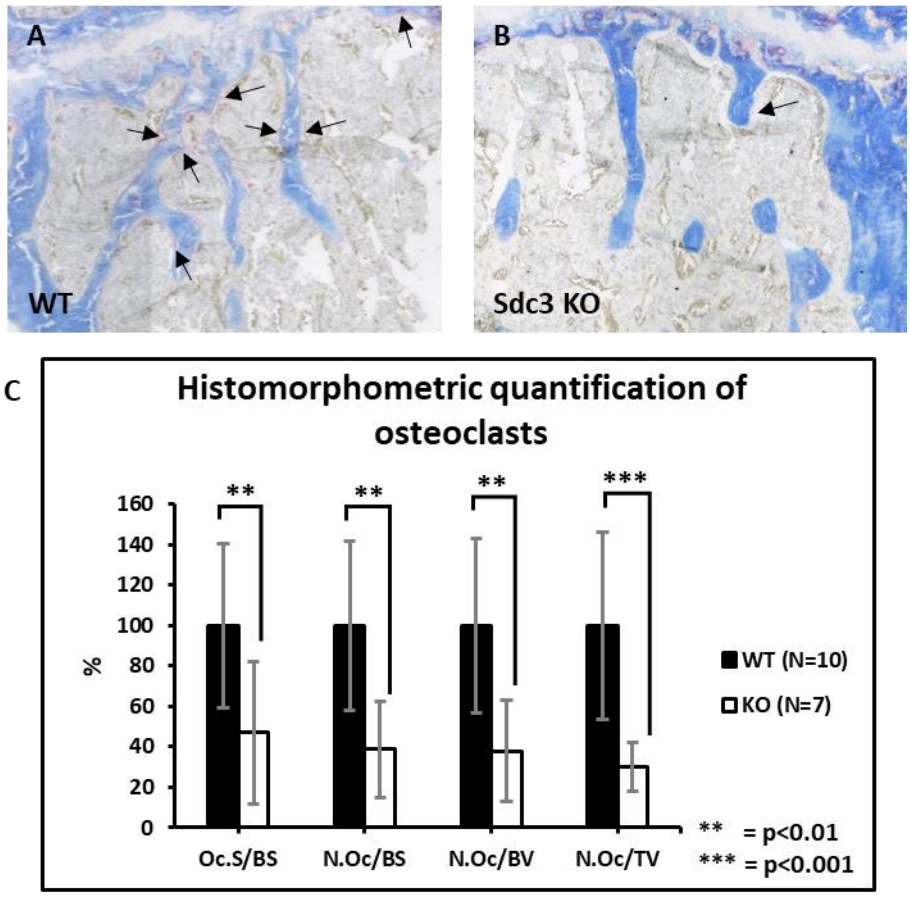

Figure 4.4: Histomorphometric quantification of osteoclasts in 6-month-old mice. Analysis of histomorphometric parameters (**A**) of tibias of 6-month-old male Sdc3 KO (N=7) shows a significant decrease in osteoclast surface per bone surface (Oc.S/BS), number of osteoclasts per bone surface (N.Oc/BS), number of osteoclasts per bone volume (N.Oc/BV) and number of osteoclasts per tissue volume (N.Oc/TV) as compared to WT (N=10). Aniline Blue and TRAcP stain of a tibia from WT and Sdc3 KO mice show more osteoclasts in the WT (**B**) compared to a reduced number of osteoclasts in Sdc3 KO mice (**C**), with osteoclasts (stained red) indicated by arrows. Measurements were normalised to 100% for the WT in **A**. Data in **A** are means ± SD. Significance is denoted by **p<0.01 and ***p<0.001.

Table 4.2: Histomorphometry analysis of osteoclasts. Results show Sdc3 KO have significantly decreased overall osteoclast numbers compared to WT mice at both 3 and 6 months of age. Values shown are means ± SD. Significance (Sdc3 KO vs age-matched WT mice) denoted by *p<0.05, **p<0.01.

	3-month-old		6-month-old	
	WT (N=13)	**Sdc3 KO (N=13)**	**WT (N=10)**	**Sdc3 KO (N=7)**
Oc.S/BS (%)	10.52 ± 5.74	**5.86 ± 4.57***	4.96 ± 2.02	**2.33 ± 1.76****
N.Oc/BS (mm^{-1})	6.50 ± 2.75	**3.62 ± 2.12****	2.96 ± 1.23	**1.15 ± 0.70****
N.Oc/BV (mm^{-2})	299.92 ± 145.67	199.26 ± 133.90	135.95 ± 58.38	**51.53 ± 34.11****
N.Oc/TV (mm^{-2})	51.71 ± 30.80	**22.15 ± 12.01****	17.69 ± 8.20	**5.31 ± 2.16****

4.3.3 Bone marrow adiposity quantification

3-month-old mice

During bone histomorphometry analysis it was noted that there were round empty spaces in the bone marrow of Sdc3 KO compared to WT mice, which were suggestive of increased bone marrow adiposity (**Figure 4.2** and **4.3**). To confirm that these voids were indeed fat cells a specific adipocyte stain, perilipin (**Figure 4.5 A** and **B**), was used. Perilipin stained the cytoplasm of the adipocytes red, as can be seen in **Figure 4.5 A** and **B**, confirming the voids were adipocytes. Next, Goldners trichrome staining was performed (**Figure 4.5 C** and **D**) in order to quantify bone marrow adiposity (**Figure 4.5 E** and **F**). Percentage fat area analysis revealed a mean of 9% for Sdc3 KO compared to a mean of only 0.1% for WT controls (**Figure 4.5 E**). Histomorphometry analysis of bone marrow adiposity (**Figure 4.5 F**) in male 3-month-old Sdc3 KO mice (N=4) revealed a 60-fold increase in bone marrow adipocytes when compared to WT mice (N=6). Sdc3 KO mice had a mean of 122mm^{-2} of fat cells per tissue volume (N.Fat cells/TV) and WT mice had a mean of only 2mm^{-2} ($p<0.001$). These data shows that Sdc3 KO mice have increased bone marrow adipose tissue when compared to WT mice.

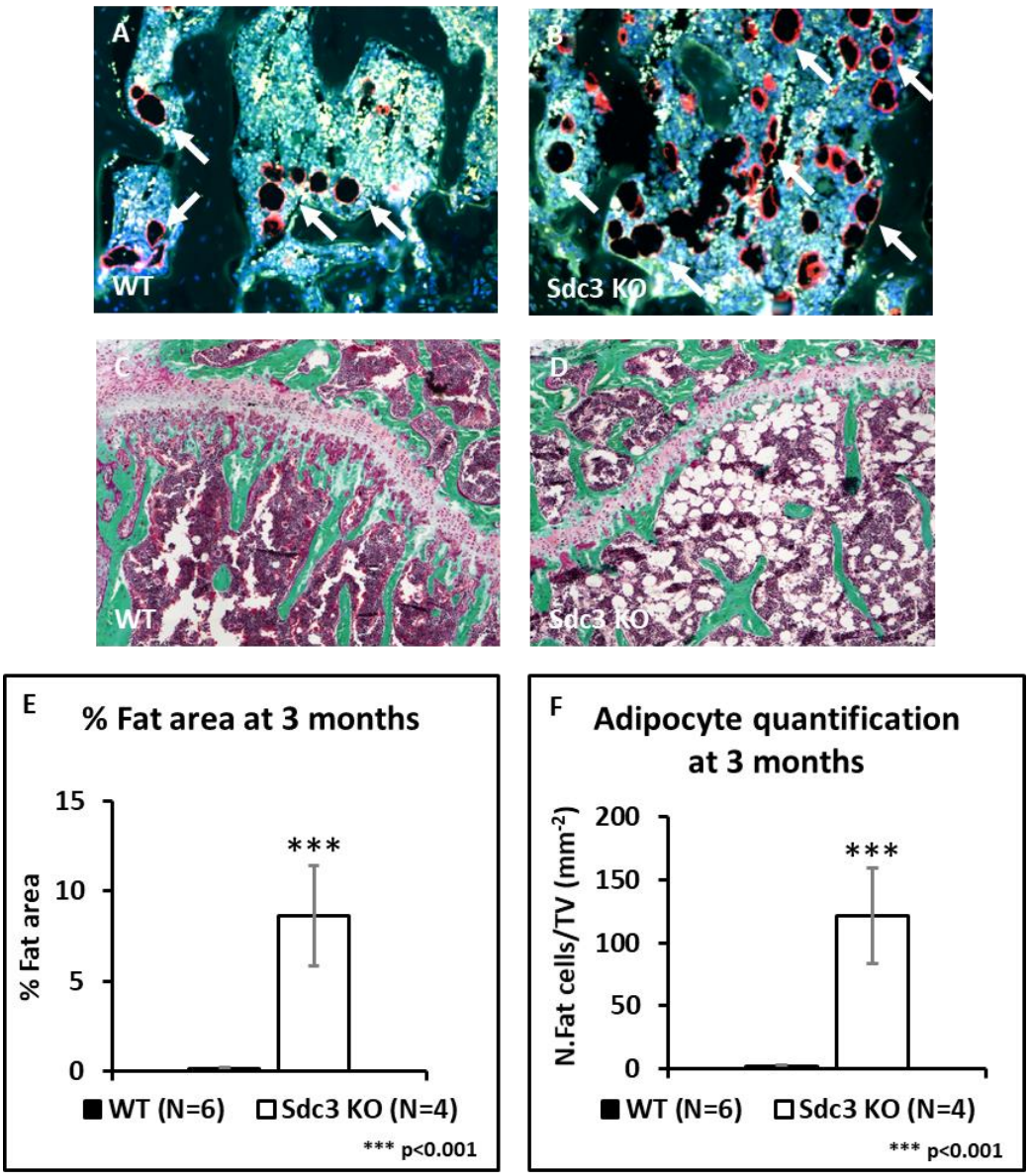

Figure 4.5: Bone marrow adiposity quantification at 3 months of age. Perilipin immunostain was performed on sections of WT (**A**) and Sdc3 KO (**B**) mice to confirm that the voids observed in the marrow area were indeed fat cells. Positive fat cells are stained red and highlighted by white arrows. Goldners trichrome staining was performed (**C** and **D**) in order to quantify bone marrow adiposity (**E** and **F**). Histomorphometry analysis of tibias of 3-month-old mice revealed a highly significant increase in percentage fat area (% fat area; **E**) and number of fat cells per tissue volume (N. Fat cells/TV; **F**) in Sdc3 KO mice (N=4) when compared to WT (N=6). Values shown in **E** and **F** are means ± SD. Significance is denoted by ***p<0.001.

6-month-old mice

The proximal metaphysis of tibias of 6-month-old Sdc3 KO continued to be occupied mostly by adipocytes (**Figure 4.6, B**) in contrast to what was observed in the same region of WT mouse tibias (**Figure 4.6, A**). Histomorphometry analysis of bone marrow adiposity (**Figure 4.6, C** and **D**) of male 6-month-old Sdc3 KO mice (N=6) revealed a mean percentage fat area of 3% for the Sdc3 KO mice in comparison to 1% in the WT mice ($p<0.001$). Analysis also revealed that Sdc3 KO mice had a mean of 65mm^{-2} of N. Fat cells/TV compared to a mean of 30mm^{-2} in WT mice ($p<0.01$). This indicates a 2-fold increase in bone marrow adiposity in Sdc3 KO mice when compared to WT mice.

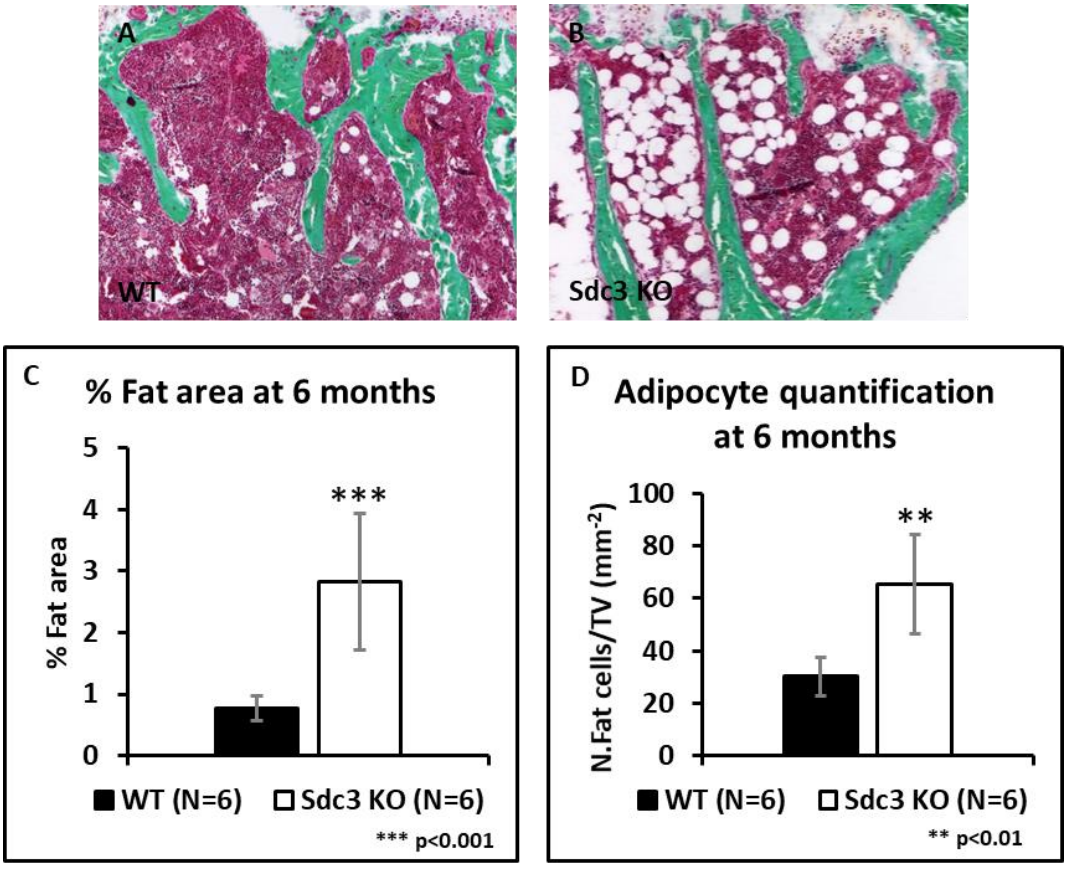

Figure 4.6: Bone marrow adiposity quantification at 6 months of age. Histomorphometry analysis of Goldners trichome stained tibias of 6-month-old WT (**A**) and Sdc3 KO (**B**) mice revealed a highly significant increase in percentage fat area (%Fat area; **C**) and in number of fat cells per tissue volume (N. Fat cells/TV; D) in Sdc3 KO mice (N=6) when compared to WT (N=6). Values shown in **C** and **D** are means ± SD. Significance is denoted by **p<0.01 and ***p<0.001.

4.3.4 Assessment of anabolic response of bone to mechanical loading

As histomorphometry data suggested decreased osteoblast-mediated bone formation in Sdc3 KO versus WT mice and as bone responds with new bone formation to mechanical loading[382], I performed mechanical loading to assess the ability of Sdc3 KO osteoblasts to form new bone. This was performed by applying an axial load on the right tibias of 3-month-old male WT and Sdc3 KO mice. To assess whether mechanical loading would induce any changes in trabecular and cortical bone I used µCT to analyse the tibias using the same method as described in Chapter 3. Dynamic histomorphometric analysis was also performed to investigate bone formation parameters also as described above.

µCT analysis of trabecular bone

When comparing loaded and not loaded tibias, Sdc3 KO showed significantly increased BV/TV ($p<0.05$) and Tb.Th ($p<0.01$), and significantly decreased Tb.Sp ($P<0.05$) and Tb. Pf ($P<0.05$) (**Table 4.3**). On the other hand, WT mice showed no significant changes in response to loading when comparing loaded leg to not loaded leg.

Table 4.3: MicroCT analysis of trabecular bone in the not loaded and loaded tibias of male WT and Sdc3 KO mice at 3 months of age. Interestingly Sdc3 KO loaded leg parameter values are significantly different from the not loaded leg parameter values as opposed to the WT mice which show no anabolic response to loading as no significant differences between loaded and not loaded leg were observed. Values shown are means ± SD. Significance denoted by *p<0.05 and **p<0.01 (Loaded vs not loaded legs of Sdc3 KO mice).

	WT (N=13)		**Sdc3 KO (N=16)**	
	Not loaded	**Loaded**	**Not loaded**	**Loaded**
BV/TV (%)	21.3 ± 2	22 ± 2	17 ± 3	**18 ± 3***
Tb.Th (µm)	57 ± 4	58 ± 5	50 ± 2	**54 ± 3****
Tb.Sp (µm)	156 ± 10	153 ± 11	166 ± 16	**163 ± 14***
Tb.N (mm)	4 ± 0.4	4 ± 0.4	3 ± 0.6	3 ± 0.5
Tb.Pf (1/mm)	17 ± 2	16 ± 2	22 ± 4	**20 ± 3***
SMI	2 ± 0.2	2 ± 0.2	2 ± 0.2	2 ± 0.2

Micro CT analysis of cortical bone

Cortical analysis showed no significant differences when comparing loaded and not loaded legs of the same genotype (**Table 4.4**).

Table 4.4: MicroCT analysis of cortical bone in the loaded versus not loaded tibias of male WT and Sdc3 KO mice at 3 months of age. No significant changes were observed between loaded and not loaded legs within genotypes. Values shown are means ± SD.

	WT (N=10)		Sdc3 KO (N=14)	
	Not loaded	**Loaded**	**Not loaded**	**Loaded**
Cort.Th (μm)	262 ± 11	260 ± 17	243 ± 13	242 ± 13
P.Pm (mm)	5 ± 1	5 ± 1	4 ± 0.5	4 ± 0.7
E.PM (mm)	4 ± 1	4 ± 1	2 ± 0.1	2 ± 0.1
MMI (mm^4)	0.2 ± 0.1	0.3 ± 0.1	0.2 ± 0.03	0.2 ± 0.1

Bone formation analysis

Histomorphometric analysis of bone formation of the loaded versus not loaded legs of 3-month-old WT and Sdc3 KO mice revealed a 34% ($p<0.001$) and a 36% ($p<0.05$) increase in MS/BS and BFR/BS, respectively, in WT mice after loading (**Figure 4.7 A; Table 4.5**). On the other hand, Sdc3 KO mice showed an increase of 12% and 21% in MS/BS and BFR/BS, respectively, after loading, but this increase did not reach significance and the response was highly variable between mice. MAR revealed a 2% and a 4% increase in WT and Sdc3 KO mice respectively which was not significant (**Figure 4.7 A**). As can be seen in **Figure 4.7 B**, WT mice have many double labels throughout the section and appear to have a very active growth plate with many single and double label. On the other hand, Sdc3 KO mice sections (**Figure 4.7 C**) have very little amount of double label, some single label, a very inactive growth plate with very little single or double label and their bone marrow space appears to have many adipocytes.

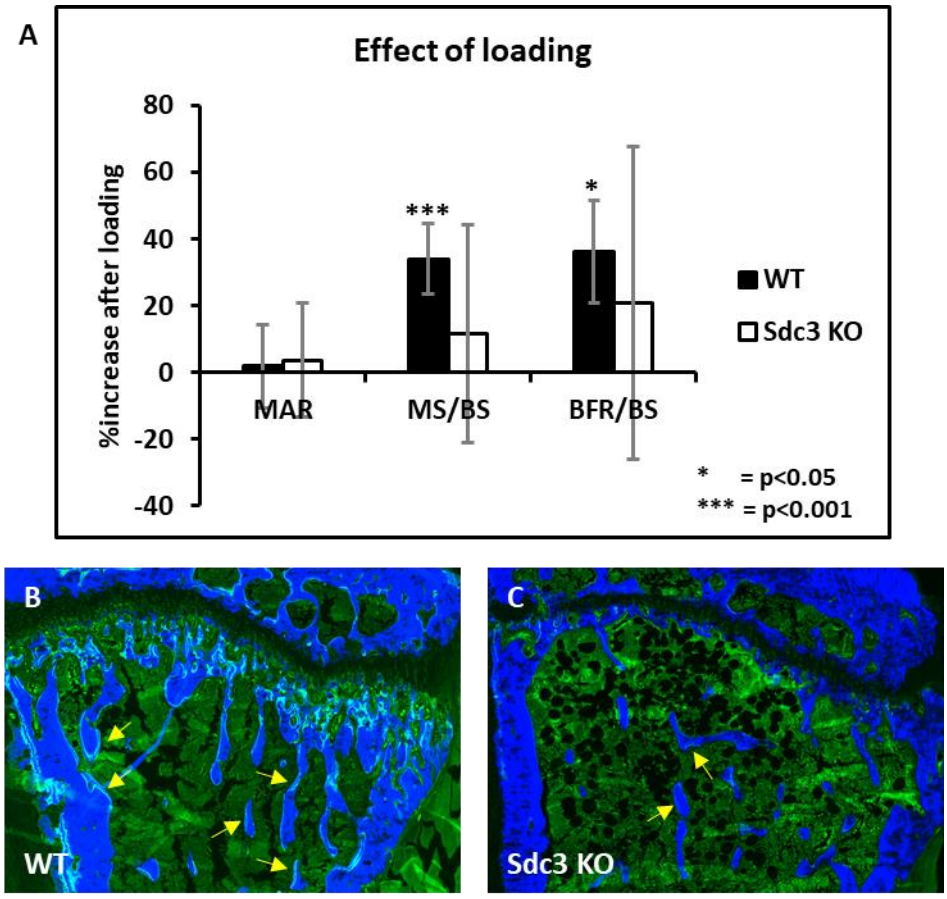

Figure 4.7: Percentage increase in bone formation parameters after loading in WT and Sdc3 KO mice analysed by dynamic histomorphometry. The effect of loading is shown by comparing not loaded leg to loaded leg of WT mice (N=6) and the same for Sdc3 KO mice (N=8). **(A)** WT have significantly increased mineralising surface per bones surface (MS/BS) and bone formation rate per bone surface (BFR/BS) when comparing loaded leg to not loaded leg, but Sdc3 KO appear to have a blunted response to loading. Mineral apposition rate (MAR) remains unchanged in both WT and Sdc3 KO. Fluorescent microscopy of tibias from WT and Sdc3 KO mice with calcein double-labelling and Calcein Blue counterstain show many areas with double label (indicated by yellow arrows) and, what appears to be, a very active growth plate in the WT mice (**B**), compared with significantly less double label surface in Sdc3 KO (**C**). Note that the Sdc3 KO mouse appears to have adipocytes in the bone marrow space and a growth plate with very little single labels. Means ± SD. Significance is denoted by *p<0.05 and ***p<0.001 (not loaded vs loaded legs).

Table 4.5: Percentage increase in bone formation parameters after loading. Values show significant increases in mineralising surface per bone surface (MS/BS) and bone formation rate per bone surface (BFR/BS) in WT mice after loading but show no significant changes in Sdc3 KO mice after loading, indicating a blunted response to loading in Sdc3 KO mice. WT mice N=6; Sdc3 KO mice N=8. Values shown are means ± SD. Significance is denoted by *p<0.05 and ***p<0.001 (not loaded vs loaded leg within genotypes).

	MAR	MS/BS	BFR/BS
WT (%)	1.90 ± 12.60	**34.10 ± 10.55*****	**36.25 ± 15.52***
Sdc3 KO (%)	3.64 ±1 7.10	11.65 ± 32.48	20.84 ± 46.76

4.4 Discussion

In the previous chapter adult Sdc3 KO mice were shown to have a low bone volume phenotype with increased bone fragility, but interestingly Sdc3 KO pups had increased bone volume and length indicating that Sdc3 has different functions at different stages of development and in bone maintenance. In order to ascertain the underlying mechanisms involved in the low bone volume phenotype observed the adult Sdc3 KO mice, dynamic histomorphometric analysis was performed. In this chapter I have shown that Sdc3 KO mice have reduced bone formation, reduced osteoclast number and increased bone marrow adiposity at 3 and 6 months of age, when compared to age matched WT mice. Through histomorphometric analysis, Sdc3 KO mice also have an impaired response to mechanical loading which could explain the reduced bone formation observed at both 3 and 6 months of age and therefore the low bone phenotype described in chapter 3.

At 6 months of age, the difference in bone formation between Sdc3 KO and WT mice was not as pronounced as the difference observed at 3 months of age. This may be explained by the lower bone formation rate which is observed in older mice[420], but also due to the variability observed between mice. Dynamic histomorphometry analysis of tibias showed a reduced amount of calcein double label in Sdc3 KO mice suggesting these mice had reduced bone formation. Therefore, tibiae were subjected to an axial load three times a week for 2 weeks in order to understand whether they had an impaired anabolic response to mechanical loading, which could have explained the impaired bone formation rate observed on dynamic histomorphometry. MicroCT analysis revealed that loading resulted in differences in

trabecular bone but not cortical bone with increases in trabecular bone volume being seen only in Sdc3 KO. Interestingly, WT mice showed no anabolic response to mechanical loading during µCT analysis. However, Sdc3 KO showed increases in BV/TV ($p<0.05$), Tb.Th ($p<0.01$) and Tb.N and decreases in Tb.Sp ($p<0.05$), Tb.Pf ($p<0.05$), and SMI. Although these values could indicate that Sdc3 KO are increasing their overall tibia bone volume after loading, it is also important to note that the resolution used for µCT analysis was 4.5µm, and some of the changes would have fallen to within this value. Therefore, the fact that a statistically significant anabolic response was reached in the Sdc3 KO may not represent a biologically significant result. In fact, this can be observed during dynamic histomorphometry analysis of bone formation parameters in which Sdc3 KO mice showed no change in bone formation parameters indicating a blunted response to loading, when compared to WT mice which had increased bone formation parameters. Another explanation for WT mice showing no response compared to the response observed in Sdc3 KO at a µCT level could be that as Sdc3 KO mice have lower bone volume and are less stiff, as observed through 3-point bending tests, the strain is expected to be higher in the Sdc3 KO mice, and therefore the anabolic effect stronger. Ideally, strain would have been calculated using either strain gages on the tibia to test both WT and Sdc3 KO mice or by performing the mechanical loading in a load cell in the microCT scanner for localized changes in strain, hut due to time constraints this was not possible. Considering the reduced bone formation in Sdc3 KO mice at both 3 and 6 months of age and the impaired response to loading, these data could indicate that Sdc3 may play a role in osteoblast regulation and function.

Bearing in mind the 60-fold increase in bone marrow adiposity, observed in 3-month-old Sdc3 KO this could indicate an imbalance between osteoblastogenesis and adipogenesis, favouring adipogenesis, which is often associated with many pathophysiological diseases such as osteoporosis[421–423]. Anorexia-nervosa has also been linked to increased bone marrow fat and early onset osteoporosis[424,425], but when monitoring Sdc3 KO mouse weights, I saw no significant changes between Sdc3 KO and WT mice with both genotypes having normal weight, as shown in chapter 3 in Figures 3.1 and 3.2. Although not specifically monitored, there was also no obvious difference in feeding pattern between Sdc3 KO and WT mice. Obesity has also been

associated with increased marrow fat[426] but interestingly, as discussed earlier, Sdc3 KO mice are resistant to diet induced obesity[376], although I did not check for visceral/peripheral fat in our Sdc3 KO and WT mice. It is important to mention that this chapter only focuses on male mice who have been reported to have decreased energy expenditure compared to female Sdc3 KO mice[376], but both were reported to have increased energy expenditure when compared to WT mice[376]. In early development, new-born mammals have practically no adipocytes in their bone marrow[317,427], however, 18 month old mice have been shown to have decreased osteoblastogenesis[428] and increased adipogenesis in the bone marrow[429] and therefore an increase in bone marrow adiposity[422,423,427]. This change in balance between osteoblastogenesis and adipogenesis may be due to the fact osteoblasts and adipocytes both have a mesenchymal origin and differentiate from a common progenitor[78,422], and there is a high degree of plasticity between both cell types[422,423,430]. It is known that different transcription factors, such as PPARγ and Runx2[431–434], in mesenchymal stem cells control what fate the precursor will commit to, which in ageing is usually adipogenesis dominant[422]. Sdc3 could possibly play a role in the expression of these transcription factors by suppressing signalling pathways which in turn could inhibit or increase their expression and therefore could lead to this increase in adipogenesis and suppression of osteoblastogenesis, characteristic of the ageing skeleton. This could explain why Sdc3 KO mice have a decrease in bone formation and an increase in bone marrow adiposity.

Histomorphometric analysis of TRAP-stained osteoclasts showed decreased osteoclast numbers in Sdc3 KO at 3 and 6 months of age, when compared to WT mice. At 3 months of age bone remodelling is still active as there is still longitudinal bone growth, but as mice mature and reach 6 months of age this growth ceases and there is very little bone remodelling[435]. Therefore, osteoclast number will decrease as mice mature in both WT and Sdc3 KO mice. With ageing there is an increase in osteoclastogenesis[436,437], but it is important to note that the mice used in these experiments cannot be considered aged yet but indeed mature mice.

The reduced bone formation observed together with increased adipocytes in the bone marrow and the lack of response to loading support the changes observed in the previous chapter in which Sdc3 KO mice were shown to have decreased bone

volume. The reduced osteoclast number in Sdc3 KO at both 3 and 6 months of age were unexpected when considering the low bone volume phenotype described in chapter 3 but may indicate that there is a greater level of osteoclast activity rather than an increase in osteoclast number in the Sdc3 KO mice. This will require further *in vitro* studies to be performed.

In summary, I observed a decrease in bone formation parameters, osteoclast number, an increase in bone marrow adiposity at 3 and 6 months of age, and a blunted response to mechanical loading at 3 months of age, in Sdc3 KO mice. These findings suggest Sdc3 KO mice may have premature ageing of the skeleton, but further *in vitro* studies are needed to understand the underlying mechanisms involved at a cellular level and if Sdc3 is involved in osteogenesis and adipogenesis. It is possible that Sdc3 plays an important role in proliferation of both osteoclasts and osteoblasts and may also be important in the regulation of the pathways involved in regulating osteoblastogenesis, adipogenesis and even osteoclastogenesis, as the results described in this chapter suggest that the lack of Sdc3 is directing the differentiation of mesenchymal stem cells to favour adipogenesis over osteoblastogenesis, which has been shown to occur in aged animals[438]. This reduction in osteoblastogenesis could also explain the reduced osteoclastogenesis which is promoted in ageing by osteoblasts[437]. In conclusion, the results obtained in this chapter together with the findings in chapter 3 imply there is increased adipogenesis together with decreased osteoblastogenesis and consequent decreased osteoclastogenesis in Sdc3 KO mice, although it will be interesting to assess osteoclast function *in vitro* to understand whether they can function normally or may be overactive. This will all be addressed in the next chapter with the *in vitro* studies.

5 The effect of Syndecan 3 deletion on bone cell function *in vitro*

5.1 Introduction

In the previous chapter, analysis of dynamic histomorphometry showed that Sdc3 KO mice had decreased bone formation and a blunted response to mechanical loading which could partially explain the low bone volume phenotype described in Chapter 3. I also found that Sdc3 KO mice had increased bone marrow adiposity. All these results were found as early as 3 months of age in Sdc3KO. According to the literature, 18 month old mice have been shown to have reduced osteoblastogenesis, indicating that skeletal ageing is also associated with increased bone marrow adiposity[428]. These age-related changes have also been shown to be similar to those that occur during human ageing, more specifically in osteoporosis, which is characterized by low bone mass and increased bone marrow adiposity with increased fracture risk[417].

Surprisingly, when analysing osteoclast numbers, Sdc3 KO mice had reduced number of osteoclasts in their tibias when compared to WT tibias. The study of the disease osteopetrosis has contributed to a more in depth understanding of the molecular mechanisms that regulate osteoclast formation and activity. Osteoclast differentiation is regulated by M-CSF, RANKL and OPG. The mechanisms involved in osteoclastogenesis have been described in detail in Chapter 1, but briefly, M-CSF is able to bind to the cell surface of osteoclast progenitors through its receptor c-Fms, which in turn leads to an upregulation of RANK, which interacts with RANKL found on osteoblast cell surface or osteocytes, leading to increased proliferation and promoting osteoclastogenesis[20,23]. It was also discovered that OPG, a decoy receptor of RANKL, can compete with RANK for RANKL and therefore inhibit osteoclastogenesis, playing an important role in regulation of bone formation[24]. In addition, binding of M-CSF to c-Fms and RANKL to RANK activates a number of pathways, including ERK, Akt, MAPK and JNK, which in turn activate a number of important transcription factors including NFATc1, which is extremely important for osteoclast differentiation[439]. Mature osteoclasts are formed by the fusion of

mononucleated cells which form large multinucleated cells. For this to happen there are a number of factors required which include DC-STAMP and OC-STAMP[440–442]. After osteoclast fusion and maturation, there are several other factors which enable osteoclasts to resorb bone. Key to this is the formation of a microenvironment, induced by the osteoclast, between the cell and the surface of the bone which is acidified by hydrochloric acid, exposing the bones organic matrix which is then degraded by cathepsin K[74,443]. All these factors, and many others not mentioned, are important for the maintenance of healthy bone.

Osteoblasts, also important for this maintenance, are the cells responsible for bone formation. These require a number of factors which regulate their formation and function. Runx2, a major transcription factor, was shown to be vital for osteoblast differentiation and bone formation during *in vivo* knockout studies in which mice lacking Runx2 had complete lack of ossification and died soon after birth[434]. In addition, Runx2 is also able to regulate the transcription factor osterix, also required for osteoblast differentiation and bone formation[4,77,234]. Late osteoblast marker genes osteonectin and osteocalcin are both essential for osteoblast maturation and function and are able to upregulate alkaline phosphatase gene expression[13].

The Wnt/β-catenin pathway appears to be the common denominator between osteoblastogenesis, adipogenesis and bone response to mechanical loading[444]. The canonical Wnt/β-catenin pathway is activated by the binding of Wnt glycoproteins, such as Wnt3a, to a complex made up of LRP5 and LRP6 co-receptors and one of ten of the frizzled receptors which leads to DVL phosphorylation and the dephosphorylation of Axin[445]. This, in turn, leads to β-catenin stabilization which is then translocated into the nucleus, where it binds to transcription factors TCF/LEF activating target genes which stimulate osteoblast formation and maturation and inhibits adipogenesis[4,7,446]. In the absence of Wnt, β-catenin is phosphorylated and targeted for degradation inhibiting bone formation and increasing adipogenesis (for details of this process please refer to **Chapter 1**)[447]. On the other hand PPARG, the main enhancer of adipogenesis, is able to inhibit Wnt activation inducing β-catenin degradation and therefore stimulate adipogenesis[446,448]. Interestingly, bone marrow adipogenesis appears to be increased in Sdc3 KO mice as described in Chapter 4.

Taking this information into account, it is possible that Sdc3 may play a role in the Wnt signalling pathway.

Therefore, in this chapter I will be investigating the effects Sdc3 deletion has on osteoclast formation and activity, osteoblast formation and function and adipocyte formation together with gene and protein studies.

For details on the pathways mentioned above please see Chapter 1.

5.2 Methods

Bone marrow, used to generate macrophages and mesenchymal stromal cells (MSCs), was obtained from 8-week-old Sdc3 KO and WT female mice by flushing out the long bones, which were also used to obtain bone chips from which osteoblasts were grown out. Two-day old Sdc3 KO and WT pups were also used for generation of osteoblasts from dissected calvaria.

For osteoclast *in vitro* work, macrophages, pre-osteoclasts and osteoclasts were generated from bone marrow, as described in chapter 2. For osteoclast number quantification, RANKL dose response was performed by stimulating macrophages with 0, 10, 25, 50 and 100 ng/ml of RANKL. Cells were fixed and stained for TRAcP. TRAcP-positive cells with more than 3 nuclei were counted as osteoclasts, under blinded conditions. Osteoclast nuclei counts were taken from wells stimulated with 100ng/ml of RANKL and also of TRAcP-positive cells containing more than 3 nuclei. For resorption assays M-CSF-dependent macrophages were seeded at $15x10^3$ cells/well density onto dentin slices and stimulated with 25ng/ml of M-CSF and 100 ng/ml of RANKL for up to 7 days. Cells were later TRAcP stained for osteoclast quantification and then removed and resorption pits were imaged using reflected light microscopy. Quantification was performed using custom software based on ImageJ developed by Prof van 't Hof. For the study of genes of interest, M-CSF dependent macrophages were grown to confluence and stimulated with 100 ng/ml RANKL for 3 days to differentiate into pre-osteoclasts and 5 days to differentiate into osteoclasts. Total RNA was isolated from M-CSF dependent macrophages, pre-osteoclasts and osteoclasts, using Qiazol (Qiagen) according to manufacturer's instructions. After storing in -80°C, RNA was later reverse transcribed using EvoScript

Universal cDNA Master (Roche). Each sample was reverse transcribed 3 times in order to obtain 3 technical replicates. cDNA was then used to perform probe-based RT-qPCR (LightCycler 480 Probes Master, Roche) for genes of interest.

For osteoblast *in vitro* work, osteoblasts were obtained from bone chips and from bone marrow MSCs (BMSCs) from 8-week-old female mice and from calvaria of 2-day-old pups. The purpose of obtaining osteoblasts from these three sources was to investigate any possible changes related to the different forms of ossification (intramembranous or endochondral) associated with these sources. These were used for mineralisation assays by stimulating cells in osteogenic conditions, as described in detail in chapter 2. After fixation, mineral was stained with 40mM Alizarin Red S. Quantification was performed by dissolving the alizarin Red in 10% (W/v) cetylpyridinium chloride in 10mM sodium phosphate and measuring absorbance at 562 nm on a SPECTROstar nano plate reader, as described in detail in chapter 2. For proliferation assays, cells were cultured on coverslips, fixed, permeabilised and then incubated in a 1:250 dilution of Anti-Ki67 rabbit primary antibody. Imaging was performed using a Zeiss Axio Scan.Z1 slide scanner with a 10x lens. For alkaline phosphatase assays, osteoblasts generated from bone chips were plated at $15x10^3$ cells/well in 96-well plates and cultured in 150 µl αMEM with 10% FCS for 24 hours. Alamar Blue (15 µl/well) was added to the culture and incubated for 2 more hours. Cell viability was measured by analysing the Alamar Blue signal using a fluorescence plate reader (excitation 560 nm and emission 590 nm). Next, the cells were fixed for 10 minutes at 4ºC using 4% paraformaldehyde in PBS, washed and stored dry at -20ºC. Alkaline phosphatase activity was measured using the conversion of para-nitrophenyl-phosphatase to p-nitrophenyl by measuring absorption at 405 nm at 1-minute intervals for 30 minutes. Alkaline phosphatase measurements were corrected for cell number by dividing by the Alamar Blue signal. For details please refer to chapter 2.

For adipogenic studies, BMSCs were grown to confluence and then cultured for up to 17 days in adipogenic differentiation medium, as described in chapter 2. Afterwards, cells were either stained with Oil Red O, to visualise adipocytes, or used for RNA extraction by using Trizol as per the manufacturer's instructions. RNA was

then reverse transcribed as described above and cDNA used for probe-based RT-qPCR (LightCycler 480 Probes Master, Roche) for genes of interest.

For protein experiments, an initial experiment was performed to assess time response to Wnt3a stimulation of osteoblasts generated from bone chips by stimulating them with 50ng/ml of recombinant mouse Wnt3a protein (Cell Signalling) for 0, 2, 6 and 24 hours. Cells were lysed with RIPA buffer and western blot was performed using standard protocols described in Chapter 2. Non-phosphorylated (active) β-catenin rabbit primary antibody at 1:1000 dilution, secondary goat anti rabbit Alexa Fluor 800 antibody at 1:10,000 dilution, primary β-actin mouse antibody at 1:5000 dilution and secondary rabbit anti mouse Alexa Fluor 680 antibody at 1:10,000 were used for probing. Membranes were visualised using the Odyssey CLx imaging system (LI-COR) and analysed using Image Studio lite (LI-COR). In subsequent experiments, osteoblasts generated from bone chips were stimulated with 50ng/ml of recombinant mouse Wnt3a protein for a time course of 0, 15, 30, 60 and 120 minutes and then lysed with RIPA buffer. Western blot was performed and analysed as described previously. To assess the optimal concentration of Wnt3a needed to induce β-catenin dephosphorylation, a dose response was performed by stimulating osteoblasts generated from bone chips with 0, 10, 15, 50 and 100 ng/ml of recombinant mouse Wnt3a protein for 2 hours. Cells were then lysed in RIPA buffer and western blotting was performed and analysed as described above.

Statistical analysis was performed using a paired two-tailed Student's *t* test.

For details on methods used in this chapter please refer to **Chapter 2**.

5.3 Results

5.3.1 The effect of Syndecan 3 deletion on osteoclast function *in vitro*

Bone histomorphometry analysis revealed reduced numbers of osteoclasts in 3-month-old Sdc3 KO compared to WT. However, firstly it was unclear whether this effect was centrally mediated and secondly, whether the reduced osteoclast number in Sdc3 KO mice translated into lower osteoclast-mediated bone resorption

capability. Therefore, studies were performed assessing osteoclastogenesis potential and bone resorption *in vitro*.

For the purpose of quantification, osteoclasts were generated *in vitro* from bone marrow macrophages by culturing them with M-CSF and after 3 days RANKL was added at increasing concentrations and cultures continued for approximately 5 days, at which point cultures were constituted primarily of osteoclasts, containing also macrophages. RANKL dose response analysis showed overall decreased osteoclast formation in Sdc3 KO compared to WT cultures (**Figure 5.1**). At 100 ng/ml of RANKL the number of osteoclasts in Sdc3 KO cultures was decreased by two-fold when compared to WT cultures ($p<0.05$; **Figure 5.1 B**).

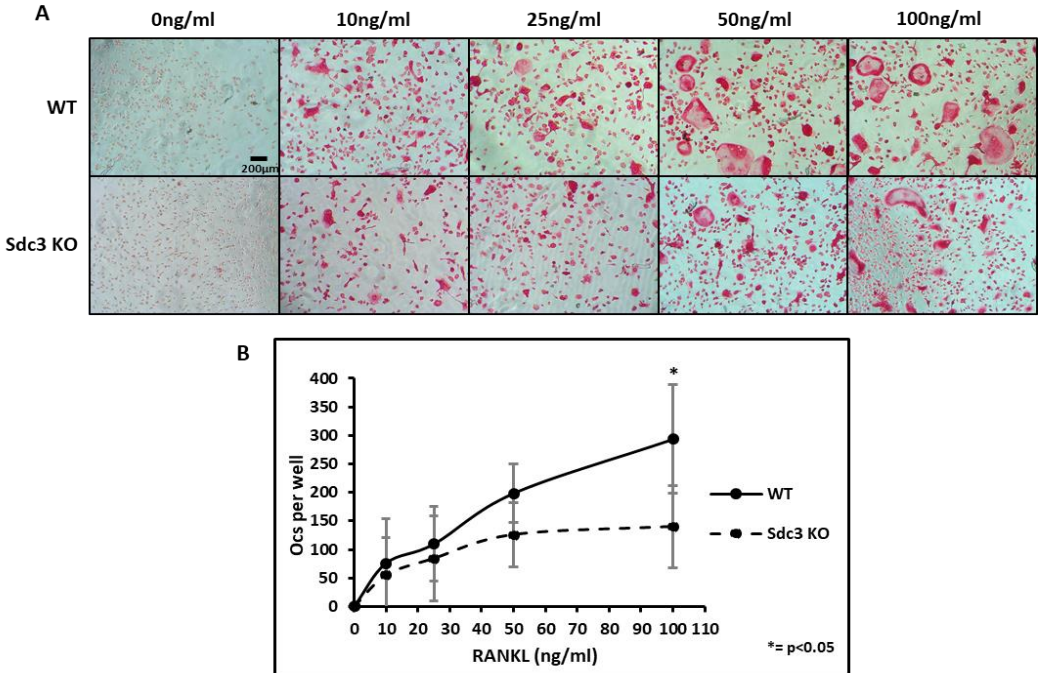

Figure 5.1: RANKL dose response assay. **(A)** Representative micrographs of TRAcP staining of bone marrow derived M-CSF dependent macrophages, of 3-month-old mice, stimulated with 0, 10, 25, 50 and 100 ng/ml RANKL grown for 5 days in 96 well plates, show less TRAcP-positive osteoclasts in Sdc3 KO cultures when compared to WT. **(B)** Quantification of osteoclast numbers shows decreased osteoclast formation in Sdc3 KO cultures after RANKL stimulation. Results in **B** represent means ± SD of 4 independent experiments performed in quintuplicate. Significance is denoted by *$p<0.05$.

During analysis of RANKL dose response it was noted that TRAcP-positive Sdc3 KO osteoclasts appeared to be smaller with less nuclei than WT osteoclasts. Therefore, nuclei counts were performed on osteoclasts generated from M-CSF

dependent macrophages and stimulated with 100ng/ml of RANKL from the RANKL dose response experiment described above. Analysis showed that Sdc3 KO cultures generate less osteoclasts than WT cultures with significantly decreased osteoclast numbers in the 3 to 5 ($p<0.001$) and 6 to 9 ($p<0.05$) nuclei groups (**Figure 5.2 A**). Sdc3 KO osteoclasts show no significant difference in percentage of total number of cells per number of nuclei group when compared to WT cultures (**Figure 5.2 B**).

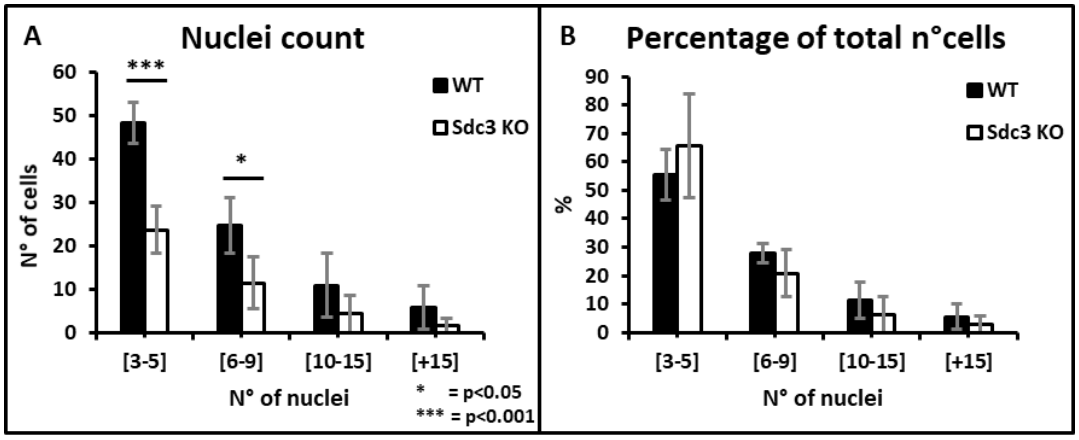

Figure 5.2: Nuclei counts and percentage of total number of cells per nuclei count group relative to total number of cells in culture of Sdc3 KO and WT osteoclasts. TRAcP positive WT osteoclasts are significantly increased in both 3 to 5 ([3-5]) and 6 to 9 ([6-9]) number of nuclei groups when compared to TRAcP positive Sdc3 KO osteoclasts (**A**). The nuclei group [3-5] is represented by more than 50% of the percentage total of both Sdc3 KO and WT osteoclasts (**B**). Results represent means ± SD of 4 independent experiments. Significance is denoted by *$p<0.05$ and ***$p<0.001$.

To assess osteoclast function, bone resorption assays were performed on dentin slices (**Figure 5.3 A and B**). Analysis of total resorption area (**Figure 5.3 C**) showed no significant difference between Sdc3 KO and WT. Osteoclast numbers showed no significant difference either (**Figure 5.3 D**), but interestingly, results show a significant increase ($p<0.01$) in resorption surface per osteoclast (ResSurf/Oc) in Sdc3 KO (**Figure 5.3 E**) when compared to WT cultures. These data indicate that although Sdc3 KO mice generate lower osteoclast numbers *in vivo*, these osteoclasts may have increased resorption activity in comparison to WT.

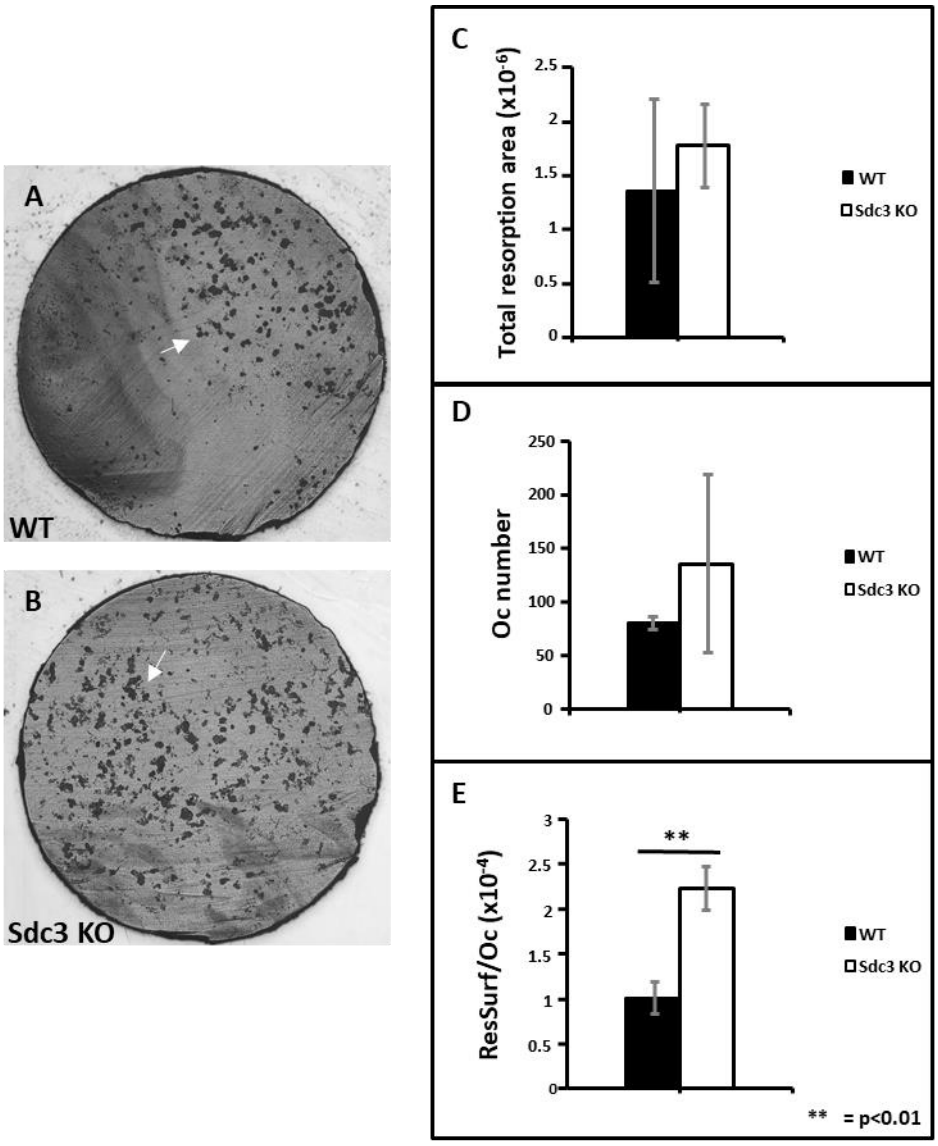

Figure 5.3: Osteoclast resorption assay. Representative micrographs of dentin slices seeded with WT (**A**) and Sdc3 KO (**B**) M-CSF dependant macrophages stimulated with 100ng/ml of RANKL for 5 days to generate osteoclasts. Arrows in white (**A** and **B**) indicate resorption pits. Osteoclasts were stained with TRAcP stain for visualisation and count, then removed and resorption pits analysed. Analysis showed no significant difference in total resorption area (**C**) and osteoclast number (Oc number; **D**) but showed a significant increase in resorption surface per osteoclast (ResSurf/Oc; **E**) in Sdc3 KO cultures. Results represent means ± SD from 3 independent experiments performed in quadruplicate. Significance is denoted by **p<0.01.

5.3.2 The effect of Syndecan 3 deletion on gene expression during osteoclastogenesis

The results described above demonstrate that Sdc3 KO have significantly lower rates of osteoclast formation induced by M-CSF and RANKL *in vitro* in

osteoclastogenesis cultures, confirming the histology findings (Chapter 4). Interestingly, cultures of osteoclasts on dentin slices did not show a difference in resorption area between Sdc3 KO and WT, however the resorption area per osteoclast was over twofold higher in Sdc3 KO compared to WT cultures, suggesting that Sdc3 promotes osteoclast differentiation but decreases mature osteoclast resorptive activity. There are certain genes involved in the regulation of osteoclast formation and function such as *Tnfrsf11a,* encoding RANK[449], which regulates osteoclastogenesis and *Nfatc1*[439], one of the main transcription factors required for osteoclastogenesis. Late osteoclast marker genes such as *Dcstamp* and *Ctsk* are also essential for osteoclast fusion and function, respectively[440,442,443,450]. Therefore, I investigated expression levels of these osteoclast marker genes in samples of cDNA obtained from Sdc3 KO and WT macrophages, pre-osteoclasts and osteoclasts.

I verified that there was no *Sdc3* expression in Sdc3 KO cells, as expected. When comparing marker gene expression between Sdc3 KO and WT cultures, *Tnfrsf11a* (encoding RANK), essential for osteoclast formation[451], was significantly decreased in Sdc3 KO macrophages compared to WT macrophages ($p<0.01$; **Figure 5.4 A**), which may explain the reduced sensitivity to RANKL observed in the Sdc3 KO RANKL dose response assays, described above in section 5.3.1 (**Figure 5.1**).

Previous literature has demonstrated the importance of β-catenin activation for osteoclastogenesis[452]. Interestingly, a paper by Maeda and colleagues showed that Wnt5a activates the FZD-mediated non-canonical Wnt pathway through receptor tyrosine kinase-like orphan receptor (Ror) proteins[453]. They found that the bone marrow macrophages highly expressed receptor components of Wnt5a, such as FZD7, which can mediate the Wnt5a-Ror2 signals and can therefore enhance RANK expression is osteoclast progenitor cells which in turn enhances RANKL-induced osteoclastogenesis[453]. Studies in *Xenopus* have revealed that FZD7 binds to SDC4 and Rspo3 promoting Wnt/PCP signalling via endocytosis[454]. Therefore, I investigated gene expression levels of *FZD7* on the above-mentioned samples and found that it was significantly decreased in Sdc3 KO macrophages ($p<0.01$) when compared to WT macrophage samples, but not at the pre-osteoclast and osteoclast stage (**Figure 5.4 F**). Given the effect Wnt5a-Ror2 signalling has on RANK expression, downregulation of *Fzd7* may in turn lead to the downregulation of *Tnfrsf11a* (encoding RANK)

observed in the Sdc3 KO macrophages. Taken together, these data suggest that syndecan 3 may enhance osteoclastogenesis through Wnt signalling and may also be important in mature osteoclasts, however the exact mechanism is still unclear.

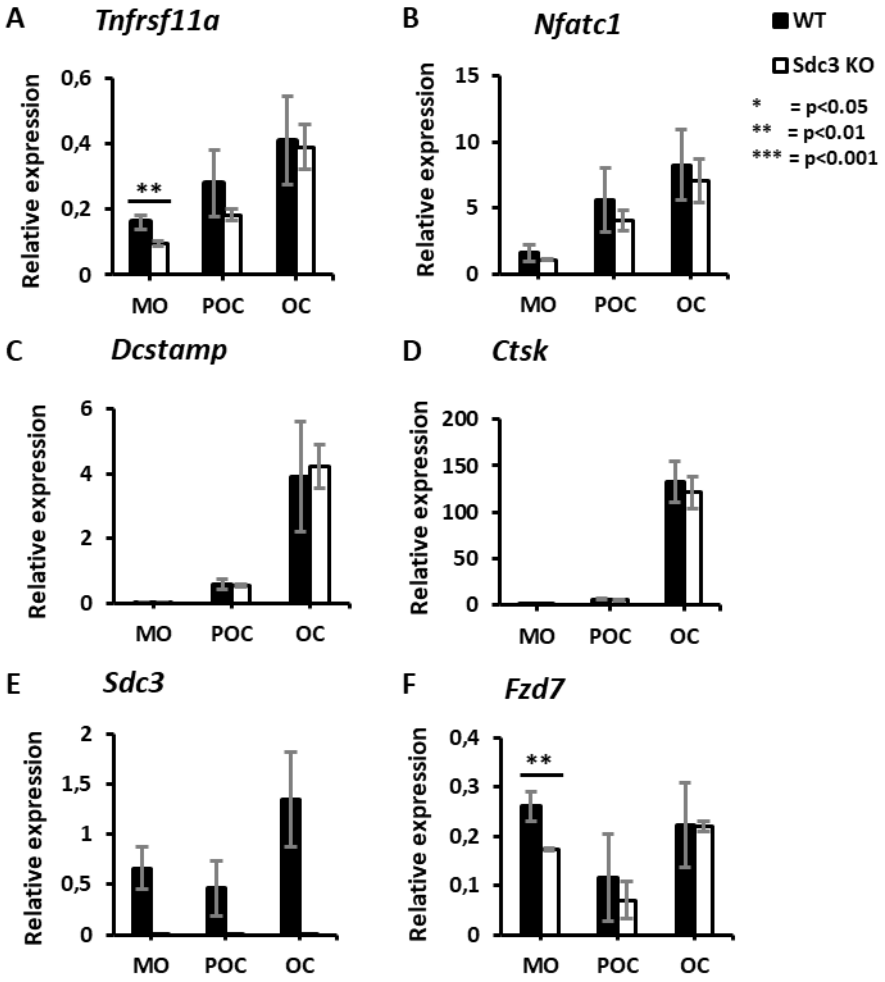

Figure 5.4: Analysis of gene expression in Sdc3 KO and WT macrophages, pre-osteoclasts and osteoclasts. M-CSF dependent macrophages (MO) were seeded at $0.6x10^6$ cells/ml in 6 well plates. Cells were grown to confluency for 2 days and the wells for pre-osteoclasts (POC) and osteoclasts (OC) were then stimulated with 25ng/ml of M-CSF and 100ng/ml of RANKL for 3 and 5 days, respectively. Wells containing only macrophages were stimulated with 100ng/ml of M-CSF until confluency. Cells were lysed and RNA was extracted. Gene expression of osteoclast marker genes was quantified by qPCR relative to *Hmbs*. There was a significant decrease in *Tnfrsf11a* (**A**) and *Fzd7* (**F**) in Sdc3 KO macrophages when compared to WT macrophages. *Sdc3* gene expression was not seen in Sdc3 KO. Values shown are mean ± SD. Significance is denoted by **p<0.01 and *p<0.05. WT are N=4 and Sdc3 KO are N=3, and all independent experiments were performed in triplicate.

5.3.3 The effect of Syndecan 3 deletion on osteoblast function *in vitro*

5.3.3.1 Mineralisation assays

Bone histomorphometry revealed lower bone formation in Sdc3 KO mice when compared to WT mice (Chapter 4), however it was unclear whether this was due to a direct defect in osteoblasts or a systemic effect. Therefore, to determine the effect of Sdc3 deletion at a cellular level, *in vitro* studies were performed assessing osteoblast formation and function.

Mineralisation assays showed a remarkable difference in Alizarin Red stained mineral between cultures of Sdc3 KO and WT osteoblasts, in which the biggest difference was noted in the osteoblasts differentiated from bone chips (**Figure 5.5 A** and **B**) where no mineral in the Sdc3 KO cultures was observed and then the osteoblasts generated from BMSCs (**Figure 5.5 C** and **D**) in which Sdc3 KO cultures showed some mineral but very little compared to WT cultures. The osteoblasts differentiated from calvaria (**Figure 5.5 E** and **F**) showed the least difference with both Sdc3 KO and WT producing mineral, although it is still noted that Sdc3 KO cultures form less mineral than WT. Quantification of mineral using Alizarin Red showed an over 2- and 6-fold reduction in mineralisation in Sdc3 KO vs WT cultures of osteoblasts differentiated from BMSCs ($p<0.05$) and from osteoblasts grown out of bone chips ($p<0.001$), respectively. Sdc3 KO cultures of osteoblasts grown out of calvaria also showed a significantly reduced mineralisation capacity when compared to WT cultures ($p<0.001$; **Figure 5.5 G**). The biggest effect was observed in cultures of mature osteoblasts obtained from bone chips. These results indicate that the low bone formation rate seen in Sdc3 KO mice in histomorphometry is due to impaired osteoblast function, however they do not exclude a systemic contributory effect.

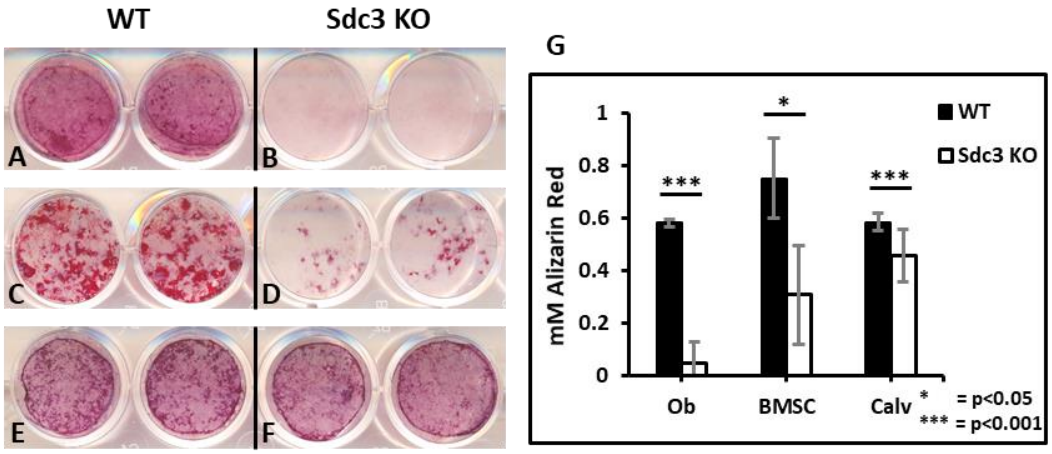

Figure 5.5: Mineralisation assays and mineralisation quantification of Sdc3 KO and WT osteoblast cultures. Representative images show osteoblasts generated from bone chips (**A** and **B**), BMSCs (**C** and **D**) and calvaria (**E** and **F**) and cultured for 21 days in mineralisation medium, fixed, and then stained with Alizarin Red. There is a significant decrease in mineral in Sdc3 KO cultures of osteoblasts from bone chips (Ob), bone marrow mesenchymal stromal cells (BMSC) and from calvaria (Calv) when compared to WT cultures (**G**). Results represent means ± SD from 3 independent experiments performed in duplicate. Significance is denoted by *p<0.05 and ***p<0.001.

5.3.3.2 Alkaline phosphatase assay

Osteoblasts secrete Alkaline phosphatase (ALP) which hydrolyses pyrophosphate, which provides phosphate for mineralisation of bone matrix[88]. ALP is also a bone formation marker[455]. Therefore, ALP activity was assessed in osteoblasts grown out of bone chips of Sdc3 KO and WT 8-week old female mice. ALP assay revealed a significant decrease in ALP activity in Sdc3 KO osteoblasts ($p<0.001$) when compared to WT cultures (**Figure 5.6**), indicating that the low bone formation rate seen in Sdc3 KO mice in histomorphometry is due to impaired osteoblast function.

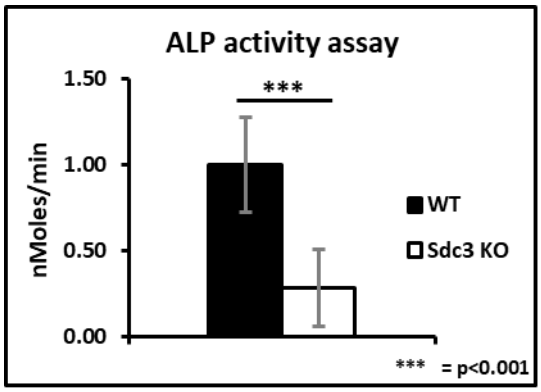

Figure 5.6 Alkaline phosphatase enzyme activity assay of Sdc3 KO osteoblasts vs WT osteoblasts. Alkaline phosphatase (ALP) activity was measured after osteoblasts generated from bone chips seeded at $15x10^3$ cells/well were cultured for 24 hours in 96 well plates with standard DMEM. Analysis shows a significant decrease in ALP activity in Sdc3 KO osteoblasts when compared to WT osteoblasts, with Sdc3 KO osteoblasts having an average of only 0.29nMoles/min and WT osteoblasts having an average of 1 nMoles/min. Alkaline phosphatase activity was corrected to cell number. Results represent means ± SD from 3 independent experiments with 6 replicates per experiment. Significance is denoted by ***p<0.001.

5.3.3.3 Cell proliferation assay

The previous results show that Sdc3 KO osteoblast cultures have reduced mineralisation and ALP activity when compared to WT cultures, however this effect could be due to reduced cell proliferation in Sdc3 KO. Therefore, to determine cell proliferation, a Ki67 assay was performed. Although the experiments were performed only twice, the obtained preliminary data show no significant difference in number of Ki67-positive cells between Sdc3 KO and WT cultures (**Figure 5.7**). This suggests that reduced mineralisation in Sdc3 KO osteoblasts is not due to diminished cell proliferation.

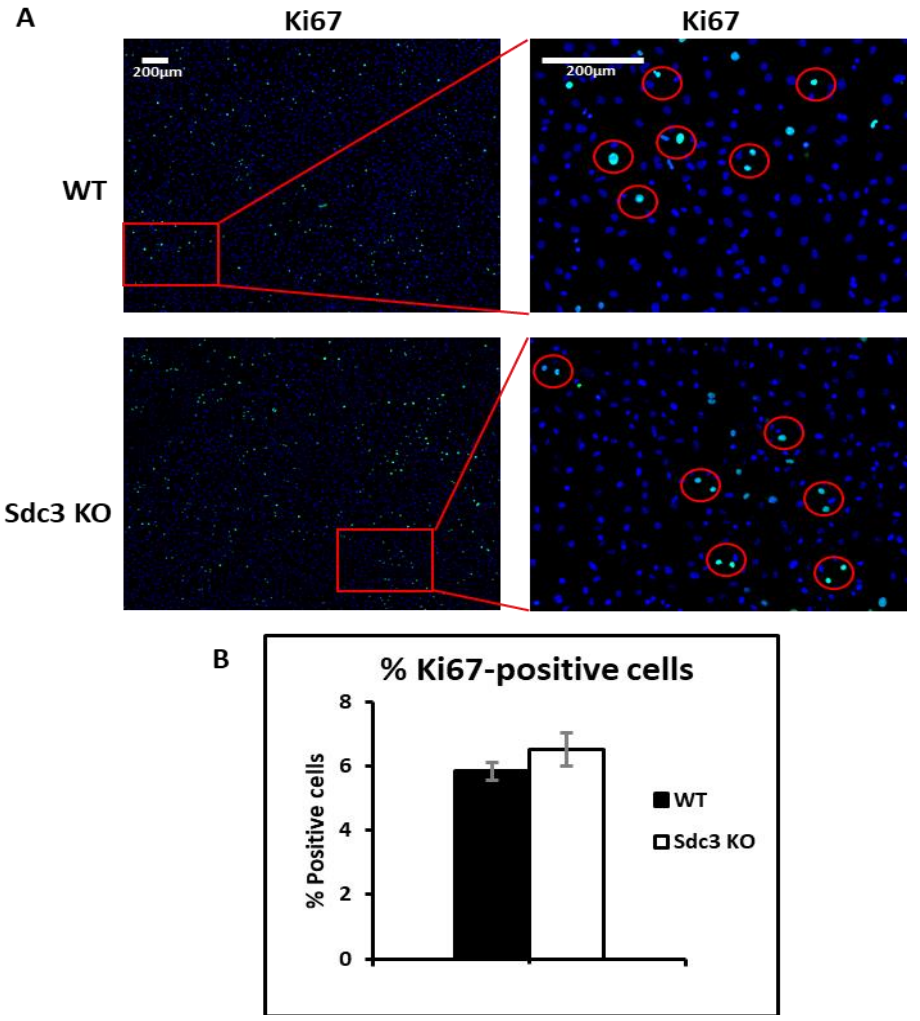

Figure 5.7: Cell proliferation assay of Sdc3 KO and WT osteoblasts. Sdc3 KO and WT osteoblasts generated from bone chips were cultured on coverslips for 24 hours, fixed and then stained for Ki67 and DAPI (**A**). Red boxes highlight the zoomed in images on the right (**A**), with the red circles on the right showing the Ki67 stained cells. Quantification of Ki67 positive cells (**B**) shows no significant difference between Sdc3 KO and WT cultures. Results represent means ± SD from 2 independent experiments with 6 replicates per experiment. Values shown are mean ± SD.

5.3.3.4 The effect of Syndecan 3 deletion on gene expression in osteoblasts

The results described above showed a decrease in mineralisation in Sdc3 KO cultures (**Figure 5.5**) when compared to WT cultures and measurement of ALP activity (**Figure 5.6**) showed a reduction in the enzyme activity in Sdc3 KO osteoblasts (**Figure 5.6**). Taking these into account and considering that ALP is a marker for bone formation[455], I next examined *Alpl* (encoding Alkaline Phosphatase) gene expression by RT-qPCR of samples of cDNA obtained from Sdc3 KO and WT osteoblasts. As shown

in **Figure 5.8 A**, *Alpl* expression was significantly reduced ($p<0.01$) in Sdc3 KO osteoblasts, when compared to WT. Osteonectin (encoded by *On*) and osteocalcin (encoded by *Bglap*), both important for osteoblast maturation and function[13], were also investigated, however I found that neither showed a significant difference in gene expression between Sdc3 KO and WT cultures (**Figure 5.8 B** and **C**, respectively). Osteoblast differentiation marker gene, *Runx2* was also investigated, in addition to *Smad6* and *Pparg* (Figure 5.9). As described in detail in Chapter 1, *Runx2* and *Smad6* are both positive regulators of osteoblast differentiation and stimulation, whereas, *Pparg* is a negative regulator of osteoblast differentiation. Both *Runx2* and *Smad6* were significantly decreased ($p<0.01$ and $p<0.05$, respectively) in Sdc3 KO osteoblasts when compared to WT osteoblasts (**Figure 5.9 A** and **B**). *Pparg* showed no significant difference between Sdc3 KO and WT cultures (**Figure 5.9 C**).

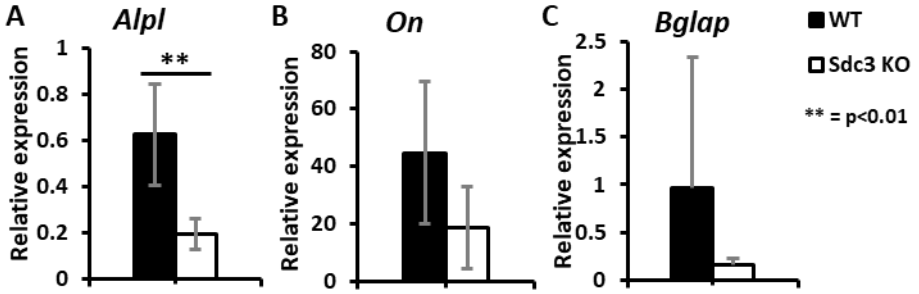

Figure 5.8: Expression of genes that regulate osteoblast function in Sdc3 KO and WT osteoblasts. Osteoblasts generated from bone chips of Sdc3 KO and WT mice were grown in standard DMEM until confluent. Analysis of relative expression of *Alpl* (encoding Alkaline phosphatase, **A**), *On* (encoding osteonectin, **B**) and *Bglap* (encoding osteocalcin, **C**) was performed but only *Alpl* was significantly decreased ($p<0.01$) in Sdc3 KO osteoblasts compared to WT osteoblasts. Results represent means ± SD of 5 independent experiments performed in triplicate and expression is relative to *Hmbs*. Significance is denoted by **$p<0.01$.

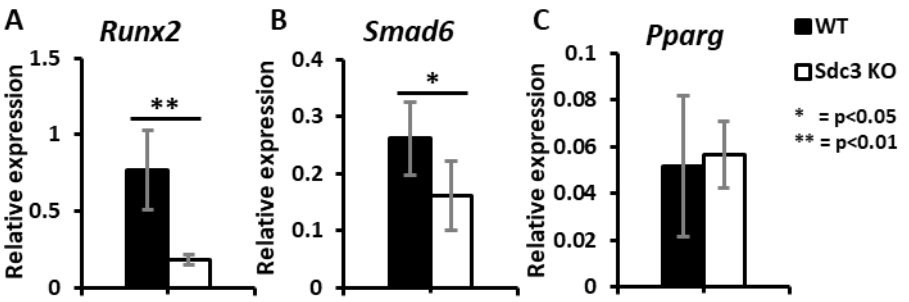

Figure 5.9: Expression of genes that regulate osteoblast differentiation in Sdc3 KO and WT osteoblasts. Osteoblasts generated from bone chips of Sdc3 KO and WT mice were grown in standard DMEM until confluent. Analysis of relative expression of *Runx2* (**A**), *Smad6* (**B**) and *Pparg* (**C**) showed significantly decreased expression in *Runx2* ($p<0.01$) and *Smad6* ($p<0.05$). Results represent means ± SD of 5 independent experiments performed in triplicate and expression is relative to *Hmbs*. Significance is denoted by **$p<0.01$.

To investigate whether any of the remaining 3 syndecans could be compensating for Sdc3 deletion, gene expression of all syndecans was also analysed. Although these appeared to be decreased in Sdc3 KO osteoblasts, the differences were not statistically significant possibly due to the low number of repeats (**Figure 5.10, A-D**), therefore there is no evidence of compensatory increase of other syndecans.

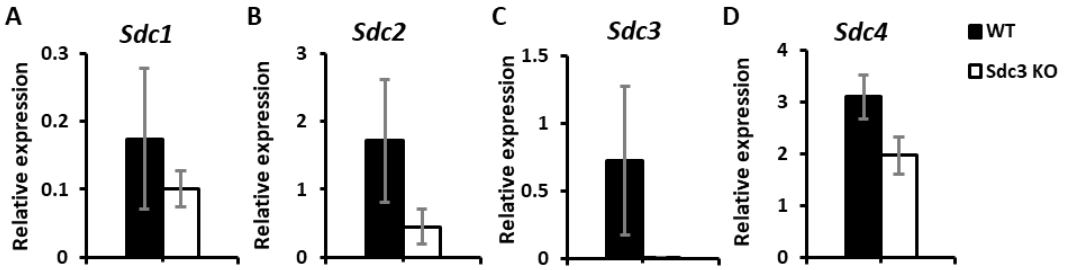

Figure 5.10: Analysis of gene expression of syndecans in Sdc3 KO and WT osteoblasts. Osteoblasts generated from bone chips of Sdc3 KO and WT mice were grown in standard DMEM until confluent. Analysis of relative expression of *Sdc1* (**A**), *Sdc2* (**B**), *Sdc3* (**C**) and *Sdc4* (**D**) showed no significant differences between Sdc3 KO and WT samples. Although it is clear that *Sdc3* is not expressed in Sdc3 KO samples compared to WT samples. Results represent means ± SD of 2 independent experiments performed in triplicate and expression is relative to *Hmbs*.

As mentioned earlier, Sdc3 KO mice have increased bone marrow fat and a blunted response to mechanical loading which could suggest involvement of Sdc3 in

the Wnt signalling pathway, possibly by enhancing the Wnt signalling. Therefore, I analysed expression levels of the main genes involved in the canonical Wnt signalling pathway (described in detail in Chapter 1) which included Wnt ligand *Wnt3a* (**Figure 5.11 A**), a major upregulator of bone metabolism[456]. Wnt proteins bind to transmembrane receptors Frizzled and co-receptors LRP5/6, triggering a cascade of intracellular events[456], therefore I analysed gene expression of *Lrp5* and *Lrp6* (**Figure 5.11 B** and **C**). *Fzd1* expression is relatively high in osteoblasts[457] and *Fzd1* is known to enhance osteoblast-mediated mineralisation[458], therefore *Fzd1* gene expression was also analysed (**Figure 5.11 D**).

Lgr4, *Lgr5* and *Lgr6* were also analysed as these potentiate Wnt/β-catenin signalling[131] and LGR4 has been shown to play an important role in bone formation[151]. Finally, downstream effectors of the Wnt pathway were also analysed, including *Axin2,* a direct target of the Wnt pathway[143], *Atf4,* a transcription factor activated by LGR4 activity promoting β-catenin expression[459], and *Ctnnb1* (encoding β-catenin) (**Figure 5.10 H, I** and **J**) required for the control of target gene expression which are important for osteogenesis[137]. Gene expression analysis showed that *Lgr4* (**Figure 5.11 E**) was significantly downregulated ($p<0.05$) in Sdc3 KO cultures but the remaining genes analysed showed no significant difference, possibly due to low N-number. Interestingly, *Atf4* (**Figure 5.11 I**), a downstream effector of LGR4 appeared to be downregulated in Sdc3 KO samples, as were *Lgr5* and *Ctnnb1*. Although these data are preliminary as only one biological experiment was performed (n=1), it may indicate that Sdc3 enhances the canonical Wnt signalling pathway in osteoblasts.

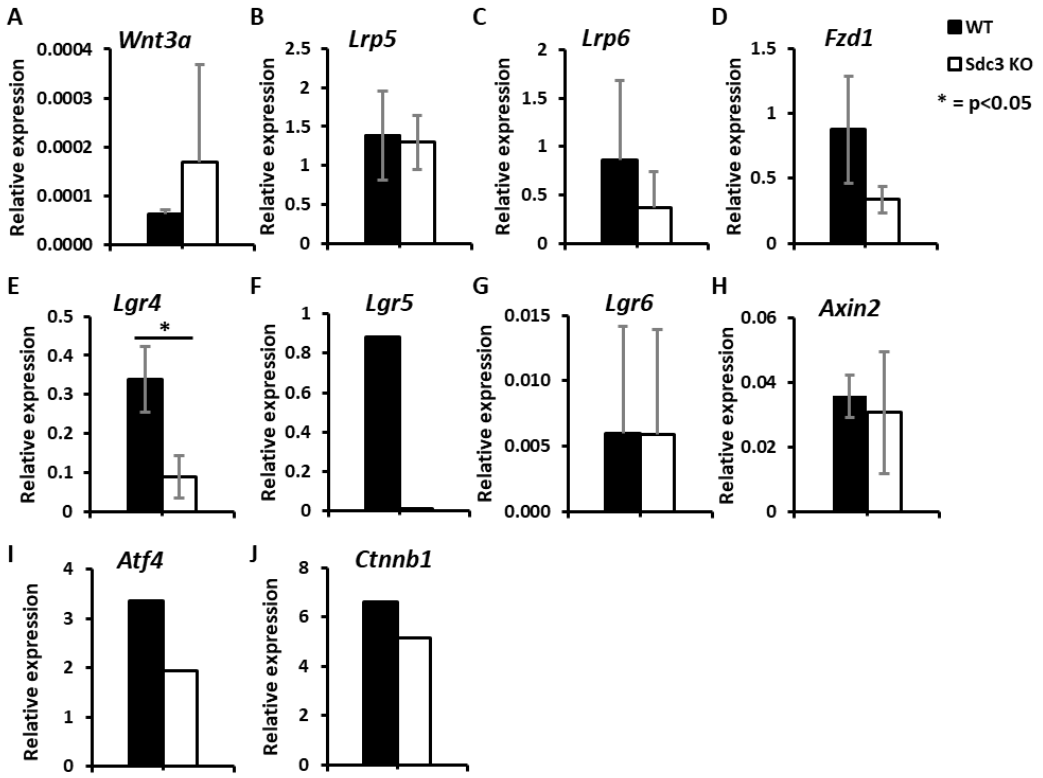

Figure 5.11: Analysis of gene expression of Wnt signalling pathway genes in Sdc3 KO and WT osteoblasts. Osteoblasts generated from bone chips of Sdc3 KO and WT mice were grown in standard DMEM until confluent. Analysis of components of the Wnt signalling pathway, which included *Wnt3a* (**A**; WT N=3 and Sdc3 KO N=2), *Lrp5* (**B**; WT N=3 and Sdc3 KO N=2), *Lrp6* (**C**; WT N=3 and Sdc3 KO N=2), *FZD1* (**D**; WT N=3 and Sdc3 KO N=2), *Lgr4* (**E**; WT N=3 and Sdc3 KO N=2), *LGR5* (**F**; WT N=1 and Sdc3 KO N=1), *Lgr6* (**G**; WT N=3 and Sdc3 KO N=2), *Axin2* (**H**; WT N=3 and Sdc3 KO N=2), *Atf4* (**I**; WT N=1 and Sdc3 KO N=1) and *Ctnnb1* (encoding β-catenin; **J**; WT N=1 and Sdc3 KO N=1) showed a significant reduction in relative expression of *Lgr4* in Sdc3 KO osteoblasts compared to WT osteoblasts. Results are means ± SD and expression is relative to *Hmbs*. Significance is denoted by *p<0.05.

To understand why there is a mineralisation defect in Sdc3 KO osteoblasts, I further investigated osteoblast marker gene expression in osteoblasts generated from MSCs grown in mineralising conditions for 21 days. These genes included *Tnfsf11* (encoding RANKL; **Figure 5.12 A**) and *TnfrsfF11b* (encoding osteoprotegerin; **Figure 5.12 B**), important for osteoblast regulation of osteoclastogenesis[66], *Alpl* (encoding alkaline phosphatase; **Figure 5.12 C**), which as mentioned earlier is essential for mineralisation[88], *Bglap* (encoding osteocalcin; **Figure 5.12 D**), the most common noncollagenous protein essential for bone formation[460], and *Col1a1* (encoding collagen type I; **Figure 5.12 E**), which is the most common type of collagen

in bone, highly expressed in osteoblasts and the main component of bone matrix[99]. These showed no significant differences between Sdc3 KO and WT samples (**Figure 5.12**).

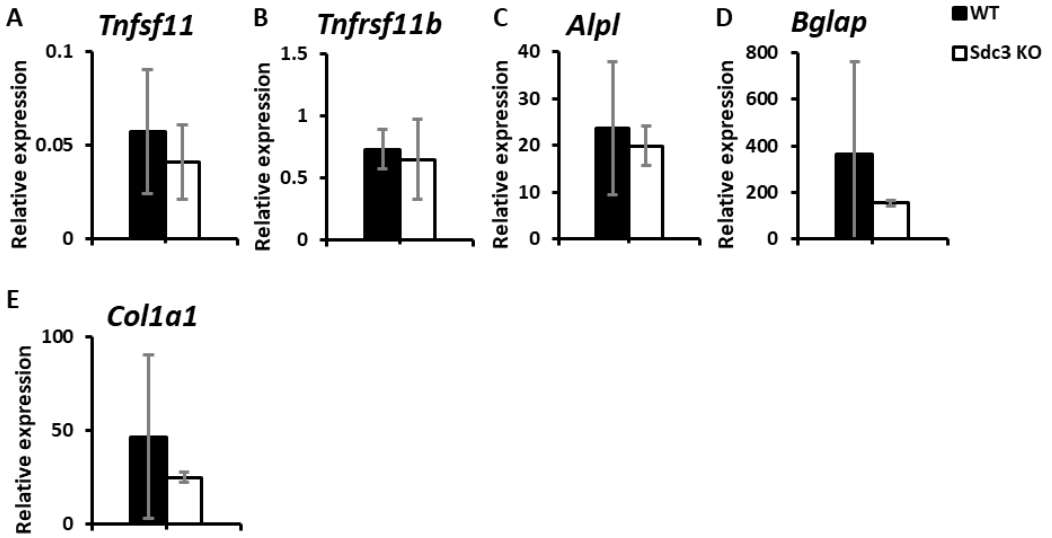

Figure 5.12: Analysis of gene expression of osteoblast marker genes in Sdc3 KO and WT mesenchymal stromal cells grown in osteogenic conditions. MSCs obtained from Sdc3 KO and WT mice were grown in standard medium until confluent and then in mineralising conditions for 21 days in order to generate mineralising osteoblasts. Analysis of relative expression showed no significant differences in *Tnfsf11* (encoding RANKL; **A**), *Tnfrsf11b* (encoding osteoprotegerin; **B**), *Alpl* (encoding alkaline phosphatase; **C**), *Bglap* (encoding osteocalcin; **D**) and *Col1a1* (encoding collagen type I; **E**) between Sdc3 KO and WT cultures. Results represent means ± SD from 3 independent experiment performed in triplicate and expression is relative to housekeeping gene *Hmbs*.

5.3.3.5 Effect of Sdc3 deletion on β-catenin

Gene expression analysis revealed a significant downregulation of *Runx2* in Sdc3 KO osteoblasts generated from bone chips (**Figure 5.9**). As Runx2 is the target gene of Wnt/β-catenin pathway inducing MSCs to differentiate into osteoblasts[144], Sdc3 could enhance Wnt/β-catenin pathway. As described in chapter 1 in section 1.2.2, activation of the Wnt pathway leads to nuclear translocation of the non-phosphorylated form of β-catenin, which in turn controls target gene transcription. Therefore, I quantified β-catenin at a protein level in osteoblasts stimulated with recombinant Wnt3a in order to activate Wnt/β-catenin signalling. In order to decide the amount of Wnt3a to use an initial literature review was performed revealing the

concentration used ranged between 20-100 ng/ml[456,461,462]. Karner *et al*., stimulated ST2 cells, which are an osteoblast-adipocyte bipotent progenitor cell line, with 50ng/ml of Wnt3a[461], Sebastian *et al*., stimulated osteoblasts generated from calvaria from Lrp5/6 KO mice with 100ng/ml of Wnt3a[456] and Grol *et al*., stimulated calvarial osteoblasts obtained from P2X7 KO mice and MC3T3-E1 osteoblast like cells with 20ng/ml of Wnt3a[462]. Taking these data into account, I decided to use a concentration of 50ng/ml of recombinant mouse Wnt3a protein to stimulate cells with. To do so, osteoblasts were generated from bone chips and after reaching confluency were placed in serum-free medium containing fortified serum replacement TCM. After 12 hours, osteoblasts were stimulated with 50ng/ml of Wnt3a for 0, 2, 6 and 24 hours. Cells were then lysed and Western Blot performed. Analysis showed that the active form of β-catenin, which is the non-phosphorylated form, increased slightly after 2 hours of incubation with Wnt3a (**Figure 5.13 A, B** and **C**). Analysis also showed that levels of non-phosphorylated (active) β-catenin showed no significant difference between Sdc3 KO cultures and WT cultures (**Figure 5.13 C**), but there appeared to be a trend towards lower levels in the Sdc3 KO cultures which may suggest a downregulation of the Wnt signalling pathway in the absence of Sdc3. To capture potential earlier effect of Wnt3a on β-catenin dephosphorylation, I performed another time course on both Sdc3 KO and WT osteoblasts which included 15, 30, 60 and 120 minutes of stimulation with 50ng/ml of recombinant mouse Wnt3a protein. Western blot analysis showed no significant changes between WT and Sdc3 KO cultures although there still appeared to be a trend towards decreased levels of active β-catenin in the Sdc3 KO when compared to WT osteoblasts (**Figure 5.14 A** and **B**). This could suggest that Sdc3 KO osteoblasts are unresponsive to Wnt3a stimulation.

In order to find the optimal concentration of Wnt3a for activating the β-catenin pathway in Sdc3 KO vs WT osteoblasts, Sdc3 KO and WT osteoblasts were stimulated for 2 hours with 0, 10, 25, 50 and 100 ng/ml of recombinant mouse Wnt3a protein. Analysis showed no significant difference in dose response between Sdc3 KO and WT. However, again the level of active β-catenin appeared to be lower in Sdc3 KO (**Figure 5.15**) which may indicate that Sdc3 KO osteoblasts are less responsive to rising concentrations of Wnt3a, but this experiment was performed only once. Therefore, these data suggest that Sdc3 deletion has an inhibitory effect on the

pathway activation. Therefore, Sdc3 may have an enhancing effect on the canonical Wnt signalling pathway in osteoblasts.

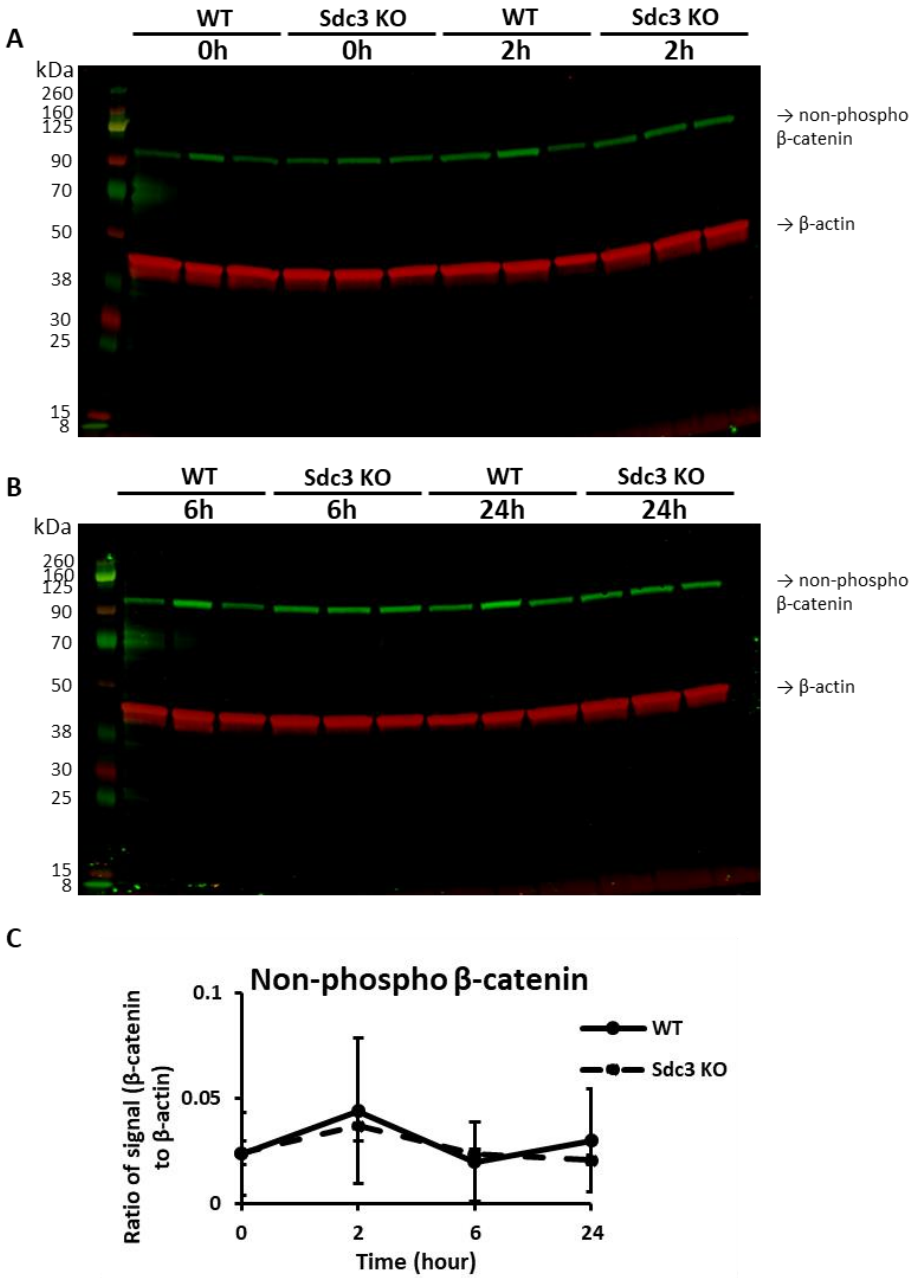

Figure 5.13: Western blot analysis of non-phosphorylated β-catenin in Sdc3 KO and WT osteoblasts after stimulation with Wnt3a. Sdc3 KO and WT osteoblasts cultures generated from bone chips were stimulated under serum-free conditions with 50ng/ml recombinant mouse Wnt3a protein for 0, 2, 6 and 24 hours after overnight incubation in serum free medium containing serum replacement TCM. Levels of non-phosphorylated (active) β-catenin at 0 and 2h (**A**) and 6 and 24h (**B**) were quantified by Western blotting. All blots were probed for β-actin as a housekeeping protein. Quantification of non-phosphorylated β-catenin (**C**) shows a slight increase at the 2-hour time point, then a slight decrease at the 6-hour time point in both Sdc3 KO and WT. Quantification showed no significant differences between Sdc3 KO cultures and WT (N=3). The expected molecular weight for non-phosphorylated β-catenin is 92 kDa and for β-actin is 42 kDa.

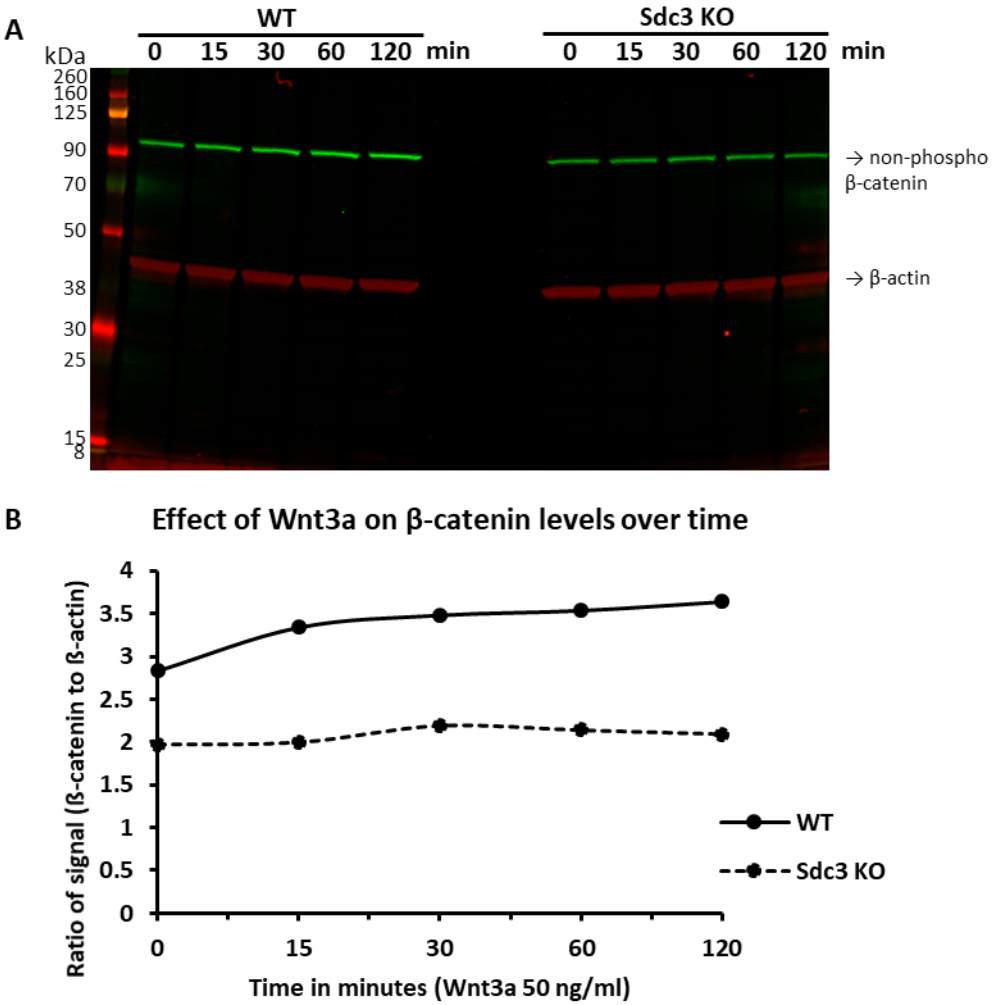

Figure 5.14: Western blot analysis of non-phosphorylated β-catenin in Sdc3 KO and WT osteoblasts after Wnt3a stimulation. Sdc3 KO and WT osteoblasts cultures generated from bone chips were stimulated under serum-free conditions with 50ng/ml recombinant mouse Wnt3a protein for 0, 15, 30, 60 and 120 minutes after 24hours in serum-free medium containing serum replacement TCM. Levels of non-phosphorylated (active) β-catenin at the different time points were examined by Western blotting (**A**). Quantification of non-phosphorylated β-catenin (**B**) shows a no significant difference in non-phosphorylated β-catenin levels as stimulation time increases between WT cells and Sdc3 KO cells. N=1. The expected molecular weight for non-phosphorylated β-catenin is 92 kDa and for β-actin is 42 kDa.

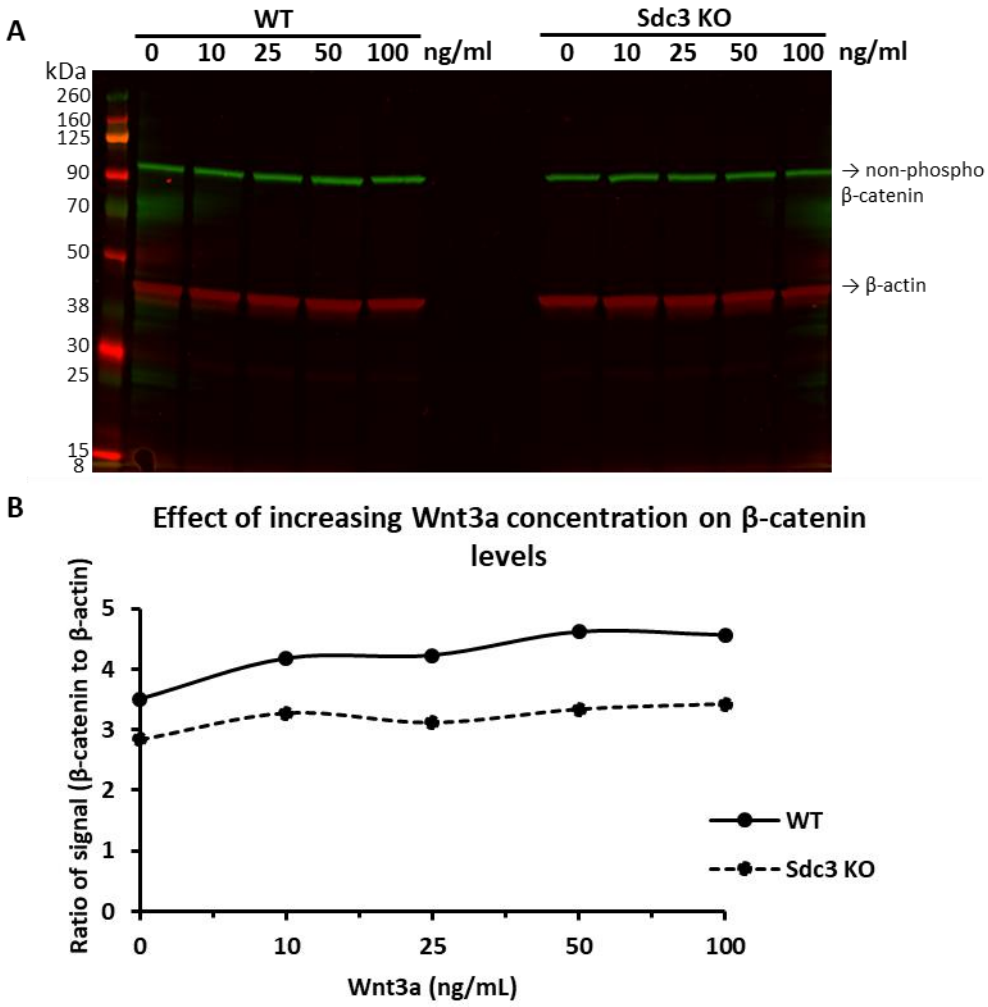

Figure 5.15: Western blot analysis of non-phosphorylated β-catenin in Sdc3 KO and WT osteoblasts after Wnt3a dose response. Sdc3 KO and WT osteoblasts cultures generated from bone chips were stimulated under serum-free conditions with 0, 10, 25, 50 and 100 ng/ml recombinant mouse Wnt3a protein for 2 hours after 24hours in serum free medium containing TCM. Levels of non-phosphorylated (active) β-catenin at the different time points were examined by Western blotting (**A**). Quantification of non-phosphorylated β-catenin (**B**) shows no significant difference in non-phosphorylated β-catenin levels in response to increased doses of Wnt3a stimulation between Sdc3 KO and WT cells. N=1. The expected molecular weight for non-phosphorylated β-catenin is 92 kDa and for β-actin is 42 kDa.

5.3.4 The effect of Syndecan 3 deletion on adipocyte formation *in vitro*

For osteoblast *in vitro* studies I extracted bone marrow MSCs (BMSCs) and grew them in osteogenic conditions in order to induce mineralisation (section **5.3.2.1**; **Figure 5.5**). During this experimental process I observed the presence of fat cells in the Sdc3 KO osteoblast cultures generated from BMSCs shown here in **Figure 5.16**.

As Sdc3 deletion leads to a phenotype which mimics premature osteoporosis and considering that Sdc3 KO mice also showed increased bone marrow adiposity during histomorphometric analysis in Sdc3 KO mice, *in vitro* studies to assess adipocyte formation were performed. Fat cells were not quantified as these cultures were used for mineralisation assay and quantification. I extracted bone marrow from the long bones of 8-week-old Sdc3 KO and WT female mice in order to obtain BMSCs. Cells were then grown in adipogenic conditions for up to 21 days. Sdc3 KO appeared to generate more adipocytes than WT cultures (**Figure 5.17**) but Oil red O staining for adipocyte quantification failed due to loss of cells during the processing, therefore I was unable to quantify them.

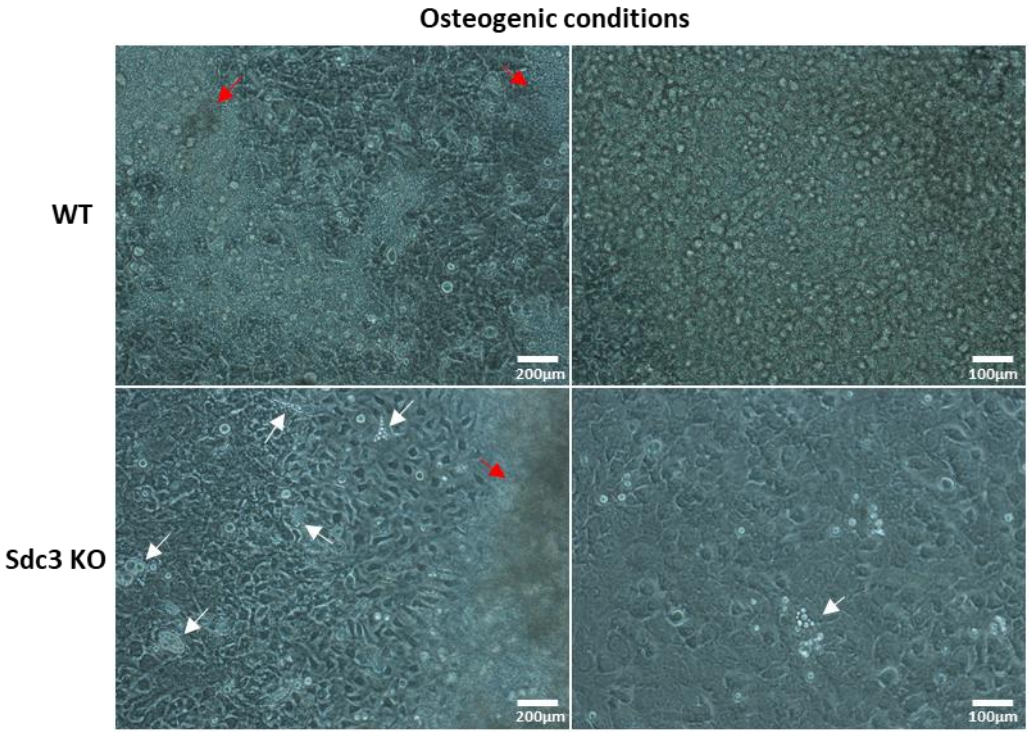

Figure 5.16: Bone marrow mesenchymal stromal cells cultured in osteogenic conditions. Representative micrographs of WT and Sdc3 KO BMSC cultures grown under osteogenic conditions show the presence of possible mineral in both cultures (indicated by red arrows). Interestingly, Sdc3 KO cultures appear to have spontaneous generation of adipocytes (indicated by white arrows). Images were taken of representative wells from 1 of 3 independent experiments performed in quadruplicate. Live cells cultures were visualised using phase contrast microscopy, magnification 10x and 20x.

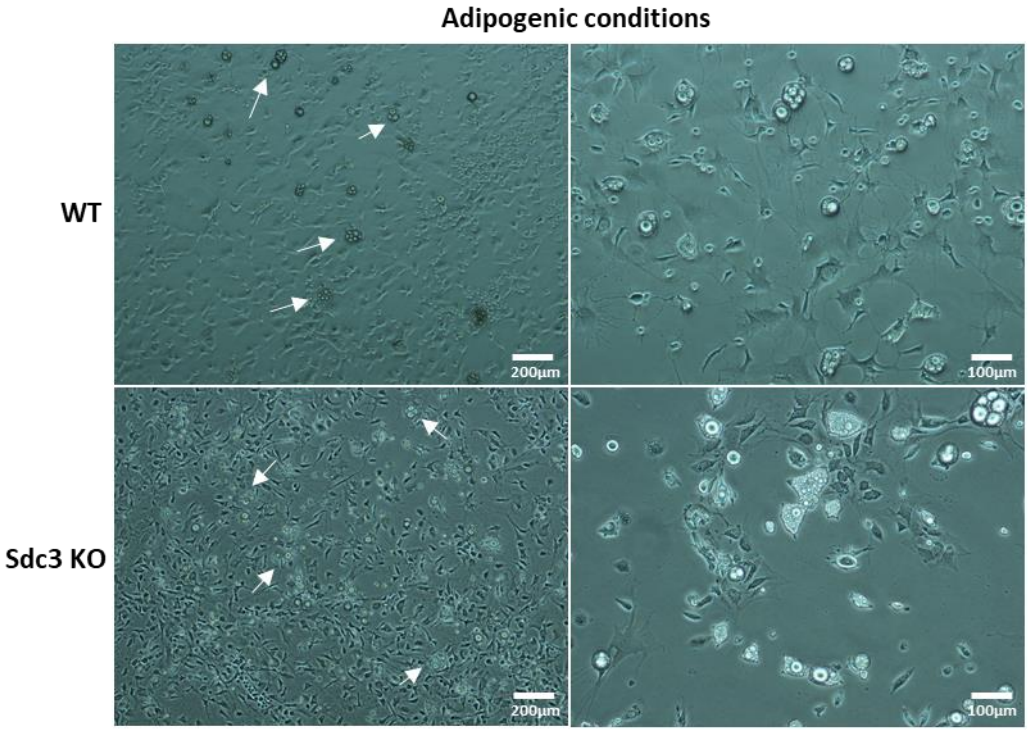

Figure 5.17: Bone marrow mesenchymal stromal cells grown under adipogenic conditions. Representative micrographs show the presence of adipocytes in both WT and Sdc3 KO cultures (indicated by white arrows). Images were taken of representative wells from 1 of 3 independent experiments performed in quadruplicate. Live cells cultures were visualised using phase contrast microscopy, magnification 10x and 20x.

5.3.3.6 The effect of Syndecan 3 deletion on gene expression in adipocytes

The results described above show that Sdc3 KO MSCs can differentiate into both mineralising osteoblasts and adipocytes in osteogenic conditions, but WT seem to form only osteoblasts under the same conditions. During histomorphometric studies, Sdc3 KO mice were also shown to have increased bone marrow adiposity when compared to WT mice. This suggests that there may be a possible dysregulation in the mechanisms governing osteoblastogenesis vs adipogenesis with a shift towards the latter in Sdc3 KO. To further understand this increased adipogenesis observed in Sdc3 KO, gene expression analysis was performed on mRNA obtained from the BMSC generated adipocyte cultures and osteoblast cultures.

Early osteoblast marker genes of differentiation analysed included *Runx2*, which is a major transcription factor in osteoblastogenesis[434], *Fgf2* and *On* (encoding

osteonectin), which positively regulate osteoblast differentiation and are essential for bone formation [463–465]. Late osteoblast marker gene analysed was *Postn* (encoding periostin), which regulates cell adhesion[466].

Adipocyte marker genes were also analysed, including early marker gene for adipogenesis, *Pparg,* which is the main regulator of adipogenesis, and late marker gene for adipogenesis, *Adipoq* (encoding adiponectin), which is highly expressed in mature adipocytes[467]. Due to the earlier suggestion of the possible involvement of Sdc3 in the enhancement of Wnt signalling, *Wnt10b* expression was also analysed. Wnt10b has been shown by Bennett *et al*., to enhance osteoblast differentiation, increasing postnatal bone formation[468]. Bennett and colleagues generated a transgenic mouse in which Wnt10b was expressed in mature osteoblasts and found that that this overexpression lead to an increase in osteoblast numbers in bone and an increase in bone formation[468]. Previous studies by the same group showed that Wnt10b stimulates osteoblastogenesis, inhibiting adipogenesis, by inducing *Runx2*, *Dlx5* and *Osterix*, and supressing *Pparg*[469].

Interestingly, as shown in **Figure 5.18**, *On* (osteonectin; **C**), a positive regulator of osteoblast differentiation, was the only gene to be significantly downregulated ($p<0.05$) in Sdc3 KO BMSCs grown in adipogenic conditions. The remaining genes showed no significant difference between genotypes in BMSCs grown in either osteogenic or adipogenic conditions.

Expression of *Hmbs*, the housekeeping gene, in WT and Sdc3 KO BMSCs grown in osteogenic conditions had an average CT value of 23.8 for both genotypes, while in BMSCs grown in adipogenic conditions *Hmbs* had an average CT value of 24.5 for WT and 25.6 for Sdc3 KO.

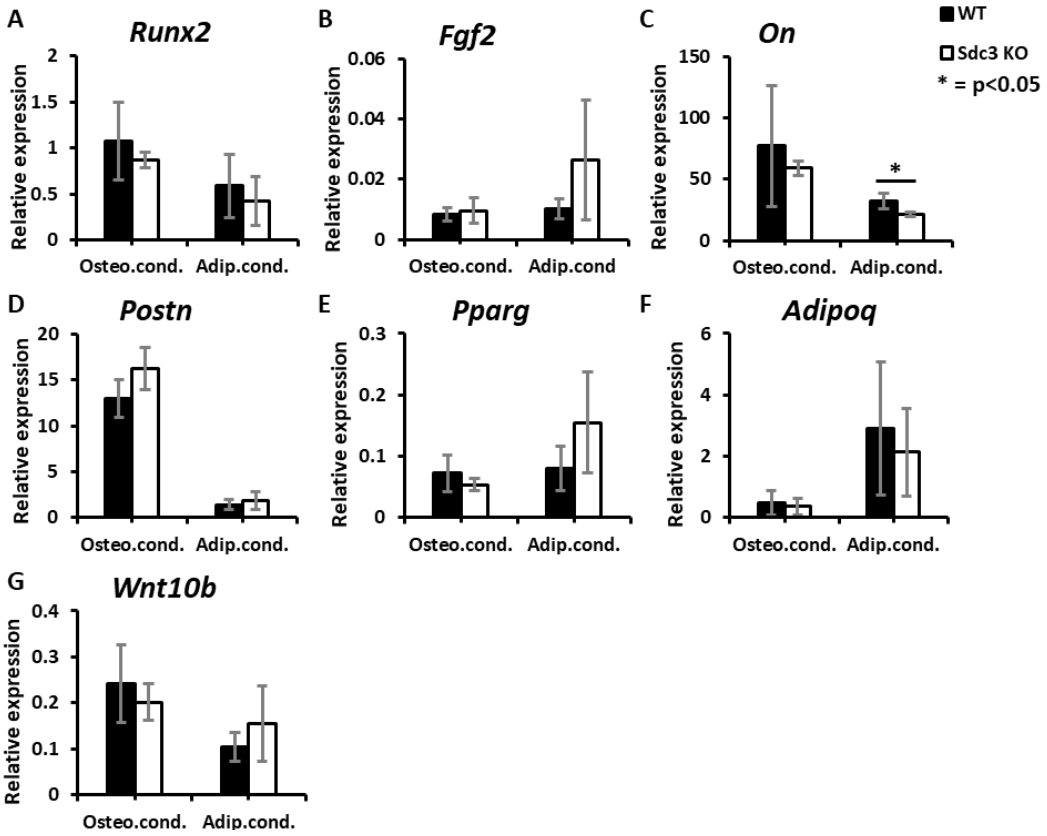

Figure 5.18: RT-qPCR analysis of osteoblast and adipogenic marker genes and *Wnt10b* in Sdc3 KO and WT BMSCs grown in osteogenic and adipogenic conditions. BMSCs obtained from Sdc3 KO and WT mice were grown in standard medium until confluent and then in mineralising or adipogenic conditions for 21 days in order to generate either mineralising osteoblasts or adipocytes. Analysis of relative expression to housekeeping gene *Hmbs* shows no significant differences in relative expression of *Runx2* **(A),** *Fgf2* **(B),** *Postn* **(D),** *Pparg* **(E),** *Adipoq* **(F)** and *Wnt10b* **(G)** between Sdc3 KO and WT**.** *On* **(C)** showed a significant downregulation in relative expression in Sdc3 KO BMSCs grown in adipogenic conditions, when compared to WT cells in the same conditions. Results represent means ± SD from 3 independent experiment performed in triplicate. Significance is denoted by *p<0.05.

5.4 Discussion

Adult Sdc3 KO mice have a low bone volume phenotype coupled with increased bone fragility. Dynamic histomorphometry showed that Sdc3 KO mice have decreased bone formation, decreased osteoclast numbers, increased bone marrow adiposity and a blunted response to mechanical loading. Sdc3 KO mice are resistant to high-fat diet-induced obesity and accumulate less adipose tissue[376], and have impaired hippocampus-dependent memory[377] suggesting that Sdc3 plays a role in the

central nervous system. This indicates that there could be a systemic factor/s dysregulation that account for the Sdc3 KO bone phenotype. Thus, it was essential to investigate the effect of Sdc3 deletion at a cellular level to understand if the effect observed *in vivo* could be replicated (or not) *in vitro*. Given the decreased bone formation coupled with increased bone adiposity and a blunted response to loading, one of the underlying mechanisms that Sdc3 may affect is the Wnt pathway, which is the major upregulator of osteoblastogenesis and inhibitor of adipogenesis and is also required for osteogenic response to mechanical loading[470,471].

In this chapter, I studied the effect Sdc3 deletion has on osteoclasts, osteoblasts and adipocytes *in vitro*. Osteoclastogenesis was decreased in Sdc3 KO osteoclasts compared to WT osteoclasts *in vitro* suggesting that Sdc3 may be important for osteoclast formation. These results are in line with the *ex vivo* findings in which Sdc3 KO had decreased osteoclast numbers. Interestingly, when investigating osteoclast activity, analysis of resorption assays showed increased resorption activity in the Sdc3 KO osteoclasts when compared to those of WT, but these results only explain in part the phenotype.

Therefore, I then performed gene expression studies which showed a downregulation of *Tnfrsf11a* (which encodes RANK) in Sdc3 KO macrophages. As mentioned in detail in Chapter 1 (Introduction), RANK is essential for osteoclast formation therefore downregulation of *Tnfrsf11a* could be reflected by the reduced sensitivity to RANKL observed in *in vitro* Sdc3 KO osteoclastogenesis cultures, but these finding still do not explain why Sdc3 KO osteoclasts have a relatively increased resorption activity vs WT.

There are many very rare diseases associated with defects in osteoclast formation or function and many of them are due to mutations in the RANK pathway[472]. Osteopetrosis, for example, is characterized by reduced bone resorption which can be either due to defective osteoclast function (“osteoclast rich”) or reduced osteoclast numbers (“osteoclast poor”) [472,473]. Thus, all forms of osteopetrosis lead to non-functional osteoclasts[472], unlike the Sdc3 KO mouse model in which Sdc3 KO osteoclasts have high bone resorption per cell although their numbers are reduced.

Dissimilar to other syndecans, studies on Sdc3 are very limited. For example, Angsana and colleagues showed that Sdc1 is able to promote macrophage motility[474], while a study by Benad-Mehner *et al*., showed that Sdc1 inhibits OPG expression, and in turn osteoclast formation[475],however, I found no difference in *Opg* or *Rankl* expression. Other proteoglycans such as small rich proteoglycans (SLRPs), which include Decorin, Biglycan and Fibromodulin, have been shown to regulate osteoclastogenesis through interactions with M-CSF, RANKL, OPG and also TNFα[476–478]. Both M-CSF and RANKL are essential for osteoclastogenesis and activate a series of pathways during osteoclastogenesis, including ERK, MAPK, JNK and AKT signalling pathways, but other studies, such as those by Maeda *et al.* have also shown that the non-canonical Wnt pathway can enhance osteoclast formation[453]. It was reported that Wnt5a enhanced the expression of RANK, mediated by FZD in osteoclast precursors, which, in turn, promoted RANKL-induced osteoclast formation[453]. Indeed, gene expression levels of *Fzd7* were downregulated in Sdc3 KO macrophages when compared to WT cultures which may also explain the downregulation in *Tnfrsf11a*, which is induced by FZD-mediated non-canonical WNT signalling pathway in which FZD7 is highly expressed[453]. Therefore, it would have been interesting to investigate the effect of Sdc3 deletion on the molecular pathways in osteoclasts in more detail.

During osteoblast *in vitro* studies I found that osteoblast cultures generated from mouse bone chips, BMSCs and from calvaria, all have impaired mineralisation, which is again consistent with my *in vivo* findings in which Sdc3 KO mice have reduced bone formation and a blunted response to mechanical loading. The decrease in mineralisation observed in Sdc3 KO cultures could be due to impaired osteoblast proliferation, but this was not reflected in cell proliferation studies as the number of Ki67+ cells showed no difference, although only preliminary, between Sdc3 KO and WT osteoblasts generated from bone chips. Gene expression studies showed that *Alpl* was reduced in Sdc3 KO osteoblasts, which is consistent with the reduced enzyme activity observed in Sdc3 KO cultures, which suggests that Sdc3 may have a positive effect on osteoblast maturation and function, and therefore mineralisation. Interestingly, to my knowledge, no other studies including the remaining syndecans have been performed investigating a possible effect on ALP activity.

Sdc3 KO osteoblast cultures also revealed decreased expression of *Runx2*, a key transcriptional regulator of osteoblast differentiation, which, interestingly, has been shown to induce ALP gene expression and enzyme activity in osteoblasts[98], which could therefore explain the decrease in *Alpl* expression and ALP enzyme activity. Interestingly, Komori and colleagues performed a study on Runx2 function by generating mice lacking the gene[434]. They found that mice lacking Runx2 die just after birth due to complete lack of bone formation due to absence of osteoblast differentiation, which completely blocked intramembranous and endochondral ossification[434], highlighting the importance of Runx2 in osteogenesis and especially in the development of osteoblasts[97,434].

Smad6, associated to BMP signalling and a positive regulator of osteoblast function together with Runx2[479,480], was also shown to be significantly reduced in Sdc3 KO cultures. Shen *et al*., performed studies on the Runx2 degradation by co-transfecting Smad6 with Runx2 and SMAD specific E3 Ubiquitination Protein Ligase 1 (Smurf1), which interacts with Smads and BMP receptors triggering their ubiquitination and degradation, in COS cells and examining any possible degradation of Runx2 by western blot[480]. They found that Smad6 significantly enhanced Smurf1-induced Runx2 degradation and that Smad6 together with Smurf1 can downregulate Runx2 protein[480]. On further investigation, Wang and colleagues found that BMP2 activates Smad6 through the interaction of Smad1 with Runx2 (**Figure 1.9**), preventing the interaction of Smurf1 with Runx2 and inhibiting Runx2 ubiquitination[479]. Both Smad6 and Runx2 are part of the BMP signalling pathway[481], and when coupled together stimulate osteoblastogenesis[479,480]. As *Smad6* is downstream from *Runx2*, *Runx2* downregulation could explain subsequent downregulation of *Smad6* in Sdc3 KO cultures, highlighting the importance of *Smad6* and *Runx2* in osteoblast formation and function.

To confirm successful deletion of *Sdc3* in Sdc3KO mice relative expression of the gene was also investigated in Sdc3 KO and WT cultures, but also of the remaining syndecans 1, 2 and 4 in order to assess any possible compensatory mechanism that could be involved in Sdc3 deletion. Sdc3 KO cultures showed no gene expression of *Sdc3* confirming that the gene was indeed knocked out. Other syndecans showed no

significant difference in gene expression between WT and Sdc3 KO cultures which could indicate that none of them are able to compensate for the lack of Sdc3.

MSCs are pluripotent cells that give rise to fibroblasts, myocytes, chondrocytes, osteoblasts and adipocytes[482]. Osteoblasts and adipocytes are both regulated by the Wnt signalling pathway[470]. Given the increase in bone marrow adipocytes found in Sdc3 KO mice coupled with decreased bone formation and blunted response to mechanical loading I investigated the effect Sdc3 deletion has on the Wnt signalling pathway. The canonical Wnt pathway is activated through the binding of Wnt ligands, such as Wnt3a, to their receptor Frizzled and co-receptor LRP5/6. Binding of the Wnt ligands activates Axin which binds to this complex formed by the Wnt ligand, frizzled and LRP5/6, preventing β-catenin phosphorylation. This signalling is enhanced by LGR4, 5 or 6. The non-phosphorylated β-catenin then accumulates in the cytoplasm, translocating into the nucleus where it can then activate target gene expression by binding to TCF/LEF transcription factors. Analysis of gene expression of members of the Wnt pathway revealed that only *Lgr4* was downregulated in Sdc3 KO cultures compared to WT cultures. *Wnt3a*, *Lrp5* and *6*, *Fzd1,* which is relatively highly expressed in osteoblasts[457] and is known to enhance osteoblast-mediated mineralisation[458], *Lgr5* and *6* and *Axin2* all showed no significant difference, but this could be due to a low number of biological replicates. Interestingly, preliminary data showed that *Atf4*, which is downstream of *Lgr4*, was downregulated in Sdc3 KO cultures, as was *Ctnnb1* (encodes β-catenin). A study by Luo *et al*., investigated the role of LGR4 in bone formation and remodelling[151]. Mice lacking LGR4 exhibited prenatal and postnatal growth retardation, characterized by shorter limbs, such as the tibias, and decreased body weight, which suggested a role of LGR4 on bone formation[151]. LGR4 function on bone formation was assessed and reported to control the expression of transcription factor Atf4 and downstream targets, *On*, *Bsp* and collagen and early differentiation marker *Runx2,* all essential for osteoblast formation and function[151]. In humans, nonsense mutations in the *Lgr4* gene has been shown to be strongly associated with low bone mineral density and with osteoporotic fractures[483]. Therefore, it is possible that Sdc3 modulates Wnt signalling, acting as a co-receptor, through stabilization of Lgr4, but the exact mechanism still remains unclear.

Protein studies performed on samples of Sdc3 KO and WT osteoblasts stimulated with Wnt3a showed no significant changes in non-phosphorylated β-catenin signal although there appeared to be a trend towards it being lower in Sdc3 KO, and while this is preliminary data it could confirm the findings observed at a gene level. This data suggests that Sdc3 may enhance the Wnt pathway. With evidence that the Sdc3 KO mouse may have early onset osteoporosis, coupled with a blunted response to mechanical loading and increased bone marrow adipogenesis, it would be of great interest to explore the possible role Sdc3 may have on the Wnt pathway when considering that this pathway has been linked to cell proliferation and function, and to cell response to loading.

I also investigated the effect of Sdc3 deletion on adipogenesis due to the observation of adipocytes in Sdc3 KO cultures grown under osteogenic conditions and the increased bone marrow adiposity observed in Sdc3 KO mice. I performed gene expression studies on osteoblast and adipocyte marker genes on both BMSC cultures grown in either osteogenic or adipogenic conditions. The only gene to show any significant difference was *Osteonectin*, which was decreased in Sdc3 KO cultures grown under adipogenic conditions. Interestingly, a study by Delany *et al*., studied osteonectin-null mice and the effect it had on osteoblasts and bone formation[464]. By performing *in vitro* studies on osteoblastic cells derived from these mice and from WT control they discovered that the osteonectin-null cultures had decreased mineralisation and were able to form adipocytes in osteoblast cultures, similar to sdc3 KO cultures. They suggest that the presence of osteonectin may lead cell differentiation to favour the osteoblastic pathway rather than the adipogenic. Adipocytes derived from bone marrow have also been shown to supress osteoblast differentiation by suppressing the BMP pathway by adipokine-induced activation of the NF-κB signalling pathway[484]. Suppressed osteoblast formation due to increased adipogenesis may be a reason for the reduced osteoclast formation. It is also important to point out that there is crosstalk between BMP pathway and the Wnt signalling pathway[485]. Zhang *et al*., found that BMP2 can stimulate *Lrp5* expression which inhibits β-catenin degradation and therefore enhancing non-phosphorylated β-catenin protein levels in osteoblasts[485]. But by deleting *Bmp2 in vitro*, osteoblast proliferation, differentiation and function was inhibited with osteoblast maker genes

Alpl and *Col1a1* being significantly downregulated in the *β-catenin*-deficient osteoblasts[485]. On the other hand, Zhang *et al*., found that the Wnt pathway is also able to modulate the BMP pathway[486]. By Wnt3a stimulation or overexpression of β-catenin/TCF4 in osteoblasts they found that this strongly induced BMP2 transcription, suggesting that Wnt signalling acts as an upstream regulator of BMP signalling[486]. It is possible that Sdc3 is able to enhance Wnt signalling, which in turn induces BMP signalling and its downstream effectors such as RUNX2, essential in osteoblastogenesis.

Due to the presence of adipocytes in Sdc3 KO osteoblast cultures generated from BMSCs grown in osteogenic conditions, I performed further gene expression studies of osteoblast marker genes as there was a possibility that these could be downregulated in Sdc3 KO explaining the increased numbers of adipocytes in these cultures. These studies showed no significant difference in relative expression between Sdc3 KO and WT cultures, but this could possibly be due to the increased sample variation, as can be seen by the large SD of the mean in both Sdc3 KO and WT cultures. As these cells were kept in culture for a prolonged time, although seeded at the same density, this could lead to variation in cell proliferation and apoptosis at the end of the experimental process which could lead to differences in gene expression observed between experimental replicates, resulting in high SD. Increase in number of replicates would be beneficial in this.

The above data suggest that Sdc3 enhances canonical Wnt signalling pathway in osteoblasts and this in turn may activate other pathways, such as the BMP pathway. It may be that in the Sdc3 KO the Wnt pathway is supressed, accounting for the increase in adipogenesis observed, which is turn decreases osteoblast function. Osteoblasts are one of the main generators of RANKL together with osteocytes. RANKL is required for activation of osteoclastogenesis through RANKL/RANK interaction, therefore if there is a decrease in this interaction, there would be a decrease in osteoclastogenesis which could explain the decreased osteoclast numbers observed in Sdc3 KO cultures. It would be of interest to perform more in-depth studies of the effect Sdc3 deletion has on the Wnt pathway and how this may be affecting other pathways such as the BMP pathway. It would also be interesting to stimulate osteoblasts with recombinant BMP2 in order to stimulate osteoblast

differentiation as it may be possible that Sdc3 KO cultures may not respond to this compared to WT which, on the other hand, could have increased osteoblast proliferation and differentiation. Co-cultures of osteoclasts and osteoblasts could be of interest to investigate a possible crosstalk between these two types of cells.

6. Summary and Discussion

Here I have shown that syndecan 3 has a novel role in bone metabolism. I demonstrated that deletion of Sdc3 leads to low bone volume, blunted response to mechanical loading and increased bone fragility, and increased bone marrow adiposity in 3-month-old young adult mice which is maintained as they mature, mimicking what is seen in premature osteoporosis.

Interestingly, I also found that Sdc3 affects bone growth differentially throughout development, as P2 Sdc3 KO mice have longer tibias than WT pups, however, at 3 months of age this is reverted, and Sdc3 KO mice develop shorter tibias. This may be explained by the role Sdc3 has in early development, in which it was shown that syndecan 3 plays a restrictive role during the formation of mesenchymal condensations by setting boundaries and limiting their size[208]. On the other hand, syndecan 3 has also been shown to be highly expressed in the periosteum and perichondrium of developing long bones[300,303], therefore suggesting it plays a role during skeletogenesis. This information leads to the assumption that the absence of Sdc3 would no longer restrict condensations and therefore would no longer limit long bone length, explaining the longer limbs observed in Sdc3 KO pups. However, this does not explain why adult Sdc3 KO mice develop shorter limbs. As Sdc3 has been shown to control chondrocyte proliferation and maturation in the growth plate during embryonic long bone development[301,374,375], therefore, it is possible that this extends into adulthood, which could explain the shorter tibias observed in adult Sdc3 KO mice. In the future, it would be of interest to investigate the effect of Sdc3 on the growth plate by also looking into to its possible role in regulating chondrocytes.

On the other hand, I also observed increased tibial bone volume in Sdc3 KO pups compared to WT pups which was also not carried into adulthood at which point Sdc3 KO adult 3-month-old mice have decreased trabecular bone volume and increased trabecular thinning and separation together with cortical thinning, compared to WT mice, and this remains low as they reach 6 months of age. Furthermore, I also found that young adult Sdc3 KO mice have decreased bone formation even after mechanical stimulation. This blunted response to mechanical loading in Sdc3 KO mice is not due to a muscle dysfunction as it has previously been

shown that Sdc3 KO mice have improved muscle homeostasis, regeneration and ageing[307].

Interestingly, Raulo *et al.* reported that Sdc3 was a receptor for HB-GAM in neurons[304], and similarly to what I have observed in Sdc3 KO mice, Imai *et al*. reported that young adult HB-GAM KO mice have shorter long bones, reduced trabecular bone volume (BV/TV), and reduced bone formation even in response to mechanical loading, compared to WT mice[487]. An earlier study performed by the same group showed that HB-GAM mediates osteoblast recruitment and enhances their function[488]. Thus, if the receptor for HB-GAM, which is Sdc3, is missing then the pathway downstream from HB-GAM/Sdc3 would be affected.

Strader *et al.* reported that Sdc3 KO mice are resistant to diet-induced obesity and have a leaner body phenotype, indicating that Sdc3 plays role in the central nervous system regulating energy balance[376]. The central nervous system plays an important role in bone metabolism and can regulate bone mass as has been shown through leptin deficient mice[258]. It could be that the in vivo phenotype may be due to a systemic effect of Sdc3 deletion. Therefore, to determine if that is or is not the case, *in vitro* studies were performed. Interestingly, osteoclastogenesis was found to be decreased in Sdc3 KO mice, like in HB-GAM KO mice, although in contrast to HB-GAM KO model, in the Sdc3 KO bone resorption was significantly increased which may partly contribute to the low bone phenotype observed in Sdc3 KO. The reduced osteoclastogenesis may be explained, in part, by the decreased expression of *Tnfrsf11a* (encoding RANK) and *Fzd7* in MCSF-dependent Sdc3 KO macrophages, explaining the reduced sensitivity to RANKL, and reduced osteoclast formation, suggesting that Sdc3 may enhance pathways which target *Fzd7*. Indeed, FZD mediates non-canonical Wnt signalling via RAC/JNK/c-Jun later inducing RANK expression[453]. Interestingly, Rspo3 was shown to bind Sdc4 which in turn associates with Fzd7, a key step in order to promote Wnt signalling during planar cell polarity in Xenopus[454]. This also activates JNK signalling[454] therefore it may be possible that Sdc3 may associate with Fzd7 during cell polarisation, an important process for osteoclast function, thus further research would be of interest in order to investigate this possibility. Furthermore, Bhat *et al.* demonstrated that Fzd7 is induced by Notch signalling in human breast epithelial cells[489], a signalling pathway which is also known to crosstalk

with Sdc3 during myogenesis[178]. Thus, it would be of interest to further investigate the crosstalk between Sdc3 and Notch in bone given that Notch plays a role in downregulating osteoblastogenesis, however, also regulates embryonic skeletal development by limiting bone growth, similar to the role Sdc3 has on condensation size[172].

As Sdc3 KO mouse showed decreased bone formation even after undergoing mechanical loading, osteoblast *in vitro* studies were also performed to further understand the role of Sdc3 in bone. Cell studies performed under mineralising BMSCs conditions showed that Sdc3 KO osteoblasts generated from bone chips, calvaria and s all have an impaired ability to mineralise their matrix. Interestingly, adipocytes were present in the Sdc3 KO osteoblast cultures grown under mineralising conditions. These observations together with the increased bone marrow adiposity seen in Sdc3 KO mice suggests mesenchymal progenitor cells may preferentially differentiate into adipocytes as opposed to osteoblasts.

The common pathway regulating the balance between adipogenesis and osteoblastogenesis and skeletal development[137], and in cartilage inducing chondrocyte hypertrophy and cartilage boundary definition, and regulating growth plate organisation [490] is the Wnt pathway[78]. Therefore, in addition to osteoblast marker genes and positive regulators of osteoblast formation, which includes *Smad6*, I focused my gene expression studies on the canonical Wnt signalling pathway using Sdc3 KO and WT osteoblasts generated from bone chips. *Alpl* (encoding alkaline phosphatase), *Runx2* and *Smad6* were decreased in Sdc3 KO osteoblast cultures indicating that Sdc3 may play a role during early osteoblast formation and maturation. On the other hand, *Sdc1*, *2* and *4* gene expression were also quantified, and it was shown that there was no significant compensatory increase, suggesting a specific role of Sdc3 in bone metabolism.

As for the members of the Wnt pathway, which included *Wnt3a*, *Lrp5* and 6*, Fzd1*, *Lgr4*, *5* and *6*, *Axin2*, *Atf4* and *Ctnnb1*, only *Lgr4* was shown to have significantly decreased expression in Sdc3 KO osteoblasts generated from bone chips. Mice lacking LGR4 exhibit growth retardation, although unlike Sdc3 KO mice, this happens both prenatally and postnatally and is driven by high osteoclasts number and high bone resorption[151,491]. However, contrary to Sdc3 KO mice, LGR4 KO mice also have

decreased body weight and renal hypoplasia together with impaired renal function which likely contributes to the phenotype[151]. Furthermore, the study by Sun *et al*. also demonstrated that LGR4 KO mice have decrease bone volume, however they also have increased BMSC cell number, with decreased apoptosis and cell migration, impaired fracture healing and decreased fat mass, contrary to Sdc3 KO mice[492]. On the other hand, preliminary work in this thesis, showed ATF4, downstream of LGR4, was decreased in Sdc3 KO cultures. Moreover, I demonstrated that, at protein level, non-phosphorylated β-catenin appeared to trend towards lower levels of activation in Sdc3 KO osteoblasts after Wnt3a stimulation. Interestingly, in the presence of RSPOs, which bind LGRs, the RSPO-LGR complex interacts with ZNRF3/RNF43 and prevents the latter from tagging FZD for degradation[493]. Thus, the high level of FZD allows for strong WNT-induced signalling[494]. Interestingly, inactivating mutation of RSPO2, which interfere with the RSPO2-LGR or -RNF43 interaction, inhibit Wnt signalling and induce limb abnormalities in humans[495] and mice[496]. Thus, it is possible that Sdc3 acts as a co-receptor for the RSPO-LGR4 complex, enhancing Wnt/β-catenin signalling which in turn activates osteoblastogenesis therefore inhibiting adipogenesis, however, as mentioned above, LGR4 deletion does not mimic the Sdc3 KO phenotype described here.

In order to understand the mineralisation defect observed in Sdc3 KO osteoblasts, which could suggest a degree of immaturity of differentiated Sdc3 KO osteoblasts, further gene expression studies were performed on osteoblasts generated from BMSC, which included *Tnfsf11*, *Tnfrsf11b*, *Alpl*, *Bglap* and *Col1a1*, but no differences were observed.

Sdc3 KO mice have a low bone volume phenotype together with impaired osteoblastic bone formation and increased bone marrow adiposity. This suggests either a preferential switch at the mesenchymal progenitor level from osteoblastogenesis to adipogenesis, or potential de-differentiation of osteoblasts towards the adipocyte lineage. Further studies were performed on BMSCs grown in osteogenic and adipogenic conditions in order to investigate the possible role of Sdc3 in regulating MSC differentiation but found no significant differences in osteoblast marker gene expression, such as *Runx2*, *Fgf2*, *On* and *Postn*, adipogenic marker gene expression, including *Pparg* and *Adipoq*, and *Wnt10b* which has been shown to

enhance osteoblast formation[468].

Although these findings suggest that Sdc3 plays a role in bone metabolism by enhancing both canonical and non-canonical Wnt signalling in osteoclast lineage and canonical Wnt signalling in osteoblast lineage, further studies are needed to fully investigate these pathways and determine the mechanism of Sdc3 involvement. These include FGF, BMP and Notch as the crosstalk between these pathways regulates osteoblast differentiation[481], and as syndecans have been shown to play roles in these pathways[181], it could be that Sdc3 acts as a co-receptor in these pathways for specific ligands enhancing downstream responses. It would also be of interest to investigate the Sdc3/HB-GAM pathway as their interaction has been shown to regulate osteoblast recruitment and enhancement of bone formation[488] as well as being associated with enhanced osteocyte expression during mechanical loading[487].

To summarize, Sdc3 deletion leads to a low bone volume phenotype together with increased bone marrow adiposity in young adult mice, increased bone fragility and a blunted response to mechanical loading. Sdc3 also appears to play different roles in pre and postnatal bone development. The decreased osteoclastogenesis and increased osteoclast bone resorption observed in Sdc3 KO may likely contribute to this low bone volume phenotype. It is possible that this anabolic effect of Sdc3 on bone is mediated through the enhancement of the Wnt/β-catenin signalling pathway, and it may be that the interaction between Sdc3 and LGR4 is important for this, however further work is required to confirm this.

Although the phenotype described herein indicates there is an osteoblast dysregulation, the increased osteoclast activity likely contributes to the Sdc3 KO phenotype. Interestingly, it has also been shown that LGR4 competes with RANK to bind RANKL negatively regulating osteoclastogenesis, as LGR4 KO mice exhibit hyperactive osteoclasts[491], similar to what I observed in Sdc3 KO osteoclast cultures. Therefore, it may be that Sdc3 also plays a role in inhibiting RANK-RANKL binding in order to control osteoclast activity. Thus, Sdc3 may be a novel therapeutic target for anabolic drug development for the treatment of osteoporosis.

References

1. Olsen, B. R., Reginato, A. M. & Wang, W. Bone Development. *Annu. Rev. Cell Dev. Biol* **16**, 191–220 (2000).
2. Ng, K. W., Romas, E., Donnan, L. & Findlay, D. M. Bone biology. *Baillieres. Clin. Endocrinol. Metab.* **11**, 1–22 (1997).
3. Datta, H. K., Ng, W. F., Walker, J. A., Tuck, S. P. & Varanasi, S. S. The cell biology of bone metabolism. *J. Clin. Pathol.* **61**, 577–587 (2008).
4. The American Society for Bone and Mineral Research. *Primer on the Metabolic Bone Diseases and Disorders of Mineral Metabolism*. *American society for bone and mineral research* (2013).
5. Clarke, B. Normal bone anatomy and physiology. *Clin. J. Am. Soc. Nephrol.* **3**, 131–139 (2008).
6. *Principles of Bone Biology*. (Academic Press).
7. Bonewald, L. F. & Johnson, M. L. Osteocytes, mechanosensing and Wnt signaling. *Bone* **42**, 606–615 (2008).
8. Sommerfeldt, D. & Rubin, C. Biology of bone and how it orchestrates the form and function of the skeleton. *Eur. Spine J.* **10**, 86–95 (2001).
9. Khurana, J. S. *Bone Pathology*. *Humana Press* (Humana Press, 2009). doi:10.1007/978-1-59745-347-9
10. Fuchs, R. K., Thompson, W. R. & Warden, S. J. Bone biology. in *Bone Repair Biomaterials* (eds. Pawelec, K. M. & Planell, J. A.) 15–52 (Woodhead Publishing, 2019). doi:10.1016/B978-0-08-102451-5.00002-0
11. Florencio-Silva, R., Sasso, G. R. da S., Sasso-Cerri, E., Simões, M. J. & Cerri, P. S. Biology of Bone Tissue: Structure, Function, and Factors That Influence Bone Cells. *Biomed Res. Int.* **2015**, (2015).
12. Viguet-Carrin, S., Garnero, P. & Delmas, P. D. The role of collagen in bone strength. *Osteoporos. Int.* **17**, 319–336 (2006).
13. Roach, H. Why does bone matrix contain non-collagenous proteins? The possible roles of osteocalcin, osteonectin, osteopontin and bone sialoprotein in bone mineralisation and resorption. *Cell Biol. Int.* **18**, 617–628 (1994).
14. Boskey, A. L. & Coleman, R. Aging and bone. *J. Dent. Res.* **89**, 1333–1348 (2010).
15. Boskey, A. L. Mineralization of Bones and Teeth. *Elements* **3**, 387–393 (2007).
16. Landis, W. J., Hodgens, K. J., Song, M. J., Arena, J., Kiyonaga, S., Marko, M., Owen, C. & McEwen, B. F. Mineralization of Collagen May Occur on Fibril Surfaces: Evidence from Conventional and High-Voltage Electron Microscopy and Three-Dimensional Imaging. *J. Struct. Biol.* **117**, 24–35 (1996).
17. Manolagas, S. C. Birth and Death of Bone Cells: Basic Regulatory Mechanisms and Implications for the Pathogenesis and Treatment of Osteoporosis. *Endocr. Rev.* **21**, 115–137 (2000).
18. Udagawa, N., Takahashi, N., Akatsu, T., Tanaka, H., Sasaki, T., Nishiharat, T., Kogat, T., Martins, T. J. & Suda, T. Origin of osteoclasts: Mature monocytes and macrophages are capable of differentiating into osteoclasts under a suitable microenvironment prepared by bone marrow-derived stromal cells. *Proc. Natl. Acad. Sci.* **87**, 7260–7264 (1990).
19. Suda, T., Takahashi, N., Udagawa, N., Jimi, E., Gillespie, M. T. & Martin, T. J. Modulation of Osteoclast Differentiation and Function by the New Members

of the Tumor Necrosis Factor Receptor and Ligand Families. *Endocr. Rev.* **20**, 345–357 (1999).

20. Lacey, D. . *et al.* Osteoprotegerin Ligand Is a Cytokine that Regulates Osteoclast Differentiation and Activation. *Cell* **93**, 165–176 (1998).
21. Teitelbaum, S. L. & Ross, F. P. Genetic regulation of osteoclast development and function. *Nat. Rev. Genet.* **4**, 638–649 (2003).
22. Insogna, K. L., Sahni, M., Grey, A. B., Tanaka, S., Horne, W. C., Neff, L., Mitnick, M., Levy, J. B. & Baron, R. Colony-stimulating Factor-1 Induces Cytoskeletal Reorganization and c-src-dependent Tyrosine Phosphorylation of Selected Cellular Proteins in Rodent Osteoclasts. *J. Clin. Invest* **100**, 2476–2485 (1997).
23. Arai, F., Miyamoto, T., Ohneda, O., Inada, T., Sudo, T., Brasel, K., Miyata, T., Anderson, D. M. & Suda, T. Commitment and differentiation of osteoclast precursor cells by the sequential expression of c-Fms and receptor activator of nuclear factor kappaB (RANK) receptors. *J. Exp. Med.* **190**, 1741–1754 (1999).
24. Simonet, W. . *et al.* Osteoprotegerin: A Novel Secreted Protein Involved in the Regulation of Bone Density. *Cell* **89**, 309–319 (1997).
25. Hofbauer, L. C., Gori, F., Riggs, B. L., Lacey, D. L., Dunstan, C. R., Spelsberg, T. C. & Khosla, S. Stimulation of Osteoprotegerin Ligand and Inhibition of Osteoprotegerin Production by Glucocorticoids in Human Osteoblastic Lineage Cells: Potential Paracrine Mechanisms of Glucocorticoid-Induced Osteoporosis [1]. *Endocrinology* **140**, 4382–4389 (1999).
26. Grey, A., Chen, Y., Paliwal, I., Carlberg, K. & Insogna, K. Evidence for a Functional Association between Phosphatidylinositol 3-Kinase and c-src in the Spreading Response of Osteoclasts to Colony-Stimulating Factor-1. *Endocrinology* **141**, 2129–2138 (2000).
27. Shinohara, M. & Takayanagi, H. Novel Osteoclast Signaling Mechanisms. *Curr. Osteoporos. Rep.* **5**, 67–72 (2007).
28. Mancini, A., Niedenthal, R., Joos, H., Koch, A., Trouliaris, S., Niemann, H. & Tamura, T. Identification of a second Grb2 binding site in the v-Fms tyrosine kinase. *Oncogene* **15**, 1565–1572 (1997).
29. Weilbaecher, K. N., Motyckova, G., Huber, W. E., Takemoto, C. M., Hemesath, T. J., Xu, Y., Hershey, C. L., Dowland, N. R., Wells, A. G. & Fisher, D. E. Linkage of M-CSF Signaling to Mitf, TFE3, and the Osteoclast Defect in Mitfmi/mi Mice. *Mol. Cell* **8**, 749–758 (2001).
30. Mckercher, S. R., Henkel, G. W. & Maki, R. A. The transcription factor PU.1 does not regulate lineage commitment but has lineage-specific effects. *J. Leukoc. Biol* **66**, 727–732 (1999).
31. Tondravi, M. M., McKercher, S. R., Anderson, K., Erdmann, J. M., Quiroz, M., Maki, R. & Teitelbaum, S. L. Osteopetrosis in mice lacking haematopoietic transcription factor PU.1. *Nature* **386**, 81–84 (1997).
32. Boyle, W. J., Simonet, W. S. & Lacey, D. L. Osteoclast differentiation and activation. *Nature* **423**, 337–342 (2003).
33. Hsu, H. *et al.* Tumor necrosis factor receptor family member RANK mediates osteoclast differentiation and activation induced by osteoprotegerin ligand. *Proc. Natl. Acad. Sci. USA* **96**, 3540–3545 (1999).
34. Darnay, B. G., Haridas, V., Ni, J., Moore, P. A. & Aggarwal, B. B. Characterization of the intracellular domain of receptor activator of NF-kappaB (RANK). *J. Biol.*

Chem. **273**, 20551–20555 (1998).
35. Rothe, M., Sarma, V., Dixit, V. M. & Goeddel, D. V. TRAF2-Mediated Activation of NF-KB by TNF Receptor 2 and CD40. *Science (80-.).* **269**, 1424–1427 (1995).
36. Nakano, H., Oshima, H., Chung, W., Williams-Abbott, L., Ware, C. F., Yagita, H. & Okumura, K. TRAF5, an activator of NF-kappaB and putative signal transducer for the lymphotoxin-beta receptor. *J. Biol. Chem.* **271**, 14661–14664 (1996).
37. Ishida, T., Mizushima, S. i, Azuma, S., Kobayashi, N., Tojo, T., Suzuki, K., Aizawa, S., Watanabe, T., Mosialos, G., Kieff, E., Yamamoto, T. & Inoue, J. Identification of TRAF6, a novel tumor necrosis factor receptor-associated factor protein that mediates signaling from an amino-terminal domain of the CD40 cytoplasmic region. *J. Biol. Chem.* **271**, 28745–28748 (1996).
38. Lomaga, M. A. *et al.* TRAF6 deficiency results in osteopetrosis and defective interleukin-1, CD40, and LPS signaling. *Genes Dev.* **13**, 1015–1024 (1999).
39. Armstrong, A. P., Tometsko, M. E., Glaccum, M., Sutherland, C. L., Cosman, D. & Dougall, W. C. A RANK/TRAF6-dependent signal transduction pathway is essential for osteoclast cytoskeletal organization and resorptive function. *J. Biol. Chem.* **277**, 44347–44356 (2002).
40. Mizukami, J., Takaesu, G., Akatsuka, H., Sakurai, H., Ninomiya-Tsuji, J., Matsumoto, K. & Sakurai, N. Receptor Activator of NF-κB Ligand (RANKL) Activates TAK1 Mitogen-Activated Protein Kinase Kinase Kinase through a Signaling Complex Containing RANK, TAB2, and TRAF6. *Mol. Cell. Biol.* **22**, 992–1000 (2002).
41. Kashiwada, M., Shirakata, Y., Inoue, J. I., Nakano, H., Okazaki, K., Okumura, K., Yamamoto, T., Nagaoka, H. & Takemori, T. Tumor necrosis factor receptor-associated factor 6 (TRAF6) stimulates extracellular signal-regulated kinase (ERK) activity in CD40 signaling along a ras-independent pathway. *J. Exp. Med.* **187**, 237–244 (1998).
42. Yamamoto, A., Miyazaki, T., Kadono, Y., Takayanagi, H., Miura, T., Nishina, H., Katada, T., Wakabayashi, K., Oda, H., Nakamura, K. & Tanaka, S. Possible Involvement of IκB Kinase 2 and MKK7 in Osteoclastogenesis Induced by Receptor Activator of Nuclear Factor κB Ligand. *J. Bone Miner. Res.* **17**, 612–621 (2002).
43. Cano, E. & Mahadevan, L. C. Parallel signal processing among mammalian MAPKs. *Trends Biochem. Sci.* **20**, 117–122 (1995).
44. Matsumoto, M., Sudo, T., Saito, T., Osada, H. & Tsujimoto, M. Involvement of p38 mitogen-activated protein kinase signaling pathway in osteoclastogenesis mediated by receptor activator of NF-kappa B ligand (RANKL). *J. Biol. Chem.* **275**, 31155–31161 (2000).
45. Boyce, B. F., Xiu, Y., Li, J., Xing, L. & Yao, Z. NF-κB-Mediated Regulation of Osteoclastogenesis. *Endocrinol. Metab.* **30**, 35–44 (2015).
46. Asagiri, M., Sato, K., Usami, T., Ochi, S., Nishina, H., Yoshida, H., Morita, I., Wagner, E. F., Mak, T. W., Serfling, E. & Takayanagi, H. Autoamplification of NFATc1 expression determines its essential role in bone homeostasis. *JEM* **202**, 1261–1269 (2005).
47. Takayanagi, H. The role of NFAT in osteoclast formation. *Ann. N. Y. Acad. Sci.* **1116**, 227–237 (2007).

48. Koga, T., Inui, M., Inoue, K., Kim, S., Suematsu, A., Kobayashi, E., Iwata, T., Ohnishi, H., Matozaki, T., Kodama, T., Taniguchi, T., Takayanagi, H. & Takai, T. Costimulatory signals mediated by the ITAM motif cooperate with RANKL for bone homeostasis. *Nature* **428**, 758–763 (2004).
49. Negishi-Koga, T. & Takayanagi, H. Ca 2+ -NFATc1 signaling is an essential axis of osteoclast differentiation. *Immunol. Rev.* **231**, 241–256 (2009).
50. Mao, D., Epple, H., Uthgenannt, B., Novack, D. V & Faccio, R. PLCgamma2 regulates osteoclastogenesis via its interaction with ITAM proteins and GAB2. *J. Clin. Invest.* **116**, 2869–2879 (2006).
51. Mócsai, A., Humphrey, M. B., Van Ziffle, J. A. G., Hu, Y., Burghardt, A., Spusta, S. C., Majumdar, S., Lanier, L. L., Lowell, C. A. & Nakamura, M. C. The immunomodulatory adapter proteins DAP12 and Fc receptor gamma-chain (FcRgamma) regulate development of functional osteoclasts through the Syk tyrosine kinase. *PNAS* **101**, 6158–6163 (2004).
52. Sato, K., Suematsu, A., Nakashima, T., Takemoto-Kimura, S., Aoki, K., Morishita, Y., Asahara, H., Ohya, K., Yamaguchi, A., Takai, T., Kodama, T., Chatila, T. A., Bito, H. & Takayanagi, H. Regulation of osteoclast differentiation and function by the CaMK-CREB pathway. *Nat. Med.* **12**, 1410–1416 (2006).
53. Kim, J. H. & Kim, N. Signaling Pathways in Osteoclast Differentiation. *Chonnam Med. J.* **52**, 12–17 (2016).
54. Takayanagi, H., Kim, S., Koga, T., Nishina, H., Isshiki, M., Yoshida, H., Saiura, A., Isobe, M., Yokochi, T., Inoue, J., Wagner, E. F., Mak, T. W., Kodama, T. & Taniguchi, T. Induction and Activation of the Transcription Factor NFATc1 (NFAT2) Integrate RANKL Signaling in Terminal Differentiation of Osteoclasts. *Dev. Cell* **3**, 889–901 (2002).
55. Wong, B. R., Besser, D., Kim, N., Arron, J. R., Vologodskaia, M., Hanafusa, H. & Choi, Y. TRANCE, a TNF Family Member, Activates Akt/PKB through a Signaling Complex Involving TRAF6 and c-Src. *Mol. Cell* **4**, 1041–1049 (1999).
56. Vanhaesebroeck, B. & Alessi, D. R. The PI3K-PDK1 connection : more than just a road to PKB. *Biochem. J* **346**, 561–576 (2000).
57. Teitelbaum, S. L. Bone resorption by osteoclasts. *Science (80-.).* **289**, 1504–1508 (2000).
58. McHugh, K. P., Hodivala-Dilke, K., Zheng, M.-H., Namba, N., Lam, J., Novack, D., Feng, X., Ross, F. P., Hynes, R. O. & Teitelbaum, S. L. Mice lacking β3 integrins are osteosclerotic because of dysfunctional osteoclasts. *J. Clin. Invest.* **105**, 433–440 (2000).
59. Hynes, R. O. Integrins: Bidirectional, Allosteric Signaling Machines. *Cell* **110**, 673–687 (2002).
60. Faccio, R., Grano, M., Colucci, S., Villa, A., Giannelli, G., Quaranta, V. & Zallone, A. Localization and possible role of two different alpha v beta 3 integrin conformations in resting and resorbing osteoclasts. *J. Cell Sci.* **115**, 2919–2929 (2002).
61. Ross, F. P. & Teitelbaum, S. L. avb3 and macrophage colony-stimulating factor: partners in osteoclast biology. *Immunol. Rev.* **208**, 88–105 (2005).
62. Helfrich, M. H., Nesbitt, S. A., Dorey, E. L. & Horton, M. A. Rat osteoclasts adhere to a wide range of rgd (arg-gly-asp) peptide-containing proteins, including the bone sialoproteins and fibronectin, via a β3 integrin. *J. Bone*

Miner. Res. **7**, 335–343 (2009).
63. Marchisio, P. C., Cirillo, D., Naldini, L., Primavera, M. V, Teti, A. & Zambonin-Zallone, A. Cell-substratum interaction of cultured avian osteoclasts is mediated by specific adhesion structures. *J. Cell Biol.* **99**, 1696–1705 (1984).
64. Suda, T., Nakamura, I., Jimi, E. & Takahashi, N. Regulation of Osteoclast Function. *J. Bone Miner. Res.* **12**, 869–879 (1997).
65. Roodman, G. D. Cell biology of the osteoclast. *Exp. Hematol.* **27**, 1229–1241 (1999).
66. Chambers, T. J. Regulation of the differentiation and function of osteoclasts. *J. Pathol.* **192**, 4–13 (2000).
67. Väänänen, H. K. & Horton, M. The osteoclast clear zone is a specialized cell-extracellular matrix adhesion structure. *J. Cell Sci.* **108**, 2729–2732 (1995).
68. Chellaiah, M., Kizer, N., Silva, M., Alvarez, U., Kwiatkowski, D. & Hruska, K. A. Gelsolin Deficiency Blocks Podosome Assembly and Produces Increased Bone Mass and Strength. *J. Cell Biol.* **148**, 665–678 (2000).
69. Blair, H. C., Teitelbaum, S. L., Ghiselli, R. & Gluck, S. Osteoclastic bone resorption by a polarized vacuolar proton pump. *Science (80-.).* **245**, 855–857 (1989).
70. Väänänen, H. K., Zhao, H., Mulari, M. & Halleen, J. M. The cell biology of osteoclast function. *J. Cell Sci.* **113**, 377–381 (2000).
71. Mattssons, J. P., Schlesingero, P. H., Keelin&, D. J., Teitelbaumn, S. L., Stonell, D. K. & Xiell, X.-S. Isolation and Reconstitution of a Vacuolar-type Proton Pump of Osteoclast Membranes. *J. Biol. Chem.* **269**, 24979–24982 (1994).
72. Baron, R., Neff, L., Louvard, D. & Courtoy, P. J. Cell-mediated Extracellular Acidification and Bone Resorption: Evidence for a Low pH in Resorbing Lacunae and Localization of a 100-kD Lysosomal Membrane Protein at the Osteoclast Ruffled Border. *J. Cell Biol* **101**, 2210–2222 (1985).
73. Teti, A., Blair, H. C., Teitelbaum, S. L., Kahn, A. J., Koziol, C., Konsek, J., Zambonin-Zallone, A. & Schlesingero, P. H. Cytoplasmic pH Regulation and Chloride/Bicarbonate Exchange in Avian Osteoclasts. *J. Clin. Invest.* **83**, 227–233 (1989).
74. Schlesinger, P. H., Blair, H. C., Teitelbaum, S. L. & Edwards, J. C. Characterization of the Osteoclast Ruffled Border Chloride Channel and Its Role in Bone Resorption. *J. Biol. Chem.* **272**, 18636–18643 (1997).
75. Salo, J., Lehenkari, P., Mulari, M., Metsikko, K. & Vaananen, H. K. Removal of Osteoclast Bone Resorption normal fluorescence microscopy, we found Products by Transcytosis. *Science (80-.).* **276**, 270–273 (1997).
76. Stenbeck, G. & Horton, M. A. Endocytic trafficking in actively resorbing osteoclasts. *J. Cell Sci.* **117**, 827–836 (2004).
77. Komori, T. Regulation of osteoblast differentiation by transcription factors. *J. Cell. Biochem.* **99**, 1233–1239 (2006).
78. Chen, Q., Shou, P., Zheng, C., Jiang, M., Cao, G., Yang, Q., Cao, J., Xie, N., Velletri, T., Zhang, X., Xu, C., Zhang, L., Yang, H., Hou, J., Wang, Y. & Shi, Y. Fate decision of mesenchymal stem cells: adipocytes or osteoblasts? *Cell Death Differ.* **23**, 1128–1139 (2016).
79. Huang, W., Yang, S., Shao, J. & Li, Y.-P. Signaling and transcriptional regulation in osteoblast commitment and differentiation. *Front Biosci.* **12**, 3068–3092

(2013).
80. Schneider, G. B., Zaharias, R. & Stanford, C. Osteoblast Integrin Adhesion and Signaling Regulate Mineralization. *J. Dent. Res.* **80**, 1540–1544 (2001).
81. Ferrari, S. L., Traianedes, K., Thorne, M., Lafage-Proust, M.-H., Genever, P., Cecchini, M. G., Behar, V., Bisello, A., Chorev, M., Rosenblatt, M. & Suva, L. J. A Role for N-Cadherin in the Development of the Differentiated Osteoblastic Phenotype. *J. Bone Miner. Res.* **15**, 198–208 (2010).
82. Rodan, G. A. Introduction to bone biology. *Bone* **13**, S3–S6 (1992).
83. Heinegard, D. & Oldberg, A. Structure and biology of cartilage and bone matrix noncollagenous macromolecules. *FASEB* **3**, 2042–2051 (1989).
84. Roberts, F., Zhu, D., Farquharson, C. & Macrae, V. E. ENPP1 in the Regulation of Mineralization and Beyond. *Trends Biochem. Sci.* **44**, 616–628 (2019).
85. Moss, D. W., Helen Eaton, R., Smith, J. K. & Whitby, A. L. G. Association of Inorganic-Pyrophosphatase Activity with Human Alkaline-Phosphatase Preparations. *Biochem. J* **102**, 53–57 (1967).
86. Majeska, R. J. & Wuthier, R. E. Studies on matrix vesicles isolated from chick epiphyseal cartilage: Association of pyrophosphatase and ATPase activities with alkaline phosphatase. *Biochim. Biophys. Acta* **391**, 51–60 (1975).
87. Johnson, K. A., Hessle, L., Vaingankar, S., Wennberg, C., Mauro, S., Narisawa, S., Goding, J. W., Sano, K., Millan, J. L. & Terkeltaub, R. Osteoblast tissue-nonspecific alkaline phosphatase antagonizes and regulates PC-1. *Am. J. Physiol. Integr. Comp. Physiol.* **279**, R1365–R1377 (2000).
88. Hessle, L., Johnson, K. A., Anderson, H. C., Narisawa, S., Sali, A., Goding, J. W., Terkeltaub, R. & Millá, J. L. Tissue-nonspecific alkaline phosphatase and plasma cell membrane glycoprotein-1 are central antagonistic regulators of bone mineralization. *PNAS* **99**, 9445–9449 (2002).
89. Murshed, M., Harmey, D., Millán, J. L., Mckee, M. D. & Karsenty, G. Unique coexpression in osteoblasts of broadly expressed genes accounts for the spatial restriction of ECM mineralization to bone. *GENES Dev.* **19**, 1093–1104 (2005).
90. Meyer, J. L. Can biological calcification occur in the presence of pyrophosphate? *Arch. Biochem. Biophys.* **231**, 1–8 (1984).
91. Hakim, F. T., Cranley, R., Brown, K. S., Eanes, E. D., Harne, L. & Oppenheim, J. J. Hereditary joint disorder in progressive ankylosis (ank/ank) mice. *Arthritis Rheum.* **27**, 1411–1420 (1984).
92. Wu, M., Chen, G. & Li, Y.-P. TGF-β and BMP signaling in osteoblast, skeletal development, and bone formation, homeostasis and disease. *Bone Res.* **4**, 1–21 (2016).
93. Celeste, A. J., Iannazzi, J. A., Wang, E. A. & Wozney, J. M. Identification of transforming growth factor B family members present in bone-inductive protein purified from bovine bone. *Proc. Nati Acad. Sci. USA.* **87**, 9843–9847 (1990).
94. Urist, M. R. Bone: Formation by Autoinduction. *Science (80-.).* **150**, 893–899 (1965).
95. Salazar, V. S., Gamer, L. W. & Rosen, V. BMP signalling in skeletal development, disease and repair. *Nat. Rev. Endocrinol.* **12**, 203–221 (2016).
96. Lee, K.-S., Kim, H.-J., Li, Q.-L., Chi, X.-Z., Ueta, C., Komori, T., Wozney, J. M., Kim,

E.-G., Choi, J.-Y., Ryoo, H.-M. & Bae, S.-C. Runx2 Is a Common Target of Transforming Growth Factor 1 and Bone Morphogenetic Protein 2, and Cooperation between Runx2 and Smad5 Induces Osteoblast-Specific Gene Expression in the Pluripotent Mesenchymal Precursor Cell Line C2C12. *Mol. Cell. Biol.* **20**, 8783–8792 (2000).

97. Otto, F., Thornell, A. P., Crompton, T., Denzel, A., Gilmour, K. C., Rosewell, I. R., Stamp, G. W. ., Beddington, R. S. ., Mundlos, S., Olsen, B. R., Selby, P. B. & Owen, M. J. Cbfa1, a Candidate Gene for Cleidocranial Dysplasia Syndrome, Is Essential for Osteoblast Differentiation and Bone Development. *Cell* **89**, 765–771 (1997).
98. Harada, H., Tagashira, S., Fujiwara, M., Ogawa, S., Katsumata, T., Yamaguchi, A., Komori, T. & Nakatsuka, M. Cbfa1 isoforms exert functional differences in osteoblast differentiation. *J. Biol. Chem. Chem.* **274**, 6972–6978 (1999).
99. Kern, B., Shen, J., Starbuck, M. & Karsenty, G. Cbfa1 contributes to the osteoblast-specific expression of type I collagen genes. *J. Biol. Chem.* **276**, 7101–7107 (2001).
100. Koga, T., Matsui, Y., Asagiri, M., Kodama, T., de Crombrugghe, B., Nakashima, K. & Takayanagi, H. NFAT and Osterix cooperatively regulate bone formation. *Nat. Med.* **11**, 880–885 (2005).
101. Nakashima, K., Zhou, X., Kunkel, G., Zhang, Z., Deng, J. M., Behringer, R. R. & de Crombrugghe, B. The Novel Zinc Finger-Containing Transcription Factor Osterix Is Required for Osteoblast Differentiation and Bone Formation. *Cell* **108**, 17–29 (2002).
102. Liu, W., Toyosawa, S., Furuichi, T., Kanatani, N., Yoshida, C., Liu, Y., Himeno, M., Narai, S., Yamaguchi, A. & Komori, T. Overexpression of Cbfa1 in osteoblasts inhibits osteoblast maturation and causes osteopenia with multiple fractures. *J. Cell Biol.* **155**, 157–166 (2001).
103. Lee, M.-H., Kim, Y.-J., Yoon, W.-J., Kim, J.-I., Kim, B.-G., Hwang, Y.-S., Wozney, J. M., Chi, X.-Z., Bae, S.-C., Choi, K.-Y., Cho, J.-Y., Choi, J.-Y. & Ryoo, H.-M. Dlx5 specifically regulates Runx2 type II expression by binding to homeodomain-response elements in the Runx2 distal promoter. *J. Biol. Chem.* **280**, 35579–35587 (2005).
104. Shimoyama, A., Wada, M., Ikeda, F., Hata, K., Matsubara, T., Nifuji, A., Noda, M., Amano, K., Yamaguchi, A., Nishimura, R. & Yoneda, T. Ihh/Gli2 Signaling Promotes Osteoblast Differentiation by Regulating Runx2 Expression and Function. *Mol. Biol. Cell* **18**, 2411–2418 (2007).
105. Wrana, J. L., Attisano, L., Wieser, R., Ventura, F. & Massagué, J. Mechanism of activation of the TGF-β receptor. *Nature* **370**, 341–347 (1994).
106. Tsukazaki, T., Chiang, T. A., Davison, A. F., Attisano, L. & Wrana, J. L. SARA, a FYVE Domain Protein that Recruits Smad2 to the TGFβ Receptor. *Cell* **95**, 779–791 (1998).
107. Macías-Silva, M., Abdollah, S., Hoodless, P. A., Pirone, R., Attisano, L. & Wrana, J. L. MADR2 Is a Substrate of the TGFβ Receptor and Its Phosphorylation Is Required for Nuclear Accumulation and Signaling. *Cell* **87**, 1215–1224 (1996).
108. Eppert, K., Scherer, S. W., Ozcelik, H., Pirone, R., Hoodless, P., Kim, H., Tsui, L.-C., Bapat, B., Gallinger, S., Andrulis, I. L., Thomsen, G. H., Wrana, J. L. & Attisano, L. MADR2 Maps to 18q21 and Encodes a TGFβ–Regulated MAD–

Related Protein That Is Functionally Mutated in Colorectal Carcinoma. *Cell* **86**, 543–552 (1996).
109. Lagna, G., Hata, A., Hemmati-Brivanlou, A. & Massagué, J. Partnership between DPC4 and SMAD proteins in TGF-β signalling pathways. *Nature* **383**, 832–836 (1996).
110. Zhang, Y., Feng, X.-H., Wu, R.-Y. & Derynck, R. Receptor-associated Mad homologues synergize as effectors of the TGF-β response. *Nature* **383**, 168–172 (1996).
111. Nakao, A., Imamura, T., Souchelnytskyi, S., Kawabata, M., Ishisaki, A., Oeda, E., Tamaki, K., Hanai, J., Heldin, C.-H., Miyazono, K. & Dijke, P. ten. TGF-β receptor-mediated signalling through Smad2, Smad3 and Smad4. *EMBO J.* **16**, 5353–5362 (1997).
112. Shioda, T., Lechleider, R. J., Dunwoodie, S. L., Li, H., Yahata, T., De Caestecker, M. P., Fenner, M. H., Roberts, A. B. & Isselbacher, K. J. Transcriptional activating activity of Smad4: Roles of SMAD hetero-oligomerization and enhancement by an associating transactivator. *Proc. Nati Acad. Sci. USA* **95**, 9785–9790 (1998).
113. Hata, A., Lo, R. S., Wotton, D., Lagna, G. & Massagué, J. Mutations increasing autoinhibition inactivate tumour suppressors Smad2 and Smad4. *Nature* **388**, 82–87 (1997).
114. Feng, X.-H., Zhang, Y., Wu, R.-Y. & Derynck, R. The tumor suppressor Smad4/DPC4 and transcriptional adaptor CBP/p300 are coactivators for Smad3 in TGF-induced transcriptional activation. *Genes DEv* **12**, 2153–2163 (1998).
115. Liu, F., Pouponnot, C. & Massagué, J. Dual role of the Smad4/DPC4 tumor suppressor in TGFbeta-inducible transcriptional complexes. *Genes Dev.* **11**, 3157–3167 (1997).
116. Li, C., Li, Y.-P., Fu, X.-Y. & Deng, C.-X. Anterior visceral endoderm SMAD4 signaling specifies anterior embryonic patterning and head induction in mice. *Int. J. Biol. Sci.* **6**, 569–583 (2010).
117. Tan, X., Weng, T., Zhang, J., Wang, J., Li, W., Wan, H., Lan, Y., Cheng, X., Hou, N., Liu, H., Ding, J., Lin, F., Yang, R., Gao, X., Chen, D. & Yang, X. Smad4 is required for maintaining normal murine postnatal bone homeostasis. *J. Cell Sci.* **120**, 2162–2170 (2007).
118. Zhang, J., Tan, X., Li, W., Wang, Y., Wang, J., Cheng, X. & Yang, X. Smad4 is required for the normal organization of the cartilage growth plate. *Dev. Biol.* **284**, 311–322 (2005).
119. Ishibashi, N., Sasaki, Y. & Asakura, Y. Myhre syndrome: a rare craniofacial disorder Myhre syndrome: a rare craniofacial disorder. *J. Craniomandib. Sleep Pract.* **32**, 300–306 (2014).
120. Le Goff, C., Mahaut, C., Abhyankar, A., Le Goff, W., Serre, V., Afenjar, A., Destrée, A., di Rocco, M., Héron, D., Jacquemont, S., Marlin, S., Simon, M., Tolmie, J., Verloes, A., Casanova, J.-L., Munnich, A. & Cormier-Daire, V. Mutations at a single codon in Mad homology 2 domain of SMAD4 cause Myhre syndrome. *Nat. Genet.* **44**, 85–88 (2012).
121. Day, T. F., Guo, X., Garrett-Beal, L. & Yang, Y. Wnt/β-Catenin Signaling in Mesenchymal Progenitors Controls Osteoblast and Chondrocyte

Differentiation during Vertebrate Skeletogenesis. *Dev. Cell* **8**, 739–750 (2005).
122. Cadigan, K. M. & Peifer, M. Wnt signaling from development to disease: insights from model systems. *Cold Spring Harb. Perspect. Biol.* **1**, (2009).
123. Jenny, A. Planar cell polarity signaling in the Drosophila eye. *Curr. Top. Dev. Biol.* **93**, 189–227 (2010).
124. Kohn, A. D. & Moon, R. T. Wnt and calcium signaling: β-Catenin-independent pathways. *Cell Calcium* **38**, 439–446 (2005).
125. Miller, J. R. The Wnts. *Genome Biol.* **3**, (2001).
126. Ackers, I. & Malgor, R. Interrelationship of canonical and non-canonical Wnt signalling pathways in chronic metabolic diseases. *Diabetes Vasc. Dis. Res.* **15**, 3–13 (2018).
127. Lerner, U. H. & Ohlsson, C. The WNT system: Background and its role in bone. *J. Intern. Med.* **277**, 630–649 (2015).
128. Tamai, K., Semenov, M., Kato, Y., Spokony, R., Liu, C., Katsuyama, Y., Hess, F., Saint-Jeannet, J.-P. & He, X. LDL-receptor-related proteins in Wnt signal transduction. *Nature* **407**, 530–535 (2000).
129. Nam, J.-S., Turcotte, T. J., Smith, P. F., Choi, S. & Yoon, J. K. Mouse cristin/R-spondin family proteins are novel ligands for the Frizzled 8 and LRP6 receptors and activate beta-catenin-dependent gene expression. *J. Biol. Chem.* **281**, 13247–13257 (2006).
130. Binnerts, M. E. *et al. R-Spondin1 regulates Wnt signaling by inhibiting internalization of LRP6*. *PNAS* **104**, (2007).
131. Carmon, K. S., Gong, X., Lin, Q., Thomas, A. & Liu, Q. R-spondins function as ligands of the orphan receptors LGR4 and LGR5 to regulate Wnt/β-catenin signaling. *PNAS* **108**, 11452–11457 (2011).
132. Willert, K., Shibamoto, S. & Nusse, R. Wnt-induced dephosphorylation of axin releases beta-catenin from the axin complex. *Genes Dev.* **13**, 1768–1773 (1999).
133. Liu, C., Li, Y., Semenov, M., Han, C., Baeg, G.-H., Tan, Y., Zhang, Z., Lin, X. & He, X. Control of β-Catenin Phosphorylation/Degradation by a Dual-Kinase Mechanism. *Cell* **108**, 837–847 (2002).
134. Yanagawa, S., Matsuda, Y., Lee, J.-S., Matsubayashi, H., Sese, S., Kadowaki, T. & Ishimoto, A. Casein kinase I phosphorylates the Armadillo protein and induces its degradation in Drosophila. *EMBO J.* **21**, 1733–1742 (2002).
135. Amit, S., Hatzubai, A., Birman, Y., Andersen, J. S., Ben-Shushan, E., Mann, M., Ben-Neriah, Y. & Alkalay, I. Axin-mediated CKI phosphorylation of beta-catenin at Ser 45: a molecular switch for the Wnt pathway. *Genes Dev.* **16**, 1066–1076 (2002).
136. Taelman, V. F., Dobrowolski, R., Plouhinec, J.-L., Fuentealba, L. C., Vorwald, P. P., Gumper, I., Sabatini, D. D. & De Robertis, E. M. Wnt signaling requires sequestration of glycogen synthase kinase 3 inside multivesicular endosomes. *Cell* **143**, 1136–48 (2010).
137. Baron, R. & Kneissel, M. WNT signaling in bone homeostasis and disease: from human mutations to treatments. *Nat. Med.* **19**, 179–192 (2013).
138. Karner, C. M. & Long, F. Wnt signaling and cellular metabolism in osteoblasts. *Cell. Mol. life Sci.* **74**, 1649–1657 (2017).
139. Daniels, D. L. & Weis, W. I. β-catenin directly displaces Groucho/TLE repressors

from Tcf/Lef in Wnt-mediated transcription activation. *Nat. Struct. Mol. Biol.* **12**, 364–371 (2005).
140. Behrens, J., von Kries, J. P., Kühl, M., Bruhn, L., Wedlich, D., Grosschedl, R. & Birchmeier, W. Functional interaction of β-catenin with the transcription factor LEF-1. *Nature* **382**, 638–642 (1996).
141. Zeng, W., Wharton, K. A., Mack, J. A., Wang, K., Gadbaw, M., Suyama, K., Klein, P. S. & Scott, M. P. naked cuticle encodes an inducible antagonist of Wnt signalling. *Nature* **403**, 789–795 (2000).
142. Roose, J., Huls, G., Beest, M. van, Moerer, P., Horn, K. van der, Goldschmeding, R., Logtenberg, T. & Clevers, H. Synergy between tumor suppressor APC and the B-catenin-Tcf4 target Tcf1. *Science (80-.).* **285**, 1923–1926 (1999).
143. Jho, E., Zhang, T., Domon, C., Joo, C.-K., Freund, J.-N. & Costantini, F. Wnt/beta-catenin/Tcf signaling induces the transcription of Axin2, a negative regulator of the signaling pathway. *Mol. Cell. Biol.* **22**, 1172–1183 (2002).
144. Gaur, T., Lengner, C. J., Hovhannisyan, H., Bhat, R. A., Bodine, P. V. N., Komm, B. S., Javed, A., van Wijnen, A. J., Stein, J. L., Stein, G. S. & Lian, J. B. Canonical WNT signaling promotes osteogenesis by directly stimulating Runx2 gene expression. *J. Biol. Chem.* **280**, 33132–33140 (2005).
145. Glass, D. A., Bialek, P., Ahn, J. D., Starbuck, M., Patel, M. S., Clevers, H., Taketo, M. M., Long, F., McMahon, A. P., Lang, R. A. & Karsenty, G. Canonical Wnt Signaling in Differentiated Osteoblasts Controls Osteoclast Differentiation. *Dev. Cell* **8**, 751–764 (2005).
146. Aberle, H., Bauer, A., Stappert, J., Kispert, A. & Kemler, R. β-catenin is a target for the ubiquitin–proteasome pathway. *EMBO J.* **16**, 3797–3804 (1997).
147. Behrens, J., Jerchow, B.-A., Wurtele, M., Grimm, J., Asbrand, C., Wirtz, R., Kuhl, M., Wedlich, D. & Birchmeier, W. Functional Interaction of an Axin Homolog, Conductin, with Beta-Catenin, APC, and GSK3B. *Science (80-.).* **275**, 596–599 (1997).
148. Hart, M. J., de los Santos, R., Albert, I. N., Rubinfeld, B. & Polakis, P. Downregulation of β-catenin by human Axin and its association with the APC tumor suppressor, β-catenin and GSK3β. *Curr. Biol.* **8**, 573–581 (1998).
149. Orford, K., Crockett, C., Jensen, J. P., Weissman, A. M. & Byers, S. W. Serine phosphorylation-regulated ubiquitination and degradation of beta-catenin. *J. Biol. Chem.* **272**, 24735–24738 (1997).
150. Morita, H., Mazerbourg, S., Bouley, D. M., Luo, C.-W., Kawamura, K., Kuwabara, Y., Baribault, H., Tian, H. & Hsueh, A. J. W. Neonatal lethality of LGR5 null mice is associated with ankyloglossia and gastrointestinal distension. *Mol. Cell. Biol.* **24**, 9736–9743 (2004).
151. Luo, J., Zhou, W., Zhou, X., Li, D., Weng, J., Yi, Z., Cho, S. G., Li, C., Yi, T., Xiushan Wu, Li, X.-Y., Crombrugghe, B. de, Höök, M. & Liu, M. Regulation of bone formation and remodeling by G-protein-coupled receptor 48. *Development* **136**, 2747–2756 (2009).
152. Xiao, G., Jiang, D., Ge, C., Zhao, Z., Lai, Y., Boules, H., Phimphilai, M., Yang, X., Karsenty, G. & Franceschi, R. T. Cooperative interactions between activating transcription factor 4 and Runx2/Cbfa1 stimulate osteoblast-specific osteocalcin gene expression. *J. Biol. Chem.* **280**, 30689–30696 (2005).
153. Yamaguchi, T. P. Heads or tails: Wnts and anterior–posterior patterning. *Curr.*

Biol. **11**, R713–R724 (2001).
154. Kawano, Y. & Kypta, R. Secreted antagonists of the Wnt signalling pathway. *J. Cell Sci.* **116**, 2627–2634 (2003).
155. Semënov, M., Tamai, K. & He, X. SOST is a ligand for LRP5/LRP6 and a Wnt signaling inhibitor. *J. Biol. Chem.* **280**, 26770–26775 (2005).
156. Li, X., Zhang, Y., Kang, H., Liu, W., Liu, P., Zhang, J., Harris, S. E. & Wu, D. Sclerostin binds to LRP5/6 and antagonizes canonical Wnt signaling. *J. Biol. Chem.* **280**, 19883–19887 (2005).
157. Semënov, M. V, Tamai, K., Brott, B. K., Kühl, M., Sokol, S. & He, X. Head inducer Dickkopf-1 is a ligand for Wnt coreceptor LRP6. *Curr. Biol.* **11**, 951–961 (2001).
158. Bafico, A., Liu, G., Yaniv, A., Gazit, A. & Aaronson, S. A. Novel mechanism of Wnt signalling inhibition mediated by Dickkopf-1 interaction with LRP6/Arrow. *Nat. Cell Biol.* **3**, 683–686 (2001).
159. Brunkow, M. E., Gardner, J. C., Van Ness, J., Paeper, B. W., Kovacevich, B. R., Proll, S., Skonier, J. E., Zhao, L., Sabo, P. J., Fu, Y.-H., Alisch, R. S., Gillett, L., Colbert, T., Tacconi, P., Galas, D., Hamersma, H., Beighton, P. & Mulligan, J. Bone dysplasia sclerosteosis results from loss of the SOST gene product, a novel cystine knot-containing protein. *Am. J. Hum. Genet.* **68**, 577–589 (2001).
160. Balemans, W., Patel, N., Ebeling, M., Van Hul, E., Wuyts, W., Lacza, C., Dioszegi, M., Dikkers, F. G., Hildering, P., Willems, P. J., Verheij, G. M., Lindpaintner, K., Vickery, B. & Foernzler, D. Identification of a 52 kb deletion downstream of the SOST gene in patients with van Buchem disease. *J MEd Genet* **39**, 91–97 (2002).
161. Loots, G. G., Kneissel, M., Keller, H., Baptist, M., Chang, J., Collette, N. M., Ovcharenko, D., Plajzer-Frick, I. & Rubin, E. M. Genomic deletion of a long-range bone enhancer misregulates sclerostin in Van Buchem disease. *Genome Res.* **15**, 928–935 (2005).
162. Gong, Y. *et al.* LDL Receptor-Related Protein 5 (LRP5) Affects Bone Accrual and Eye Development. *Cell* **107**, 513–523 (2001).
163. Balemans, W. *et al.* Increased bone density in sclerosteosis is due to the deficiency of a novel secreted protein (SOST). *Hum. Mol. Genet.* **10**, 537–543 (2001).
164. McClung, M. R. Romosozumab for the treatment of osteoporosis. *Osteoporos. Sarcopenia* **4**, 11–15 (2018).
165. Fietz, M. J., Concordet, J.-P., Barbosa, R., Johnson, R., Krauss, S., McMahon, A. P., Tabin, C. & Lngham, P. W. The hedgehog gene family in Drosophila and vertebrate development. *Development* 43–51 (1994).
166. Hooper, J. E. & Scott, M. P. Communicating with Hedgehogs. *Nat. Rev. Mol. Cell Biol.* **6**, 307–317 (2005).
167. Long, F., Chung, U., Ohba, S., McMahon, J., Kronenberg, H. M. & McMahon, A. P. Ihh signaling is directly required for the osteoblast lineage in the endochondral skeleton. *Development* **131**, 1309–1318 (2004).
168. St-Jacques, B., Hammerschmidt, M. & Mcmahon, A. P. Indian hedgehog signaling regulates proliferation and differentiation of chondrocytes and is essential for bone formation. *GENES Dev.* **13**, 2072–2086 (1999).
169. Deregowski, V., Gazzerro, E., Priest, L., Rydziel, S. & Canalis, E. Notch 1 overexpression inhibits osteoblastogenesis by suppressing Wnt/beta-catenin but not bone morphogenetic protein signaling. *J. Biol. Chem.* **281**, 6203–6210

(2006).
170. Ehebauer, M., Hayward, P. & Martinez-Arias, A. Notch Signaling Pathway. *Sci STKE* **364**, (2006).
171. Lindsell, C. E., Boulter, J., DiSibio, G., Gossler, A. & Weinmaster, G. Expression Patterns ofJagged, Delta1, Notch1, Notch2, and Notch3Genes Identify Ligand–Receptor Pairs That May Function in Neural Development. *Mol. Cell. Neurosci.* **8**, 14–27 (1996).
172. Hilton, M. J., Tu, X., Wu, X., Bai, S., Zhao, H., Kobayashi, T., Kronenberg, H. M., Teitelbaum, S. L., Ross, F. P., Kopan, R., Long, F. & Author, N. M. Notch signaling maintains bone marrow mesenchymal progenitors by suppressing osteoblast differentiation. *Nat Med* **14**, 306–314 (2008).
173. Kopan, R. & Goate, A. A common enzyme connects notch signaling and Alzheimer's disease. *Genes Dev.* **14**, 2799–2806 (2000).
174. Artavanis-Tsakonas, S., Rand, M. D. & Lake, R. J. Notch Signaling: Cell Fate Control and Signal Integration in Development. *Scie* **284**, 770–776 (1999).
175. Ohtsuka, T., Ishibashi, M., Gé Rald Gradwohl, G., Nakanishi, S., Ois Guillemot, F. & Kageyama, R. Hes1 and Hes5 as Notch effectors in mammalian neuronal differentiation. *EMBO J.* **18**, 2196–2207 (1999).
176. Iso, T., Sartorelli, V., Poizat, C., Iezzi, S., Wu, H.-Y., Chung, G., Kedes, L. & Hamamori, Y. HERP, a Novel Heterodimer Partner of HES/E(spl) in Notch Signaling. *Mol. Cell. Biol.* **21**, 6080–6089 (2001).
177. Zamurovic, N., Cappellen, D., Rohner, D. & Susa, M. Coordinated activation of notch, Wnt, and transforming growth factor-beta signaling pathways in bone morphogenic protein 2-induced osteogenesis. *J. Biol. Chem.* **279**, 37704–37715 (2004).
178. Pisconti, A., Cornelison, D. D. W., Olguín, H. C., Antwine, T. L. & Olwin, B. B. Syndecan-3 and Notch cooperate in regulating adult myogenesis. *J. Cell Biol.* **190**, 427–441 (2010).
179. Marie, P. J. Fibroblast growth factor signaling controlling osteoblast differentiation. *Gene* **316**, 23–32 (2003).
180. Jaye, M., Schlessinger, J. & Dionne, C. A. Fibroblast growth factor receptor tyrosine kinases: molecular analysis and signal transduction. *Biochim. Biophys. Acta* **1135**, 185–199 (1992).
181. Ornitz, D. M. & Marie, P. J. Fibroblast growth factor signaling in skeletal development and disease. *Genes Dev.* **29**, 1463–1486 (2015).
182. Marie, P. J., Miraoui, H. & Sévère, N. Growth Factors FGF/FGFR signaling in bone formation: Progress and perspectives. *Growth Factors* **30**, 117–123 (2012).
183. Klagsbrun, M. & Baird, A. A dual receptor system is required for basic fibroblast growth factor activity. *Cell* **67**, 229–231 (1991).
184. Takei, Y., Minamizaki, T. & Yoshiko, Y. Functional diversity of fibroblast growth factors in bone formation. *Int. J. Endocrinol.* **2015**, 1–12 (2015).
185. Yayon, A., Klagsbrun, M., Esko, J. D., Leder, P. & Ornitz, D. M. Cell surface, heparin-like molecules are required for binding of basic fibroblast growth factor to its high affinity receptor. *Cell* **64**, 841–848 (1991).
186. Schlessinger, J., Plotnikov, A. N., Ibrahimi, O. A., Eliseenkova, A. V., Yeh, B. K., Yayon, A., Linhardt, R. J. & Mohammadi, M. Crystal Structure of a Ternary FGF-

FGFR-Heparin Complex Reveals a Dual Role for Heparin in FGFR Binding and Dimerization. *Mol. Cell* **6**, 743–750 (2000).
187. Newberry, E. P., Willis, D., Latifi, T., Boudreaux, J. M. & Towler, D. A. Fibroblast Growth Factor Receptor Signaling Activates the Human Interstitial Collagenase Promoter via the Bipartite Ets-AP1 Element. *Mol. Endocrinol.* **11**, 1129–1144 (1997).
188. Mansukhani, A., Bellosta, P., Sahni, M. & Basilico, C. *Signaling by Fibroblast Growth Factors (FGF) and Fibroblast Growth Factor Receptor 2 (FGFR2)-activating Mutations Blocks Mineralization and Induces Apoptosis in Osteoblasts*. *The Journal of Cell Biology* **149**, (2000).
189. Debiais, F., Lemonnier, J., Hay, E., Delannoy, P., Caverzasio, J. & Marie, P. J. Fibroblast growth factor-2 (FGF-2) increases N-cadherin expression through protein kinase C and Src-kinase pathways in human calvaria osteoblasts. *J. Cell. Biochem.* **81**, 68–81 (2001).
190. Xiao, G., Jiang, D., Gopalakrishnan, R. & Franceschi, R. T. Fibroblast Growth Factor 2 Induction of the Osteocalcin Gene Requires MAPK Activity and Phosphorylation of the Osteoblast Transcription Factor, Cbfa1/Runx2. *J. Biol. Chem.* **277**, 36181–36187 (2002).
191. Kim, H.-J., Kim, J.-H., Bae, S.-C., Choi, J.-Y., Kim, H.-J. & Ryoo, H.-M. The protein kinase C pathway plays a central role in the fibroblast growth factor-stimulated expression and transactivation activity of Runx2. *J. Biol. Chem.* **278**, 319–326 (2003).
192. Kozawa, O., Tokuda, H., Matsuno, H. & Uematsu, T. Involvement of p38 Mitogen-Activated Protein Kinase in Basic Fibroblast Growth Factor-Induced Interleukin-6 Synthesis in Osteoblasts. *J. Cell. Biochem* **74**, 479–485 (1999).
193. Jilka, R. L., Weinstein, R. S., Bellido, T., Parfitt, A. M. & Manolagas, S. C. Osteoblast Programmed Cell Death (Apoptosis): Modulation by Growth Factors and Cytokines. *J. Bone Miner. Res.* **13**, 793–802 (1998).
194. Rodan, G. A. & Martin, T. J. Role of Osteoblasts in Hormonal Control of Bone Resorption - A Hypothesis. *Calcif. Tissue Int* **33**, 349–351 (1981).
195. Franz-Odendaal, T. A., Hall, B. K. & Witten, P. E. Buried alive: How osteoblasts become osteocytes. *Dev. Dyn.* **235**, 176–190 (2006).
196. Baude, C. A. Submicroscopic Structure and Functional Aspects of the Osteocyte. *Clin. Orthop. Relat. Res.* **56**, 227–236 (1968).
197. Knothe Tate, M. L. "Whither flows the fluid in bone?" An osteocyte's perspective. *J. Biomech.* **36**, 1409–1424 (2003).
198. Goldring, S. R. The osteocyte: key player in regulating bone turnover. *RMD Open* **1**, (2015).
199. Verborgt, O., Tatton, N. A., Majeska, R. J. & Schaffler, M. B. Spatial Distribution of Bax and Bcl-2 in Osteocytes After Bone Fatigue: Complementary Roles in Bone Remodeling Regulation? *J. Bone Miner. Res.* **17**, 907–914 (2002).
200. Nakashima, T., Hayashi, M., Fukunaga, T., Kurata, K., Oh-hora, M., Feng, J. Q., Bonewald, L. F., Kodama, T., Wutz, A., Wagner, E. F., Penninger, J. M. & Takayanagi, H. Evidence for osteocyte regulation of bone homeostasis through RANKL expression. *Nat. Med.* **17**, 1231–1234 (2011).
201. Xiong, J., Onal, M., Jilka, R. L., Weinstein, R. S., Manolagas, S. C. & O'Brien, C. A. Matrix-embedded cells control osteoclast formation. *Nat. Med.* **17**, 1235–

1241 (2011).
202. Poole, K. E. S., Van Bezooijen, R. L., Loveridge, N., Hamersma, H., Papapoulos, S. E., Löwik, C. W. & Reeve, J. Sclerostin is a delayed secreted product of osteocytes that inhibits bone formation. *FASEB J.* **19**, 1842–1844 (2005).
203. Morvan, F., Boulukos, K., Clément-Lacroix, P., Roman, S. R., Suc-Royer, I., Vayssière, B., Ammann, P., Martin, P., Pinho, S., Pognonec, P., Mollat, P., Niehrs, C., Baron, R. & Rawadi, G. Deletion of a Single Allele of the Dkk1 Gene Leads to an Increase in Bone Formation and Bone Mass. *J. Bone Miner. Res.* **21**, 934–945 (2006).
204. Robling, A. G., Niziolek, P. J., Baldridge, L. A., Condon, K. W., Allen, M. R., Alam, I., Mantila, S. M., Gluhak-Heinrich, J., Bellido, T. M., Harris, S. E. & Turner, C. H. Mechanical stimulation of bone in vivo reduces osteocyte expression of Sost/sclerostin. *J. Biol. Chem.* **283**, 5866–5875 (2008).
205. Lefebvre, V. & Bhattaram, P. Vertebrate skeletogenesis. *Curr. Top. Dev. Biol.* **90**, 291–317 (2010).
206. Berendsen, A. D. & Olsen, B. R. Bone development. *Bone* **80**, 14–18 (2015).
207. Shum, L., Coleman, C. M., Hatakeyama, Y. & Tuan, R. S. Morphogenesis and dysmorphogenesis of the appendicular skeleton. *Birth Defects Res.* **69**, 102–122 (2003).
208. Hall, B. K. & Miyake, T. All for one and one for all: condensations and the initiation of skeletal development. *BioEssays* **22**, 138–147 (2000).
209. Ornitz, D. M. FGF signaling in the developing endochondral skeleton. *Cytokine Growth Factor Rev* **16**, 205–213 (2005).
210. Kronenberg, H. M. Developmental regulation of the growth plate. *Nature* **423**, 332–336 (2003).
211. Long, F. & Ornitz, D. M. Development of the endochondral skeleton. *Cold Spring Harb. Perspect. Biol.* **5**, (2013).
212. Iyama, K.-I., Ninomiya, Y., Olsen, B. R., Linsenmayer, T. F., Trelstad, R. L. & Hayashi, M. Spatiotemporal pattern of type X collagen gene expression and collagen deposition in embryonic chick vertebrae undergoing endochondral ossification. *Anat. Rec.* **229**, 462–472 (1991).
213. Vu, T. H., Shipley, J. M., Bergers, G., Berger, J. E., Helms, J. A., Hanahan, D., Shapiro, S. D., Senior, R. M. & Werb, Z. MMP-9/Gelatinase B Is a Key Regulator of Growth Plate Angiogenesis and Apoptosis of Hypertrophic Chondrocytes. *Cell* **93**, 411–422 (1998).
214. Maes, C., Kobayashi, T., Selig, M. K., Torrekens, S., Roth, S. I., Mackem, S., Carmeliet, G. & Kronenberg, H. M. Osteoblast Precursors, but Not Mature Osteoblasts, Move into Developing and Fractured Bones along with Invading Blood Vessels. *Dev. Cell* **19**, 329–344 (2010).
215. Hunziker, E. B. Mechanism of longitudinal bone growth and its regulation by growth plate chondrocytes. *Microsc. Res. Tech.* **28**, 505–519 (1994).
216. Roach, H. I., Mehta, G., Oreffo, R. O. C., Clarke, N. M. P. & Cooper, C. Temporal Analysis of Rat Growth Plates: Cessation of Growth with Age Despite Presence of a Physis. *J. Histochem. Cytochem.* **51**, 373–383 (2003).
217. Abzhanov, A., Rodda, S. J., McMahon, A. P. & Tabin, C. J. Regulation of skeletogenic differentiation in cranial dermal bone. *Development* **134**, 3133–3144 (2007).

218. Hall, B. K. & Miyake, T. The membranous skeleton: the role of cell condensations in vertebrate skeletogenesis. *Anat Embryol* **186**, 107–124 (1992).
219. Biewener, A. A., Swartz, S. M. & Bertram, J. E. A. Bone Modeling During Growth: Dynamic Strain Equilibrium in the Chick Tibiotarsus. *Calcif Tissue Int.* **39**, 390–395 (1986).
220. Frost, H. M. Wolff's Law and bone's structural adaptations to mechanical usage: an overview for clinicians. *The Angle Osthodontist* **64**, 175–188 (1994).
221. Wolff, J. Gesetz der Transformation der Knochen. *ci.nii.ac.jp* (1982).
222. Kontulainen, S., Sievänen, H., Kannus, P., Pasanen, M. & Vuori, I. Effect of Long-Term Impact-Loading on Mass, Size, and Estimated Strength of Humerus and Radius of Female Racquet-Sports Players: A Peripheral Quantitative Computed Tomography Study Between Young and Old Starters and Controls. *J. Bone Miner. Res.* **18**, 352–359 (2003).
223. Lindsay, R., Cosman, F., Zhou, H., Bostrom, M. P., Shen, V. W., Cruz, J. D., Nieves, J. W. & Dempster, D. W. A Novel Tetracycline Labeling Schedule for Longitudinal Evaluation of the Short-Term Effects of Anabolic Therapy With a Single Iliac Crest Bone Biopsy: Early Actions of Teriparatide. *J. Bone Miner. Res.* **21**, 366–373 (2005).
224. Ubara, Y., Tagami, T., Nakanishi, S., Sawa, N., Hoshino, J., Suwabe, T., Katori, H., Takemoto, F., Hara, S. & Takaichi, K. Significance of minimodeling in dialysis patients with adynamic bone disease. *Kidney Int.* **68**, 833–839 (2005).
225. Raggatt, L. J. & Partridge, N. C. Cellular and molecular mechanisms of bone remodeling. *J. Biol. Chem.* **285**, 25103–25108 (2010).
226. Eriksen, E. F. Cellular mechanisms of bone remodeling. *Rev. Endocr. Metab. Disord.* **11**, 219–227 (2010).
227. Dobnig, H. & Turner, R. T. Evidence that intermittent treatment with parathyroid hormone increases bone formation in adult rats by activation of bone lining cells. *Endocrinology* **136**, 3632–3638 (1995).
228. Tatsumi, S., Ishii, K., Amizuka, N., Li, M., Kobayashi, T., Kohno, K., Ito, M., Takeshita, S. & Ikeda, K. Targeted Ablation of Osteocytes Induces Osteoporosis with Defective Mechanotransduction. *Cell Metab.* **5**, 464–475 (2007).
229. Chambers, T. J., Darby, J. A. & Fuller, K. Cell and Tissue Research Mammalian collagenase predisposes bone surfaces to osteoclastic resorption. *Cell Tissue Res* **241**, 671–675 (1985).
230. Parikka, V., Väänänen, A., Risteli, J., Salo, T., Sorsa, T., Väänänen, H. K. & Lehenkari, P. Human mesenchymal stem cell derived osteoblasts degrade organic bone matrix in vitro by matrix metalloproteinases. *Matrix Biol.* **24**, 438–447 (2005).
231. Baron, R. Molecular mechanisms of bone resorption by the osteoclast. *Anat. Rec.* **224**, 317–324 (1989).
232. Tang, Y., Wu, X., Lei, W., Pang, L., Wan, C., Shi, Z., Zhao, L., Nagy, T. R., Peng, X., Hu, J., Feng, X., Van Hul, W., Wan, M. & Cao, X. TGF-β1-induced Migration of Bone Mesenchymal Stem Cells Couples Bone Resorption and Formation. *Nat Med* **15**, 757–765 (2009).
233. Martin, T. J. & Sims, N. A. Osteoclast-derived activity in the coupling of bone formation to resorption. *TRENDS Mol. Med.* **11**, 76–81 (2005).

234. Ikebuchi, Y., Aoki, S., Honma, M., Hayashi, M., Sugamori, Y., Khan, M., Kariya, Y., Kato, G., Tabata, Y., Penninger, J. M., Udagawa, N., Aoki, K. & Suzuki, H. Coupling of bone resorption and formation by RANKL reverse signalling. *Nature* **561**, 195–200 (2018).
235. Hill, P. A. Bone remodelling. *Br. J. Orthod.* **25**, 101–107 (1998).
236. Siddiqui, J. A. & Partridge, N. C. Physiological Bone Remodeling: Systemic Regulation and Growth Factor Involvement. *Physiology* **31**, 233–245 (2016).
237. Bouillon, R., Carmeliet, G., Verlinden, L., Van Etten, E., Verstuyf, A., Luderer, H. F., Lieben, L., Mathieu, C. & Demay, M. Vitamin D and Human Health: Lessons from Vitamin D Receptor Null Mice. *Endocr. Rev.* **29**, 726–776 (2008).
238. Jeon, S.-M. & Shin, E.-A. Exploring vitamin D metabolism and function in cancer. *Jeon Shin Exp. Mol. Med.* **50**, (2018).
239. Holick, M. F. Vitamin D deficiency. *N. Engl. J. Med.* **357**, 266–281 (2007).
240. Reichel, H., Koeffler, H. P. & Norman, A. W. The role of the vitamin D endocrine system in health and disease. *N. Engl. J. Med.* **320**, 980–991 (1989).
241. Lips, P. & van Schoor, N. M. The effect of vitamin D on bone and osteoporosis. *Best Pract. Res. Clin. Endocrinol. Metab.* **25**, 585–591 (2011).
242. Friedman, P. A. Mechanisms of Renal Calcium Transport. *Exp Nephrol* **8**, 343–350 (2000).
243. Lips, P. Vitamin D Deficiency and Secondary Hyperparathy-roidism in the Elderly: Consequences for Bone Loss and Fractures and Therapeutic Implications. *Endocr. Rev.* **22**, 477–501 (2001).
244. Goltzman, D. Studies on the mechanisms of the skeletal anabolic action of endogenous and exogenous parathyroid hormone. *Arch. Biochem. Biophys.* **473**, 218–224 (2008).
245. Juppner, H., Abou-Samra, A.-B., Freeman, M., Kong, X. F., Schipani, E., Richards, J., Lee F. Kolakowski, J., Hock, J., John T. Potts, J., Kronenberg, H. M. & Segre, G. V. A G Protein-Linked Receptor for Parathyroid Hormone and Parathyroid Hormone-Related Peptide. *Science (80-.).* **254**, 1024–1026 (1990).
246. Shevde, N. K., Bendixen, A. C., Dienger, K. M. & Pike, J. W. Estrogens suppress RANK ligand-induced osteoclast differentiation via a stromal cell independent mechanism involving c-Jun repression. *PNAS* **97**, 7829–7834 (2000).
247. Hofbauer, L. C. & Schoppet, M. Clinical Implications of the Osteoprotegerin / RANKL / RANK System for Bone. *J. Am. Med. Assoc.* **292**, 490–495 (2004).
248. Weitzmann, M. N. & Pacifici, R. Estrogen deficiency and bone loss: an inflammatory tale. *J. Clin. Invest.* **116**, 1186–1194 (2006).
249. Eghbali-Fatourechi, G., Khosla, S., Sanyal, A., Boyle, W. J., Lacey, D. L. & Riggs, B. L. Role of RANK ligand in mediating increased bone resorption in early postmenopausal women. *J. Clin. Invest.* **111**, 1221–1230 (2003).
250. Kimble, R. B., Srivastava, S., Ross, F. P., Matayoshi, A. & Pacifici, R. Estrogen deficiency increases the ability of stromal cells to support murine osteoclastogenesis via an interleukin-1and tumor necrosis factor-mediated stimulation of macrophage colony-stimulating factor production. *J. Biol. Chem.* **271**, 28890–28897 (1996).
251. Kousteni, S., Bellido, T., Plotkin, L. I., O'Brien, C. A., Bodenner, D. L., Han, L., Han, K., DiGregorio, G. B., Katzenellenbogen, J. A., Katzenellenbogen, B. S., Roberson, P. K., Weinstein, R. S., Jilka, R. L. & Manolagas, S. C. Nongenotropic,

Sex-Nonspecific Signaling through the Estrogen or Androgen Receptors. *Cell* **104**, 719–730 (2001).
252. Kousteni, S., Han, L., Chen, J.-R., Almeida, M., Plotkin, L. I., Bellido, T. & Manolagas, S. C. Kinase-mediated regulation of common transcription factors accounts for the bone-protective effects of sex steroids. *J. Bone Miner. Res* **111**, 1651–1664 (2003).
253. Keller, J. *et al.* Calcitonin controls bone formation by inhibiting the release of sphingosine 1-phosphate from osteoclasts. *Nat. Commun.* **5**, (2014).
254. Davey, R. A., Turner, A. G., Mcmanus, J. F., Chiu, W. S. M., Tjahyono, F., Moore, A. J., Atkins, G. J., Anderson, P. H., Ma, C., Glatt, V., Maclean, H. E., Vincent, C., Bouxsein, M., Morris, H. A., Findlay, D. M. & Zajac, J. D. Calcitonin Receptor Plays a Physiological Role to Protect Against Hypercalcemia in Mice. *J. Bone Miner. Res.* **23**, 1182–1193 (2008).
255. Zaidi, M., Moonga, B. S. & Abe, E. Calcitonin and bone formation: a knockout full of surprises Historical perspectives. *J. Clin. Invest.* **110**, 1769–1771 (2002).
256. Imel, E. A., Biggin, A., Schindeler, A. & Munns, C. F. FGF23, Hypophosphatemia, and Emerging Treatments. *J. bone Miner. Res.* **3**, 310190 (2019).
257. Carpenter, T. O., Shaw, N. J., Portale, A. A., Ward, L. M., Abrams, S. A. & Pettifor, J. M. Rickets. *Nat. Rev.* **4**, (2017).
258. Hamrick, M. W., Pennington, C., Newton, D., Xie, D. & Isales, C. Leptin deficiency produces contrasting phenotypes in bones of the limb and spine. *Bone* **34**, 376–383 (2004).
259. Dimitri, P. & Rosen, C. The Central Nervous System and Bone Metabolism: An Evolving Story. *Calcif. Tissue Int.* **100**, 476–485 (2017).
260. Zhang, Y., Proenca, R., Maffei, M., Barone, M., Leopold, L. & Friedman, J. M. Positional cloning of the mouse obese gene and its human homologue. *Nature* **372**, 425–432 (1994).
261. Ducy, P., Amling, M., Takeda, S., Priemel, M., Schilling, A. F., Beil, F. T., Shen, J., Vinson, C., Rueger, J. M. & Karsenty, G. Leptin Inhibits Bone Formation through a Hypothalamic Relay: A Central Control of Bone Mass. *Cell* **100**, 197–207 (2000).
262. Andreoli, M. F., Donato, J., Cakir, I. & Perello, M. Leptin resensitisation: A reversion of leptin-resistant states. *J. Endocrinol.* **241**, R81–R96 (2019).
263. Couchman, J. R. & Pataki, C. A. An Introduction to Proteoglycans and Their Localization. *J. Histochem. Cytochem.* **60**, 885–897 (2012).
264. Couchman, J. R. Transmembrane Signaling Proteoglycans. *Annu. Rev. Cell Dev. Biol.* **26**, 89–114 (2010).
265. Iozzo, R. V. & Murdoch, A. D. Proteoglycans of the extracellular environment: clues from the gene and protein side offer novel perspectives in molecular diversity and function. *FASEB* **10**, 598–614 (1996).
266. Schaefer, L. & Schaefer, R. M. Proteoglycans: from structural compounds to signaling molecules. *Cell Tissue Res* **339**, 237–246 (2010).
267. Yanagishita, M. Function of proteoglycans in the extracellular matrix. *Acta Pathol. Jpn.* **43**, 283–293 (1993).
268. Bulow, H. E. & Hobert, O. The Molecular Diversity of Glycosaminoglycans Shapes Animal Development. *Annu. Rev. Cell Dev. Biol* **22**, 375–407 (2006).
269. Habuchi, H., Habuchi, O. & Kimata, K. Sulfation pattern in glycosaminoglycan:

Does it have a code? *Glycoconj. J.* **21**, 47–52 (2004).
270. Kingma, S. D. K., Wagemans, T., IJlst, L., Bronckers, A. L. J. J., van Kuppevelt, T. H., Everts, V., Wijburg, F. A. & van Vlies, N. Altered interaction and distribution of glycosaminoglycans and growth factors in mucopolysaccharidosis type I bone disease. *Bone* **88**, 92–100 (2016).
271. Wang, X., Hua, R., Ahsan, A., Ni, Q., Huang, Y., Gu, S. & Jiang, J. X. Age-Related Deterioration of Bone Toughness Is Related to Diminishing Amount of Matrix Glycosaminoglycans (GAGs); Age-Related Deterioration of Bone Toughness Is Related to Diminishing Amount of Matrix Glycosaminoglycans (GAGs). *JBMR* **2**, 164–173 (2018).
272. Picke, A.-K., Salbach-Hirsch, J., Hintze, V., Rother, S., Rauner, M., Kascholke, C., Möller, S., Bernhardt, R., Rammelt, S., Pisabarro, M. T., Ruiz-Gómez, G., Schnabelrauch, M., Schulz-Siegmund, M., Hacker, M. C., Scharnweber, D., Hofbauer, C. & Hofbauer, L. C. Sulfated hyaluronan improves bone regeneration of diabetic rats by binding sclerostin and enhancing osteoblast function. *Biomaterials* **96**, 11–23 (2016).
273. Mansouri, R., Jouan, Y., Hay, E., Blin-Wakkach, C., Frain, M., Ostertag, A., Le Henaff, C., Marty, C., Geoffroy, V., Marie, P. J., Cohen-Solal, M. & Modrowski, D. Osteoblastic heparan sulfate glycosaminoglycans control bone remodeling by regulating Wnt signaling and the crosstalk between bone surface and marrow cells. *Cell Death Dis.* **8**, (2017).
274. Bernfield, M., Kokenyesi, R., Kato, M., Hinkes, M. T., Spring, J., Gallo, R. L. & Lose, E. J. Biology of the syndecans: A Family of Transmembrane Heparan Sulfate Proteoglycans. *Annu. Rev. Cell Biol.* **8**, 365–393 (1992).
275. Bernfield, M., Götte, M., Park, W., Reizes, O., Fitzgerald, M. L., Lincecum, J. & Zako, M. Functions of cell surface heparan sulfate proteoglycans. *Annu. Rev. Biochem* **68**, 729–777 (1999).
276. Sarrazin, S., Lamanna, W. C. & Esko, J. D. Heparan Sulfate Proteoglycans. *Cold Spring Harb Perspect Biol* **3**, (2011).
277. Lin, X. Functions of heparan sulfate proteoglycans in cell signaling during development. *Development* **131**, 6009–6021 (2004).
278. Kjellen, L., Pettersson, I. & Hook, M. Cell-surface heparan sulfate: An intercalated membrane proteoglycan. *Proc. Nati Acad. Sci. USA* **78**, 5371–5375 (1981).
279. David, G., Lories, V., Decock, B., Marynen, P., Cassiman, J.-J. & Van Den Berghe, H. Molecular Cloning of a Phosphatidylinositol-anchored Membrane Heparan Sulfate Proteoglycan from Human Lung Fibroblasts. *J. Cell Biol.* **111**, 3165–3176 (1990).
280. Carey, D. J. Syndecans: multifunctional cell-surface co-receptors. *Biochem. J.* **327**, 1–16 (1997).
281. Deepa, S. S., Yamada, S., Zako, M., Goldberger, O. & Sugahara, K. Chondroitin Sulfate Chains on Syndecan-1 and Syndecan-4 from Normal Murine Mammary Gland Epithelial Cells Are Structurally and Functionally Distinct and Cooperate with Heparan Sulfate Chains to Bind Growth Factors. *J. Biol. Chem.* **279**, 37368–37376 (2004).
282. Afratis, N. A., Nikitovic, D., Multhaupt, H. A. B., Theocharis, A. D., Couchman, J. R. & Karamanos, N. K. Syndecans – key regulators of cell signaling and

biological functions. *FEBS J.* **284**, 27–41 (2017).
283. Barbouri, D., Afratis, N., Gialeli, C., Vynios, D. H., Theocharis, A. D. & Karamanos, N. K. Syndecans as Modulators and Potential Pharmacological Targets in Cancer Progression. *Front. Oncol.* **4**, (2014).
284. Bellin, R., Capila, I., Lincecum, J., Park, P. W., Reizes, O. & Bernfield, M. R. Unlocking the secrets of syndecans: Transgenic organisms as a potential key. *Glycoconj. J.* **19**, 295–304 (2002).
285. Saunders, S., Jalkanen, M., O'Farrell, S. & Bernfield, M. Molecular Cloning of Syndecan, an Integral Membrane Proteoglycan. *J. Cell Biol.* **108**, 1547–1556 (1989).
286. Marynen, P., Zhang, J., Cassiman, J.-J., Van Den Berghe, H. & David, G. *Partial Primary Structure of the 48-and 90-Kilodalton Core Proteins of Cell Surface-associated Heparan Sulfate Proteoglycans of Lung Fibroblasts PREDICTION OF AN INTEGRAL MEMBRANE DOMAIN AND EVIDENCE FOR MULTIPLE DISTINCT CORE PROTEINS AT THE CELL SURFACE*. *THE JOURNAL OF BIOLOGICAL CHEMISTRY* **264**, (1989).
287. Pierce, A., Lyons, M., Hampson, I. N., Cowling, G. J. & Gallagher, J. T. Molecular Cloning of the Major Cell Surface Heparan Sulfate Proteoglycan from Rat Liver. *J. Biol. Chem.* **267**, 3894–3900 (1992).
288. Carey, D. J., Evans, D. M., Stahl, R. C., Asundi, V. K., Conner, K. J., Garbes, P. & Cizmeci-Smith, G. Molecular cloning and characterization of N-syndecan, a novel transmembrane heparan sulfate proteoglycan. *J. Cell Biol.* **117**, 191–201 (1992).
289. Gould, S. E., Upholtt, W. B. & Kosher, R. A. Syndecan 3: A member of the syndecan family of membrane- intercalated proteoglycans that is expressed in high amounts at the onset of chicken limb cartilage differentiation. *Dev. Biol.* **89**, 3271–3275 (1992).
290. Kojimas, T., Shworak, N. W. & Rosenbergl, R. D. *Molecular Cloning and Expression of Two Distinct cDNA-encoding Heparan Sulfate Proteoglycan Core Proteins from a Rat Endothelial Cell Line*. *The Journal of Biological Chemistry* **267**, (1992).
291. Rapraeger, A. C. & Bernfield, M. *Heparan Sulfate Proteoglycans from Mouse Mammary Epithelial Cells*. *THE JOURNAL OF BIOLOGICAL CHEMISTRY* **258**, (1983).
292. Rapraeger, A., Jalkanen, M. & Bernfield, M. Cell Surface Proteoglycan Associates with the Cytoskeleton at the Basolateral Cell Surface of Mouse Mammary Epithelial Cells. *J. Cell Biol.* **103**, 2683–2696 (1986).
293. Hui-Fang Teng, Y., Aquino, R. S. & Woo Park, P. Molecular functions of syndecan-1 in disease. *Matrix Biol.* **31**, 3–16 (2012).
294. Zhang, X., Wu, C., Song, J., Gotte, M. & Sorokin, L. Syndecan-1, a Cell Surface Proteoglycan, Negatively Regulates Initial Leukocyte Recruitment to the Brain across the Choroid Plexus in Murine Experimental Autoimmune Encephalomyelitis. *J. Immunol.* **191**, 4551–4561 (2013).
295. Voyvodic, P. L., Min, D., Liu, R., Williams, E., Chitalia, V., Dunn, A. K. & Baker, A. B. Loss of Syndecan-1 Induces a Pro-inflammatory Phenotype in Endothelial Cells with a Dysregulated Response to Atheroprotective Flow. *J. Biol. Chem.* **289**, 9547–9559 (2014).

296. Averbeck, M., Kuhn, S., Bühligen, J., Götte, M., Simon, J. C. & Polte, T. Syndecan-1 regulates dendritic cell migration in cutaneous hypersensitivity to haptens. *Exp. Dermatol.* **26**, 1060–1067 (2017).
297. Ren, Z., van Andel, H., de Lau, W., Hartholt, R. B., Maurice, M. M., Clevers, H., Kersten, M. J., Spaargaren, M. & Pals, S. T. Syndecan-1 promotes Wnt/β-catenin signaling in multiple myeloma by presenting Wnts and R-spondins. *Blood* **131**, 982–994 (2018).
298. Lories, V., Cassiman, J.-J., Van Den Berghe, H. & David, G. Differential Expression of Cell Surface Heparan Sulfate Proteoglycans in Human Mammary Epithelial Cells and Lung Fibroblasts. *J. Biol. Chem.* **267**, 1116–1122 (1992).
299. David, G., Bai, X. M., Schueren, B. Van der, Marynen, P., Cassiman, J.-J. & Berghe, H. Van den. Spatial and temporal changes in the expression of fibroglycan (syndecan-2) during mouse embryonic development. *Development* **119**, 841–854 (1993).
300. Gould, S. E., Upholt, W. B. & Kosher, R. A. Characterization of Chicken Syndecan-3 as a Heparan Sulfate Proteoglycan and Its Expression during Embryogenesis. *Dev. Biol.* **168**, 438–451 (1995).
301. Shimazu, A., Nah, H. D., Kirsch, T., Koyama, E., Leatherman, J. L., Golden, E. B., Kosher, R. A. & Pacifici, M. Syndecan-3 and the control of chondrocyte proliferation during endochondral ossification. *Exp. Cell Res.* **229**, 126–136 (1996).
302. Koyama, E., Leatherman, J. L., Shimazu, A., Nah, H. -D & Pacifici, M. Syndecan-3, tenascin-C, and the development of cartilaginous skeletal elements and joints in chick limbs. *Dev. Dyn.* **203**, 152–162 (1995).
303. Koyama, E., Shimazu, A., Leatherman, J. L., Golden, E. B., Nah, H.-D. & Pacifici, M. Expression of syndecan-3 and tenascin-C: Possible involvement in periosteum development. *J. Orthop. Res.* **14**, 403–412 (1996).
304. Raulo, E., Chernousovo, M. A., Carey, D. J., Nolo, R. & Rauvala, H. Isolation of a Neuronal Cell Surface Receptor of Heparin Binding Growth-associated Molecule (HB-GAM). *J. Biol. Chem.* **269**, 12999–13004 (1994).
305. Dreyfus, J., Brunet-de Carvalho, N., Duprez, D., Raulais, D. & Vigny, M. HB-GAM/pleiotrophin: localization of mRNA and protein in the chicken developing leg. *Int. J. Dev. Biol.* **42**, 189–198 (1998).
306. Cornelison, D. D. W., Wilcox-adelman, S. a, Goetinck, P. F., Rauvala, H., Rapraeger, A. C. & Olwin, B. B. Essential and separable roles for Syndecan-3 and Syndecan-4 in skeletal muscle development and regeneration Essential and separable roles for Syndecan-3 and Syndecan-4 in skeletal muscle development and regeneration. *Genes Dev.* **18**, 2231–2236 (2004).
307. Pisconti, A., Banks, G. B., Babaeijandaghi, F., Betta, N. D., Rossi, F. M. V., Chamberlain, J. S. & Olwin, B. B. Loss of niche-satellite cell interactions in syndecan-3 null mice alters muscle progenitor cell, improving muscle regeneration. *Skelet. Muscle* **6**, 1–14 (2016).
308. Kosher, R. A. Syndecan-3 in limb skeletal development. *Microsc. Res. Tech.* **43**, 123–130 (1998).
309. Stanley, M. J., Liebersbach, B. F., Liu, W., Anhalt, D. J. & Sanderson, R. D. Heparan sulfate-mediated cell aggregation. Syndecans-1 and -4 mediate intercellular adhesion following their transfection into human B lymphoid

cells. *J. Biol. Chem.* **270**, 5077–5083 (1995).
310. Gallo, R., Kim, C., Kokellyesi, R., Adzick, N. S. & Bernfield, M. Syndecans-1 and -4 Are Induced During Wound Repair of Neonatal but Not Fetal Skin. *J. Invest. Dermatol.* **107**, 676–683 (1996).
311. Woods, A. & Couchman, J. R. Syndecan 4 Heparan Sulfate Proteoglycan Is a Selectively Enriched and Widespread Focal Adhesion Component. *Mol. Biol. Cell* **5**, 183–192 (1994).
312. Muñoz, R., Moreno, M., Oliva, C., Orbenes, C. & Larraín, J. Syndecan-4 regulates non-canonical Wnt signalling and is essential for convergent and extension movements in Xenopus embryos. *Nat. Cell Biol.* **8**, 492–500 (2006).
313. Bertrand, J., Stange, R., Hidding, H., Echtermeyer, F., Nalesso, G., Godmann, L., Timmen, M., Bruckner, P., Dell'Accio, F., Raschke, M. J., Pap, T. & Dreier, R. Syndecan 4 supports bone fracture repair, but not fetal skeletal development, in mice. *Arthritis Rheum.* **65**, 743–752 (2013).
314. Consensus development conference: prophylaxis and treatment of osteoporosis. in *The American Journal of Medicine* **90**, 107–110 (1991).
315. Eastell, R., O'Neill, T. W., Hofbauer, L. C., Langdahl, B., Reid, I. R., Gold, D. T. & Cummings, S. R. Postmenopausal osteoporosis. *Nat. Rev. Dis. Prim.* **2**, 1–17 (2016).
316. Kanis, J. A. & Kanis, J. A. Assessment of fracture risk and its application to screening for postmenopausal osteoporosis: Synopsis of a WHO report. *Osteoporos. Int.* **4**, 368–381 (1994).
317. Justesen, J., Stenderup, K., Ebbesen, E. N., Mosekilde, L., Steiniche, T. & Kassem, M. Adipocyte tissue volume in bone marrow is increased with aging and in patients with osteoporosis. *Biogerontology* **2**, 165–171 (2001).
318. What is Osteoporosis? | International Osteoporosis Foundation. Available at: https://www.iofbonehealth.org/what-is-osteoporosis. (Accessed: 25th August 2019)
319. Klotzbuecher, C. M., Ross, P. D., Landsman, P. B., Abbott, T. A. & Berger, M. Patients with Prior Fractures Have an Increased Risk of Future Fractures: A Summary of the Literature and Statistical Synthesis. *J. Bone Miner. Res.* **15**, 721–739 (2010).
320. Ström, O., Borgström, F., Kanis, J. A., Compston, J., Cooper, C., McCloskey, E. V. & Jönsson, B. Osteoporosis: burden, health care provision and opportunities in the EU. *Arch. Osteoporos.* **6**, 59–155 (2011).
321. Johnell, O. & Kanis, J. A. An estimate of the worldwide prevalence and disability associated with osteoporotic fractures. *Osteoporos. Int.* **17**, 1726–1733 (2006).
322. Hernlund, E., Svedbom, A., Ivergård, M., Compston, J., Cooper, C., Stenmark, J., McCloskey, E. V., Jönsson, B. & Kanis, J. A. *Osteoporosis in the European Union: Medical management, epidemiology and economic burden*. *Archives of Osteoporosis* **8**, (Springer London, 2013).
323. Cummings, S. R. & Melton, L. J. Epidemiology and outcomes of osteoporotic fractures. *Lancet* **359**, 1761–1767 (2002).
324. Cooper, C., Cole, Z., Holroyd, C., Earl, S., Harvey, N., Dennison, E., Melton, L., Cummings, S., Kanis, J. & Cyrus Cooper FMedSci, P. Secular trends in the incidence of hip and other osteoporotic fractures Europe PMC Funders Group. *Osteoporos Int* **22**, 1277–1288 (2011).

325. *Prevention and management of osteoporosis : report of a WHO scientific group*. *World Health Organization* (2003). doi:10.1016/j.mpmed.2017.06.004
326. Xia, W.-B., He, S.-L., Xu, L., Liu, A.-M., Jiang, Y., Li, M., Wang, O., Xing, X.-P., Sun, Y. & Cummings, S. R. Rapidly increasing rates of hip fracture in Beijing, China. *J. Bone Miner. Res.* **27**, 125–129 (2012).
327. World Health Organization. *Assessment of fracture risk and its application to screening for postmenopausal osteoporosis*. *WHO technical report series* **843**, (1994).
328. Pocock, N. A., Eisman, J. A., Hopper, J. L., Yeates, M. G., Sambrook, P. N. & Eberi, S. Genetic Determinants of Bone Mass in Adults A Twin Study. *J. Clin. Invest.* **80**, 706–710 (1987).
329. Snieder, H., Macgregor, A. J. & Spector, T. D. Genes Control the Cessation of a Woman's Reproductive Life: A Twin Study of Hysterectomy and Age at Menopause. *J. Clin. Endocrinol. Metab.* **83**, 1875–1880 (1998).
330. Ralston, S. H. & Uitterlinden, A. G. Genetics of Osteoporosis. *Endocr. Rev.* **31**, 629–662 (2010).
331. Makovey, J., Nguyen, T. V, Naganathan, V., Wark, J. D. & Sambrook, P. N. Genetic Effects on Bone Loss in Peri- and Postmenopausal Women: A Longitudinal Twin Study. *J. Bone Miner. Res.* **22**, 1773–1780 (2007).
332. Christian, J. C., Yu, P.-L., Slemenda, C. W. & Conrad Johnston Jr., C. Heritability of Bone Mass: A Longitudinal Study in Aging Male Twins. *Am. J. Hum. Genet* **44**, 429–433 (1989).
333. Estrada, K. *et al.* Genome-wide meta-analysis identifies 56 bone mineral density loci and reveals 14 loci associated with risk of fracture. *Nat Genet* **44**, 491–501 (2012).
334. Velázquez-Cruz, R., García-Ortiz, H., Castillejos-López, M., Quiterio, M., Valdés-Flores, M., Orozco, L., Villarreal-Molina, T., Salmerón, J., Velázquez-Cruz, R., García-Ortiz, H., Orozco, L., Quiterio, M. & Salmerón, J. WNT3A gene polymorphisms are associated with bone mineral density variation in postmenopausal mestizo women of an urban Mexican population: findings of a pathway-based high-density single nucleotide screening. *Age (Omaha).* **36**, 1483–1492 (2014).
335. Albright, F., Bloomberg, E. & Smith, P. Postmenopausal osteoporosis. *Trans Assoc Am Physicians* **55**, 298–305 (1940).
336. Riggs, B. L., Wahner, H. W., Seeman, E., Offord, K. P., Dunn, W. L., Mazess, R. B., Johnson, K. A. & Melton III, L. J. Changes in Bone Mineral Density of the Proximal Femur and Spine with Aging. *J Clin Invest1* **70**, 716–723 (1982).
337. Langdahl, B., Ferrari, S. & Dempster, D. W. Bone modeling and remodeling: potential as therapeutic targets for the treatment of osteoporosis. *Ther. Adv. Musculoskelet. Dis.* **8**, 225–235 (2016).
338. Dempster, D. W. & Lindsay, R. Pathogenesis of osteoporosis. *Lancet* **341**, 797–801 (1993).
339. Syed, F. A., Oursler, M. J., Hefferanm, T. E., Peterson, J. M., Riggs, B. L. & Khosla, S. Effects of estrogen therapy on bone marrow adipocytes in postmenopausal osteoporotic women. *Osteoporos. Int.* **19**, 1323–1330 (2008).
340. Ivey, J. L. & Baylink, D. J. Postmenopausal osteoporosis: proposed roles of defective coupling and estrogen deficiency. *Metab. Bone Dis. Relat. Res.* **3**, 3–

7 (1981).
341. Lee, K., Jessop, H., Suswillo, R., Zaman, G. & Lanyon, L. Bone adaptation requires oestrogen receptor-a. *Nature* **424**, 389–390 (2003).
342. Il Modder, U., Clowes, J. A., Hoey, K., Peterson, J. M., McCready, L., Oursler, M. J., Riggs, L. & Khosla, S. Regulation of Circulating Sclerostin Levels by Sex Steroids in Women and in Men. *J. Bone Miner. Res.* **26**, 27–34 (2011).
343. Fujita, K., Roforth, M. M., Demaray, S., Mcgregor, U., Kirmani, S., Mccready, L. K., Peterson, J. M., Drake, M. T., Monroe, D. G. & Khosla, S. Effects of Estrogen on Bone mRNA Levels of Sclerostin and Other Genes Relevant to Bone Metabolism in Postmenopausal Women. *J Clin Endocrinol Metab* **99**, E81–E88 (2014).
344. Khosla, S., Melton III, L. J., Atkinson, E. J. & O'Fallon, W. M. *Relationship of Serum Sex Steroid Levels to Longitudinal Changes in Bone Density in Young Versus Elderly Men*. *The Journal of Clinical Endocrinology & Metabolism* **86**, (2001).
345. Felson, D. T., Zhang, Y., Hannan, M. T. & Anderson, J. J. Effects of weight and body mass index on bone mineral density in men and women: The framingham study. *J. Bone Miner. Res.* **8**, 567–573 (2009).
346. Zhao, L.-J., Jiang, H., Papasian, C. J., Maulik, D., Drees, B., Hamilton, J. & Deng, H.-W. Correlation of Obesity and Osteoporosis: Effect of Fat Mass on the Determination of Osteoporosis. *J Bone Min. Res* **23**, 17–29 (2008).
347. Heim, M., Frank, O., Kampmann, G., Sochocky, N., Pennimpede, T., Fuchs, P., Hunziker, W., Weber, P., Martin, I. & Bendik, I. The Phytoestrogen Genistein Enhances Osteogenesis and Represses Adipogenic Differentiation of Human Primary Bone Marrow Stromal Cells. *Endocrinology* **145**, 848–859 (2004).
348. Brenza, H. L., Kimmel-Jehan, C., Jehan, F., Shinki, T., Wakino, S., Anazawa, H., Suda, T. & Deluca, H. F. Parathyroid hormone activation of the 25-hydroxyvitamin D 3-1-hydroxylase gene promoter. *Proc. Nati Acad. Sci. USA* **95**, 1387–1391 (1998).
349. Bischoff-Ferrari, H. A., Dawson-Hughes, B., Willett, W. C., Staehelin, H. B., Bazemore, M. G., Zee, R. Y. & Wong, J. B. Effect of Vitamin D on Falls. *JAMA* **291**, 1999 (2004).
350. Sambrook, P. N., Chen, J. S., March, L. M., Cameron, I. D., Cumming, R. G., Lord, S. R., Zochling, J., Sitoh, Y. Y., Lau, T. C., Schwarz, J. & Seibel, M. J. Serum Parathyroid Hormone Predicts Time to Fall Independent of Vitamin D Status in a Frail Elderly Population. *J. Clin. Endocrinilogy Metab.* **89**, 1572–1576 (2004).
351. Hofbauers, L. C., Khosla, S., Dunstan, C. R., Lacey, D. L., Spelsberg, T. C. & Riggs, B. L. Estrogen stimulates gene expression and protein production of osteoprotegerin in human osteoblastic cells. *Endocrinology* **140**, 4367–4370 (1999).
352. Silverberg, S. J. & Lindsay, R. Postmenopausal Osteoporosis. *Med. Clin. North Am.* **71**, 41–57 (1987).
353. Glaser, D. L. & Kaplan, F. S. Osteoporosis: Definition and Clinical Presentation. *Spine (Phila. Pa. 1976).* **22**, 12S-16S (1997).
354. Kanis, J. A. Diagnosis of osteoporosis and assessment of fracture risk. *Lancet* **359**, 1929–1936 (2002).
355. Kanis, J. A. FRAX: WHO Fracture Risk Assessment Tool.

https://www.shef.ac.uk/FRAX/tool.jsp. (2016).
356. Compston, J. E., McClung, M. R. & Leslie, W. D. Osteoporosis. *Lancet* **393**, 364–376 (2019).
357. Sims, N. A. & Ng, K. W. Implications of Osteoblast-Osteoclast Interactions in the Management of Osteoporosis by Antiresorptive Agents Denosumab and Odanacatib. *Curr Osteoporos. Rep* **12**, 98–106 (2014).
358. Ebetino, F. H., Hogan, A.-M. L., Sun, S., Tsoumpra, M. K., Duan, X., Triffitt, J. T., Kwaasi, A. A., Dunford, J. E., Barnett, B. L., Oppermann, U., Lundy, M. W., Boyde, A., Kashemirov, B. A., McKenna, C. E. & Russell, R. G. G. The relationship between the chemistry and biological activity of the bisphosphonates. *Bone* **49**, 20–33 (2011).
359. Murad, M. H., Drake, M. T., Mullan, R. J., Mauck, K. F., Stuart, L. M., Lane, M. A., Elnour, N. O. A., Erwin, P. J., Hazem, A., Puhan, M. A., Li, T. & Montori, V. M. Comparative Effectiveness of Drug Treatments to Prevent Fragility Fractures: A Systematic Review and Network Meta-Analysis. *J Clin Endocrinol Metab* **97**, 1871–1880 (2012).
360. Black, D. M. *et al.* Once-Yearly Zoledronic Acid for Treatment of Postmenopausal Osteoporosis. *N. Engl. J. Med.* **356**, 1809–1822 (2007).
361. Khosla, S. & Hofbauer, L. C. Osteoporosis treatment: recent developments and ongoing challenges. *lancet. Diabetes Endocrinol.* **5**, 898–907 (2017).
362. Lenart, B. A., Neviaser, A. S., Lyman, S., Chang, C. C., Edobor-Osula, F., Steele, B., van der Meulen, M. C. H., Lorich, D. G. & Lane, J. M. Association of low-energy femoral fractures with prolonged bisphosphonate use: a case control study. *Osteoporos. Int.* **20**, 1353–1362 (2009).
363. Marx, R. E. Pamidronate (Aredia) and zoledronate (Zometa) induced avascular necrosis of the jaws: a growing epidemic. *J. Oral Maxillofac. Surg.* **61**, 1115–7 (2003).
364. Cummings, S. R., Martin, J. S., Mcclung, M. R., Siris, E. S., Eastell, R., Reid, I. R., Delmas, P., Zoog, H. B., Austin, M., Wang, A., Kutilek, S., Adami, S., Zanchetta, J., Libanati, C., Siddhanti, S. & Christiansen, C. Denosumab for Prevention of Fractures in Postmenopausal Women with Osteoporosis. *N. Engl. J. Med.* **361**, 756–765 (2009).
365. Vahle, J. L., Long, G. G., Sandusky, G., Westmore, M., Linda, Y. M. & Sato, M. Bone Neoplasms in F344 Rats Given Teriparatide [rhPTH(1-34)] Are Dependent on Duration of Treatment and Dose. *Toxicol. Pathol.* **32**, 426–438 (2004).
366. Cosman, F., Crittenden, D. B., Ferrari, S., Khan, A., Lane, N. E., Lippuner, K., Matsumoto, T., Milmont, C. E., Libanati, C. & Grauer, A. FRAME Study: The Foundation Effect of Building Bone With 1 Year of Romosozumab Leads to Continued Lower Fracture Risk After Transition to Denosumab. *J. Bone Miner. Res.* **33**, 1219–1226 (2018).
367. Saag, K. G., Petersen, J., Brandi, M. L., Karaplis, A. C., Lorentzon, M., Thomas, T., Maddox, J., Fan, M., Meisner, P. D. & Grauer, A. Romosozumab or Alendronate for Fracture Prevention in Women with Osteoporosis. *N. Engl. J. Med.* **377**, 1417–1427 (2017).
368. Cauley, J. A., Robbins, J., Chen, Z., Cummings, S. R., Jackson, R. D., LaCroix, A. Z., LeBoff, M., Lewis, C. E., McGowan, J., Neuner, J., Pettinger, M., Stefanick, M. L., Wactawski-Wende, J., Watts, N. B. & Investigators, for the W. H. I.

Effects of Estrogen Plus Progestin on Risk of Fracture and Bone Mineral Density. *JAMA* **290**, 1729–1738 (2003).
369. Writing Group for the Women's Health Initiative Investigators, W. G. for the W. H. I. Risks and Benefits of Estrogen Plus Progestin in Healthy Postmenopausal Women: Principal Results From the Women's Health Initiative Randomized Controlled Trial. *JAMA* **288**, 321–333 (2002).
370. Ralston, S. H. & de Crombrugghe, B. Genetic regulation of bone mass and susceptibility to osteoporosis. *Genes Dev.* **20**, 2492–2506 (2006).
371. Varanasi, S. S., Olstad, O. K., Swan, D. C., Sanderson, P., Gautvik, V. T., Reppe, S., Francis, R. M., Gautvik, K. M. & Datta, H. K. Skeletal Site-Related Variation in Human Trabecular Bone Transcriptome and Signaling. *PLoS One* **5**, e10692 (2010).
372. Peacock, M., Turner, C. H., Econs, M. J. & Foroud, T. Genetics of Osteoporosis. *Endocr. Rev.* **23**, 303–326 (2002).
373. Kram, V. & Young, M. F. Bone Matrix Proteoglycans in Skeletal Function. in *Osteogenesis Imperfecta* 85–95 (Academic Press, 2014). doi:10.1016/B978-0-12-397165-4.00008-3
374. Shimo, T., Gentili, C., Iwamoto, M., Wu, C., Koyama, E. & Pacifici, M. Indian Hedgehog land Syndecans-3 Coregulate Chondrocyte Proliferation and Function during Chick Limb Skeletogenesis. *Dev. Dyn.* **229**, 607–617 (2004).
375. Pacifici, M., Shimo, T., Gentili, C., Kirsch, T., Freeman, T. A., Enomoto-Iwamoto, M., Iwamoto, M. & Koyama, E. Syndecan-3: A cell-surface heparan sulfate proteoglycan important for chondrocyte proliferation and function during limb skeletogenesis. *J. Bone Miner. Metab.* **23**, 191–199 (2005).
376. Strader, A. D., Reizes, O., Woods, S. C., Benoit, S. C. & Seeley, R. J. Mice lacking the syndecan-3 gene are resistant to diet-induced obesity. *J. Clin. Invest.* **114**, 1354–1360 (2004).
377. Kaksonen, M., Pavlov, I., Võikar, V., Lauri, S. E., Hienola, A., Riekki, R., Lakso, M., Taira, T. & Rauvala, H. Syndecan-3-Deficient Mice Exhibit Enhanced LTP and Impaired Hippocampus-Dependent Memory. *Mol. Cell. Neurosci.* **21**, 158–172 (2002).
378. Dempster, D. W., Compston, J. E., Drezner, M. K., Glorieux, F. H., Kanis, J. A., Malluche, H., Meunier, P. J., Ott, S. M., Recker, R. R. & Parfitt, A. M. Standardized Nomenclature, Symbols, and Units for Bone Histomorphometry: A 2012 Update of the Report of the ASBMR Histomorphometry Nomenclature Committee. *J. bone Miner. Res.* **28**, 2–17 (2013).
379. van 't Hof, R. J., Rose, L., Bassonga, E. & Daroszewska, A. Open source software for semi-automated histomorphometry of bone resorption and formation parameters. *Bone* **99**, 69–79 (2017).
380. Chappard, D., Alexandre, C. & Riffat, G. Histochemical identification of osteoclasts. Review of current methods and reappraisal of a simple procedure for routine diagnosis on undecalcified human iliac bone biopsies. *Basic Appl.Histochem.* **27**, 75–85 (1983).
381. Sheehan, D. C. & Hrapchak, B. B. *Theory and practice of histotechnology*. (Battelle Press, 1987).
382. De Souza, R. L., Matsuura, M., Eckstein, F., Rawlinson, S. C. F., Lanyon, L. E. & Pitsillides, A. A. Non-invasive axial loading of mouse tibiae increases cortical

bone formation and modifies trabecular organization: A new model to study cortical and cancellous compartments in a single loaded element. *Bone* **37**, 810–818 (2005).
383. Poulet, B., Hamilton, R. W., Shefelbine, S. & Pitsillides, A. A. Characterizing a novel and adjustable noninvasive murine joint loading model. *Arthritis Rheum.* **63**, 137–147 (2011).
384. Hummon, A. B., Lim, S. R., Difilippantonio, M. J. & Ried, T. *Isolation and solubilization of proteins after TRIZOL extraction of RNA and DNA from patient material following prolonged storage*. *BioTechniques* **42**, (2007).
385. Stephens, A. S., Stephens, S. R. & Morrison, N. A. Internal control genes for quantitative RT-PCR expression analysis in mouse osteoblasts, osteoclasts and macrophages. *BMC Res. Notes* **4**, (2011).
386. Taichman, R. S., Liu, Z. Y. & Groopman, J. E. Blood and bone: two tissues whose fates are intertwined to create the hematopoietic stem-cell niche. *Blood* **105**, 2631–2639 (2005).
387. Kini, U. & Nandeesh, B. N. Physiology of Bone Formation, Remodeling, and Metabolism. in *Radionuclide and Hybrid Bone Imaging* 29–57 (Springer Berlin Heidelberg, 2012). doi:10.1007/978-3-642-02400-9_2
388. Wang, Y., Li, Y.-P., Paulson, C., Shao, J.-Z., Zhang, X., Wu, M. & Chen, W. Wnt and the Wnt signaling pathway in bone development and disease. *Front Biosci* **19**, 379–407 (2014).
389. Bartl, R. & Bartl, C. Modelling and Remodelling of Bone. in *Bone Disorders* 21–30 (Springer International Publishing, 2017). doi:10.1007/978-3-319-29182-6_3
390. Raisz, L. G. Physiology and Pathophysiology of Bone Remodeling. *Clin. Chem.* **45**, 1353–1358 (1999).
391. Mulder, J. E., Kolatkar, N. S. & LeBoff, M. S. Drug Insight: existing and emerging therapies for osteoporosis. *Nat. Clin. Pract. Endocrinol. Metab.* **2**, 670–680 (2006).
392. Gori, F., Lerner, U., Ohlsson, C. & Baron, R. A new WNT on the bone: WNT16, cortical bone thickness, porosity and fractures. *Bonekey Rep.* **4**, (2015).
393. Lanyon, L. E. Functional strain in bone tissue as an objective, and controlling stimulus for adaptive bone remodelling. *J. Biomech.* **20**, 1083–1093 (1987).
394. Singer, B. R., McLauchlan, G. J., Robinson, C. M. & Christie, J. Epidemiology of fractures in 15,000 adults: the influence of age and gender. *J. Bone Joint Surg. Br.* **80**, 243–8 (1998).
395. John A Kanis on behalf of the World Health Organization Scientific Group. *Assessment of osteoporosis at the primary health-care level. Technical Report.* (2007).
396. Cramer, J. A., Gold, D. T., Silverman, S. L. & Lewiecki, E. M. A systematic review of persistence and compliance with bisphosphonates for osteoporosis. *Osteoporos. Int.* **18**, 1023–1031 (2007).
397. Rossini, M., Bianchi, G., Di Munno, O., Giannini, S., Minisola, S., Sinigaglia, L. & Adami, S. Determinants of adherence to osteoporosis treatment in clinical practice. *Osteoporos. Int.* **17**, 914–921 (2006).
398. Appelman-Dijkstra, N. M. & Papapoulos, S. E. Clinical advantages and disadvantages of anabolic bone therapies targeting the WNT pathway. *Nat.*

Rev. Endocrinol. **14**, 605–623 (2018).
399. Lane, N. E. & Kelman, A. A review of anabolic therapies for osteoporosis. *Arthritis Res. Ther.* **5**, 214–222 (2003).
400. Karsenty, G. The complexities of skeletal biology. *Nature* **423**, 316–318 (2003).
401. Karsenty, G. & Wagner, E. F. Review Reaching a Genetic and Molecular Understanding of Skeletal Development patterning were not really involved in the control of cell differentiation. Thus, the development of the skeleton encompasses. *Dev. Cell* **2**, 389–406 (2002).
402. Couchman, J. R. Syndecans: proteoglycan regulators of cell-surface microdomains? *Nat. Rev. Mol. Cell Biol.* **4**, 926–938 (2003).
403. Ng, K. W. Regulation of glucose metabolism and the skeleton. *Clin. Endocrinol. (Oxf).* **75**, 147–155 (2011).
404. Wang, Z., Telci, D. & Griffin, M. Importance of syndecan-4 and syndecan -2 in osteoblast cell adhesion and survival mediated by a tissue transglutaminase−fibronectin complex. *Exp. Cell Res.* **317**, 367–381 (2011).
405. Kwon, M. J., Jang, B., Yi, J. Y., Han, I. O. & Oh, E. S. Syndecans play dual roles as cell adhesion receptors and docking receptors. *FEBS Lett.* **586**, 2207–2211 (2012).
406. Couchman, J. R., Gopal, S., Lim, H. C., Nørgaard, S. & Multhaupt, H. A. B. Syndecans: From peripheral coreceptors to mainstream regulators of cell behaviour. *Int. J. Exp. Pathol.* **96**, 1–10 (2015).
407. Choi, Y., Chung, H., Jung, H., Couchman, J. R. & Oh, E. S. Syndecans as cell surface receptors: Unique structure equates with functional diversity. *Matrix Biol.* **30**, 93–99 (2011).
408. Glatt, V., Canalis, E., Stadmeyer, L. & Bouxsein, M. L. Age-Related Changes in Trabecular Architecture Differ in Female and Male C57BL/6J Mice. *J. Bone Miner. Res.* **22**, 1197–1207 (2007).
409. Halloran, B. P., Ferguson, V. L., Simske, S. J., Burghardt, A., Venton, L. L. & Majumdar, S. Changes in Bone Structure and Mass With Advancing Age in the Male C57BL/6J Mouse. *J. Bone Miner. Res.* **17**, 1044–1050 (2002).
410. Mansouri, R., Haÿ, E., Marie, P. J. & Modrowski, D. Role of syndecan-2 in osteoblast biology and pathology. *Bonekey Rep.* **4**, (2015).
411. Kehoe, O., Kalia, N., King, S., Eustace, A., Boyes, C., Reizes, O., Williams, A., Patterson, A. & Middleton, J. Syndecan-3 is selectively pro-inflammatory in the joint and contributes to antigen-induced arthritis in mice. *Arthritis Res. Ther.* **16**, 1–14 (2014).
412. Oh, E.-S. & Couchman, J. R. Syndecans-2 and -4; close cousins, but not identical twins. *Mol. Cells* **17**, 181–187 (2004).
413. Klaus Elenius and Markku Jalkanen. Function of the syndecans - a family of cell surface proteoglycans. *J. Cell Sci.* **107**, 2975–2982 (1994).
414. Kirsch, T., Koyama, E., Liu, M., Golub, E. E. & Pacifici, M. Syndecan-3 is a selective regulator of chondrocyte proliferation. *J. Biol. Chem.* **277**, 42171–42177 (2002).
415. Kesavan, C., Mohan, S., Srivastava, A. K., Kapoor, S., Wergedal, J. E., Yu, H. & Baylink, D. J. Identification of genetic loci that regulate bone adaptive response to mechanical loading in C57BL/6J and C3H/HeJ mice intercross. *Bone* **39**, 634–643 (2006).

416. Verma, S., Rajaratnam, J. H., Denton, J., Hoyland, J. A. & Byers, R. J. Adipocytic proportion of bone marrow is inversely related to bone formation in osteoporosis. *J. Clin. Pathol.* **55**, 693–698 (2002).
417. Rosen, C. J. & Bouxsein, M. L. Mechanisms of Disease: is osteoporosis the obesity of bone? *Nat. Clin. Pract. Rheumatol.* **2**, 35–43 (2006).
418. Cohen, A. *et al.* Abnormal Bone Microarchitecture and Evidence of Osteoblast Dysfunction in Premenopausal Women with Idiopathic Osteoporosis. *J. Clin. Endocrinol. Metab.* **96**, 3095–3105 (2011).
419. Cohen, A., Dempster, D. W., Stein, E. M., Nickolas, T. L., Zhou, H., McMahon, D. J., Müller, R., Kohler, T., Zwahlen, A., Lappe, J. M., Young, P., Recker, R. R. & Shane, E. Increased Marrow Adiposity in Premenopausal Women with Idiopathic Osteoporosis. *J. Clin. Endocrinol. Metab.* **97**, 2782–2791 (2012).
420. Ferguson, V. L., Ayers, R. A., Bateman, T. A. & Simske, S. J. Bone development and age-related bone loss in male C57BL/6J mice. *Bone* **33**, 387–398 (2003).
421. Demontiero, O., Vidal, C. & Duque, G. Aging and bone loss: new insights for the clinician. *Ther. Adv. Musculoskelet. Dis.* **4**, 61–76 (2012).
422. Berendsen, A. D. & Olsen, B. R. Osteoblast-adipocyte lineage plasticity in tissue development, maintenance and pathology. *Cell. Mol. life Sci.* **71**, 493–497 (2014).
423. Bethel, M., Chitteti, B. R., Srour, E. F. & Kacena, M. A. The changing balance between osteoblastogenesis and adipogenesis in aging and its impact on hematopoiesis. *Curr. Osteoporos. Rep.* **11**, 99–106 (2013).
424. Bredella, M. A., Fazeli, P. K., Miller, K. K., Misra, M., Torriani, M., Thomas, B. J., Ghomi, R. H., Rosen, C. J. & Klibanski, A. Increased Bone Marrow Fat in Anorexia Nervosa. *J. Clin. Endocrinol. Metab.* **94**, 2129–2136 (2009).
425. Mehler, P. S., Cleary, B. S. & Gaudiani, J. L. Osteoporosis in Anorexia Nervosa. *Eat. Disord.* **19**, 194–202 (2011).
426. Ambrosi, T. H., Scialdone, A., Graja, A., Gohlke, S., Jank, A.-M., Bocian, C., Woelk, L., Fan, H., Logan, D. W., Schürmann, A., Saraiva, L. R. & Schulz, T. J. Adipocyte Accumulation in the Bone Marrow during Obesity and Aging Impairs Stem Cell-Based Hematopoietic and Bone Regeneration. *Cell Stem Cell* **20**, 771–784 (2017).
427. Kajkenova, O., Lecka-Czernik, B., Gubrij, I., Hauser, S. P., Takahashi, K., Parfitt, A. M., Jilka, R. L., Manolagas, S. C. & Lipschitz, D. A. Increased Adipogenesis and Myelopoiesis in the Bone Marrow of SAMP6, a Murine Model of Defective Osteoblastogenesis and Low Turnover Osteopenia. *J. Bone Miner. Res.* **12**, 1772–1779 (1997).
428. Rauner, M., Sipos, W. & Pietschmann, P. Age-dependent Wnt gene expression in bone and during the course of osteoblast differentiation. *Age (Omaha).* **30**, 273–282 (2008).
429. Takahashi, K., Tsuboyama, T., Matsushita, M., Kasai, R., Okumura, H., Yamamuro, T., Okamoto, Y., Toriyama, K., Kitagawa, K. & Takeda, T. Modification of strain-specific femoral bone density by bone marrow-derived factors administered neonatally: a study on the spontaneously osteoporotic mouse, SAMP6. *Bone Miner.* **24**, 245–255 (1994).
430. Bowers, R. R. & Daniel Lane, M. Wnt signaling and adipocyte lineage commitment. *Cell Cycle* **7**, 1191–1196 (2008).

431. Ducy, P., Zhang, R., Geoffroy, V., Ridall, A. L. & Karsenty, G. Osf2/Cbfa1: A Transcriptional Activator of Osteoblast Differentiation. *Cell* **89**, 747–754 (1997).
432. Rangwala, S. M. & Lazar, M. A. Transcriptional control of adipogenesis. *Annu. Rev. Nutr.* **20**, 535–559 (2000).
433. Rosen, E. D. & Spiegelman, B. M. PPARgamma : a nuclear regulator of metabolism, differentiation, and cell growth. *J. Biol. Chem.* **276**, 37731–37734 (2001).
434. Komori, T., Yagi, H., Nomura, S., Yamaguchi, A., Sasaki, K., Deguchi, K., Shimizu, Y., Bronson, R. ., Gao, Y.-H., Inada, M., Sato, M., Okamoto, R., Kitamura, Y., Yoshiki, S. & Kishimoto, T. Targeted Disruption of Cbfa1 Results in a Complete Lack of Bone Formation owing to Maturational Arrest of Osteoblasts. *Cell* **89**, 755–764 (1997).
435. Nilsson, O. & Baron, J. Fundamental limits on longitudinal bone growth: growth plate senescence and epiphyseal fusion. *Trends Endocrinol. Metab.* **15**, 370–374 (2004).
436. Koshihara, Y., Suematsu, A., Feng, D., Okawara, R., Ishibashi, H. & Yamamoto, S. Osteoclastogenic potential of bone marrow cells increases with age in elderly women with fracture. *Mech. Ageing Dev.* **123**, 1321–1331 (2002).
437. Cao, J. J., Wronski, T. J., Iwaniec, U., Phleger, L., Kurimoto, P., Boudignon, B. & Halloran, B. P. Aging Increases Stromal/Osteoblastic Cell-Induced Osteoclastogenesis and Alters the Osteoclast Precursor Pool in the Mouse. *J. Bone Miner. Res.* **20**, 1659–1668 (2005).
438. Moerman, E. J., Teng, K., Lipschitz, D. A. & Lecka-Czernik, B. Aging activates adipogenic and suppresses osteogenic programs in mesenchymal marrow stroma/stem cells: the role of PPAR-γ2 transcription factor and TGF-β/BMP signaling pathways. *Aging Cell* **3**, 379–389 (2004).
439. Kim, J. H. & Kim, N. Regulation of NFATc1 in Osteoclast Differentiation. *J. Bone Metab.* **21**, 233 (2014).
440. Yagi, M., Miyamoto, T., Sawatani, Y., Iwamoto, K., Hosogane, N., Fujita, N., Morita, K., Ninomiya, K., Suzuki, T., Miyamoto, K., Oike, Y., Takeya, M., Toyama, Y. & Suda, T. DC-STAMP is essential for cell–cell fusion in osteoclasts and foreign body giant cells. *J. Exp. Med.* **202**, 345–351 (2005).
441. Witwicka, H., Hwang, S. Y., Reyes-Gutierrez, P., Jia, H., Odgren, P. E., Donahue, L. R., Birnbaum, M. J. & Odgren, P. R. Studies of OC-STAMP in osteoclast fusion: A new knockout mouse model, rescue of cell fusion, and transmembrane topology. *PLoS One* **10**, 1–25 (2015).
442. Kukita, T., Wada, N., Kukita, A., Kakimoto, T., Sandra, F., Toh, K., Nagata, K., Iijima, T., Horiuchi, M., Matsusaki, H., Hieshima, K., Yoshie, O. & Nomiyama, H. RANKL-induced DC-STAMP Is Essential for Osteoclastogenesis. *J. Exp. Med.* **200**, 941–946 (2004).
443. Wilson, S. R., Peters, C., Saftig, P. & Brömme, D. Cathepsin K activity-dependent regulation of osteoclast actin ring formation and bone resorption. *J. Biol. Chem.* **284**, 2584–2592 (2009).
444. Robinson, J. A., Chatterjee-Kishore, M., Yaworsky, P. J., Cullen, D. M., Zhao, W., Li, C., Kharode, Y., Sauter, L., Babij, P., Brown, E. L., Hill, A. A., Akhter, M. P., Johnson, M. L., Recker, R. R., Komm, B. S. & Bex, F. J. Wnt/beta-catenin

signaling is a normal physiological response to mechanical loading in bone. *J. Biol. Chem.* **281**, 31720–31728 (2006).
445. Grainger, S. & Willert, K. Mechanisms of Wnt signaling and control. *WIREs Syst Biol Med* **e1422**, (2018).
446. Christodoulides, C., Lagathu, C., Sethi, J. K. & Vidal-Puig, A. Adipogenesis and WNT signalling. *Trends Endocrinol. Metab.* **20**, 16–24 (2009).
447. Ross, S. E., Hemati, N., Longo, K. A., Bennett, C. N., Lucas, P. C., Erickson, R. L. & MacDougald, O. A. Inhibition of adipogenesis by Wnt signaling. *Science (80-.).* **289**, 950–953 (2000).
448. Cawthorn, W. P., Bree, A. J., Yao, Y., Du, B., Hemati, N., Martinez-Santibañez, G. & MacDougald, O. A. Wnt6, Wnt10a and Wnt10b inhibit adipogenesis and stimulate osteoblastogenesis through a β-catenin-dependent mechanism. *Bone* **50**, 477–489 (2012).
449. Li, J. *et al.* RANK is the intrinsic hematopoietic cell surface receptor that controls osteoclastogenesis and regulation of bone mass and calcium metabolism. *PNAS* **97**, 1566–1571 (2000).
450. Gowen, M., Lazner, F., Dodds, R., Kapadia, R., Feild, J., Tavaria, M., Bertoncello, I., Drake, F., Zavarselk, S., Tellis, I., Hertzog, P., Debouck, C. & Kola, I. Cathepsin K Knockout Mice Develop Osteopetrosis Due to a Deficit in Matrix Degradation but Not Demineralization. *J. Bone Miner. Res.* **14**, 1654–1663 (1999).
451. Boyce, B. F. & Xing, L. Biology of RANK, RANKL, and osteoprotegerin. *Arthritis Res. Ther.* **9**, (2007).
452. Wei, W., Zeve, D., Suh, J. M., Wang, X., Du, Y., Zerwekh, J. E., Dechow, P. C., Graff, J. M. & Wan, Y. Biphasic and dosage-dependent regulation of osteoclastogenesis by β-catenin. *Mol. Cell. Biol.* **31**, 4706–4719 (2011).
453. Maeda, K., Kobayashi, Y., Udagawa, N., Uehara, S., Ishihara, A., Mizoguchi, T., Kikuchi, Y., Takada, I., Kato, S., Kani, S., Nishita, M., Marumo, K., Martin, T. J., Minami, Y. & Takahashi, N. Wnt5a-Ror2 signaling between osteoblast-lineage cells and osteoclast precursors enhances osteoclastogenesis. *Nat. Med.* **18**, 405–412 (2012).
454. Ohkawara, B., Glinka, A. & Niehrs, C. Rspo3 Binds Syndecan 4 and Induces Wnt/PCP Signaling via Clathrin-Mediated Endocytosis to Promote Morphogenesis. *Dev. Cell* **20**, 303–314 (2011).
455. Yadav, M. C., Simão, A. M. S., Narisawa, S., Huesa, C., Mckee, M. D., Farquharson, C. & Millán, J. L. Loss of Skeletal Mineralization by the Simultaneous Ablation of PHOSPHO1 and Alkaline Phosphatase Function: A Unified Model of the Mechanisms of Initiation of Skeletal Calcification. *JBMR* **26**, 286–297 (2011).
456. Sebastian, A., Hum, N. R., Murugesh, D. K., Hatsell, S., Economides, A. N. & Loots, G. G. Wnt co-receptors Lrp5 and Lrp6 differentially mediate Wnt3a signaling in osteoblasts. *PLoS One* **12**, e0188264 (2017).
457. Eijken, M., Meijer, I. M. J., Westbroek, I., Koedam, M., Chiba, H., Uitterlinden, A. G., Pols, H. A. P. & Van Leeuwen, J. P. T. M. Wnt signaling acts and is regulated in a human osteoblast differentiation dependent manner. *J. Cell. Biochem.* **104**, 568–579 (2008).
458. Yu, S., Yerges-Armstrong, L. M., Chu, Y., Zmuda, J. M. & Zhang, Y. E2F1 effects on osteoblast differentiation and mineralization are mediated through up-

regulation of frizzled-1. *Bone* **56**, 234–241 (2013).
459. Yu, S., Zhu, K., Lai, Y., Zhao, Z., Fan, J., Im, H.-J., Chen, D. & Xiao, G. ATF4 promotes β-catenin expression and osteoblastic differentiation of bone marrow mesenchymal stem cells. *Int. J. Biol. Sci.* **9**, 256–266 (2013).
460. Ducy, P., Desbois, C., Boyce, B., Pinero, G., Story, B., Dunstan, C., Smith, E., Bonadio, J., Goldstein, S., Gundberg, C., Bradley, A. & Karsenty, G. Increased bone formation in osteocalcin-deficient mice. *Nature* **382**, 448–452 (1996).
461. Karner, C. M., Esen, E., Chen, J., Hsu, F.-F., Turk, J. & Long, F. Wnt Protein Signaling Reduces Nuclear Acetyl-CoA Levels to Suppress Gene Expression during Osteoblast Differentiation. *J. Biol. Chem.* **291**, 13028–13039 (2016).
462. Grol, M. W., Brooks, P. J., Pereverzev, A. & Dixon, S. J. P2X7 nucleotide receptor signaling potentiates the Wnt/β-catenin pathway in cells of the osteoblast lineage. *Purinergic Signal.* **12**, 509–520 (2016).
463. Fei, Y., Xiao, L., Doetschman, T., Coffin, D. J. & Hurley, M. M. Fibroblast Growth Factor 2 Stimulation of Osteoblast Differentiation and Bone Formation Is Mediated by Modulation of the Wnt Signaling Pathway. *J. Biol. Chem.* **286**, 40575–40583 (2011).
464. Delany, A. M., Kalajzic, I., Bradshaw, A. D., Sage, E. H. & Canalis, E. Osteonectin-Null Mutation Compromises Osteoblast Formation, Maturation, and Survival. *Endocrinology* **144**, 2588–2596 (2003).
465. Delany, A. M., Amling, M., Priemel, M., Howe, C., Baron, R. & Canalis, E. Osteopenia and decreased bone formation in osteonectin-deficient mice. *J. Clin. Invest.* **105**, 915–923 (2000).
466. Horiuchi, K., Amizuka, N., Takeshita, S., Takamatsu, H., Katsuura, M., Ozawa, H., Toyama, Y., Bonewald, L. F. & Kudo, A. Identification and Characterization of a Novel Protein, Periostin, with Restricted Expression to Periosteum and Periodontal Ligament and Increased Expression by Transforming Growth Factor β. *J. Bone Miner. Res.* **14**, 1239–1249 (1999).
467. Scherer, P. E., Williams, S., Fogliano, M., Baldini, G. & Lodish, H. F. A novel serum protein similar to C1q, produced exclusively in adipocytes. *J. Biol. Chem.* **270**, 26746–26749 (1995).
468. Bennett, C. N., Ouyang, H., Ma, Y. L., Zeng, Q., Gerin, I., Sousa, K. M., Lane, T. F., Krishnan, V., Hankenson, K. D. & MacDougald, O. A. Wnt10b Increases Postnatal Bone Formation by Enhancing Osteoblast Differentiation. *J. Bone Miner. Res.* **22**, 1924–1932 (2007).
469. Bennett, C. N., Longo, K. A., Wright, W. S., Suva, L. J., Lane, T. F., Hankenson, K. D. & MacDougald, O. A. Regulation of osteoblastogenesis and bone mass by Wnt10b. *PNAS* **102**, 3324–3329 (2005).
470. Nuttall, M. E. & Gimble, J. M. Controlling the balance between osteoblastogenesis and adipogenesis and the consequent therapeutic implications. *Curr. Opin. Pharmacol.* **4**, 290–294 (2004).
471. Tu, X., Rhee, Y., Condon, K. W., Bivi, N., Allen, M. R., Dwyer, D., Stolina, M., Turner, C. H., Robling, A. G., Plotkin, L. I. & Bellido, T. Sost downregulation and local Wnt signaling are required for the osteogenic response to mechanical loading. *Bone* **50**, 209–217 (2012).
472. Crockett, J. C., Mellis, D. J., Scott, D. I. & Helfrich, M. H. New knowledge on critical osteoclast formation and activation pathways from study of rare

genetic diseases of osteoclasts: focus on the RANK/RANKL axis. *Osteoporos. Int.* **22**, 1–20 (2011).
473. Del Fattore, A., Cappariello, A. & Teti, A. Genetics, pathogenesis and complications of osteopetrosis. *Bone* **42**, 19–29 (2008).
474. Angsana, J., Chen, J., Smith, S., Xiao, J., Wen, J., Liu, L., Haller, C. A., Chaikof, E. L. & Carolyn Haller, or A. Syndecan-1 Modulates the Motility and Resolution Responses of Macrophages. *Arter. Thromb Vasc Biol* **35**, 332–340 (2015).
475. Benad-Mehner, P., Thiele, S., Rachner, T. D., Göbel, A., Rauner, M. & Hofbauer, L. C. Targeting syndecan-1 in breast cancer inhibits osteoclast functions through up-regulation of osteoprotegerin. *J. bone Oncol.* **3**, 18–24 (2014).
476. Xaus, J., Comalada, M., Cardó, M., Valledor, A. F. & Celada, A. Decorin inhibits macrophage colony-stimulating factor proliferation of macrophages and enhances cell survival through induction of p27(Kip1) and p21(Waf1). *Blood* **98**, 2124–2133 (2001).
477. Théoleyre, S., Kwan Tat, S., Vusio, P., Blanchard, F., Gallagher, J., Ricard-Blum, S., Fortun, Y., Padrines, M., Rédini, F. & Heymann, D. Characterization of osteoprotegerin binding to glycosaminoglycans by surface plasmon resonance: Role in the interactions with receptor activator of nuclear factor κB ligand (RANKL) and RANK. *Biochem. Biophys. Res. Commun.* **347**, 460–467 (2006).
478. Kram, V., Kilts, T. M., Bhattacharyya, N., Li, L. & Young, M. F. Small leucine rich proteoglycans, a novel link to osteoclastogenesis. *Sci. Rep.* **7**, 12627 (2017).
479. Wang, Q., Wei, X., Zhu, T., Zhang, M., Shen, R., Xing, L., O'Keefe, R. J. & Chen, D. Bone morphogenetic protein 2 activates Smad6 gene transcription through bone-specific transcription factor Runx2. *J. Biol. Chem.* **282**, 10742–10748 (2007).
480. Shen, R., Chen, M., Wang, Y.-J., Kaneki, H., Xing, L., O'Keefe, R. J. & Chen, D. Smad6 interacts with Runx2 and mediates Smad ubiquitin regulatory factor 1-induced Runx2 degradation. *J. Biol. Chem. Chem.* **281**, 3569–3576 (2006).
481. Lin, G. L. & Hankenson, K. D. Integration of BMP, Wnt, and notch signaling pathways in osteoblast differentiation. *J. Cell. Biochem.* **112**, 3491–3501 (2011).
482. Pittenger, M. F., Mackay, A. M., Beck, S. C., Jaiswal, R. K., Douglas, R., Mosca, J. D., Moorman, M. A., Simonetti, D. W., Craig, S. & Marshak, D. R. Multilineage potential of adult human mesenchymal stem cells. *Science (80-.).* **284**, 143–147 (1999).
483. Styrkarsdottir, U. *et al.* Nonsense mutation in the LGR4 gene is associated with several human diseases and other traits. *Nature* **497**, 517–520 (2013).
484. Abdallah, B. M. Marrow adipocytes inhibit the differentiation of mesenchymal stem cells into osteoblasts via suppressing BMP-signaling. *J. Biomed. Sci.* **24**, 1–10 (2017).
485. Zhang, M., Yan, Y., Lim, Y.-B., Tang, D., Xie, R., Chen, A., Tai, P., Harris, S. E., Xing, L., Qin, Y.-X. & Chen, D. BMP-2 modulates beta-catenin signaling through stimulation of Lrp5 expression and inhibition of beta-TrCP expression in osteoblasts. *J. Cell. Biochem.* **108**, 896–905 (2009).
486. Zhang, R., Oyajobi, B. O., Harris, S. E., Chen, D., Tsao, C., Deng, H.-W. & Zhao, M. Wnt/β-catenin signaling activates bone morphogenetic protein 2

expression in osteoblasts. *Bone* **52**, 145–56 (2013).
487. Imai, S., Heino, T. J., Hienola, A., Kurata, K., Büki, K., Matsusue, Y., Väänänen, H. K. & Rauvala, H. Osteocyte-derived HB-GAM (pleiotrophin) is associated with bone formation and mechanical loading. *Bone* **44**, 785–794 (2009).
488. Imai, S., Kaksonen, M., Raulo, E., Kinnunen, T., Fages, C., Meng, X. J., Lakso, M. & Rauvala, H. Osteoblast recruitment and bone formation enhanced by cell matrix-associated heparin-binding growth-associated molecule (HB- GAM). *J. Cell Biol.* **143**, 1113–1128 (1998).
489. Bhat, V., Sun, Y. J., Weger, S. & Raouf, A. Notch-Induced Expression of FZD7 Requires Noncanonical NOTCH3 Signaling in Human Breast Epithelial Cells. *Stem Cells Dev.* **25**, 522–529 (2016).
490. Tamamura, Y., Otani, T., Kanatani, N., Koyama, E., Kitagaki, J., Komori, T., Yamada, Y., Costantini, F., Wakisaka, S., Pacifici, M., Iwamoto, M. & Enomoto-Iwamoto, M. Developmental Regulation of Wnt/β-Catenin Signals Is Required for Growth Plate Assembly, Cartilage Integrity, and Endochondral Ossification. *J. Biol. Chem.* **280**, 19185–19195 (2005).
491. Luo, J. *et al.* LGR4 is a receptor for RANKL and negatively regulates osteoclast differentiation and bone resorption. *Nat. Med.* **22**, 539–546 (2016).
492. Sun, P., Jia, K., Zheng, C., Zhu, X., Li, J., He, L., Siwko, S., Xue, F., Liu, M. & Luo, J. Loss of *Lgr4* inhibits differentiation, migration and apoptosis, and promotes proliferation in bone mesenchymal stem cells. *J. Cell. Physiol.* **234**, 10855–10867 (2019).
493. Hao, H.-X. *et al.* ZNRF3 promotes Wnt receptor turnover in an R-spondin-sensitive manner. *Nature* **485**, 195–200 (2012).
494. Lehoczky, J. A. & Tabin, C. J. Rethinking WNT signalling. *Nature* **557**, 495–496 (2018).
495. Szenker-Ravi, E. *et al.* RSPO2 inhibition of RNF43 and ZNRF3 governs limb development independently of LGR4/5/6. *Nature* **557**, 564–569 (2018).
496. Bell, S. M., Schreiner, C. M., Wert, S. E., Mucenski, M. L., Scott, W. J. & Whitsett, J. A. R-spondin 2 is required for normal laryngeal-tracheal, lung and limb morphogenesis. *Development* **135**, 1049–1058 (2008).

Appendix 1 - Solutions and Buffers

A1.1 - Goldner's Trichrome staining solutions:

Weigert's Ferric Haematoxylin:
Solution A:

- 1g Haematoxylin
- 100mL 96% Ethanol

Solution B:

- 4mL 30% Ferric chloride
- 1mL 37% Hydrochloric acid
- 100mL distilled water

Working solution: equal parts of solution A and solution B

Ponceau Acid Fuchsin:
Solution A:

- 1g Ponceau 2R
- 100mL distilled water

Solution B:

- 1g Acid Fuchsin
- 100mL distilled water

Working solution:

- 6mL Solution A
- 2mL Solution B
- 9mL 2% Acetic Acid
- 73mL distilled water

Phosphotungstic-acid (or Phosphomolybdic)- Orange G solution:

- 3-5g Phosphotungstic acid
- 2g Orange G
- 100mL distilled water

Light green solution:

- 0.2-0.3g Light green
- 0.2mL Acetic acid
- 100mL distilled water

A1.2 - TRAP staining Reagents for fixed cells:

Reagents required:

Naphthol–AS-BI-phosphate
Veronal Buffer
Acetate buffer
Pararosanilin
Sodium Nitrite (NaNO2)
Dimethylformamide

Stock Buffers:

Veronal Buffer in 100ml dH_2O
1.17g Sodium Acetate Anhydrous
2.94g Veronal (sodium barbiturate)

Acetate Buffer 0.1n, pH5.2
a/ 0.82g Sodium Acetate Anhydrous in 100ml dH_2O
b/ 0.6ml glacial acetic acid made up to 100ml with dH_2O
Adjust pH of solution a to 5.2 with solution b

Pararosanilin
Add 1g to 20ml dH_2O and add 5ml concentrated HCl, Heat carefully in a waterbath while stirring until fully dissolved do this in the fume cupboard. Filter after cooling to room temp.

4% Sodium Nitrite
4g in 100mls dH2O

Prepare staining solution:
Stocks to be made fresh each time:
Naphthol –AS-BI-phosphate stock 10mg/ml in dimethylformamide
Stable for about two weeks at 4ºC

Solution 1
Must add in this order and mix the Naphthol and Veronal buffers together very well before adding the next ingredients.

150ul Naphthol–AS-BI-phosphate stock to be made fresh each time
750ul Veronal buffer
900ul Acetate buffer
900ul Acetate buffer with 100mM tartrate

Solution 2
This needs time to react before adding to solution 1 so prepare before fixing the cells.
120ul Pararosanilin
120ul NaNO2 (4%)
Mix solution 1 and 2 together (the above amounts give a volume of 2.94mls). Then filter through 0.2um filter.

Total volume of solution prepared using these volumes is 2.94mls

A1.3 - RIPA Buffer

Final Concentrations
Triton 1%
Na Deoxycholate 0.5% w/v
SDS 0.1% w/v
Tris HCL pH 7.4 50mM
NaCl 150mM

To make up 1l of RIPA Buffer
10ml Triton
5g Na deoxycholate
1g SDS
50ml 1M TRIS HCl pH 7.4
8.77g

Appendix 2 – CTAN Macro for trabecular analysis

Step 1: Filtering	
Mode	Median (2D space)
Kernel	Square
Radius	1
Step 2: Thresholding	
Mode	Global
Lower grey threshold	70
Upper grey threshold	255
Step 3: Despeckle	
Type	Remove white speckles (3D space)
Volume	Less than 100 voxels
Apply to	Image
Step 4: Bitwise operations	
	<Region of Interest>=COPY<Image>
Step 5: Morphological operations	
Type	Closing (2D space)
Kernel	Round
Radius	5
Apply to	Region of interest
Step 6: Despeckle	
Type	Remove black speckles (2D space)
Area	Less than 250 pixels
Apply to	Region of interest
Step 7: Despeckle	
Type	Remove white speckles (2D space)
Area	Less than 100 pixels
Apply to	Region of interest
Step 8: Morphological operations	
Type	Opening (3D space)
Kernel	Round
Radius	1
Apply to	Region of interest
Step 9: Despeckle	
Type	Sweep (3D space)
Remove	All except the largest object
Apply to	Region of interest
Step 10: Despeckle	

Type	Remove white speckles (2D space)
Remove	All except the largest object
Area	Less than 100 pixels
Apply to	Region of interest
Step 11: Bitwise operations	
	<Image> =COPY <Region of Interest>
Step 12: ROI shrink-wrap	
Mode	Fill-out (2D space)
Step 13: Bitwise operations	
	<Region of Interest>=<Image>XOR<Region of Interest>
Step 14: Morphological operations	
Type	Opening (3D space)
Kernel	Round
Radius	2
Apply to	Region of Interest
Step 15: Despeckle	
Type	Sweep (3D space)
Remove	All except the largest object
Apply to	Region of interest
Step 16: Morphological operations	
Type	Closing (2D space)
Kernel	Round
Radius	15
Apply to	Region of Interest
Step 17: Despeckle	
Type	Remove pores (2D space)
Detected by	By image borders
Apply to	Region of interest
Step 18: Morphological operations	
Type	Erosion (2D space)
Kernel	Round
Radius	12
Apply to	Region of Interest
Step 19: Despeckle	
Type	Sweep (2D space)
Remove	All except the largest object
Apply to	Region of interest
Step 20: Morphological operations	

Type	Dilation (2D space)	
Kernel	Round	
Radius	12	
Apply to	Region of Interest	
Step 21: Morphological operations		
Type	Opening (3D space)	
Kernel	Round	
Radius	4	
Apply to	Region of Interest	
Step 22: Morphological operations		
Type	Erosion (2D space)	
Kernel	Round	
Radius	2	
Apply to	Region of Interest	
Step 23: Save bitmaps (only ROI)		
File format	bmp	
Step 24: Save bitmaps		
	<Image> = COPY <Clipboard>	
Step 25: 3D analysis		
	Abbreviation	**Unit**
Tissue volume	TV	μm^3
Bone volume	BV	μm^3
Percent bone volume	BV/TV	%
Tissue surface	TS	μm^2
Bone surface	BS	μm^2
Intersection surface	i.S	μm^2
Bone surface/ volume ratio	BS/BV	1/ µm
Bone surface density	BS/TV	1/ µm
Trabecular pattern factor	Tb.Pf	1/ µm
Centroid (x)	Crd.X	µm
Centroid (y)	Crd.Y	µm
Centroid (z)	Crd.Z	µm
Structure model index	SMI	
Trabecular thickness	Tb.Th	µm
Trabecular number	Tb.N	1/ µm
Trabecular separation	Tb.Sp	µm
Degree of anisotropy	DA	
Eigenvalue 1		
Eigenvalue 2		
Eigenvalue 3		
Fractal dimension	FD	
Number of objects	Obj.N	
Number of closed pores	Po.N(cl)	

Volume of closed pores	Po.V(cl)	μm^3
Surface of closed pores	Po.S(cl)	μm^2
Closed porosity (percent)	Po(cl)	%
Volume of open pore space	Po.V(op)	μm^3
Open porosity	Po(op)	%
Total volume of pore space	Po.V(tot)	μm^3
Total porosity (percent)	Po(tot)	%
Euler number	Eu.N	
Connectivity	Conn	
Connectivity density	Conn.Dn	$1/ \mu m^3$

Appendix 3 – CTAN Macro for cortical analysis

Step 1: Filtering		
Mode	Median (2D space)	
Kernel	Round	
Radius	1	
Step 2: Thresholding		
Mode	Global	
Lower grey threshold	70	
Upper grey threshold	255	
Step 3: Despeckle		
Type	Sweep (3D space)	
Remove	All except the largest object	
Apply to	Image	
Step 4: Morphological operations		
Type	Closing (2D space)	
Kernel	Round	
Radius	3	
Apply to	Image	
Step 5: Bitwise operations		
	<Region of Interest>=COPY<Image>	
Step 6: Despeckle		
Type	Remove pores (2D space)	
Detected by	By image borders	
Apply to	Region of interest	
Step 7: Bitwise operations		
	<Clipboard> = <Region of Interest> XOR <Image>	
Step 8: 3D analysis		
	Abbreviation	**Unit**
Tissue volume	TV	μm^3
Bone volume	BV	μm^3
Percent bone volume	BV/TV	%
Tissue surface	TS	μm^2
Bone surface	BS	μm^2
Intersection surface	i.S	μm^2
Bone surface/ volume ratio	BS/BV	1/ µm
Bone surface density	BS/TV	1/ µm
Trabecular pattern factor	Tb.Pf	1/ µm
Centroid (x)	Crd.X	µm
Centroid (y)	Crd.Y	µm
Centroid (z)	Crd.Z	µm

Trabecular thickness	Tb.Th	µm
Trabecular number	Tb.N	1/ µm
Step 9: 2D analysis		
Mean Polar moment of inertia	MMI(polar)	μm^4
Step 10: Bitewise operation	<Image> = SWAP <Clipboard>	
Step 11: 3D analysis		
Tissue volume	TV	μm^3
Bone volume	BV	μm^3
Percent bone volume	BV/TV	%
Tissue surface	TS	μm^2
Bone surface	BS	μm^2
Intersection surface	i.S	μm^2
Bone surface / volume ratio	BS/BV	1/ µm
Bone surface density	BS/TV	1/ µm
Trabecular pattern factor	Tb.Pf	1/ µm
Centroid (x)	Crd.X	µm
Centroid (Y)	Crd.Y	µm
Centroid (Z)	Crd.Z	µm
Trabecular thickness	Tb.Th	µm
Trabecular number	Tb.N	1/ µm
Step 13: 2D analysis		
Tissue volume	TV	μm^3
Bone volume	BV	μm^3
Percent bone volume	BV/TV	
Tissue surface	TS	μm^2
Peripheral tissue surface	TS(per)	μm^2
Bone surface	BS	μm^2
Peripheral bone surface	BS(per)	μm^2
Bone surface / volume ratio	BS/BV	1/µm
Mean total crossectional tissue area	T.Ar	μm^2
Mean total crossectional tissue perimeter	T.Pm	µm
Mean total crossectional bone area	B.Ar	μm^2
Mean total crossectional bone perimeter	B.Pm	µm
Mean number of objects per slice	Obj.N	
Average principal moment of inertia (max)	Av.MM(max)	μm^4
Average principal moment of inertia (min)	Av.MM(min)	μm^4
Mean eccentricity	Ecc	
Crossectional thickness	Cs.Th	µm

Trabecular thickness (plate model)	Tb.Th(pl)	µm
Step 14: Bitewise operations	<Image> = SWAP <Clipboard>	
Step 15: 3D model		
Model creation algorithm	Adaptive rendering	
Apply to	Image	
Smoothing	On	
Locality	1	
Tolerance	0.250000	
Step 16: Save bitmaps		

Appendix 4 – CTAN Macro for L5 analysis

Step 1: Filtering		
Mode	Median (2D space)	
Kernel	Round	
Radius	2	
Step 2: Thresholding		
Mode	Automatic (Otsu mode)	
Background	Dark	
Step 3: Despeckle		
Type	Remove white speckles (3D space)	
Volume	Less than 100 voxels	
Apply to	Image	
Step 4: 3D analysis		
	Abbreviation	**Unit**
Tissue volume	TV	μm^3
Bone volume	BV	μm^3
Percent bone volume	BV/TV	%
Tissue surface	TS	μm^2
Bone surface	BS	μm^2
Intersection surface	i.S	μm^2
Bone surface/ volume ratio	BS/BV	1/ µm
Bone surface density	BS/TV	1/ µm
Trabecular pattern factor	Tb.Pf	1/ µm
Centroid (x)	Crd.X	µm
Centroid (y)	Crd.Y	µm
Centroid (z)	Crd.Z	µm
Structure model index	SMI	
Trabecular thickness	Tb.Th	µm
Trabecular number	Tb.N	1/ µm
Trabecular separation	Tb.Sp	µm
Fractal dimension	FD	
Number of objects	Obj.N	
Number of closed pores	Po.N(cl)	
Volume of closed pores	Po.V(cl)	μm^3
Surface of closed pores	Po.S(cl)	μm^2
Closed porosity (percent)	Po(cl)	%
Volume of open pore space	Po.V(op)	μm^3
Open porosity (percent)	Po(op)	%
Total volume of pore space	Po.V(tot)	μm^3
Total porosity (percent)	Po(tot)	%
Euler number	Eu.N	
Connectivity	Conn	

Connectivity density	Conn.Dn	
Degree of anisotropy	DA	
Eigenvalue 1		
Eigenvalue 2		
Eigenvalue 3		

Appendix 5 – CTAN macro for P2 leg analysis

Step 1: Filtering		
Mode	Median (2D space)	
Kernel	Square	
Radius	2	
Step 2: Thresholding		
Mode	Global	
Lower grey threshold	80	
Upper grey threshold	240	
Step 3: Despeckle		
Type	Remove white speckles (3D space)	
Volume	Less than 100 voxels	
Apply to	Image	
Step 4: Save bitemaps (only image)		
File format	Bmp	
Step 5: 3D analysis		
	Abbreviation	**Unit**
Tissue volume	TV	μm^3
Bone volume	BV	μm^3
Percent bone volume	BV/TV	%
Tissue surface	TS	μm^2
Bone surface	BS	μm^2
Intersection surface	i.S	μm^2
Bone surface/ volume ratio	BS/BV	1/ µm
Bone surface density	BS/TV	1/ µm
Trabecular pattern factor	Tb.Pf	1/ µm
Centroid (x)	Crd.X	µm
Centroid (y)	Crd.Y	µm
Centroid (z)	Crd.Z	µm